NATIONAL AERONAUTICS AND SPACE ADMINISTRATION
Grant NsG-641

Final Report for the Period 1 May 1966 to 31 October 1967

HETEROGENEOUS IGNITION OF METALS:

MODEL AND EXPERIMENT

by

Arthur M. Mellor

Aerospace and Mechanical Sciences Report No. 816

Approved By: Irvin Glassman

Irvin Glassman
Professor of Aerospace Sciences
Principal Investigator

Guggehneim Laboratories for the Aerospace Propulsion Sciences
Department of Aerospace and Mechanical Sciences
PRINCETON UNIVERSITY
Princeton, New Jersey

1967

ABSTRACT

Inefficient ignition and combustion of metallic additives in solid propellant rocket motors has stimulated interest in the fundamental processes involved in the ignition of metals. A physical model of this heterogeneous process is presented, compared with other theories of ignition in view of literature studies of metal ignition, and finally tested by detailed experimentation in an induction furnace facility.

Three temperatures form the basis of the model for any metal-oxidizing gas system. The first is a spontaneous ignition temperature, which is called the critical temperature, the second is the ignition temperature, at which immediate inflammation of the metallic fuel occurs, and the last is the transition temperature, which is invoked due to a problem unique to metal ignition. Because reacting metal-gas systems form solid-phase products on the reaction surface at low temperatures, the chemical reaction can be inhibited by the product film thus formed. The transition temperature is that temperature at and above which this product layer becomes non-protective in the sense that a reaction rate independent of time describes the behavior of the system at constant temperature.

The model postulates that the ignition temperature, at which a flame appears, will exceed both the critical temperature, at and above which sample self-heating is possible, and the transition temperature, which reflects the protective ability of the product film. Furthermore, the minimum possible ignition temperature of any metal-oxidizer system is the transition temperature appropriate to the particular product film. Because the transition temperature is relatively independent of en-

vironmental conditions (in particular the heat losses from the solid metallic fuel), and because this temperature can be estimated from the metal oxidation literature in many cases of interest, it then is an important and useful design criterion for efficient ignition of metals, because only if the transition temperature is exceeded can ignition and combustion occur.

Both experimental results on metal ignition available in the literature and of the present investigation indicate that the present model is much more general than other theories of metal ignition and is able to correlate ignition data in a completely self-consistent manner. In particular, the present results obtained with Mg and Ca in various oxidizing gases demonstrate the existence of the critical and ignition temperatures and the behavior of these temperatures with respect to variations in the independent experimental parameters. For example, for Mg in O_2 at 300 torr, as the metal surface area to volume ratio is increases from 10^{-1} to 10^{1} mm^{-1}, the ignition temperature decreases from about 650°C to 450°C; this latter value is comparable to the transition temperature, as the model predicts. The observed non-unique nature of the critical and ignition temperatures reinforces the importance of the transition temperature.

ACKNOWLEDGEMENTS

The author wishes to acknowledge the guidance and encouragement which he has received from Professor Irvin Glassman, both during the author's graduate and undergraduate careers at Princeton. Many extended discussions with Professor Glassman, as well as with Doctor Alvin S. Gordon, Professor Robert F. Sawyer, and Doctor James G. Hansel, were extremely helpful in the formulation of the model presented in this report.

Special thanks go to Mr. Anthony Bozowski who assisted the writer in innumerable ways, including sample preparation, apparatus construction, and particularly apparatus design. Mr. Bozowski's creative imagination in the latter category deserves special mention. Mr. Joseph Sivo also helped with the mechanical construction of the equipment.

Mr. Jack Cooper designed and constructed the electronic components used during the investigation. His enthusiasm and interest in the design of the temperature differentiating control system guaranteed its successful operation.

The assistance of Mr. Normand Laurendeau in the final stages of the experimental work is appreciated.

Mr. Tony Poli, Mrs. Ann Jansak, and Mr. Donald Neiler prepared the figures in the present report, and Mr. Poli assisted in the design of the mechanical apparatus.

Miss Dorothy Morris, Miss Claire Hartmann, and Miss Christine Walch typed both of the drafts of the manuscript. The author particularly wishes to acknowledge the special talents of Miss Morris.

The author is pleased to acknowledge the receipt of the Air Reduction Company Fellowship in Aerothermochemistry. The National Aeronautics and Space Administration made this research possible through Grant NsG-641, Pre-Ignition and Ignition Processes of Metals. The special interest of Mr. Robert Ziem of the Solid Propellant Group of NASA and Mr.Warren Dowler of the Advanced Technology Group of JPL is most appreciated.

TABLE OF CONTENTS

NOMENCLATURE

Throughout the text, all symbols are defined as they are used. The following list includes particular temperatures which are used often and the number of the page on which they are defined.

T_{oxid}	Oxidation Temperature	28
T_{crit}	Critical Temperature	29
T_f	Flame Temperature	29
T_{ign}	Ignition Temperature	31
T_{trans}	Transition Temperature	39

LIST OF TABLES

LIST OF FIGURES

CHAPTER I - INTRODUCTION

In recent years the chemistry of high-temperature metal-gas reactions has become of greater importance in aerospace research. At elevated temperatures metals undergo oxidation, ignition, and combustion reactions, and the chemical properties of metals in the presence of hot gases are of tantamount importance in various areas of modern aerospace activity.

Interest in high-temperature metallurgy stems from application involving metallic structures at elevated temperatures, applications such as re-entry vehicles and nuclear rockets. In this and similar uses, catastrophic oxidation, or combustion, of structural members is obviously unwanted.

In the second major application, combustion is desired. Because of their characteristically high heat release per unit mass upon combustion, the light metals, particularly Mg, Al, and Be, have come into use as additives to solid propellant rocket systems, and much of the future of chemical propulsion depends upon the proper utilization of the metallic elements. Unfortunately, in solid propellants inability to attain theoretical performance is encountered. Three reasons have been offered for this inefficiency: firstly, inefficient ignition of the metal particles, due to high ignition temperatures; secondly, inefficient combustion, because of slow surface-burning processes rather than the desired rapid vapor-phase combustion, possibly a result of lack of ignition; and lastly, two-phase flow losses in the expansion nozzle due to the presence of small particles of metal oxide smoke resulting from the combustion process. It is the first two of these possible causes which is the subject of this study.

In 1959, Glassman published four observations on metal ignition and metal combustion, which were based on simple physical reasoning (1, 2):[1]

(1) The boiling point of the metal oxides limits the flame temperature of the metals.

This statement is based on the observation that in most cases the heat available from a metal-oxygen reaction is less than the heat of vaporization or dissociation of the appropriate metal oxide formed during the reaction.

(2) If the boiling point of the metal oxide is greater than that of the metal, then "steady-state" combustion takes place in the vapor phase; the contra condition, the metal temperature greater than the oxide temperature, predicts a surface combustion process.

Since the temperature of the metal particle is limited to its boiling point, for the vapor-phase diffusion flame in which heat transfer from the reaction zone to the particle is necessary, the boiling point of the metal oxide (that is, the flame temperature) must be greater than the boiling point of the metal.

In a later paper (3), it was pointed out that this condition for vapor-phase combustion was necessary but not sufficient, as heat losses from the reaction zone could lower its temperature below the boiling point of the oxide, or even below that of the metal, thus establishing a surface-burning configuration.

(3) Radiation plays an important part in metal combustion.

Statement (3) results from a consideration of the high

---

[1] Numbers in parentheses refer to references listed at the end of this report.

number density of condensed phase particles of metal oxide smoke formed in the flame zone during the combustion reaction and the high boiling points of the oxides.

(4) Ignition phenomena could be entirely different from the controlling steady combustion phenomena.

This statement reflects the fact that ignition can be the transition from surface oxidation, during the pre-ignition reaction, to vapor-phase combustion.

The simple thermodynamic criterion for vapor-phase combustion in O_2, statement (2), was used to predict that Al, Mg, Li, Na, K, Ca, and Be would burn in the vapor-phase, and that B, Si, Ti, and Zr would burn on the surface (1). More recent thermodynamic data, shown in Table 1 and taken from Ref. (4) - (6), predict that Li, Be, Mg, Al, Si(?), Ca, Cr, Rb, Sr, Y, Zr, Sb, Ba, La, Ce, Bi, and Th will burn in the vapor phase, under the assumption that the heat of vaporization or dissociation of the oxide is greater than the available heat of reaction.

Brzustowski (7, 8) developed a burning rate theory for metals based on the classical hydrocarbon diffusion flame theory but modified to include the characteristics peculiar to metal combustion. He also performed an extensive experimental investigation of the combustion of magnesium ribbons and anodized and unanodized aluminum wires in O_2-Ar mixtures (7, 9)[2]. He found regions of vapor-phase burning for both of these metals, as well as agreement with trends predicted by the metal diffusion flame burning rate theory. There

[2]Because of space limitations, only a few details of the metal combustion literature will be given here. Three surveys of this literature are available (7,10,11). Most of the more recent work not included in these surveys may be found in Ref. (12)-(14). The metal ignition literature will be reviewed in detail in Chapter IV.

TABLE 1.

METAL AND OXIDE BOILING POINTS AT ONE ATMOSPHERE FOR THOSE METALS WHICH CAN BURN IN THE VAPOR PHASE

Atomic Number	Metal	Predominant Metal Oxide	Boiling Points, °C	
			Metal	Oxide
3	Li	Li_2O	1365(4)[1]	2563(4)
4	Be	BeO	2484(4)	3787(4)
12	Mg	MgO	1105(4)	3600(5)
13	Al	Al_2O_3	2463(4)	2980(5)
14	Si	SiO_2	3167(4)	3273(4)
20	Ca	CaO	1240(5)	2850(5)
24	Cr	Cr_2O_3	2480(5)	4000(5)
37	Rb	Rb_2O_2	700(5)	1010(5)
38	Sr	SrO	1366(5)	3000(5)
39	Y	Y_2O_3	1427(5)	4300(6)
40	Zr	ZrO_2	4474(4)	5000(5)
51	Sb	Sb_2O_5	1380(5)	1550(5)
56	Ba	BaO	1527(5)	2000(5)
57	La	La_2O_3	3470(5)	4200(5)
58	Ce	CeO_2	2417(5)	2700(6) decomposes
83	Bi	Bi_2O_3	1470(5)	1890(6)
90	Th	ThO_2	4230(5)	4400(5)

[1]Numbers in parentheses refer to references listed at the end of the report.

was substantially no difference between the ignition and combustion of the two types of Al wire in O_2.

In particular, Brzustowski found a correspondence between the ignition temperature of aluminum in O_2 and the melting point of aluminum oxide (7, 9). It had been predicted previously that the surface temperature of an aluminum particle must exceed this temperature in order to avoid slow heterogeneous reactions and rather to burn in the vapor phase (3). Experimental work by Friedman and Macek led these investigators to the same conclusions (15, 16), and more recent work by Kuehl (17, 18) has demonstrated that the ignition temperature of Al in O_2 is generally equal to the melting point of Al_2O_3.

In an extension of Brzustowski's experimental investigation, Mellor studied the ignition and combustion of aluminum and magnesium in O_2-CO_2 and CO_2-Ar mixtures (19, 20). The ignition and combustion of unanodized and anodized Al wires in O_2-CO_2 mixtures was found to differ little from that in O_2-Ar mixtures, except for the presence of C in the products of combustion. However, Mg ribbons could not be ignited in O_2-CO_2 mixtures except at high O_2 partial pressures, in contrast to Brzustowski's earlier results in O_2-Ar atmospheres. One possible explanation of this effect of CO_2 was that the outflow of Mg vapor required for the characteristic gas-phase ignition of Mg in O_2 was unhibited by an oxide-carbide film which formed during the pre-ignition reactions in O_2-CO_2 mixtures (20). Mg ribbons could not be ignited in CO_2-Ar mixtures. These observations indicate that the ignition temperature of Mg in CO_2-Ar mixtures and in low O_2 partial pressure O_2-CO_2 mixtures is above the melting point of the metal whereas in O_2-Ar mixtures or in pure O_2 it is at or below

the metal melting point.[3]

Although unanodized Al wires could not be ignited in CO_2-Ar mixtures, the anodized wires, on which a thick oxide film was present at the start of an experiment, were easily ignited in this gas mixture. In fact, the power required to ignite these wires (using resistance heating) was less than that required at similar pressures in O_2-CO_2 mixtures (19, 20). Furthermore, whereas ignition occurred when the wire broke in oxygen-containing atmospheres, at the lower pressures in CO_2-Ar mixtures a cylindrical vapor-phase ignition flame was observed over the surface of the wire before its breaking. The appearance of this flame was attributed to the porous nature of the anodized coating present upon the wires. It was argued that in oxygen-containing atmospheres and in CO_2-Ar mixtures at the higher pressures investigated these pores were filled during the pre-ignition oxidation reactions.[4]

In a later paper (21), these experimental observations of the ignition of Mg ribbons and anodized and unanodized Al wires were correlated to present a physical model of metal ignition. Fig. 4 of Ref. (21) is presented here as Fig. 1 for convenience. The appearance of a vapor-phase flame before the wire or ribbon broke was correlated with the formation of a porous non-protective product film on the surface of the metal during the pre-ignition reactions in the particular oxidizing atmosphere.[5]

Upon examination of the metal oxidation liter-

---

[3] In the experimental apparatus used in these investigations, it is necessary that the metal wires or ribbons support themselves in order to maintain ohmic heating. See Chapter V.

[4] Kuehl (17) has observed a similar mode of ignition in O_2-Ar mixtures and has offered a somewhat different explanation which will be discussed in detail in Chapter VI and Appendix II.

[5] V_f/V_m in Fig. 1 is the Pilling and Bedworth ratio, the

ature, it was found that in general all metals at low temperatures form protective oxide films, as indicated by the nature of their low-temperature oxidation rate laws, and at high temperatures these oxide films become non-protective. The temperature which distinguishes these two regimes was defined as the transition temperature (21). It was also argued that metal-oxidizer systems would exhibit a spontaneous ignition temperature, at which the rate of heat generation by the chemical reaction just exceeds the rate of heat loss from the system, as in homogeneous and other heterogeneous systems described by the classical stationary thermal ignition theory (see for example Ref. (23)). This spontaneous ignition temperature was renamed the critical temperature (21).

The physical criterion for metal ignition was then formulated simply: the ignition temperature observed for a particular metal-oxidizer system will be greater than both the transition and critical temperatures for that particular system (21). Estimations of these two latter temperatures were made from the metal oxidation and metal ignition literature for the Al-O_2, Mg-O_2, Mg-CO_2, Ca-O_2, and Mo-O_2 systems, and were then compared with the ignition temperatures observed by other investigators. In all cases, the metal ignition criterion was obeyed and in some cases apparent controversies were eliminated (21).

It is the development and refinement of this ignition criterion which forms the subject matter of the present report; critical experimentation which has been

---

[5] volume of (oxide) film formed divided by the volume of metal required to form it (22). Values of the ratio less than one indicate a non-protective product film, greater than one a protective film, and much greater than one again a non-protective film due to mechanical stresses set up by its formation.

FIGURE 1

TYPES OF IGNITION

1. 

VAPOR-PHASE

2. 

a) HIGH TEMP., VAPOR PHASE
b) LOW TEMP., SURFACE

OCCURRENCE	SURFACE FILM	OCCURRENCE	SURFACE FILM
1. CLEAN Mg IN O_2-Ar	MgO	1. CLEAN Mg IN O_2-CO_2	MgO + C
2. ANODIZED Al IN CO_2-Ar	POROUS-Al_2O_3	2. ANODIZED Al IN O_2-Ar	Al_2O_3
3. ANODIZED Al IN H_2O-Ar	POROUS-Al_2O_3	3. ANODIZED Al IN CO_2-O_2	Al_2O_3
4. ANODIZED Al IN H_2O-CO_2	POROUS-Al_2O_3	4. CLEAN Al IN O_2-Ar	Al_2O_3
		5. CLEAN Al IN CO_2-O_2	Al_2O_3

COMMON CHARACTERISTIC OF SURFACE FILM

$V_f / V_M < 1$ $\qquad$ $V_f / V_M > 1$

performed at Princeton to test the criterion is described.

In Chapter II, after a brief review of classical theories of thermal ignition, the classical stationary thermal ignition theory is applied to the case of heterogeneous systems forming gas-phase reaction products (that is, hydrocarbon droplets, solid-propellant fuel slabs, and so forth). In the next section of the chapter the possibility of formation of solid-phase products on the reaction surface is allowed, and the transition temperature is introduced. An extension of the stationary theory is then given to show that the general features of the metal ignition model do not change when a time dependence is considered.

Section 4 of Chapter II is a discussion of metal pyrophoricity, that is, the property of small metal particles to self-heat and ignite when exposed to air at room temperature. The final section of Chapter II is a consideration of augmented metal ignition efficiency based on concepts generated by the model of metal ignition.

Literature values of transition and critical temperatures are given in Appendices I and II and are analyzed in view of ignition temperatures observed by other investigators. These data are summarized in Chapters III and IV.

The experimental apparatus used in the present investigation is described in Chapter V, and results obtained on the ignition of Mg, Al, and Ca are discussed in view of the metal ignition criterion in the following two chapters (VI and VII).

The final chapter is a review of the experimental verification by the present investigation of the metal ignition criterion developed in Chapter II.

CHAPTER II - THE PHYSICAL MODEL OF METAL IGNITION

Because of the possibility of the formation of solid-phase products of metal-oxidizer pre-ignition reactions on the reacting surface, metal ignition can be much more complicated than the ignition of other heterogeneous fuel-oxidizer systems. At low temperatures this product film is generally protective in the sense that it inhibits the reaction in time, and thus ignition (immediate temperature runaway on the reacting surface ending in steady-state, self-sustained combustion) is impossible to achieve.

Before discussing a general metal-oxidizer system, a review of the classical thermal theories of homogeneous ignition and a treatment of the simple heterogeneous system in which no solid-phase product forms on the reacting surface will be given. This latter treatment will then be extended to the area of metal-gas reactions; finally, the basis of metal pyrophoricity and augmented ignition efficiency which results from the ignition model will be discussed.

1. Classical Thermal Theories of Homogeneous Ignition

Although many authors have contributed to the thermal theories of homogeneous ignition, probably the most comprehensive and instructive demonstration is given by Frank-Kamenetskii in his classic work, Ref. (23). The present model of heterogeneous ignition is based to a large extent on this reference. Furthermore, for this section dealing with homogeneous ignition, Frank-Kamenetskii's analysis will be followed in detail.

In general, one considers a static homogeneous mixture of a gaseous fuel and oxidizer; this mixture is

placed in a vessel of defined geometry with wall temperature T_w (^oK) at time zero. For certain values of T_w below some critical value, little if any change in the gas temperature T_g will be observed in time. For values of T_w greater than the critical value, the gas temperature will increase rapidly to a steady state value:

$$T_{max} = T_w + Q/c_p \qquad \text{(II-1)}$$

where T_{max} is the maximum gas temperature attainable from the chemical reaction, Q is the heat released by the reaction (cal/g), and c_p is the heat capacity (cal/g^oK; it is assumed that the heat capacities of the reactant and product mixtures are equal).

The critical value of wall temperature which separates these two very different regimes of temporal behavior of the reacting mixture may be considered as an ignition or explosion temperature. It is the purpose of the thermal theory of homogeneous ignition to calculate this value.

For this purpose, the non-steady Fourier heat conduction equation with distributed heat sources is used:

$$\rho c_p \frac{\partial T_g}{\partial t} = \nabla \cdot (K \nabla T_g) + \dot{q} \qquad \text{(II-2)}$$

where ρ is the density of the mixture (g/cm^3), t is time (sec), k is the thermal conductivity of the mixture (cal/cm sec^oK), and $\dot{q}$ is the heat release rate per unit volume of the mixture (cal/cm^{3}sec).

Depending on the method of approach to the solution of the problem, the theory is referred to as stationary (time independent) or non-stationary (time dependent). In the former case, the temporal dependence of Eqn. (II-2) is neglected, and Eqn. (II-3) is solved:

$$\nabla \cdot (K \nabla T_g) = -\dot{q} \qquad \text{(II-3)}$$

Ignition is said to occur at the value of T_w for which no stationary value of T_g may be obtained from the solution of Eqn. (II-3).

In the non-stationary theory, it is assumed that the entire mixture is a uniform temperature equal to T_g. Under this assumption Eqn. (II-4) must be solved (in the actual formulation of this theory a heat loss term is also included; see Section 1.b):

$$\rho c_p \frac{dT_g}{dt} = \dot{q} \qquad \text{(II-4)}$$

Ignition is determined by the failure of T_g to attain a steady-state value. Each of these methods of solution will be reviewed briefly. The reader is referred to Ref. (23) for details.

a. The Stationary Theory

As noted, the appropriate equation to be solved is Eqn. (II-3) under the time-independent assumption of the stationary theory. If it is further assumed that the thermal conductivity is temperature independent, then Eqn. (II-3) may be written:

$$K\nabla^2 T_g = -\dot{q} \qquad \text{(II-5)}$$

where the particular form of the Laplacian operator will depend on the geometry of the vessel under consideration.

If x_0 is the radius of a spherical vessel or an infinite cylindrical vessel (or the half-width of an infinite plane-sided vessel), then the boundary conditions appropriate to Eqn. (II-5) are as follows:

$$\left.\frac{dT_g}{dx}\right|_{x=0} = 0 \qquad \text{(II-6)}$$

$$T_g(x=x_0) = T_w \qquad \text{(II-7)}$$

If it is assumed that an Arrhenius-type expression will represent satisfactorily the temperature dependence of the reaction rate for the homogeneous mixture, then $\dot{q}$ is given by Eqn. (II-8):

$$\dot{q} = ZQe^{-E/RT_g} \tag{II-8}$$

where Z is a function of pressure and composition of the mixture (but not of T_g; $g/cm^3 sec$), E is the activation energy (cal/mole), and R is the universal gas constant ($cal/mole\,^{\circ}K$).

Non-dimensional parameters are introduced as follows:

$$\xi = x/x_o \tag{II-9}$$

$$\theta = E(T_g - T_w)/RT_w^2 \tag{II-10}$$

By virtue of Eqn. (II-8) through (II-10), Eqn. (II-5) through (II-7) become:

$$\nabla_\xi^2 \theta = \frac{Q}{K}\frac{E}{RT_w^2} x_o^2 Z \exp\left\{-\frac{E}{RT_w}\left(\frac{1}{1+RT_w\theta/E}\right)\right\} \tag{II-11}$$

$$\left.\frac{d\theta}{d\xi}\right|_{\xi=0} = 0 \tag{II-12}$$

$$\theta(\xi=1) = 0 \tag{II-13}$$

Because the stationary solution of Eqn. (II-11) is sought below the critical value of T_w, it can be assumed that $T_g \cong T_w$, that is, $(T_g - T_w)/T_w \ll 1$. Then, if the argument of the exponential in Eqn. (II-11) is expanded into a power series, all terms involving powers of $(T_g - T_w)/T_w$ greater than one can be neglected, and the exponential may be approximated:

$$\exp\left\{-\frac{E}{RT_w}\left(\frac{1}{1+RT_w\theta/E}\right)\right\} \cong \exp\left\{-\frac{E}{RT_w}\right\}\exp\{\theta\} \qquad \text{(II-14)}$$

Eqn. (II-11) then becomes:

$$\nabla^2_\xi \theta = \delta \exp\{\theta\} \qquad \text{(II-15)}$$

where

$$\delta \equiv \frac{Q}{K}\frac{E}{RT_w^2} X_o^2 Z \exp\left\{-\frac{E}{RT_w}\right\} \qquad \text{(II-16)}$$

which is a single parameter involving all of the independent variables of the geometry and gas mixture.

The solution of Eqn. (II-15) will be of the form

$$\theta = \theta(\xi; \delta) \qquad \text{(II-17)}$$

and thus only the value of δ can determine if a stationary

temperature distribution within the vessel is possible, that is, if ignition will not occur for a given set of boundary conditions. Therefore, the critical ignition condition may be expressed as

$$\delta_{crit} = \text{constant} \qquad \text{(II-18)}$$

The values of δ_{crit} are found by numerical integration of Eqn. (II-15) for the three geometries of interest and equal 3.32, 2.00, and 0.88 for a spherical, cylindrical, and plane-parallel vessel, respectively.

Therefore, for a given geometry and a given gas mixture, one may calculate δ as a function of T_w. For values of T_w such that $\delta < \delta_{crit}$, no ignition will occur, and vice versa.

In the next section, the non-stationary theory of thermal ignition is developed. In particular, it will be demonstrated that the critical conditions of ignition are equivalent in both the stationary and non-stationary theories.

b. The Non-Stationary Theory

In the non-stationary theory of thermal ignition for homogeneous gas mixtures, any temperature gradients within the gas are neglected, and it is assumed that the entire gas is at uniform temperature T_g, which however is not necessarily equal to the wall temperature T_w. The heat transfer from the gas to the wall is expressed as:

$$hS(T_g - T_w) \qquad \text{(II-19)}$$

where h is the heat exchange coefficient ($cal/cm^2 sec$) and S is the wall surface area (cm^2).

Eqn. (II-2) then becomes:

$$\rho c_p V \frac{dT_g}{dt} = QVZe^{-E/RT_g} - hS(T_g - T_w) \qquad \text{(II-20)}$$

where V is the volume of the vessel (cm^3). The initial condition may be expressed as:

$$T_g(t=0) = T_w \qquad \text{(II-21)}$$

Again Eqn. (II-10) is used to define the non-dimensionalization scheme, and Eqn. (II-20) and (II-21) become:

$$\frac{d\theta}{dt} = \frac{Q}{\rho c_p} \frac{E}{RT_w^2} Ze^{-E/RT_w} e^{\theta} - \frac{hS}{\rho c_p V} \theta \qquad \text{(II-22)}$$

$$\theta(t=0) = 0 \qquad \text{(II-23)}$$

There are two dimensional groups in Eqn. (II-22) having the dimension of time:

$$\tau_1 = \left[\frac{Q}{\rho c_p} \frac{E}{RT_w^2} Ze^{-E/RT_w}\right]^{-1} \qquad \text{(II-24)}$$

$$\tau_2 = \left[\frac{hS}{\rho c_p V}\right]^{-1} \qquad \text{(II-25)}$$

Division of Eqn. (II-22) by either τ_1 or τ_2 will yield a dimensionless equation which will have a solution of the form:

$$\theta = \theta\left(\frac{t}{\tau_i}; \frac{\tau_2}{\tau_1}\right) \qquad i = 1,2 \qquad \text{(II-26)}$$

and it is apparent that a critical constant value of τ_1/τ_2 will define the condition of ignition.

The heat exchange coefficient h is defined in terms of the Nusselt number Nu, which for a static gas configuration (neglecting mass diffusion and convection) is constant:

$$h = NuK/x_0 \qquad \text{(II-27)}$$

Thus the critical conditions of ignition resulting from the stationary and non-stationary theories are essentially equivalent:

$$\left(\frac{\tau_2}{\tau_1}\right)_{crit} = \frac{x_0 V}{NuS}\,\frac{Q}{K}\,\frac{E}{RT_w^2}\,Z\exp\left\{-\frac{E}{RT_w}\right\} \qquad \text{(II-28)}$$

$$= \left(\frac{V}{x_0 NuS}\right)\delta_{crit} \qquad \text{(II-29)}$$

and differ only by a constant geometrical factor.

c. Summary

For homogeneous gas systems, two approaches to the problem of thermal ignition or thermal explosion are

available; these are the stationary theory, in which temporal variation of gas temperature is neglected, and the non-stationary theory, in which the gas mixture is assumed at equal temperature throughout. The defining condition for ignition can be shown to be the same as obtained from either theory.

More sophisticated approaches including reactant consumption, and so forth, are available, and the reader is referred to Ref. (23) for details. This reference also demonstrates the agreement between experiment and theory.

In the stationary theory, if the heat transfer term per unit volume involving the wall temperature is expressed as in the non-stationary theory, that is,

$$\dot{q}_{loss} = hS(T_g - T_w)/V \qquad \text{(II-30)}$$

then the defining equation for the stationary theory may be expressed as

$$\dot{q}_{chem} = \dot{q}_{loss} \qquad \text{(II-31)}$$

where as before $\dot{q}_{chem}$ is the heat release rate of the chemical reaction per unit volume (cal/cm^{3}sec):

$$\dot{q}_{chem} = ZQe^{-E/RT_g} \qquad \text{(II-32)}$$

a) STATIONARY THEORY

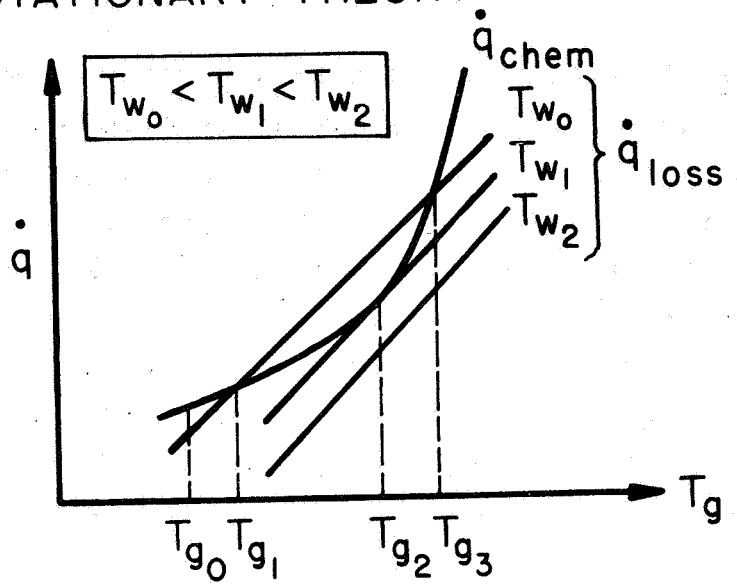

b) NON-STATIONARY THEORY

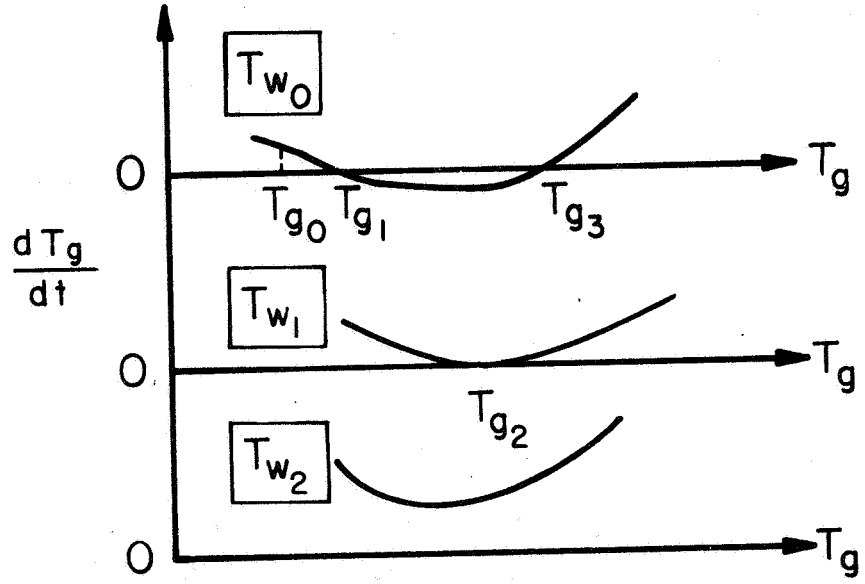

GRAPHICAL REPRESENTATIONS OF THE CLASSICAL THEORIES OF HOMOGENEOUS IGNITION

FIGURE 2

AD29-4044-67

It is seen that a simple graphical representation, as suggested by Semenoff (24), can demonstrate the cogent features of the theory. In Fig. 2a, $\dot{q}_{chem}$ and $\dot{q}_{loss}$ are plotted versus the gas temperature T_g; the former is shown for three values of the wall temperature T_w.[1] Depending on the particular value of T_w, various behaviors of the gas temperature are encountered.

For T_{w0}, with $T_{w0} < T_{w1} < T_{w2}$, if the initial value of the gas temperature is T_{g0}, the mixture will self-heat to the stable temperature T_{g1} because $\dot{q}_{chem}$ exceeds $\dot{q}_{loss}$ between T_{g0} and T_{g1}. Explosion does not occur since the gas temperature cannot rise above T_{g1} spontaneously.

For T_{w1}, with initial gas temperature just greater than T_{g2}, since at these gas temperatures $\dot{q}_{chem}$ exceeds $\dot{q}_{loss}$, explosion will occur.

Finally, for T_{w2}, explosion will occur for any value of T_g.

Thus it is seen that T_{w1} is a minimum wall temperature required for ignition of the gas mixture, that is, a critical condition of ignition or explosion. T_{w1} is referred to as the ignition or explosion temperature of the particular gas mixture and is a function of gas pressure and temperature and geometry of the containing vessel.

Semenoff obtained an analytical expression for the explosion temperature from the defining equations at T_{g2} (24), for T_{w1}:

$$(\dot{q}_{chem})\Big|_{T_g=T_{g2}} = (\dot{q}_{loss})\Big|_{T_g=T_{g2}} \qquad \text{(II-33)}$$

$$\left(\frac{\partial \dot{q}_{chem}}{\partial T_g}\right)\Big|_{T_g=T_{g2}} = \left(\frac{\partial \dot{q}_{loss}}{\partial T_g}\right)\Big|_{T_g=T_{g2}} \qquad \text{(II-34)}$$

[1] Semenoff actually considered three values of $\dot{q}_{chem}$ for three values of Z (that is, for three values of gas mixture pressure) (24).

The essential features of the non-stationary theory may also be represented conveniently in graphical form, as is shown in Fig. 2b. Since the defining equation for this theory is

$$\rho c_p \frac{dT_g}{dt} = \dot{q}_{chem} - \dot{q}_{loss} \qquad \text{(II-35)}$$

dT_g/dt is proportional to the difference between $\dot{q}_{chem}$ and $\dot{q}_{loss}$ and may be plotted versus T_g. According to the value of T_w, the temporal behavior of T_g is then obtained. It is seen from Fig. 2b that the non-stationary representation predicts the same trends as that of the stationary theory. In particular, explosion will occur for all values of T_g with $T_w=T_{w2}$ and for $T_g > T_{g2}$ with $T_w=T_{w1}$ (since dT_g/dt is positive). For $T_{g0} \leq T_g < T_{g3}$ with T_{w0}, a stationary state will be attained with $T_g=T_{g1}$. The significance of the $\dot{q}_{chem}$ and $\dot{q}_{loss}$ intersection at T_{g3}, with $T_w = T_{w0}$, will be discussed in a latter section.

In the following discussions of heterogeneous ignition it will be convenient to use similar graphical representations to study the physical situation of interest. Although the stationary approach will be emphasized, certain features of the non-stationary theory will be included.

2. Heterogeneous Ignition Involving Gas-Phase Reaction Products

The ignition of solid-phase fuels with gaseous oxidizers through reactions which form gaseous reaction products is discussed in this section. Examples of such heterogeneous systems are solid propellant fuel strands,

hydrocarbon droplets, or carbon particles reacting in air or oxygen. Much of the present discussion is based on the physical analysis of Frank-Kamenetskii (23).

Several features within a theory of heterogeneous ignition change from their counterparts in a theory of homogeneous ignition. For example, because the exothermic reaction occurs on a surface as opposed to throughout a reaction volume, the surface temperature T_s replaces the gas temperature T_g, and all heating terms are expressed in terms of unit area rather than unit volume.

Consider a spherical fuel particle whose central point temperature is 293°K. The particle is placed in a stagnant mixture of oxidizing and inert gases whose temperature at infinity is also 298°K. During reaction, reactant depletion is neglected. Reaction proceeds on the surface at temperature T_s, but, for the sake of simplicity, the gas-phase products are continuously removed as they appear at temperature T_s and are not allowed to participate in any heat transfer to the environment.

This case of no product heat transfer by means of mass transfer is of interest because in the generalization to metal ignition, which is characterized by a surface deposition of solid-phase products, such products cannot transport heat from the reacting surface to the environment.

In principle, two equations may be written for a thin control volume at uniform temperature T_s enclosing only the reacting surface; the first is the rate of heat input to the volume, which includes the chemical heat release rate, and the second is the rate of heat loss from the control volume to the environment (which includes the fuel volume interior to the reaction surface), where both equations are functions of the surface temperature, T_s. Both equations are cal-

culated at some specific time, say $t = t^*$,[2] and the entire control volume is assumed at uniform temperature equal to T_s.

The chemical energy release rate may be written as:

$$\dot{q}_{chem} = \dot{m} Q \qquad \text{(II-36)}$$

$$\dot{q}_{chem} = \dot{m} \left\{ \sum_{\substack{\text{reactants} \\ i}} n_i \Delta H_{i,T_s} - \sum_{\substack{\text{products} \\ j}} n_j \Delta H_{j,T_s} \right\} \qquad \text{(II-37)}$$

where:

$$\Delta H_{\ell,T_s} = \Delta H_{f,\ell}^{298} + (H_{T_s} - H_{298})_\ell \qquad [\ell \equiv i, j] \qquad \text{(II-38)}$$

where subscript i indicates reactants and j products, and where

$\dot{q}_{chem}$ = chemical energy release rate, cal/cm^{2}sec;

$\dot{m}$ = molar reaction rate, mole fuel/cm^{2}sec;

Q = chemical energy release, cal/mole fuel;

T_s = surface temperature, $^\circ$K;

n_k = number of moles of species k per mole of fuel, mole k/mole fuel;

---

[2] Although reaction depletion is not considered, in general the heat loss terms to be discussed below will be functions of time.

a) $\dot{q}_{chem}$ VS T_s

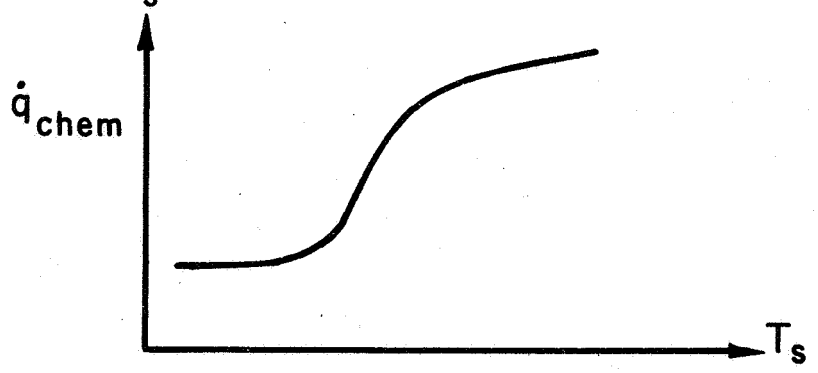

b) $\dot{q}_{loss}$ VS T_s

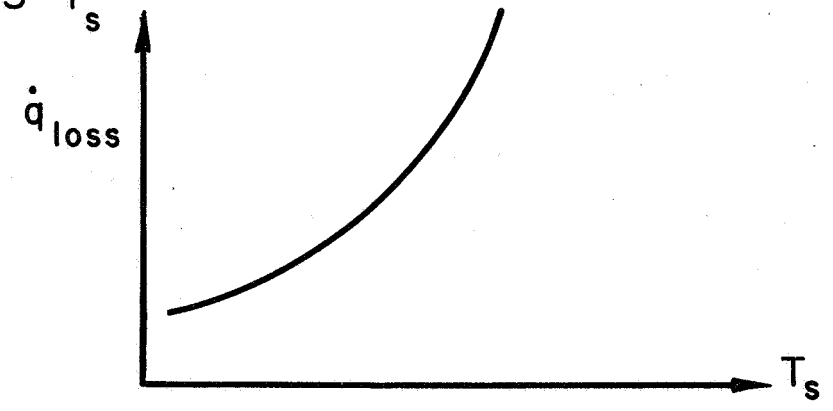

c) $\dot{q}_{chem}$ AND $\dot{q}_{loss}$ VS T_s

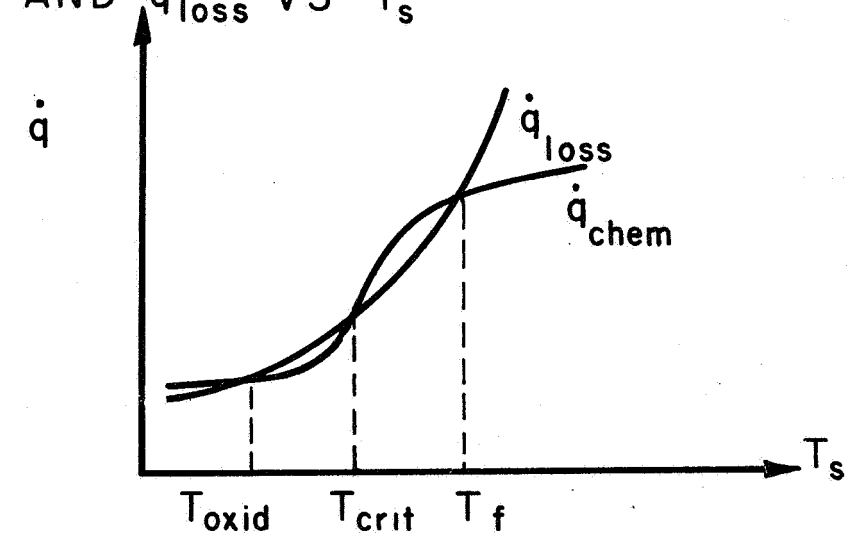

HETEROGENEOUS IGNITION:
RATE OF CHEMICAL ENERGY RELEASE AND RATE OF HEAT LOSS VS SURFACE TEMPERATURE

FIGURE 3

$\Delta H^{298}_{f,k}$ = standard heat of formation of species k at 298°K, cal/mole k;

$H_{T,k}$ = enthalpy of species k at T°K, cal/mole k.

The general form of $\dot{q}_{chem}$ versus T_s is displayed in Fig. 3a. At low temperatures, the dependence is exponential due to the controlling kinetic Arrhenius factor.[3] As the surface temperature of the particle is increased, diffusion of the oxidizer through the inert gas to the particle surface will become rate-controlling, and the $\dot{q}_{chem}$ curve will have a smaller, but still positive slope, as is shown in Fig. 3a.[4] A contribution to the lessening of the slope also results from dissociation of the products.[5]

In the diffusional regime, if it is assumed that all portions of the surface are equally accessible with respect to diffusion, then $\dot{m}$ may be written in the form (23):

$$\dot{m} = \beta(c - c') \qquad \text{(II-39)}$$

where c is the oxidizer concentration in the gas, c' is the oxidizer concentration at the surface (both in mole fuel/cm^3), and is the diffusion velocity coefficient

---

[3]Throughout these discussions it is assumed of course that T_s is less than the maximum temperature attainable from the reaction, $T_{max} = T_o + Q/(\bar{c}_p)$ (for Lewis Number equal to unity (271), where T_o is the initial reactant temperature and $(\bar{c}_p)$ is a specific heat averaged over products.

[4]Gas phase diffusion coefficients usually increase with the 1.67 power of temperature (25).

[5]Note that the S-shape of the $\dot{q}_{chem}$ curve occurs also in homogeneous gas-phase reactions, but that in this case the leveling at high temperature is due only to dissociation of the products.

(cm/sec), which Frank-Kamenetskii defines as follows(23):

$$\beta = Nu D/r \qquad \text{(II-40)}$$

In Eqn. (II-40), Nu is the diffusional Nusselt number, D is the diffusivity of the oxidizer (cm^2/sec), and r is the characteristic dimension of the system (cm). See Reference (272) for limitations of Eqn. (II-39).

Under the assumption that the reaction at the surface is first order with respect to oxidizer, in the kinetic regime at low surface temperature $\dot{m}$ may be expressed as:

$$\dot{m} = Kc^{r} \qquad \text{(II-41)}$$

where k is the rate constant (cm/sec) with an Arrhenius-type temperature dependence, as noted above:

$$K = Ae^{-E/RT_s} \qquad \text{(II-42)}$$

Here A is the pre-exponential factor (cm/sec), E is the activation energy (cal/mole), and R is the universal gas constant (cal/mole$^{\circ}$K).

For the entire temperature range of interest $\dot{m}$ may then be written as (23):

$$\dot{m} = \frac{K\beta}{K+\beta} c \qquad \text{(II-43)}$$

and thus Eqn. (II-37) becomes:

$$\dot{q}_{chem} = \frac{K\beta}{K+\beta} C \left\{ \sum_i n_i \Delta H_{i,T_s} - \sum_j n_j \Delta H_{j,T_s} \right\} \qquad \text{(II-44)}$$

As noted, the variation of $\dot{q}_{chem}$ with surface temperature has been denoted schematically in Fig. 3a: at low temperatures in the kinetic range, $k << \beta$, and the temperature dependence is exponential; at high temperatures in the diffusional range, $\beta << k$, and the temperature dependence is given predominantly by the diffusivity D in Eqn. (II-40).

When the geometry and heat transfer characteristics of the system have been given, it is possible in principle to calculate a heat loss term, $\dot{q}_{loss}$, including conduction into the fuel particle,[6] conduction into the static oxidizing gas, and radiation to the surroundings, at $t = t^*$, and as a function of the interface temperature. Recall that the products formed do not participate in the heat transfer.

$$\dot{q}_{loss} = K_f \left.\frac{\partial T}{\partial r}\right|_{r=r_{0-}} + K_g \left.\frac{\partial T}{\partial r}\right|_{r=r_{0+}} + \epsilon\sigma\left(T_s^4 - T_r^4\right) \qquad \text{(II-45)}$$

where

$\dot{q}_{loss}$ = rate of heat loss, cal/cm^{2}sec;

k = thermal conductivity of the fuel (subscript f) or oxidizer gas (g), cal/cm sec ^oK;

$\frac{\partial T}{\partial r}$ = temperature gradient evaluated at the surface

---

[6] Recall that the control volume includes only the reaction surface. The importance of this conduction loss term in metal ignition will be demonstrated in Section 4.

($r = r_0$) either into the fuel (r_{0-}) or into the oxidizer (r_{0+}), $^{o}K/cm$;

ϵ = surface emissivity, dimensionless;

σ = Stephan-Boltzmann constant, $cal/cm^2 sec (^{o}K)^4$;

T_r = effective radiation temperature of the environment, ^{o}K.

If any other form of heat input were of interest, such as ohmic heating, then the model would be much more complicated, since part of the this term would add to the right hand side of Eqn. (II-44) to obtain the total heat input rate. Also, because the interior of the fuel is not included in the control volume, and because the extra heating term may affect the temperature distribution within the fuel particle, the conduction loss into the fuel on the right hand side of Eqn. (II-45) must also be modified. For the purposes of the present discussion, only chemical heat input will be considered, so that Eqn. (II-44) and (II-45) are complete as they stand.

The general form of the $\dot{q}_{loss}$ versus T_s curve is shown in Fig. 3b.

Combining Fig. 3a and 3b (Fig. 3c), there will be in general three intersections which define equilibrium conditions for the surface. That which occurs at the lowest temperature is a stable equilibrium (with respect to small perturbations in surface temperature) since

$$\left(\frac{\partial \dot{q}_{chem}}{\partial T_s}\right)\Bigg|_{T_s=T_{oxid}} < \left(\frac{\partial \dot{q}_{loss}}{\partial T_s}\right)\Bigg|_{T_s=T_{oxid}} \qquad \text{(II-46)}$$

The temperature at which this intersection occurs is referred to as the oxidation temperature (T_{oxid}); the intersection has physical significance in that it represents ordinary low-temperature oxidation. Since the $\dot{q}_{chem}$ and $\dot{q}_{loss}$ curves may be nearly tangent at T_{oxid},

this single temperature may be more realistically represented by a temperature range.

The center intersection of the $\dot{q}_{chem}$ and $\dot{q}_{loss}$ curves is said to occur at the critical temperature (T_{crit}). Note that this equilibrium is unstable, since

$$\left(\frac{\partial \dot{q}_{chem}}{\partial T_s}\right)\Bigg|_{T_s=T_{crit}} > \left(\frac{\partial \dot{q}_{loss}}{\partial T_s}\right)\Bigg|_{T_s=T_{crit}} \qquad \text{(II-47)}$$

T_{crit} is the spontaneous ignition temperature, that is, it is the lowest initial temperature from which the surface may self-heat to a combustion configuration. However, to avoid confusion with the experimental ignition temperature which will be defined later, this temperature will always be referred to as the critical temperature.

The final intersection is again a stable equilibrium because

$$\left(\frac{\partial \dot{q}_{chem}}{\partial T_s}\right)\Bigg|_{T_s=T_f} < \left(\frac{\partial \dot{q}_{loss}}{\partial T_s}\right)\Bigg|_{T_s=T_f} \qquad \text{(II-48)}$$

This intersection represents the flame temperature (T_f) and physically, of course, is the steady-state, self-sustained combustion configuration.

By comparison of Fig. 2 and 3 it is seen that T_{crit} is equivalent to T_{g3} in the homogeneous ignition theory. In the development of the homogeneous theory, the independent variables of interest are the total pressure of the reacting gas mixture and the heat transfer to the environment as determined by the wall temperature and the size of the containing vessel. In this case it is convenient to consider an ignition limit (for T_{w1} in Fig. 2a) where the heating curves are tangent, rather than an ignition temperature T_{g3} (for T_{wO} in Fig. 2a), because the convenient experimental measurements then involve

the minimum explosion pressure (for fixed wall temperature and container size), and so forth. In other words, the behavior of the mixture as the gas temperature is raised by external means (for fixed wall temperature, container size, and gas pressure) is not of interest.

However, note that if the gas temperature is raised by external heating to T_{g3}, explosion will occur at T_{g3}, and thus this temperature is an ignition or explosion temperature.

In applications involving the ignition of metals, or of other heterogeneous systems, generally it is this type of configuration which is appropriate; that is, the behavior of the surface temperature of the fuel as it is raised by external means is of interest. If the experimental configuration is such that three intersections of the heating curves exist, as in Fig. 3c, then there will be a spontaneous ignition or critical temperature at and above which the surface will eventually self-heat to the stable combustion configuration at T_f.

With reference to Fig. 3c, it is possible to envision certain special cases in which only one intersection of the $\dot{q}_{chem}$ and $\dot{q}_{loss}$ curves occurs, and thus only steady-state oxidation or steady-state combustion is possible, or in which the curves are tangent (that is, the ignition or extinction limits (23), as in the homogeneous theory of thermal ignition). However, for the reasons given previously, only the more general case involving a triple intersection (and thus defining a critical temperature) is considered here.

Also, note that the $\dot{q}_{chem}$ and $\dot{q}_{loss}$ curves are similar for both the case of homogeneous gas-phase reactants, in which the flame temperature is determined by dissociation of the products (see Footnote 5 of this chapter), and the case of heterogeneous reactants, in which T_f

is controlled not only by dissociation of the products, but also by gas-phase diffusion of the reactants. The latter case can then be generalized to any non-premixed system, including gas-phase diffusion flames. Thus any chemical system involving thermal ignition may be described by curves of the general form shown in Fig. 3.

In defining an ignition temperature (T_{ign}), it is convenient to choose a definition which is directly related to that of the experimental ignition temperature, since comparison will be made with values of the latter. For systems which burn on the surface, the experimental definition of ignition is usually taken to be the point of most rapid rate of change with time of sample temperature or of light intensity emitted by the fuel sample; for metals which burn in the vapor phase, ignition is sometimes defined by the appearance of the vapor-phase flame.

Because the control volume has been assumed to be at uniform temperature, the rate of change of the temperature of the control volume T_s may be expressed as follows, as in the non-stationary homogeneous ignition theory:

$$\frac{m_{c.v.}\, c_p}{S} \frac{\partial T_s}{\partial t} = \dot{q}_{chem} - \dot{q}_{loss} \qquad \text{(II-49)}$$

where

$m_{c.v.}$ = mass of the control volume, g;
c_p = fuel specific heat, cal/g^{o}K;
S = sample surface area, cm^2.

If the volume of the control volume (V) is taken as

$$V = \delta S \tag{II-50}$$

where δ is the thickness of the control volume and

$$\delta \neq 0 \tag{II-51}$$

then Eqn. (II-49) may be written

$$\rho \delta c_p \frac{\partial T_s}{\partial t} = \dot{q}_{chem} - \dot{q}_{loss} \tag{II-52}$$

where ρ is the density of the fuel (g/cm^3). Thus, the experimental definition of ignition in terms of the $\dot{q}_{chem}$ and $\dot{q}_{loss}$ curves is the temperature at which the magnitude of $(\dot{q}_{chem} - \dot{q}_{loss})$ is greatest. The ignition temperature must be above the critical temperature, of course, because only above the latter temperature can the thermal non-equilibrium result in stable combustion at T_f. This definition of ignition is demonstrated graphically in Fig. 4.

Mathematically, the ignition temperature is defined by the equation:

$$\left[(\dot{q}_{chem})\Big|_{T_s = T_{ign}} - (\dot{q}_{loss})\Big|_{T_s = T_{ign}} \right] = \text{maximum} \tag{II-53}$$

Thus

$$\frac{\partial}{\partial T_s} (\dot{q}_{chem} - \dot{q}_{loss})\Big|_{T_s = T_{ign}} = 0 \tag{II-54}$$

or

$$\left(\frac{\partial \dot{q}_{chem}}{\partial T_s} \right)\Big|_{T_s = T_{ign}} = \left(\frac{\partial \dot{q}_{loss}}{\partial T_s} \right)\Big|_{T_s = T_{ign}} \tag{II-55}$$

a) STATIONARY APPROACH

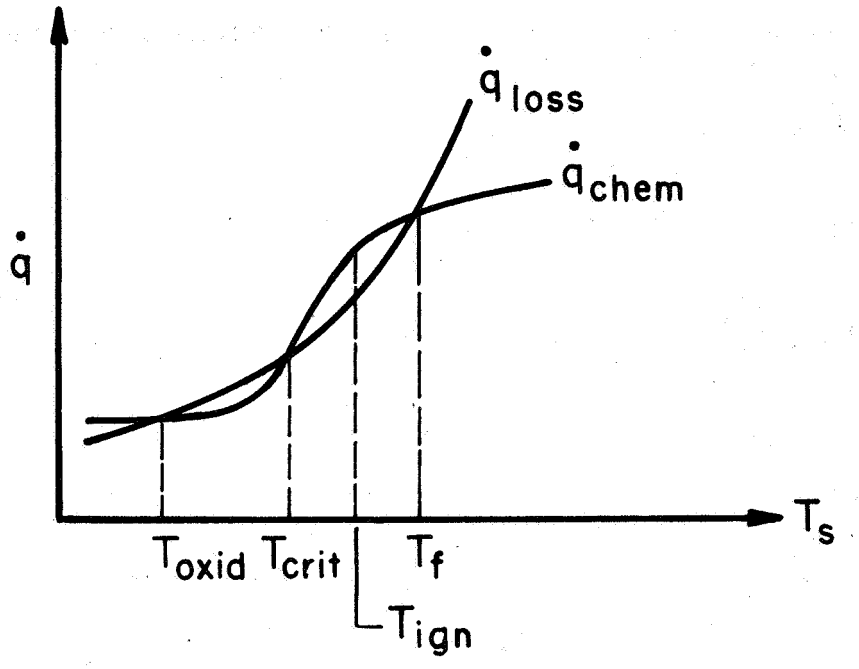

b) NON-STATIONARY APPROACH

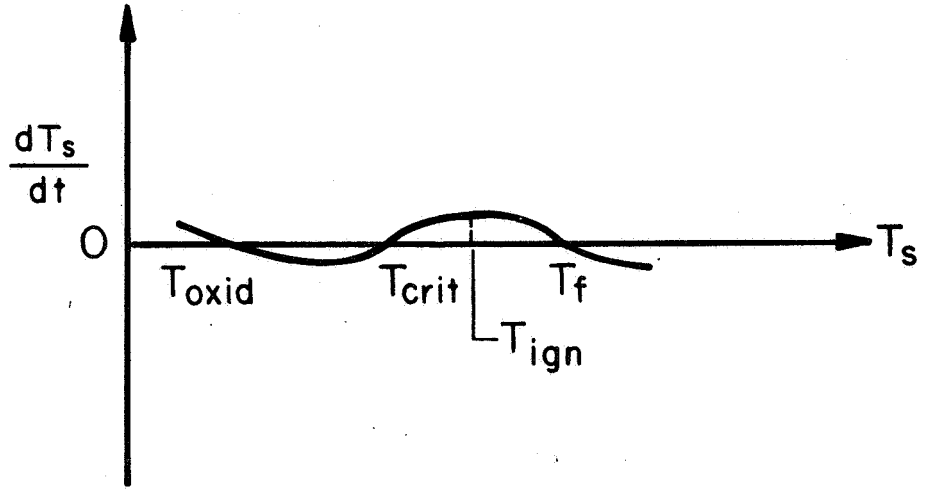

HETEROGENEOUS IGNITION:
THE DISTINCTION BETWEEN THE CRITICAL
AND IGNITION TEMPERATURES

FIGURE 4

Therefore, in terms of the $\dot{q}$ versus T_s diagram, the ignition temperature occurs at that point above the critical temperature at which the slopes, but not magnitudes, of $\dot{q}_{chem}$ and $\dot{q}_{loss}$ are equal.

Physically, the ignition temperature is the temperature at which immediate inflammation occurs, whereas the critical temperature is the spontaneous ignition temperature; thus an important distinction between these two temperatures is the possibility of an ignition delay time.[7]

It is obviously the ignition rather than the critical temperature which is of interest in rocket propulsion applications since a long self-heating period before ignition, upon attainment of the critical temperature, could be extremely detrimental to ignition efficiency.

Note that in defining the ignition temperature both experimentally and theoretically in terms of the maximum rate of change of surface temperature (or of light intensity emitted by the sample), a discrepancy between this definition of the model and the true experimental definition has been introduced, because experimentally the ignition temperature is the surface temperature just prior to rapid temperature runaway. In other words, rather than that surface temperature at which the time derivative of temperature is a maximum, the temperature immediately before fast temperature runaway is taken as the ignition temperature experimentally.

Also, since for the heterogeneous system the leveling of the S-shaped $\dot{q}_{chem}$ curve results from diffusional control of the reaction, the definition used in the model implies that at ignition diffusional processes have become important.

---

[7] In Section 4 of this chapter another important distinction between these two temperatures will be demonstrated.

In reality, however, the ignition temperature as defined experimentally can be kinetically controlled.[8]

In the following, this discrepancy between the experimental and theoretical definitions of ignition will be neglected. The latter definition is convenient because it presents a mathematical defining equation for ignition (Eqn. II-55), which will be used in subsequent chapters for comparison with other theories of metal ignition and for interpretation of various trends in experimental results.

At this point, at least in principle, T_{crit} and T_{ign} can be calculated for any fuel-oxidizer system from their defining equations

$$\left(\dot{q}_{chem}\right)\Big|_{T_s = T_{crit}} = \left(\dot{q}_{loss}\right)\Big|_{T_s = T_{crit}} \qquad \text{(II-56)}$$

and

$$\left(\frac{\partial \dot{q}_{chem}}{\partial T_s}\right)\Big|_{T_s = T_{ign}} = \left(\frac{\partial \dot{q}_{loss}}{\partial T_s}\right)\Big|_{T_s = T_{ign}} \qquad \text{(II-57)}$$

---

[8] See Chapter VII.

by a numerical iterative procedure. However, uncertainty in the numerical values of the parameters involved in Eqn. (II-44) and (II-45) as a function of temperature (especially for metal-oxidizer systems) and difficulty in evaluating the two conduction heat loss terms in Eqn. (II-45) make such a calculation of questionable value; thus it was not attempted.

To summarize, the classical stationary thermal ignition theory has been applied to the case of heterogeneous ignition involving reactants which form gaseous products. By consideration of the rate of heat generation and rate of heat loss from a control volume centered at the reaction surface, steady-state stable regimes of oxidation (at low temperatures) and combustion (at high temperatures) have been found. These are separated by the critical temperature, which is an unstable equilibrium with respect to perturbations in temperature.

A distinction has been made between this critical, or spontaneous ignition temperature, and the ignition temperature which is defined by the appearance of a flame in an experiment, to allow for the possibility of sample self-heating.

The next section of this chapter is a discussion of metal ignition, that is, heterogeneous systems involving the formation of solid-phase products on the reaction surface, in terms of the classical stationary theory of heterogeneous ignition.

3. Heterogeneous Ignition Involving Solid-Phase Reaction Products

a. The Stationary Theory

The geometry and assumptions of the previous section are maintained. Furthermore, those products which form on the reaction surface are included in the control volume and are assumed to be at uniform temperature equal

to the surface temperature, so that there is no effect of their presence on the heat transfer characteristics of the configuration (See however Reference (272)). As before, reactnat depletion is neglected. Thus the equations and concepts developed in Section 2 remain valid for the case of solid-phase product formation.

In general, as found at low temperatures in isothermal oxidation experiments, the presence of this product film leads to so-called protective oxidation rate laws (6, 26, 27), of the form:

$$\frac{dx}{dt} = \frac{K_n}{x^n} \qquad \text{(II-58)}$$

where

x = thickness of product film formed at time t, cm;
k_n = rate constant, $(cm)^{n+1}/sec$;
n = oxidation index, dimensionless.

Eqn. (II-58) integrates to Eqn. (II-59) or (II-60) for n = +1 or +2 respectively:

$$x^2 = 2K_1 t + C_1 \qquad \text{(II-59)}$$

$$x^3 = 3K_2 t + C_2 \qquad \text{(II-60)}$$

Another protective rate law is the logarithmic law:

$$x = K \ln t + C \qquad \text{(II-61)}$$

---

[9] Specific examples are discussed Appendix I.

where all c_n are constants. These rate laws are referred to as parabolic, cubic, or logarithmic, respectively (6,26, 27). See these references just cited for discussions of the microscopic derivations of these rate laws.

The non-protective rate law which is generally exhibited by metal-oxidizer systems at higher temperatures is obtained by integrating Eqn. (II-58) with n = 0:

$$x = K_0 t + c_0 \qquad \text{(II-62)}$$

This law is known as the linear rate law (6,26,27) and may result from a porous or cracked oxide film, since the rate is independent of oxide thickness.

Note that the linear oxidation rate law may be attributed to physical mechanisms other than a porous, non-protective reaction product film. For example, if there is a protective, non-porous barrier layer between an outer porous layer and the metal substrate, and if this barrier layer maintains a constant thickness with respect to time, then a linear oxidation rate will be observed for this system. Other physical mechanisms, such as rate-controlling phase boundary reactions, may also be responsible for the appearance of a linear oxidation rate law (6,26,27).

To summarize briefly, so-called protective oxidation rate laws are characterized by inhibition of the reaction rate by the product film; such rate laws are observed for metal-oxidizer systems at low temperatures. At higher temperatures, the non-protective linear rate law usually occurs; in this case the reaction rate is independent of the instantaneous product film thickness.

The temperature which separates these two rate regimes is defined as the transition temperature (T_{trans}). It is the lowest temperature at and above which the metal-oxidizer system exhibits a linear oxidation rate law at the start[10] of ordinary isothermal oxidation rate experiments and is estimated from the appropriate empirical metal oxidation literature.

The transition from a protective rate law to the linear rate law may be attributed to one of six different physical mechanisms:

(a) The volume of oxide formed may be less than the volume of metal used in its formation (that is, the volume ratio, or Pilling and Bedworth ratio (22), may be less than one);

(b) The oxide may melt or sublime thus exposing fresh metal surface;

(c) Mechanical stress cracking may result from expansion or contraction due to a phase change or crystallization in scale or substrate;

(d) Mechanical stress cracking may result from a chemical composition change in the film;

(e) Thermal stress cracking may result from large differences in coefficients of thermal expansion of metal and product film;

(f) Mechanical stress cracking may result from a Pilling and Bedworth ratio much greater or less than one, perhaps when some critical oxide thickness is attained.

It is seen immediately that in general mechanism (b) places an upper temperature limit on the transition temperature, although if the molten oxide were extremely

---

[10] There is generally a brief induction period at the beginning of an oxidation experiment before steady-state conditions are established (see Appendix I).

viscous, it is conceivable that the transition temperature could be higher than the oxide melting point.[11]

The effect of the transition temperature will be felt in the kinetic regime and, in particular, in the $\dot{m}$ term of Eqn. (II-36), that is, in the pre-exponential factor and activation energy of Eqn. (II-42). The presence of the protective product film will lower the reaction rate from the value expected for a clean surface; therefore, $\dot{q}_{chem}$ will decrease in the real case. When the transition temperature is attained, the chemical heat release term will approach its value for a clean surface.

The metal ignition criterion for the two possible cases $T_{trans} < T_{crit}$ and $T_{trans} > T_{crit}$ is indicated in Figure 5b and 5c according to the definitions given above. (The case with no solid-phase product formation is shown in Fig. 5a.). The dashed $\dot{q}_{chem}$ curves indicate the rate for a clean surface. The metal ignition criterion may be summarized mathematically:

$$\text{If } T_{trans} < T_{crit}, \text{ then } T_{ign} \geq T_{crit}. \qquad \text{(II-63)}$$

$$\text{If } T_{trans} > T_{crit}, \text{ then } T_{ign} \geq T_{trans}. \qquad \text{(II-64)}$$

The equal sign will apply in Eqn. (II-63) only at the ignition limit where $\dot{q}_{chem}$ and $\dot{q}_{loss}$ curves are tangent and in Eqn. (II-64) only if the magnitude of

---

[11] SiO_2 formed in the $Si-O_2$ reaction may be an example of this phenomenon. See Appendix I.

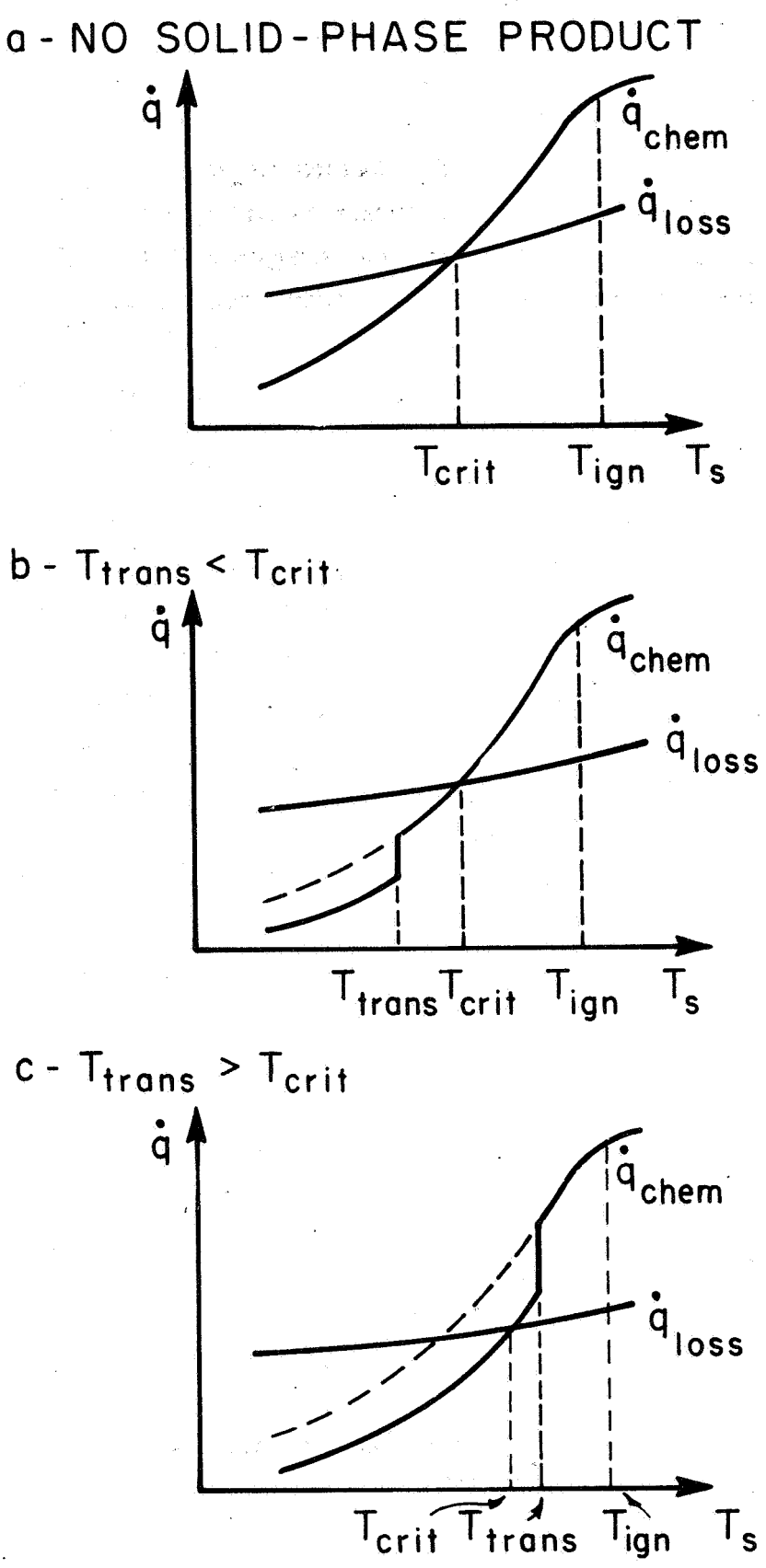

THE IGNITION CRITERION

FIGURE 5

$(\dot{q}_{chem} - \dot{q}_{loss})$ is largest at the transition temperature.

In Fig. 5c it is seen that the critical temperature is a function of oxide thickness, as the $\dot{q}_{chem}$ curve shifts to the left as a clean metal surface is approached. Thus in cases for which $T_{trans} > T_{crit}$, T_{crit} is expected to depend on the oxide thickness present on the metal sample.

According to Fig. 5b, for $T_{crit} > T_{trans}$, T_{crit} should not depend on this parameter. However, in the real physical situation, after T_{trans} is exceeded, the oxidation rate will not attain its value for a clean surface even if the oxide is non-protective, simply because such an oxide covers part of the metal surface (and the reaction rate per unit area is lower). Thus even in the case for which $T_{trans} < T_{crit}$, T_{crit} may be a function of oxide thickness.

Note that in estimating the transition temperature strictly on the basis of the observation of a linear oxidation rate law at that particular temperature, it is possible that the reaction product film is not truely non-protective, that is, is not porous or cracked. However, since nonetheless the reaction rate is not inhibited in time as a result of the thickening product film, the ignition criterion as depicted in Fig. 5 does not change.

Furthermore, it is necessary that the oxidation rate be linear at all higher temperatures between T_{trans} and T_{ign}. Two well-known examples of metals which exhibit linear rates at intermediate temperatures but protective rates at higher temperatures are Al and Be in O_2.[12] Al exhibits a linear rate in O_2 at 500°C (28) and a protective

[12] See Appendix I for a detailed discussion of the oxidation of these metals.

rate above 660°C (29). Likewise, the oxidation rate of Be in O_2 is linear between 700 and 750°C (30) but parabolic between 840 and 970°C (31). The correspondence between the ignition temperatures of these metals and the respective oxide melting points (18) suggests that the oxides are generally protective at higher temperatures until they melt, and indicates that caution must be exercised in estimating the transition temperature. Nevertheless, the proper value of the transition temperature is the lowest possible ignition temperature, according to the metal ignition criterion.

It must be pointed out that the transition temperature is generally estimated on the basis of isothermal oxidation experiments, whereas it is generally applied in non-isothermal situations, such as for particles in a rocket motor, for wires subjected to a linearly increasing potential difference across their length, and so forth. Unfortunately, very few non-isothermal oxidation rate experiments have been conducted, and any effect is presently unclear. The specific examples which are available will be presented and discussed in Chapter III.

To summarize, a transition temperature has been introduced which delineates regimes of time-dependent and time-independent reaction rates for metal-oxidizer systems. It is postulated that above this temperature metal ignition occurs exactly as for other heterogeneous systems, and that in general, ignition, as defined by appearance of a flame, will not occur until this temperature is exceeded.

In the next section of this chapter, a simplified temporal dependence is included within the stationary ignition theory which has been used up to this point, in order to examine the validity of the concepts generated by the latter.

b. The Temporal Extension

As before, it is assumed that any thickness of solid-phase products formed on the metal surface during the pre-ignition reactions is at uniform temperature equal to the metal surface temperature. Thus the products of reaction are assumed not to participate in heat transfer to the environment.

Furthermore, to simplify the discussion, it is required that several properties are constant in time; specifically, the effective radiation temperature of the environment, T_r, the emissivity of the reacting surface, the oxidizer temperature at infinity, $T_{ox,\infty}$, and the oxidizer concentration at the fuel particle surface, $C_{ox}(g/cm^3)$, are constant. Holding this concentration constant is equivalent to assuming that the chemical reaction proceeding at the fuel surface has a constant oxidizer requirement in time, which may not be strictly valid. Nevertheless, this assumption is made to clarify the discussion.

Conceptually, for the thin control volume centered around the metal surface, the rate of heat generation at the surface by chemical reaction and the rate of heat loss from the control volume will be examined for a fixed surface temperature as a function of time.

$\dot{q}_{loss}$ consists of three terms: the conduction loss into the metal, $\dot{q}_{cond,f}$; the conduction loss into the ambient gas, $\dot{q}_{cond,g}$; and the radiation loss to the environment, $\dot{q}_r$:

$$\dot{q}_{loss} = \dot{q}_{cond,f} + \dot{q}_{cond,g} + \dot{q}_r \qquad \text{(II-65)}$$

Eqn. (II-45) expresses each of these terms explicitly, and is repeated here for convenience:

$$\dot{q}_{loss} = K_f \left.\frac{\partial T}{\partial r}\right|_{r=r_{o-}} + K_g \left.\frac{\partial T}{\partial r}\right|_{r=r_{o+}} + \epsilon\sigma(T_s^4 - T_r^4) \quad \text{(II-45)}$$

Because T_s and T_r are constant, and because the emissivity of the surface has been assumed constant, $\dot{q}_r$ is independent of time.

Furthermore, because the thermal conductivity of the gas is much less than that of the metal, and because $T_{ox,\infty}$ and T_s are constant, $\dot{q}_{cond,g}$ can also be considered independent of time. Thus any variation of $\dot{q}_{loss}$ with time is due only to $\dot{q}_{cond,f}(t)$.

For a thermally conducting medium at uniform internal temperature at t = 0, with constant surface temperature T_s imposed upon the surface at t = 0+, the temperature gradient at the surface, and thus $\dot{q}_{cond,f}$ decay exponentially with time (32). Because of this exponential time dependence, $\dot{q}_{loss}$ at a given T_s will converge to a limiting value in time. When $\dot{q}_{loss}$ is examined for other values of T_s a similar temporal behavior will be encountered. Thus it is possible to draw a family of curves of $\dot{q}_{loss}$ (T_s, t^*) for the various t* considered above. This behavior is demonstrated in Fig. 6a.

Note that if the properties at infinity were not held constant, then as time approached infinity the problem would approach an adiabatic configuration, as the temperature everywhere would approach T_s. Since any system involving an exothermic chemical reaction will always self-heat (and in this case ignite) in an adiabatic situation, this particular case is not of physical interest.

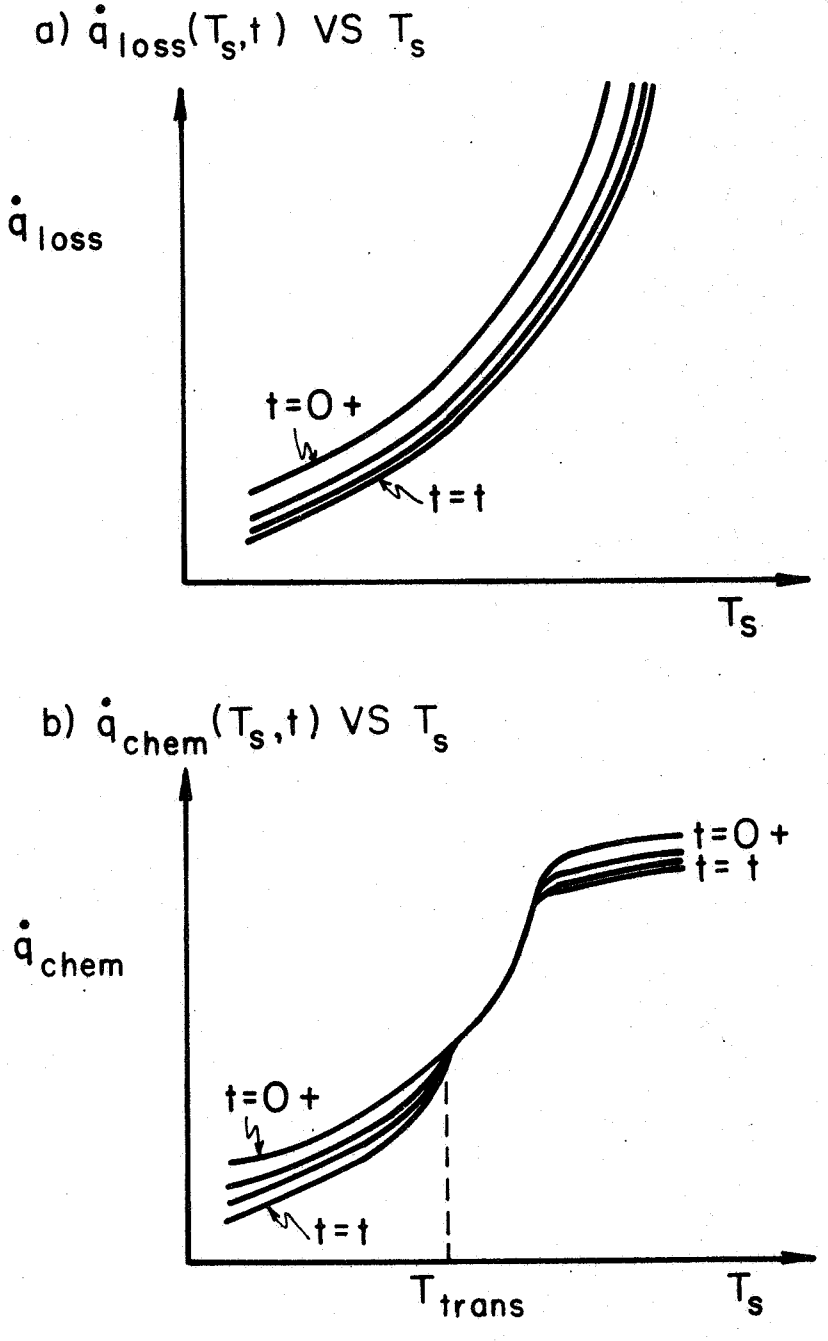

$\dot{q}_{chem}$ AND $\dot{q}_{loss}$ AS FUNCTIONS OF SURFACE TEMPERATURE AND TIME

FIGURE 6

In discussing the behavior of the $\dot{q}_{chem}$ curve, one must distinguish between the regimes controlled by chemical kinetics and by gas-phase diffusion, as has been shown in the earlier portions of this chapter. Furthermore, in the case of metal ignition, in the kinetic regime one must distinguish between the low-temperature protective and high-temperature non-protective oxidation rates, which are separated by the transition temperature. Although it is assumed here that the reactants are in large enough supply such that consumption of the reactants may be neglected, the parabolic rate law to be discussed below could be construed as a reactant depletion with a time independent reaction rate.

From Eqn. (II-36):

$$\dot{q}_{chem} = \dot{m}Q \qquad \text{(II-36)}$$

For purposes of this discussion, the parabolic rate law, Eqn. (II-59), is chosen to represent the low-temperature protective rate and is rewritten in slightly different form:

$$(\Delta m)^2 = K_p t + c \qquad \text{(II-66)}$$

where

Δm = amount of metal consumed at time t per unit area, g/cm^2;

k_p = parabolic rate constant, g^2/cm^4 sec;

c = integration constant, g^2/cm^4.

Therefore,

$$\dot{m} = \frac{d\Delta m}{dt} = \frac{K_p}{2\Delta m} = \frac{1}{2}\sqrt{\frac{K_p}{t}} \qquad \text{(II-67)}$$

and, at low temperatures, $\dot{q}_{chem}$ is inversely proportional to the square root of time. As has been discussed, in the kinetic regime the temperature dependence is given by the Arrhenius-type behavior of k_p and the weak temperature dependence of Q.

Above the transition temperature, metal-oxidizer systems exhibit the non-protective linear oxidation rate. Rewriting Eqn. (II-62):

$$\Delta m = K_l t + c' \qquad \text{(II-68)}$$

where k_l is the linear rate constant in $g/cm^2 sec$ and c' is an integration constant in g/cm^2. Thus in this case:

$$\dot{m} = K_l \qquad \text{(II-69)}$$

and $\dot{q}_{chem}$ is independent of time. Again, the temperature dependence is given by the exponential behavior of k_l and the slight dependence of Q.

At higher temperatures, gas-phase diffusion of the oxidizer to the surface (and in the case of volatile metals such as Mg and Ca, perhaps gas-phase diffusion of the metal vapor to a reaction zone above the metal surface)

becomes rate-controlling, and the temperature dependence of $\dot{q}_{chem}$ is given predominantly by that of the appropriate diffusion coefficient, which is usually proportional to the 1.67 power of temperature (25). Dissociation of the products also enters through Q. Thus at higher temperatures, the $\dot{q}_{chem}$ curves will exhibit a lesser slope with respect to surface temperature.

The temporal dependence of $\dot{q}_{chem}$ in the diffusionally controlled regime at high temperatures may be examined as follows: upon insertion of the metal particle at t = 0+, the oxidizer concentration gradient at the surface will be infinite and will decay exponentially in time to some limiting value, in strict analogy with the heat conduction into the interior of the metal. (Recall that the oxidizer concentration at the particle surface is held constant.)

The behavior of the $\dot{q}_{chem}$ curve with surface temperature and time is shown in Fig. 6b. In the exponential, kinetic regime below the transition temperature, $\dot{q}_{chem}$ is inversely proportional to the square root of time, due to the parabolic oxidation rate. Above the transition temperature, because of the linear oxidation rate law, $\dot{q}_{chem}$ is independent of time. At still higher temperatures where diffusion of the oxidizer becomes rate-controlling, the exponential decay of the oxidizer gradient at the surface yields a similar behavior for $\dot{q}_{chem}$.

When the $\dot{q}_{chem}$ and $\dot{q}_{loss}$ curves are combined as in the classical stationary thermal ignition theory, in those cases in which an ignition temperature exists there will be three intersections of the curves, which will occur at the oxidation temperature, the critical temperature, and the flame temperature. The possible combinations of the curves are shown in Fig. 7. Note that only two of the time family of curves are shown, in order to simplify the graphs. Fig. 7a and 7b from the

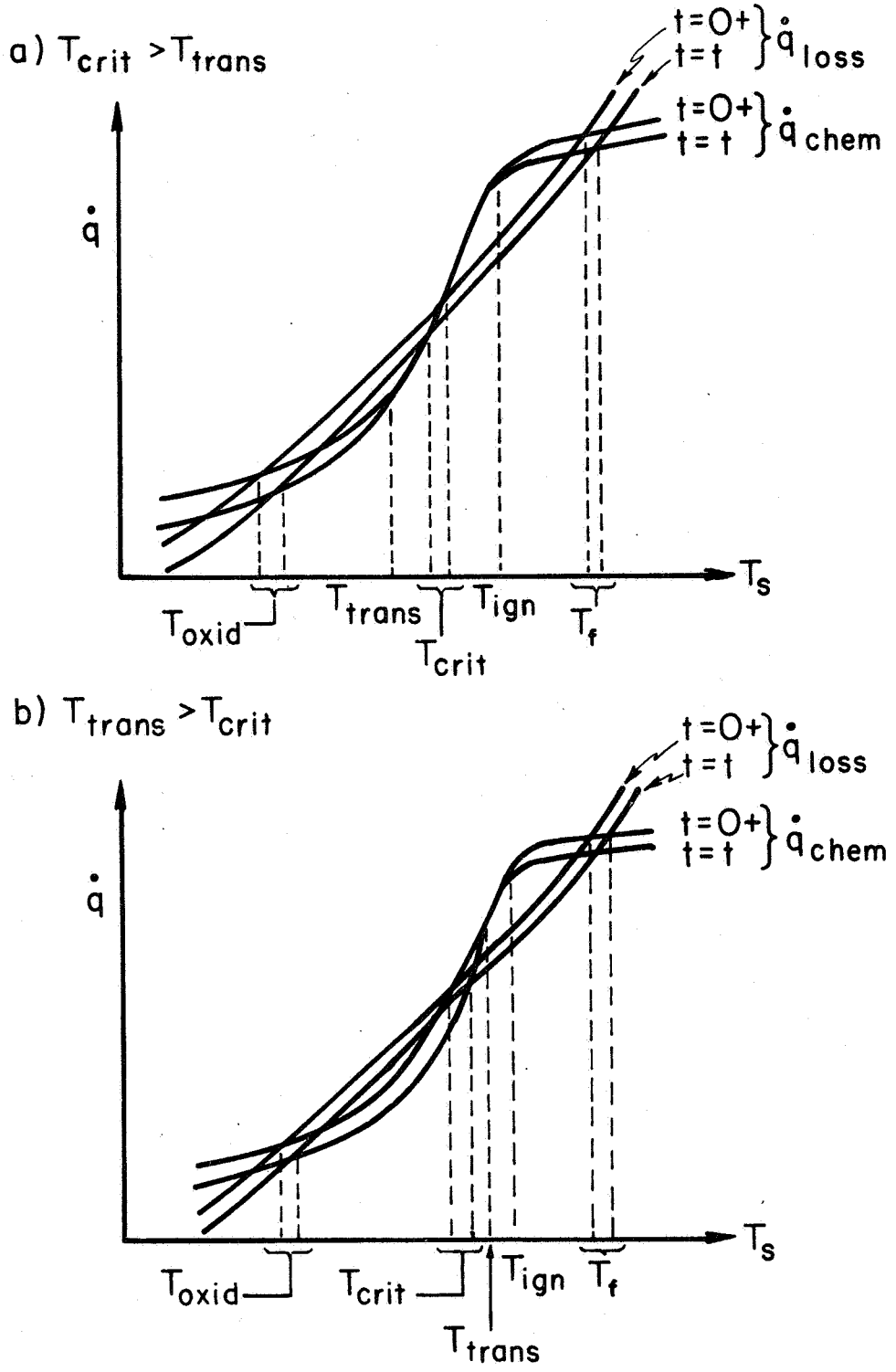

$\dot{q}_{chem}$ AND $\dot{q}_{loss}$ AS FUNCTIONS OF SURFACE TEMPERATURE AND TIME: THE COMBINED CURVES

FIGURE 7

temporal extension, are to be compared with Fig. 5b and 5c, from the stationary theory.

The important point to note is that since in the temporal extension the relative intersections of the curves remain the same in time, the stability of the system with respect to changes in surface temperature, and thus the conceptual definitions of T_{oxid}, T_{crit}, and T_f, based on the stability criterion, do not change.

Furthermore, for an initial surface temperature ($T_{s,0}$) not equal to one of these three "stable" values, the temporal variation of the surface temperature is as follows:

$T_{s,0} < T_{oxid,0}$, then $T_s \longrightarrow T_{oxid,t}$;

$T_{oxid,0} < T_{s,0} < T_{crit,0}$, then $T_s \longrightarrow T_{oxid,t}$;

$T_{crit,0} < T_{s,0} < T_{f,0}$, then $T_s \longrightarrow T_{f,t}$;

$T_{s,0} > T_{f,0}$, then $T_s \longrightarrow T_{f,t}$,

where subscript 0 represents initial conditions, and subscript t represents conditions approaching the time limit. These values are indicated by the brackets on the temperature axes in Fig. 7. Note that these trends predicted for the temporal behavior of surface temperature by the temporal extension of the stationary theory are exactly those predicted by the simple stationary theory.

In conclusion, it is seen that the general concepts of oxidation, critical, and flame temperatures, originating in the classical stationary thermal ignition theory, can be retained without modification in an extension of the thermal theory including time dependence. The com-

plicating factor, unique to metal ignition, of time-dependent reaction rates below the transition temperature in the kinetically controlled regime may also be included, and the metal ignition criterion, that the ignition temperature be greater than the larger of the transition and critical temperatures, is not affected by the temporal extension.

In the final two sections of this chapter, two important applied aspects of metal ignition are discussed in view of the ignition criterion. These topics are metal pyrophoricity and augmented metal ignition efficiency, respectively.

4. Metal Pyrophoricity

Pyrophoricity is the property of small metal particles to self-heat to ignition when exposed to an oxidizer at room temperature. Probably the best known example of pyrophoricity is the ignition of iron filings dispersed in air, although the cigarette lighter flint makes use of essentially the same phenomenon. It is presently a problem of great practical interest to the Atomic Energy Commission, because uranium and zirconium particles are pyrophoric and have been responsible for many explosions in factories (33).

In approaching the problem of metal pyrophoricity, the influence of sample volume on the transition, critical, and ignition temperature must be examined. It is postulated that the transition temperature will remain constant as the volume of the fuel sample is changed (see Chapter III). However, the critical temperature will not remain constant.

Inspection of Eqn. (II-44) and (II-45) reveals only two possible functions of sample volume in the kinetic regime (that is, $k << \beta$), the two conduction heat loss terms in Eqn. (II-45). Because the thermal conductivity of the metal greatly exceeds that of the oxidizing gas,

only conduction into the interior of the particle will be considered here.

The dependence of this conduction loss term on sample volume may be evaluated by consideration of a simpler, but related problem. Consider a sphere of radius r_0 initially at temperature $T_0 = 0$ except at $r = r_0$, where the temperature is T_s which is constant in time. The solution of the non-steady Fourier heat conduction equation for this system is (32):

$$T = T_s + \frac{2r_0 T_s}{\pi r} \sum_{n=1}^{\infty} \frac{(-1)^n}{n} \sin\left(\frac{n\pi r}{r_0}\right) \exp\left\{-\alpha n^2 \pi^2 t / r_0^2\right\} \quad \text{(II-70)}$$

where all symbols have their previous meanings and where

n = summation variable taking all integral values between 1 and ∞, dimensionless;

α = fuel thermal diffusivity, cm^2/sec.

Since the series (II-70) is uniformly convergent for $t > 0$ and $0 \leq r \leq r_0$, it may be differentiated term by term and multiplied by the thermal conductivity of the fuel to obtain the conduction heat loss term:

$$\dot{q}_{cond}(r,t) = K_f \frac{\partial T}{\partial r} \quad \text{(II-71)}$$

$$\dot{q}_{cond}(r,t) = \frac{2r_0 K_f T_s}{\pi r} \sum_{n=1}^{\infty} \frac{(-1)^n}{n} \left[\frac{n\pi}{r_0} \cos\left(\frac{n\pi r}{r_0}\right) - \frac{1}{r} \sin\left(\frac{n\pi r}{r_0}\right)\right] \exp\left\{-\alpha n^2 \pi^2 t / r_0^2\right\} \quad \text{(II-72)}$$

Evaluating $\dot{q}_{cond}(r,t)$ at the particle surface:

$$\dot{q}_{cond}(r_{0-},t) \equiv \dot{q}_{cond,f} \tag{II-73}$$

$$\dot{q}_{cond,f} = \frac{2K_f T_s}{r_0} \sum_{n=1}^{\infty} \exp\{-\alpha n^2 \pi^2 t / r_0^2\} \tag{II-74}$$

in the limit as $r \rightarrow r_0$.

If then

$$\frac{\partial \dot{q}_{cond,f}}{\partial r_0} > 0 \tag{II-75}$$

it is apparent that a small decrease in r_0 (or the sample volume) will decrease the conduction heat loss term accordingly. Thus the critical intersection of the $\dot{q}_{chem}$ and $\dot{q}_{loss}$ curves will move toward lower temperatures as the volume of the sample is decreased, and

$$\frac{\partial T_{crit}}{\partial r_0} > 0 \tag{II-76}$$

that is, the critical temperature of the system will decrease as the radius (or volume) of the sample is decreased.

From Eqn. (II-74):

$$\frac{\partial \dot{q}_{cond,f}}{\partial r_0} = 2K_f T_s \sum_{n=1}^{\infty} \exp\{-\alpha n^2 \pi^2 t / r_0^2\} \left[-\frac{1}{r_0^2} + \frac{2\alpha n^2 \pi^2 t}{r_0^4} \right] \tag{II-77}$$

Since the term outside the brackets on the right hand side of Eqn. (II-77) is positive, the criterion for Eqn. (II-75) and (II-76) becomes

$$\sum_{n=1}^{\infty} \frac{2\alpha n^2 \pi^2 t}{r_0^2} > 1 \qquad \text{(II-78)}$$

or

$$\frac{2\alpha \pi^2 t}{r_0^2} > \frac{1}{\sum_{n=1}^{\infty} n^2} = 0 \qquad \text{(II-79)}$$

Since the property of uniform convergence applies only for $t > 0$, the criterion (II-76) is satisfied for all finite values of r_0.

The same conclusion can be reached on purely physical grounds. Taking as the appropriate size index the surface area-volume ratio (S/V) which indicates the approximate magnitudes of the total chemical heat release and total heat capacity of the fuel particle, the effect of heat loss will decrease with increasing S/V (smaller systems). Thus the critical temperature will decrease with decreasing particle size. Note that the transition temperature still must be exceeded before ignition can occur and that as the sample size is decreased ignition may shift from that depicted in Fig. 5b ($T_{crit} > T_{trans}$) to that in Fig. 5c ($T_{crit} < T_{trans}$).[13]

After the volume of the sample exceeds a certain value, as far as events on the particle surface are

[13] This is the second distinction between the critical and ignition temperatures mentioned in Footnote 6 of the present chapter.

concerned, the volume is essentially infinite. At and above this critical size the critical temperature becomes relatively independent of size; such samples are said to be in the bulk configuration.

The size dependence of the ignition temperature may also be examined: the defining equation for ignition is Eqn. (II-55):

$$\left(\frac{\partial \dot{q}_{chem}}{\partial T_s}\right)\Bigg|_{T_s=T_{ign}} = \left(\frac{\partial \dot{q}_{loss}}{\partial T_s}\right)\Bigg|_{T_s=T_{ign}} \qquad \text{(II-55)}$$

Again it is assumed that the conduction heat loss into the fuel particle is the most strongly dependent on sample size, and therefore the criterion for a decrease in ignition temperature with decreasing particle size is Eqn.(II-80), which is to be compared with Eqn. (II-76):

$$\frac{\partial}{\partial r_0}\left(\frac{\partial \dot{q}_{cond,f}}{\partial T_s}\right) > 0 \qquad \text{(II-80)}$$

Eqn. (II-77) then becomes:

$$\frac{\partial}{\partial r_0}\left(\frac{\partial \dot{q}_{cond,f}}{\partial T_s}\right) = 2K_f \sum_{n=1}^{\infty} \exp\left\{-\alpha n^2 \pi^2 t / r_0^2\right\}\left[-\frac{1}{r_0^2} + \frac{2\alpha n^2 \pi^2 t}{r_0^4}\right] \qquad \text{(II-81)}$$

and the criterion (II-79) is unchanged.

Recall, however, that the transition temperature is postulated to be independent of sample size. Thus the ignition temperature dependence discussed above applies

only to cases in which the bulk ignition is controlled by the critical temperature, that is, the critical and ignition temperatures will decrease with decreasing particle size until they are approximately equal to the transition temperature. The critical temperature will continue to decrease, but the ignition temperature will remain equal to the transition temperature, that is, will be independent of sample size.

Thus for metals whose bulk ignition is controlled by the critical temperature, the ignition temperature is expected to demonstrate the following size dependence: in the bulk regime for large samples in which the critical temperature is relatively independent of size, the ignition temperature will also be relatively independent of size; in an intermediate size regime, the critical and ignition temperatures will decrease with decreasing sample size until the latter is approximately equal to the transition temperature; upon further reduction in sample size, the ignition temperature will remain constant and equal to the transition temperature. However, it must be noted that in experimental environments such that the metal sample is heated uniformly, no size dependence of either the critical or ignition temperatures will be found if the assumption is correct that the conduction heat loss into the metal is the source of the size effect.

Results of the literature survey on the size effect in metal ignition will be given in Chapter IV of this report. Attempts to measure the critical and ignition temperatures versus S/V will be discussed in Chapter VII.

In summary, it has been shown that the critical temperature of a given metal-oxidizer system decreases with decreasing system size. In other words, a small particle may self-heat to the transition temperature and thus ignition, whereas a larger sample will not. Note

that for the purposes of the discussion of metal pyrophoricity no assumption has been made concerning the initial condition of the metal particle when it is exposed to the oxidizer, that is, it is not necessary that the surface be free of oxide initially. As long as $\dot{m}$ in Eqn. (II-36) is non-zero, the possibility of eventual ignition exists.

5. Augmented Ignition Efficiency for Metals

Since the critical temperature of a given metal-oxidizer system decreases as the metal sample volume is decreased, the transition temperature will eventually become the controlling factor in metal ignition. For some metals (for example, Mg and Ca [14]) which have low transition temperatures in oxygen, inefficient ignition would not be expected, but with other metals such as Al and Be with high transition temperatures,[14] difficulties have been encountered in metal combustion applications such as chemical rocket systems.

Lowering the transition temperature is equivalent to destroying the protective quality of the product film at a low temperature, or eliminating its formation entirely. An excellent example of the former technique is the amalgamation of Al, and this metal so treated exhibits lower ignition temperatures than that with the ordinary thermal oxide film present (17,18).

The latter technique is exemplified by coating clean Al with Mg or Ca. Assuming that alloying does not occur, it would be hoped that the coating metal would react preferentially during the pre-ignition time, and that its ignition would be controlled by its low transition temperature. After the coating metal had ignited, the clean Al

[14] See Appendix I.

(or Be) substrate would ignite and burn during the subsequent temperature rise without the limitations imposed by its high transition temperature.

In the following chapter, estimations of transition temperatures of several metals are listed and discussed. These estimates are reviewed in detail in Appendix I with the help of the metal oxidation literature.

CHAPTER III - ESTIMATES OF TRANSITION TEMPERATURES

Inhibition of heterogeneous metal-gas reactions occurs as the reaction progresses because of build-up of the product on the reaction surface. At low temperatures this product film impedes the reaction, as it presents a physical barrier between the reactants. Some of the pertinent empirical metal oxidation literature is reviewed in Appendix I in order to estimate the transition temperature at which the product film becomes non-protective, as defined in Chapter II. The metals which are discussed are Mg, Li, Ca, Al, Be, U, Zr, Ti, Ta, Mo, and Si. In those cases for which literature is available, the oxidizing gases of interest will include O_2, N_2, air, CO_2, and H_2O.

These particular metals were chosen for study for the following reasons: Mg, Al, and Be are of interest in chemical propulsion applications, and the latter two are noted for their ignition difficulties; Li and Ca are studied and compared with Mg in order to extend the metal ignition criterion to the alkali and alkaline earth metals; and U and Zr are known to be pyrophoric, as was mentioned in Chapter II.

Some metals were selected because of certain properties of the metal or oxide. During its low-temperature oxidation, U forms two oxides, UO_2 and U_3O_8. Gases are highly soluble in Zr and Ti at low temperatures. Ta and Mo are refractory metals which are of interest in high-temperature structural applications, and the latter forms the volatile oxide MoO_3. Finally, the semi-conductor Si forms a glassy oxide.

All of the above material forms the basis for a critique of the transition temperature given in this chapter. This critique includes a discussion of

sample size and surface preparation effects on the transition temperature, as well as a review of non-isothermal oxidation experiments. All of these effects could be significant in applications of the transition temperature in design situations:

The reader interested in the details of the literature survey should refer directly to Appendix I.

1. A Critique of the Transition Temperatures

For convenience, those transition temperatures estimated in Appendix I are listed in Table 13.[1] The appropriate pressure range and the postulated mechanism causing the transition to the linear oxidation rate are given. Where one or two primary references have been used as the source of the data they are also listed.

Although the definition of a transition temperature and its connection with metal ignition is original to the present investigation, it should be noted that other authors have recognized that metals which form non-protective oxides will have characteristically low ignition

---

[1] Tables 2 through 12 and Ref. (34) through (193) may be found in Appendix I.

temperatures. For example, Dean and Thompson (194) stated that "those metals which form a non-porous oxide film which adheres tightly to the base metal are immune to further oxidation. Ignition of the metal will not normally occur unless this protective film is broken. . . However, if the oxide film is porous, or does not adhere to the base metal, oxidation will occur. This results in destruction of the metal through complete conversion to the oxide form. Ignition occurs more readily for metals forming such films."

Nor is the present investigation the first to join linear oxidation rates (which may or may not indicate a non-protective oxide film) with metal ignition. When reviewing the literature on the oxidation of U, it was learned that Loriers (73,78,195) had discussed the relationship between the linear oxidation of U and Ce and their ignition.

Furthermore, Grosse and Conway (196) remarked "it is not clear if there is any correlation between this transformation temperature (from parabolic to linear oxidation) and the ignition temperature. . . Perhaps this transition must take place before ignition, although such a statement lacks experimental verification."

One of the more important contributions of the present investigation is the combination of the transition temperature, which relies on the field of metal oxidation for its estimation, with the classical theory of thermal ignition for heterogeneous reactant systems, which was developed within the fields of physical chemistry and combustion. Although the resulting model is too cumbersome for calculation (even if the necessary data were available), certain trends are predicted which explain clearly some discrepancies found in the metal ignition literature.[2]

[2]For a discussion of this literature, both experimental and theoretical, see Appendix II.

TABLE 13.

ESTIMATED TRANSITION TEMPERATURES

System	Estimated T_{trans}, °C	Pressure Range	Physical Mechanism	Primary Reference
Mg-O_2	475	2-200 torr	(f) or (c)	(35)
	400	2.64 atm	(f) or (c)	(28, 34)
Mg-N_2	300	20-200 torr	---	(41)
Mg-air	450	---	(f)	(44)
Mg-CO_2	≥500	1 atm	---	(42)
	≥550	15 atm	---	(42, 45)
Mg-H_2O	≤425	31-208 torr	(f)	(46, 47)
Li-H_2O	≤25	2.5-12.6 torr	(f)	(53)
Ca-O_2	400	100-760 torr	(f)	(56)
Al-O_2	2030	---	(b)	---
Be-O_2	2530	---	(b)	---
U-O_2	150	20-800 torr	(d) or (f)	---
U-air	150	200 torr	---	(74)
Zr-O_2	925 ± 100	1-211 torr	(c), (e), or (f)	(100, 105)
Zr-air	925 ± 100	---	(c) or (e)	---
Ti-O_2	900	10^{-3}-760 torr	(f)	---
Ta-O_2	500	10 torr-40 atm	(f)	(156)
Ta-air	800	1 atm	(f)	(157)
Mo-O_2	600	76 torr	(f) or (b)	(177)
	725	1 atm	(f) or (b)	(178)
Mo-air	595	1 atm	---	(183)
Si-O_2	>1400, ≤1610	1 atm	(b)?	(191)
Si-H_2O	<500	25-400 atm	---	(193)

Upon examination of Table 13, it is noted immediately that mechanism (a), as discussed in Chapter II, is not a contributing factor to the breakdown of the oxide film in any of the cases considered. Recall that mechanism (a) states that for a Pilling and Bedworth ratio less than one, the oxide film will be non-protective at any temperature. This mechanism is essentially the basis of the statement of Dean and Thompson (194) which was quoted above. Thus for metals such as Mg and Ca, whose oxides have Pilling and Bedworth ratios which are less than one (0.81 and 0.64, respectively, (6)), one might expect ignition to be possible at any temperature.

It is shown in Appendix I, however, that the transition temperatures of these two metals in O_2 are on the order of 400°C; the transitions apparently result from mechanical stress cracking at a critical oxide thickness. That mechanism (a) is not an important factor in cases such as these (that is, for metals with Pilling and Bedworth ratios less than one) is not a surprising result: for thin oxide films, a uniform covering of the metal substrate would be expected; this covering would assume the microscopic geometry of the metal surface. Only when some critical thickness of oxide is attained would the stresses within the oxide become sufficient to stretch the oxide to the point at which some breakdown would occur. This process is in fact mechanism (f) mechanical stress cracking.

Thus another contribution of the present investigation to the area of metal ignition is the recognition that a simple criterion for the protective ability of the oxide film based solely on the Pilling and Bedworth ratio is invalid and that rather the concept that the film's protective ability varies with temperature must

be applied to the problem if quantitative predictions are to be made.[3]

In the final portions of this chapter, the effect of sample purity, sample size, and sample pretreatment on the transition temperature will be discussed. Finally, where available, the results of non-isothermal experiments will be compared with those of the more common isothermal experiments.

a. The Effect of Sample Purity and Sample Size

As might be expected, sample purity has a relatively important influence on the reaction rate. In the case of Al in O_2 in the temperature range 400-550°C, the rate constant, but not the rate law was found to depend on sample purity (61), but in other cases the effect was more pronounced. For example, for Zr in O_2 a cubic oxidation rate was observed for high purity Zr in the temperature range 700-900°C, and the law approached a quartic dependence for less pure samples (103).

For Ti in O_2 over a wide pressure range, at 1000°C a linear rate was observed for the reaction with high purity Van Arkel Ti, but with commercial purity Kroll Ti a parabolic rate was found at the same temperature (135). Unfortunately this was the highest temperature studied in this investigation and thus further discrepancies were not reported. However, in the lower temperature range from 300° to 950°C, the two types of Ti showed the same rate laws in the same temperature regimes (135).

[3] That the concept of Pilling and Bedworth is an oversimplification of the physical situation is, of course, clearly understood in the field of metal oxidation. This does not detract from the original contribution of these authors, who were the first to apply this type of ratio to the oxidation of metals in order to elucidate the structure of the oxide film (22).

Also for Ti in O_2, in the temperature range 650-950°C, breakaways were not observed with impure samples, whereas they were found with more pure Ti (139).

Thus one may conclude that sample purity will have an important effect on the transition temperature. In applying the transition temperature to a practical case, the purity of the sample in question may have a strong effect on the ignition of the metal.

Recall that it was postulated in Chapter II that the transition temperature will remain independent of sample size. The size dependence of the critical temperature was examined, and a model for metal pyrophoricity resulted. The initial postulate is now examined.

In general, for samples of differing surface area to volume ratios, the same type of rate law has been observed. For example, for Mg ribbon or powder in O_2 (37), for Mg cog-shaped samples or plates in air or CO_2 (42), for U foil or cylinders in H_2O (83), for Zr foil or spheres in O_2 (91), for Zr cylinders of differing sizes in O_2 (96), for Zr foil or cylinders in air (113,114) and in H_2O (117), for Ta foils of differing sizes in O_2 (175), and for Mo foil or wire in air (182) the same rate law has been used in each particular case to correlate the experimental data for the different types of samples. The rate constant may differ, however (Ti powder or bars in O_2 (133), Mo cylinders of varying sizes in O_2 (178)); for Zr foil or blocks in O_2, a slightly faster rate was found for the smaller samples (95).

In only one case of which the author is aware has a different rate law been observed; for sputtered Ta films 600 to 2500 Å thick in O_2, a logarithmic law was found throughout the temperature range 100-600°C, in contrast with the linear law usually observed with larger samples in the temperature range 500-600°C (151).

To summarize, then, for samples of differing sizes, different rates, but similar rate laws have been observed. Since the transition temperature is defined in terms of a linear rate law, with no regard to the rate constant, the transition temperature will indeed remain the same irrespective of sample size, as was postulated in Chapter II.

b. The Effect of Sample Pretreatment

By sample pretreatment one means the type of surface polishing, generally mechanical, chemical, or electrochemical, which is used previous to experimentation in oxidation studies. Induction periods, which are observed during the initial stages of the oxidation, before the appearance of the "steady-state" rate laws (which have been discussed in the earlier sections of this chapter), are associated with the clean metal surface which results from these sample pretreatments. That is, induction periods reflect the initial processes of adsorption and reaction on the clean metal surfaces. For experiments starting with, say the room-temperature thickness of oxide on the metal surface, an induction period would not be expected. Artificial coatings on the metal substrate, such as anodized films or metallic mirrors, are not included in the present discussion.

As was the case for different sample sizes, different sample pretreatments generally affect the rate constant, but not the rate law which is observed. For Mg foil in O_2, air, or CO_2 in the approximate temperature range 503-575^{o}C, there was no effect of differing degrees of mechanical polishing (40). Gulbransen (28,34) found that the parabolic to linear shift for Al in O_2 in the range 400^{o} to 500^{o}C was independent of the surface preparation technique. Similar laws but differing rates were found

in the oxidation of U in O_2, N_2, or air (74), U in H_2O (82), and Zr in O_2 or N_2 (87) as the pretreatment method was varied.

For U cubes in O_2 from 125° to 250°C a linear law was found with some effect of surface preparation on the initial portion of the oxidation only (75,76). For the oxidation of Zr and Mo in O_2, only a small effect was noted (91,176). Chemical polishing generally gives a somewhat slower rate than mechanical abrasion, as has been observed with Al in O_2 (61), and Zr in O_2 (92,93), and this effect has been attributed to the surface roughness induced by mechanical abrasion, that is, a higher effective surface area per unit geometrical surface area results from mechanical polishing (93).

In the Zr-O_2 reaction in the temperature range 400-900°C, mechanically abraded samples exhibited a somewhat faster rate than chemically polished samples only at the lower temperatures investigated (95), Finally, longer induction periods were observed with chemical pretreatments than with mechanical polishing in the oxidation of Ta in O_2 in the temperature range 500° to 700°C (155).

In conclusion, sample surface pretreatment does not appear to affect the transition temperature, as the induction period and the rate constant, but not the rate law change with the method of sample preparation.

c. The Effect of an Applied Heating Rate

As has been mentioned previously, very few non-isothermal experiments have been reported in the metal oxidation literature. The results of such studies are important in metal ignition because in almost every experiment or application an externally applied heating rate is necessary for ignition. Non-isothermal conditions could lead to thermal gradients across the oxide film and thus a lower transition temperature.

A method involving a linearly increasing temperature has been used by both Baur et al. (36) and by Kofstad (101,197). The appropriate theory is derived as follows (101,197): as in Chapter II, the oxidation rate constant may be written:

$$K_n = x^n \frac{dx}{dt} \qquad \text{(III-1)}$$

where x is the thickness of oxide formed at time t, n is the oxidation index (n = 0 gives a linear rate law, n = 1 a parabolic rate law, and n = 2 a cubic rate law), and k_n is the oxidation rate constant. The temperature dependence of the rate constant may be expressed by an Arrhenius type relation:

$$K_n = A_n e^{-E_n/RT} \qquad \text{(III-2)}$$

where A_n is the pre-exponential factor, E_n is the activation energy, R is the universal gas constant, and T is the temperature. Thus

$$x^n \frac{dx}{dt} = A_n e^{-E_n/RT} \qquad \text{(III-3)}$$

For oxidation with a linear increase in temperature,

$$T = at + T_o \qquad \text{(III-4)}$$

or

$$dT = a\,dt \qquad \text{(III-5)}$$

where a is the rate of temperature rise and T_0 is the

initial temperature. Eqn. (III-3) then becomes:

$$x^n \frac{dx}{dT} = B_n e^{-E_n/RT} \qquad \text{(III-6)}$$

where B_n is a constant equal to A_n/a.

Taking the logarithm of Eqn. (III-6), one obtains:

$$n \ln x + \ln(dx/dT) = \ln B_n - E_n/RT \qquad \text{(III-7)}$$

which may be rewritten:

$$(n+1)\ln x + \ln(d\ln x/dT) = \ln B_n - E_n/RT \qquad \text{(III-8)}$$

Thus a graph of the left hand side of Eqn. (III-8) versus 1/T should yield a straight line of slope $(-E_n/R)$. Accordingly, then, breaks in the curve will indicate the temperature regimes of different rate laws (that is, different n).

Baur et al. (36) studied the oxidation of Mg, Zr, Ti, Ta, and Mo in O_2 at a temperature rise rate equal to 5 $^{\circ}$C/min. For Mg in 6.7 atm of O_2 they found only a slight reaction; ignition occurred at 591°C. No correlation with the isothermal transition temperature is possible here. For Zr and Ti in 6.7 atm of O_2, no indication of a transition from a protective rate was observed in the temperature range from 450° to 790°C. Comparison with the isothermal transition temperatures at lower pressures listed in Table 13 shows no discrepancy with the isothermal results.

For Ta in O_2 in the pressure range 1 through 6.7 atm and in the temperature range 450-790°C, a break in the curve, leading to an approximately linear law, was observed

at about 560°C, which indicates a rise in the transition temperature from the isothermal value of 500°C (156). For Mo in 6.7 atm of O_2, the only break observed occurred at 560°C and led to an apparently protective rate law; ignition occurred at 725°C, which is equal to the Mo-O_2 transition temperature at 1 atm listed in Table 13.

Kofstad (101,197) investigated the oxidation of Ti and Zr in O_2, presumably at a pressure of 1 atm, with a linear temperature rise rate of 3.86 °C/min. For Ti he found a parabolic regime in the temperature range 700-900°C, followed by a linear regime in the range 900-1100°C. These results are in complete agreement with the isothermal transition temperature. However, for Zr, a cubic dependence was observed in the range 650-950°C, and a parabolic dependence from 950° to 1100°C, which is in disagreement with the estimated isothermal transition temperature of 925°C $\pm$ 100°C (Table 13), but in agreement with the isothermal results of Pemsler (107,132). (See also Section 7.b of Appendix II.)

To summarize, the effect of heating rate on transition temperature is unclear because of the scarcity of non-isothermal oxidation studies. Excellent agreement with isothermal experiments has been obtained, however, for Mo in O_2 (36), for Ti in O_2, and for Zr in O_2 at temperatures below the estimated isothermal transition temperature (36, 101,197). The transition temperature was observed to increase with heating rate about 60°C for Ta in O_2 (36), and an increase was also found for Zr in O_2 (101,197). Until more data become available, this important effect cannot be examined further.

d. Summary

In this chapter the transition temperatures of

several metal-oxidizer systems have been listed; in Appendix I these are estimated from isothermal oxidation experiments in cases for which sufficient data are available in the metal oxidation literature. In general, the transition temperature is essentially independent of sample size and of sample surface pretreatment. Sample purity and non-isothermal conditions may have an effect on its value.

Recall that the transition temperature is postulated to be the lowest possible ignition temperature for any metal-oxidizer system (see Chapter II). In the next chapter, the physical model of metal ignition is tested with the help of the metal oxidation - metal ignition literature. Literature values of critical and ignition temperatures are cited in Appendix II for those systems discussed in this chapter.

CHAPTER IV - LITERATURE TEST OF THE IGNITION MODEL

The metal ignition criterion states that the ignition temperature, as defined by the appearance of a flame, must be greater than both the transition temperature, at which the oxide film becomes non-protective, and the critical temperature, at and above which sample self-heating is possible. Furthermore, the appropriate transition temperature is thus the minimum ignition temperature of any metal-oxidizer system of any size.

In Appendix II, literature values of critical and ignition temperatures are cited for those metals whose transition temperatures were estimated in Appendix I. As before, wherever possible, the oxidizing gases of interest include O_2, N_2, air CO_2, and H_2O. In this chapter a critique of the physical model of metal ignition will be given in light of the metal ignition literature.

Also, other models and theories of metal ignition presented in the literature are reviewed and discussed in Appendix II. In the present chapter comparison of the present model with these other theories is made. The reader concerned with the detailed critical and ignition temperatures, the appropriate experimental methods, and specific discussion of these data as well as other theories, should consult Appendix II.

1. A Critique of Metal Ignition Criterion

Before reviewing the ability of the metal ignition criterion to correlate, explain, and interpret metal ignition data presented in the literature, let us briefly review the more significant predictions of the model.

Firstly, as developed in Chapter II, the model predicts that the ignition temperature will be greater than the larger of the transition and critical temperatures; care must be taken, however, to make such comparisons in restricted ranges of surface area to volume ratio and of oxidizer pressure, as the critical temperature is thought to depend strongly on the sample S/V, and both temperatures may depend on the gas pressure.

At a given pressure, by virtue of the criterion, the minimum possible ignition temperature at any surface to volume ratio is the transition temperature. However, in certain types of experiments which are prone to low critical temperatures (namely QP[1] and DD[1] experiments) or suffer from an inability to diagnose sample self-heating (namely DD and SP[1] experiments), critical temperature interference with ignition temperature determinations may occur.

If the ignition temperature is controlled by the transition temperature, then no variation in ignition temperature with S/V is expected.

If the ignition temperature is controlled by the critical temperature, then three ranges of dependence of the former on S/V are expected: (1) for large samples in which the rate of heat transfer to the interior of the sample is relatively independent of the sample size, the critical and ignition temperature will be

---

[1] Experiments are designated as follows: QP is a quiescent pile, DD is a dust dispersion, and SP is a single particle experiment (See Appendix II).

TABLE 25.

SUMMARY OF LITERATURE REVIEW

System	T_{trans}, °C and Associated Pressure Range	T_{crit}, °C and Associated Pressure Range	S/V, mm^{-1} for T_{crit}	Controlling	T_{ign}, °C and Associated Pressure Range	S/V, mm^{-1} for T_{ign}	$(T_{ign})_{minimum}$, °C Experiment, and Pressure
$Mg-O_2$	475-400, 2 torr -2.64 atm	575, 1 atm	0.579 -1.23	T_{crit}	623, 1 atm	0.579	591, B, flowing
$Mg-N_2$	300, 20-200 torr	---	---	---	520-575, 1 atm?	---	520, QP, 1 atm?
Mg-air	450, ---	575, 1 atm	0.579 -1.23	T_{crit}	645, 1 atm?	0.74 -1.23	470, QP, 1 atm?
$Mg-CO_2$	$\geq$ 500-550, 1-15 atm	$\leq$ 790, 15 atm	1.23	T_{crit}	920, 15 atm	1.23	600, QP, 1 atm?
$Mg-H_2O$	$\leq$ 425, 31-208 torr	---	---	---	635, flowing	---	635, B, flowing
$Li-N_2$	---	$\leq$ 239, 110-200 torr	---	---	170-399, 1 atm? & flowing	---	170, QP, 1 atm?
$Ca-O_2$	400, 100-760 torr	$\leq$ 350-300, 100-760 torr	---	T_{trans}	550, 1 atm	---	550, B, 1 atm
$Al-O_2$	2030, ---	$<$ 2030, flowing	171	T_{trans}	2030, 0.067-66.7 atm	7.8	590, QP, 1 atm?
$Be-O_2$	2530, ---	$<$ 2530, 0.1-2 atm	158	T_{trans}	$\approx$ 2530, 0.1-2 atm	158	$\approx$2530, SP, flowing
$U-O_2$	150, 20-800 torr	$\leq$ 300, 20-800 torr	---	T_{crit}	535, flowing	2.1	240, QP, flowing

TABLE 25.(Concluded)

System	T_{trans}, °C and Associated Pressure Range	T_{crit}, °C and Associated Pressure Range	S/V, mm^{-1} for T_{crit}	Controlling	T_{ign}, °C and Associated Pressure Range	S/V, mm^{-1} for T_{ign}	$(T_{ign})_{minimum}$, °C Experiment, and Pressure
U-air	150, 200 torr	400, 1 atm	2.1	T_{crit}	645, 1 atm	2.1	25, DD, 1 atm?
$Zr-O_2$	>1300, flowing	800-1000, 76-760 torr	1.41 -15.05	T_{trans}	>1300, flowing	---	855, B, flowing
$Ti-O_2$	900, 10^{-3}-760 torr	1150, 33.3 atm	2.56	T_{crit}	815, 20 atm	2.25-7.88	815, B, 20 atm
$Ta-O_2$	500, 10 torr - 40 atm	≤1250, 1 atm	0.845	T_{crit}	1300, 1 atm	0.845	1000, B, ---
Ta-air	800, 1 atm	---	---	---	1238-1282[1], 1-7 atm	4.32	300, QP, 1 atm?
$Mo-O_2$	600-725, 76-760 torr	≤725, 1 atm	2.33	?	750, 1 atm	2.33	725, B, 6.7 atm
Mo-air	595, 1 atm	---	---	---	720, 1 atm?	---	360, QP, 1 atm?

[1] Brightness temperature

relatively independent of size: (2) in an intermediate regime, the critical and ignition temperatures will decrease monotonically; (3) when the ignition temperature becomes equal to the transition temperature, it will remain equal to this value for further increases in S/V, even though the critical temperature continues to decrease.

The results of the surveys of the metal oxidation and metal ignition literatures which have been presented in detail in Appendices I and II are summarized in Table 25.[2] For each system characterized by sufficient oxidation or ignition data, the estimated transition and critical temperatures and their associated pressure ranges are listed. The appropriate S/V for the critical temperature is also given. The larger of these two temperatures is selected as controlling in ignition. Wherever possible, an ignition temperature is cited which was obtained in a similar pressure and S/V range. Finally, the minimum ignition temperature observed for each system and the experiment in and the pressure at which it was found are listed.

For convenience, the success of the physical model of metal ignition is demonstrated schematically in Table 26. From Tables 25 and 26 it is seen that the ignition criterion (T_{ign} greater than larger of T_{crit} and T_{trans}) is satisfied for the following systems (the ignition controlling temperature is given in parentheses): Mg-O_2 (T_{crit}); Mg-air (T_{crit}); Mg-CO_2 (T_{crit}); Ca-O_2 (T_{trans}); Al-O_2 (T_{trans}); Be-O_2 (T_{trans}); U-O_2 (T_{crit}); U-air (T_{crit}); Zr-O_2 (T_{trans}); Ta-O_2 (T_{crit}); and Mo-O_2 (either T_{trans} or T_{crit}). Insufficient data are available to test the ignition criterion for the following

[2] Tables 14 through 24, Fig. 8 through 15, and Ref. (198) through (246) are discussed in Appendix II.

TABLE 26.

LITERATURE TEST OF THE METAL IGNITION CRITERION

System	T_{trans} Estimated	T_{crit} Estimated	Controlling	Criterion Satisfied	$(T_{ign})_{min} \geq T_{trans}$ in the Following Experiments: All	(-QP)	-(QP + DD)
$Mg-O_2$	x	x	T_{crit}	x	x	x	x
$Mg-N_2$	x	---[1]	---	---	x	x	x
Mg-air	x	x	T_{crit}	x	x	x	x
$Mg-CO_2$	x	x	T_{crit}	x	x	x	x
$Mg-H_2O$	x	---	---	---	x	x	x
$Li-N_2$	---	x	---	---	---	---	---
$Li-H_2O$	x	---	---	---	---	---	---
$Ca-O_2$	x	x	T_{trans}	x	x	x	x
$Al-O_2$	x	x	T_{trans}	x	no	no	x
$Be-O_2$	x	x	T_{trans}	x	x	x	x
$U-O_2$	x	x	T_{crit}	x	x	x	x
U-air	x	x	T_{crit}	x	no	no	x
$Zr-O_2$	x	x	T_{trans}	x	no	no	no
$Ti-O_2$	x	x	T_{crit}	no	no	no	no
$Ta-O_2$	x	x	T_{crit}	x	x	x	x
Ta-air	x	---	---	---	no	no	x
$Mo-O_2$	x	x	?[2]	x	x	x	x
Mo-air	x	---	---	---	no	x	x
$Si-O_2$	x	---	---	---	---	---	---
$Si-H_2O$	x	---	---	---	---	---	---

[1] Insufficient data.

[2] Either T_{trans} or T_{crit}.

systems: Mg-N_2; Mg-H_2O; Li-N_2; Li-H_2O; Ta-air; Mo-air; Si-O_2; and Si-H_2O. Finally, the ignition criterion is not satisfied in the case of the Ti-O_2 system.

Note that for this former system, the failure of the ignition criterion is based on only one piece of experimental evidence: the Ti-O_2 ignition temperature of 815°C measured by Dean and Thompson (194) at an O_2 pressure of 20 atm. These authors stated "the results indicate that in an oxygen atmosphere, ignition of titanium will take place when the metal temperature exceeds 1500°F (815°C)." If this value which they have named is in actuality a critical or spontaneous ignition temperature, then the metal ignition criterion is absolved.

Because the transition temperature controls the ignition of at least four of the twelve systems for which a prediction has been made, it is concluded that the statement that the ignition temperature will be greater than the transition temperature is not trivial.

Furthermore, the stronger statement that the ignition temperature will be greater than or equal to the transition temperature for any metal-oxidizer system with any sample S/V (that is, the transition temperature is the minimum possible ignition temperature) has been verified in all types of experiments for the following systems: Mg-O_2, Mg-N_2, Mg-air, Mg-CO_2, Mg-H_2O, Ca-O_2, Be-O_2, U-O_2, Ta-O_2, and Mo-O_2 (See Table 26). If quiescent pile experiments are excluded because of their characteristically low critical temperatures[3], then the Mo-air system also falls into this category. Finally, if only bulk or single particle experiments are considered to yield meaningful ignition temperature data to be compared with the model, then the Al-O_2, U-air, and Ta-air systems also demonstrate the validity of this hypothesis.

[3]See Appendix II: in QP experiments the critical temperature is low because of the high surface area available for reaction compared to the low surface area available for heat loss to the surroundings.

Recall that the ignition criterion itself may not be satisfied for the Ti-O_2 system, and that the transition temperature of the Zr-O_2 system was changed on the basis of the available ignition data (see Appendix II). Difficulties with predictions about the ignition of these metals in O_2 may be a result of the solubility of this gas in the metals, which was documented in Appendix I. It is possible that either the transition temperature concept (and thus the metal ignition criterion) fails when gas solubility is important at temperatures near to the ignition temperature because of possible continuous variation of concentration from pure metal to pure oxide, or that the discrepancies in the experimental data, upon which the estimated transition temperatures and attempted verification of the criterion are based, are a result of varying initial gas concentrations within the metallic samples from experiment to experiment.

In general the expected trends with respect to sample size are found for all of the systems considered. The data are too sparse, however, to study the details with respect to sample surface to volume ratio for cases in which the bulk ignition is controlled by the critical temperature.

It is concluded that the critical temperature is a necessary part of the ignition criterion for several reasons: firstly, because sample self-heating and/or spontaneous ignition have been encountered in many oxidation and ignition experiments, notably with Mg in O_2 and air (Fig. 8) and with U in air (Fig. 11), the importance of this effect in ignition is clear; secondly, since it has been shown in Chapter III that the transi-

tion temperature is independent of sample size, whereas it has been shown in Chapter II that the critical temperature decreases with decreasing sample size, the size effect observed in some systems in ignition temperature can be explained on the basis of the S/V dependence of critical temperature. Finally, for those twelve metal-oxidizer systems for which a comparision of transition and critical temperatures is possible, the latter temperature controls the bulk ignition of at least seven of these systems.

Literature verification of the metal ignition criterion and of trends expected on the basis of the physical model of metal ignition is quite good. It is concluded that the model will satisfactorily correlate experimental data and will remove discrepancies in existing data by distinguishing between critical and ignition temperatures.

The final section of the present chapter is devoted to a summary of the critical review of other theories of metal ignition which have been published in the literature (see Appendix II).

2. Summary of Other Theories of Metal Ignition

Let us briefly review each of the theories of metal ignition which have been discussed in Appendix II and summarize their weak points. In general, all of these theories are extensions of the ignition theory of Semenov and Frank-Kamenetskii (23, 24) and fail to include or realize the inhibiting effect of the metal oxidation product surface film, as reflected in the present model in the transition temperature. Some theories are in excellent agreement with experiment, however, for limited ranges of variation of the experimental parameters.

The theory of Eyring and Zwolinski (48) allows calculation of the critical temperature. It is valid

only for systems undergoing linear oxidation, that is, only above the transition temperature. No dependence of critical temperature on oxidizer pressure or on metal sample size is predicted, and the theory fails for clean metal surfaces, that is, for zero oxide thicknesses.

Hill et al. (213) have also provided a theory for calculation of the critical temperature. This theory, however, shows the wrong dependence of critical temperature on sample size (that is, the critical temperature decreases with increasing sample size), and also fails for zero oxide thickness.

Reynolds (220) developed a theory for calculation of the ignition temperature, but used incorrect reasoning to obtain the defining equation for ignition. Agreement with theory was found experimentally only if convective heat losses to the oxidizing gas were neglected in the former. The ignition temperature is independent of sample size and of oxidizer pressure, and the theory fails for metals exhibiting the parabolic oxidation rate if zero oxide thicknesses are considered.

Talley's theory (245) yields values of critical temperature only for large samples; the critical temperature is predicted to be independent of pressure.

The theory of Friedman and Macek (15) is valid only for small particles whose ignition temperature can be associated with some fixed temperature, such as the melting point of the appropriate oxide. It provides an estimate of the critical temperature under such circumstances. The wrong size dependence of critical temperature is predicted.

The theory of Cassel and Liebman (217) is also valid only for small particles, and predicts the incorrect

size dependence of ignition temperature.[4]

Theories yielding the critical temperature have been developed for specific types of experimental configurations: dust dispersions, by Nagy and Surincik (246); quiescent piles, by Anderson and Belz (236), by Tetenbaum, Mishler, and Schnizlein (233), and by Murray, Buddery, and Taylor, as quoted by Tetenbaum et al.

In general these latter specialized theories give good agreement between calculated critical temperatures and measured "ignition temperatures", and show the correct trends with respect to sample size and oxidizer pressure. As was inferred by means of the physical model of metal ignition developed within the present report, so-called ignition temperatures measured in QP and DD experiments are actually critical temperatures, as is also indicated by the theoretical agreement.

To summarize, the basic difficulties of the quantitative theories which have been discussed in this chapter are their restriction to limited ranges of sample size, generally either large or small samples, their inability to predict the observed size dependence of critical or ignition temperature and any dependence of these temperatures on oxidizer pressure, and their failure for a clean metal surface (or for zero oxide thickness).

On the other hand, the physical model of metal ignition, as developed in Chapter II of this report, is valid for any size of sample. It is interesting to note that, if the conduction heat losses into the fuel and/or oxidizer included in $\dot{q}_{loss}$ (Eqn. II-45) are approximated by a linear temperature profile inversely proportional to the particle radius, then the incorrect size dependence of the critical temperature is predicted; that is, since then $\dot{q}_{loss}$ increases with decreasing particle size (for

[4]As discussed in Appendix II, however, their analysis may be valid under particular experimental conditions.

both terms representing cooling), the critical temperature intersection on the $\dot{q}$ versus T_s diagram moves to higher temperatures.

This is exactly the reason that most of the theories cited above show the wrong size dependence. In order to facilitate calculations, this simplifying approximation was made. It was shown in Section 4 of Chapter II that if a more realistic temperature profile into the metal sample is considered, the experimentally observed trend of critical temperature with sample size is predicted. Unfortunately, however, the ability to calculate critical and ignition temperatures is sacrificed when the complicated nature of these two heat loss terms is considered. Thus analytical calculations based on the model developed in Chapter II would be extremely difficult, and one must be satisfied to examine the trends predicted by the model.

Dependence on oxidizer pressure has not been considered in the physical model of metal ignition up to this point. However, in order to explain observed experimental results on the ignition of Mg, such a dependence will be investigated (again in terms of a trend) in Chapter VII.

Finally, difficulties with zero initial oxide thickness will develop in the model only if protective oxidation rate laws are used to describe the initial states of oxidation of a clean metal surface. In the nomenclature of Chapter II, these laws may be written:

$$\frac{dx}{dt} = K_n / x^n \qquad \text{(IV-1)}$$

where $n \neq 0$. Since then

$$\dot{m} \sim dx/dt = K_n/x^n \qquad \text{(IV-2)}$$

mathematical difficulty will always occur for $x = 0$. If it is remembered that in fact, although the oxidation rate for a clean surface is initially no doubt extremely large, but finite, then this purely mathematical dilemma common to all of the theories (including the present model) is resolved.

To summarize, although the present model is not readily useful for calculation of critical or ignition temperatures, it is more general than quantitative theories of metal ignition, and it predicts several experimentally observed trends of which other theories are incapable or yield the inverse dependence. As was shown in Section 1 of this chapter, experimental agreement is excellent with the quantitative aspects and with the relatively qualitative trend predictions of the model.

In the following chapters, the present model is used to assist in explanation of experimental results obtained at Princeton on the ignition of metal wires and is tested critically by experiments in an induction furnace. Materials and details of the equipment are presented in Chapter V.

Because of space limitations, certain qualitative studies, performed with wires, of the ignition and combustion of Ta and Mo and of means of improving the ignition efficiencies for metals such as Al and Be (that is, providing low artificial transition temperatures), as suggested by the model of metal ignition (see Section II.5), will not be reviewed here. The reader is referred to References (247,248) and (249), respectively, for details of these investigations.

CHAPTER V - EXPERIMENTAL DESCRIPTION

The materials and apparatus used in the present investigation are discussed in this chapter. Two major types of experiments were performed: in the first, Al wires and Mg ribbons were ignited by ohmic heating; as this apparatus, referred to as the wire-burning apparatus, was designed primarily for the study of metal combustion rather than metal ignition, the data obtained are necessarily qualitative. Nevertheless, as the original model of metal ignition was developed from such qualitative data (as will be discussed in Chapter VI), valuable information can be obtained from these experiments.

The second type of experiment was performed in an induction furnace facility. In this apparatus, metal ignition rather than combustion is studied primarily, because of various experimental characteristics which will be discussed in Section 3 of this chapter. Quantitative ignition data were obtained for Mg and Ca samples of various sizes. Preliminary experiments were performed with Al.

The first section of the chapter is devoted to a description of the various materials used in this investigation. The wire-burning apparatus and induction furnace are described in the following sections. Finally, miscellaneous techniques, such as still photography, are reviewed in the last section.

1. Materials

a. Gases

Throughout the present investigation, the ambient atmospheres of interest consisted of O_2, CO_2, Ar, and H_2O. For the first three gases listed, commercially pure samples were used, and typical analyses of these gases, which were obtained from the Liquid Carbonic Division of General Dynamics, are listed in Table 27. H_2O was obtained where desired by evaporating distilled water.

TABLE 27.

TYPICAL ANALYSES OF GASES

1. Argon 99.998%	
N_2	< 10 ppm
O_2	< 10 ppm
H_2O	< 5 ppm
2. Oxygen 99.5%	
$N_2 + H_2$	< 5000 ppm
H_2O	< 11 ppm
3. Carbon Dioxide 99.5% Average	
O_2	< 900 ppm
N_2	< 500 ppm
H_2O	< 45 ppm

In general, in both the investigation in the wire-burning apparatus and also that in the induction furnace, the gas compositions used were as follows: pure O_2, pure CO_2, pure Ar, pure H_2O, and 50 volume percent-50 volume percent mixtures of O_2-Ar, O_2-CO_2, O_2-H_2O, CO_2-Ar, CO_2-H_2O, and H_2O-Ar. An abbreviated composition designation of the form X-Y is understood to indicate a 50%-50% mixture of gases X and Y, unless otherwise noted.

The total gas pressures of interest were generally as follows: 50, 100, 300, 500 torr, and 1, 2, and 5 atm (that is, 760, 1520, and 3800 torr). Exceptions will be noted where they occur. Static gas atmospheres were used throughout (except for free convection around the heated sample).

b. Metal Wires and Ribbons

The ignition and combustion of Mg and Al were studied in the wire-burning apparatus. Mg was obtained

in ribbon form from Baker and Adamson (Code 1901). The average width of the ribbon was 0.29 cm, the average thickness 0.016 cm, and its average weight was 7.7 mg/cm. The only impurities seen in the Mg flame spectrum were Mn and Na (7, 19).

Al wire of 0.889 mm diameter was obtained from the Fisher Scientific Company (Catalogue Number A-557). A typical analysis of the wire is shown in Table 28; however, only Cu, Ga, and Na were observed as trace impurities in the flame spectrum (7, 19).

Some of this Al wire was anodized commercially prior to experimentation. Anodization was performed in a H_2SO_4 bath and oxide layers of 5 to 10 μ were thus obtained. Finally, the wire was immersed in boiling H_2O.

The nature of the H_2SO_4-anodized film which is produced on Al under these conditions is extremely well documented (250-256, 259).[1] The anodic oxide film consists of two layers: the inner layer, called the barrier layer, is amorphous and non-porous, much like the ordinary low-temperature thermal oxide coating which forms on Al; the thickness of this barrier layer depends on several parameters of the anodization process, such as the potential, electrolyte concentration, and so forth, but is much less than 1 μ. The outer layer of oxide, which is extremely thick, is porous; the number density and dimensions of the pores are strong functions of the electrolizing conditions. The porosity of the outer layer of film is attributed to the solvent action of the electrolyte, as non-porous anodic films can be formed in weak acids.

---

[1] Only some of the more recent references on this subject are listed here. See these references for a more extensive literature review.

TABLE 28.

TYPICAL ANALYSIS OF 0.889 mm DIAMETER Al WIRE

Si	0.10%
N	0.001
Cu	0.02
Fe	0.10
Mn	0.001
Ti	0.02
As	Trace
Al (by difference)	99.758%

The subsequent H_2O immersion process partially seals these pores by reaction of the H_2O with the Al_2O_3 to produce boehmite, AlOOH ($Al_2O_3 \cdot H_2O$) (250,255-259). This sealing is not effective at high temperatures, however, as boehmite decomposes at 300°C to Al_2O_3 and H_2O (6). Thus, at the temperatures associated with the ignition of the Al wires, the majority of the anodized oxide coating can be considered porous if no further reaction occurs during the ohmic heating process.

The unanodized wire averaged 16.9 mg/cm in weight and was of 0.889 mm diameter; the anodized wire of 0.800 mm diameter weighed 16.2 mg/cm on the average.

Throughout the investigation, 11 cm lengths of each metal wire or ribbon were used. Brzustowski (7) found that the qualitative aspects of the ignition and combustion of 8.8 or 15.1 cm Mg ribbons in O_2-Ar atmospheres were the same. The surface area to volume ratios of the various samples were thus 13.2, 4.53, and 5.02 mm^{-1} for the Mg ribbon, unanodized Al, and anodized Al wires, respectively.

Unless otherwise noted, the only pretreatment of the ribbons and various wires was light wiping with tissue paper in order to remove surface dirt and oil.

c. Metal Rods and Foils

Various sized samples of Mg, Ca, or Al were

cut from rods or foils for use in the induction furnace. Specific sample dimensions and weights will be described in Chapter VII. Impurity analyses of some of the various materials, all of which were supplied by A. D. MacKay, Inc., are given in Tables 29 through 31. The only pretreatment given any of the Mg or Al rod or foil samples was a light wiping.

According to the supplier, the Ca samples were typically 99.9% Ca with 0.5% Mg maximum impurity; 2.34 cm rod and 0.508 and 0.889 mm foil were used in the investigation. All of the Ca samples were shipped, stored, and machined under mineral oil. Prior to testing the samples were wiped, washed in hexane for one hour at room temperature, and then degassed in a vacuum desiccator (with continuous pumping) for at least 16 hours.

To examine the effect of the hexane pretreatment, some samples were washed in methanol until rapid dissolution of the Ca began (about 30 min at room temperature). As far as ignition temperatures were concerned, there was no significant difference between the two pretreatments: thus the C_6H_{14} wash was used. The C_6H_{14} was replaced every 25 samples.

The freshly machined surfaces of the Ca samples maintained their metallic luster to the time of experimentation. However, those surfaces not machined during the sample preparation were covered by a thick black, brown, and white oxide (and nitride) film. Removal of this film from either the rod or foils was not found to affect the appropriate ignition temperatures. Thus most experiments were conducted with this film present.

2. Wire-Burning Apparatus

The wire-burning apparatus used in the present

TABLE 29.

TYPICAL ANALYSIS OF 2.38 cm DIAMETER Mg ROD

Al	0.007%
Ni	<0.0005
Cu	<0.001
Fe	0.001
Mn	0.002
Si	0.006
Ca	0.004
Pb	0.001
Zn	0.01
Ag	<0.0005
Na	<0.001
Mg (by difference)	99.966%

TYPICAL ANALYSIS OF 2.54 cm DIAMETER Al ROD

Cu	0.001%
Fe	0.001
Si	0.002
Mn	0.000
Mg	0.001
Zn	0.005
Others	0.000
Al (by difference)	99.99%

TABLE 30.

TYPICAL ANALYSIS OF 0.127 AND 0.254 mm Mg FOILS

Fe	0.03%
Mn	0.04
Cu	0.003
Al	0.003
Mg (typical)	99.9%

TABLE 31.

TYPICAL ANALYSIS OF 0.254 mm Al FOIL

Cu	0.001%
Fe	0.001
Si	0.002
Mn	0.000
Mg	0.001
Zn	0.005
Others	0.000
Al (typical)	99.99%

investigation was essentially the same as that used by Brzustowski (7, 9) and Mellor (19), with only minor modifications.

a. Apparatus Description

A photograph of the apparatus is shown in Fig. 16. The pressure vessel which houses the wire and test atmosphere is at the right and the control panel is at the left. Fig. 17 is a schematic drawing of the system.

The test vessel was a steel cylinder of about 25 cm diameter and 30 cm length, or of 16.4 ℓ volume. The maximum operating pressure of the vessel was 20 atm. Quartz windows of 2.54 cm diameter were mounted on the centerline plane and on the front and back plates; these windows allowed visual and photographic observation of the heated wires. Access to the interior of the chamber was gained by means of the front plate, which was mounted on a hinge. The exterior of the cylinder was wrapped with resistance heating tapes so that the chamber could be heated in experiments involving H_2O. Vapor pressures as high as 100 torr could be obtained without difficulty. The H_2O vapor pressure was deduced from the temperature as given by a iron-constantan thermocouple mounted within the chamber.

The drying chamber which is shown in Fig. 17 was a small pressure vessel which was filled with Drierite. All gases were passed through the dryer at a slow rate before entering the chamber if H_2O was not a constituent of the test atmosphere.

Blowers at the back of the chamber were used to assist in mixing of the gas combinations; these may be seen in the background of Fig. 18, which also shows

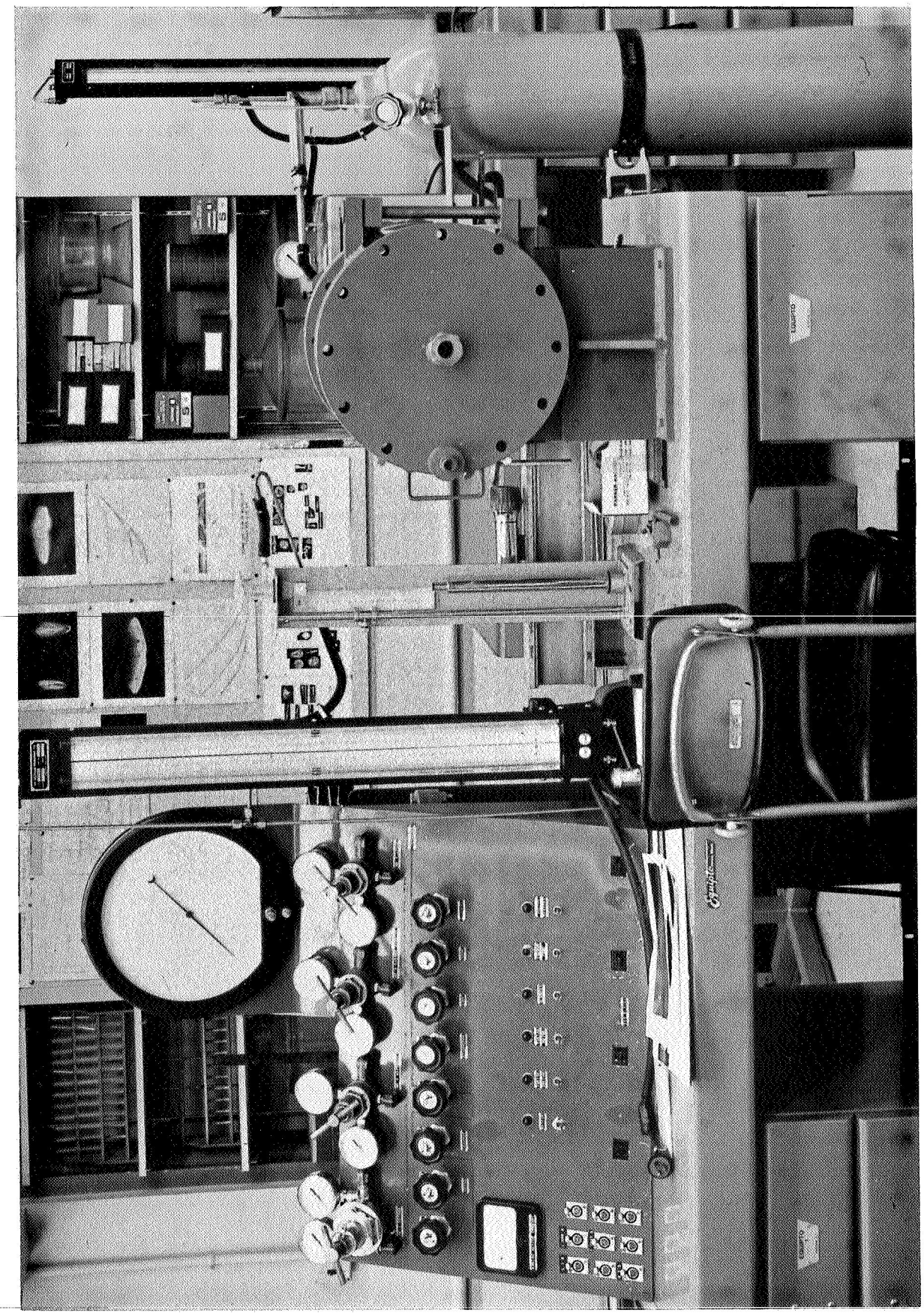

FIGURE 16

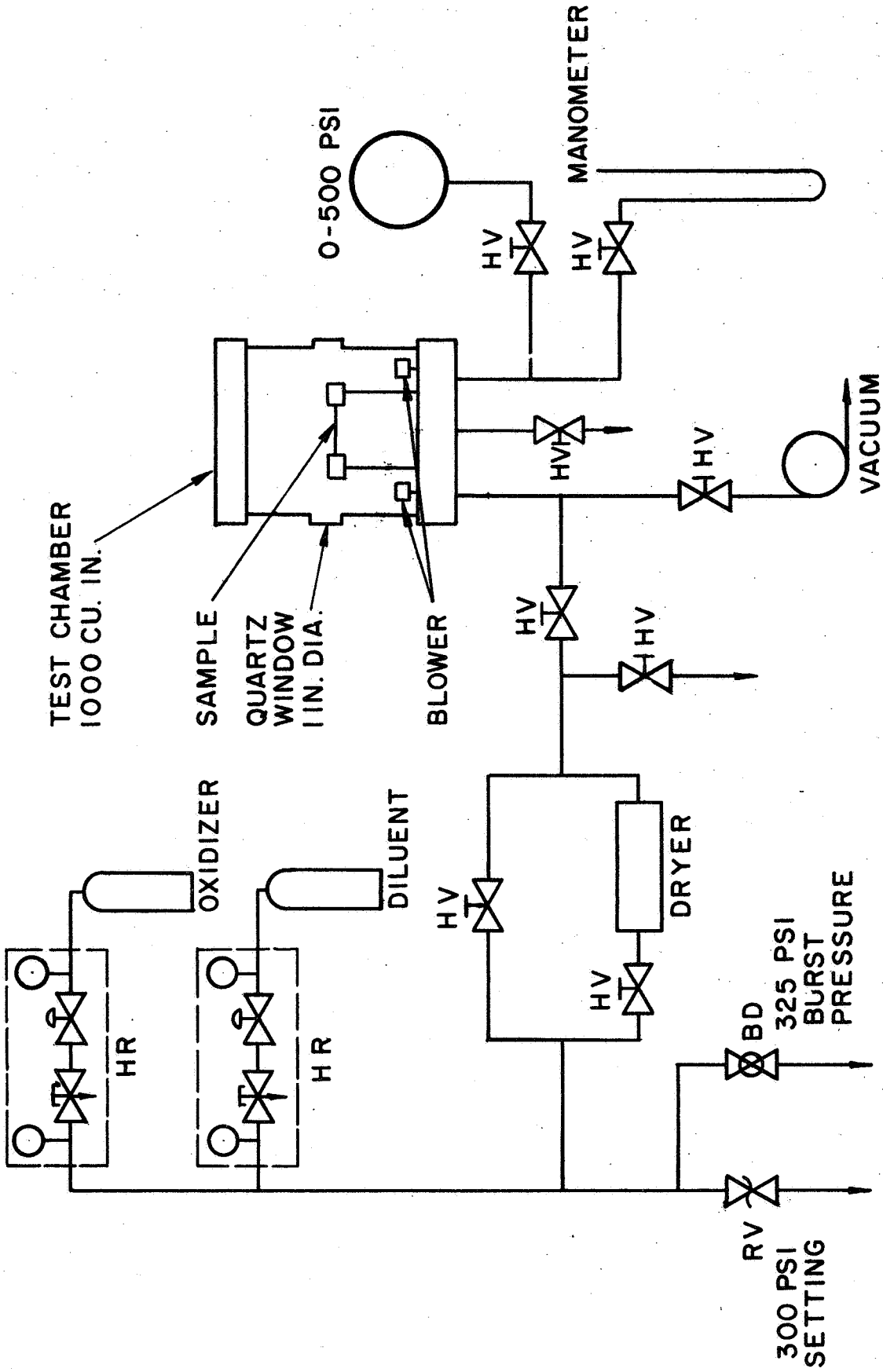

WIRE-BURNING APPARATUS SCHEMATIC

FIGURE 17

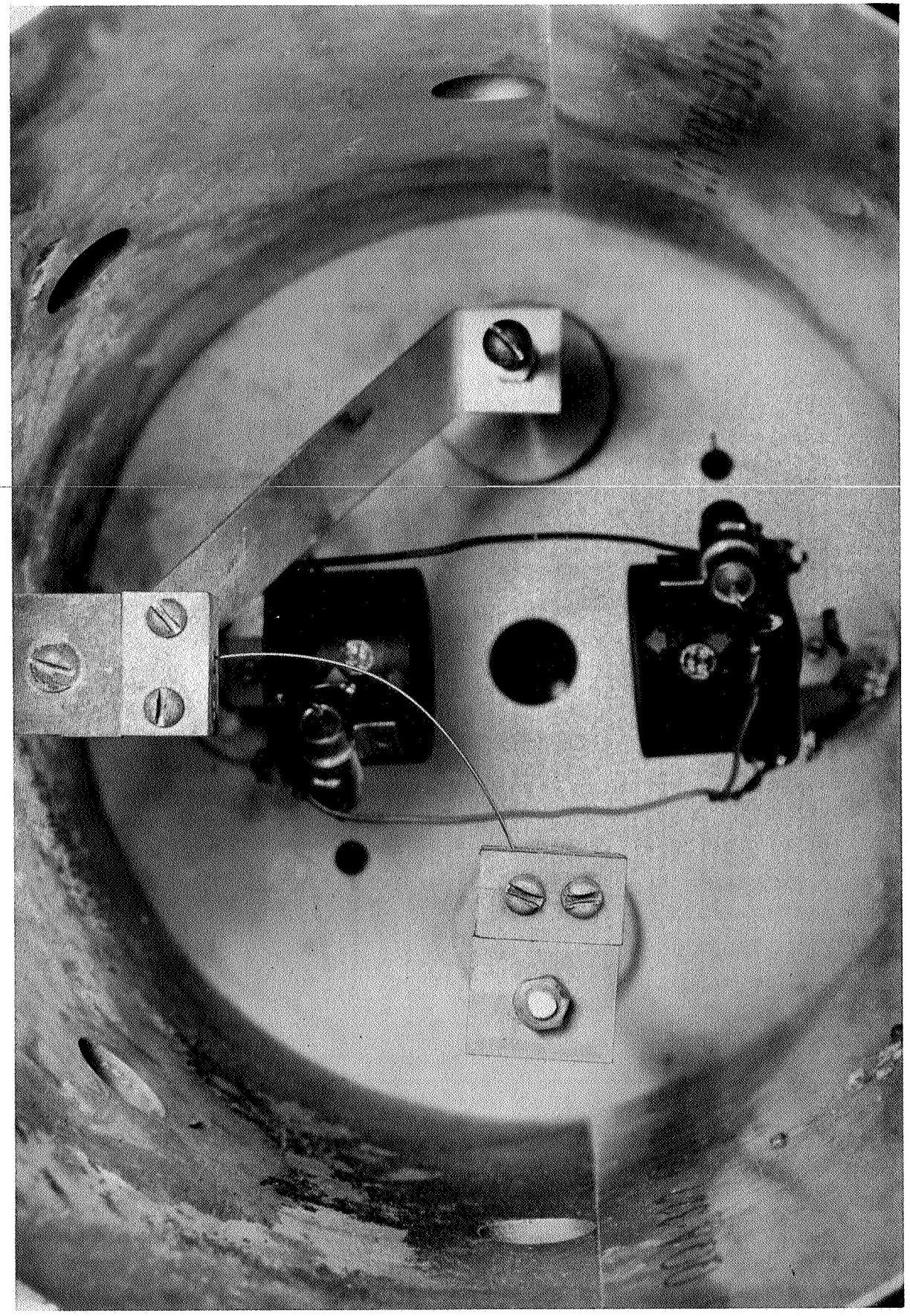

FIGURE 18

a wire sample mounted in the electrode blocks. Large brass electrode blocks were used so that they would withstand the effect of the burning metal wire. The "L" mounting of the sample which is shown in Fig. 18 was chosen for convenience in photographic observation.

As has been noted, the samples were ignited by ohmic heating. Reproducible results were obtained if a voltage increasing linearly with time was applied across the electrodes. A 2.4 KVA step-down transformer relayed the output of a 20 amp variac, which was driven at a constant rate, to the electrodes. The no load voltage rise rate was 0.120 v/sec; measured approximate voltage rise rates which were used for the various samples were 0.106 v/sec for Mg and 0.110 for Al. Note that the sample must maintain mechanical integrity in order to continue ohmic heating; that is, for some metals under some circumstances, the ignition experiment will automatically end when the sample breaks at the metal melting point.

The voltage across the electrodes, the current passing through the sample, and the light intensity emitted by the sample were continuously recorded during an experiment on a Honeywell Model 1406 Visicorder.

One unfortunate disadvantage of the wire-burning apparatus is the lack of quantitative temperature measurement, which, of course, is extremely desirable in ignition experiments. Temperature measurements by means of thermocouples were discarded for several reasons: firstly, because of the small size of the samples, mounting a thermocouple is difficult; secondly, because of non-uniform heating along the wire, placement of the thermocouple near to the hottest spot at which ignition will occur is little more than guesswork; finally, because of the large

number of samples involved, any use of thermocouples mounted on the individual wires would have been prohibitingly time-consuming. Although this method of temperature measurement could have been at attempted, the wire self-support limitation restricts the usefulness of the wire-burning apparatus.

Optical methods of temperature measurement are also difficult and of questionable value because of focusing problems and because of wire movement during the pre-ignition heating period. A two color pyrometer, which yields the true temperature of a solid body under the gray body emissivity assumption, was constructed and tested. It was found unsatisfactory because of the various focusing problems and because of the low light intensities involved.

Thus most of the information obtained from the wire-burning apparatus is qualitative; as will be seen in Chapter VI, however, valuable insight into the ignition process can be gained.

b. Experimental Procedure

An 11 cm length of ribbon or wire was wiped clean and weighed on a Mettler Electric Balance, Type H15. The sample was then mounted between the electrode blocks, generally in the "L" configuration shown in Fig. 18. The front door of the chamber was closed and the system was evacuated. When a total pressure on the order of one torr was attained in the vessel, the first gas appropriate to the test atmosphere was admitted through the drier to the test chamber. When the desired partial pressure was attained, the second gas was admitted in a similar manner. Mixing was accomplished by the use of the blowers. At all times, it was attempted to maintain the chamber leakage rate at a level of less than 2 mm/hr, so that leakage into or out of the chamber during an experiment was negligible (this rate represents a maximum error of 4% in composition at the lowest pressure of interest, 50 torr, for an experiment duration of 1 hr.).

When the desired test conditions were obtained, the voltage across the electrodes was increased from zero linearly. After the sample had ignited and burned, this voltage was turned off and the chamber was opened, and any recoverable macroscopic products of combustion were removed.

3. Induction Furnace

As was mentioned in the previous section of this chapter, the wire-burning apparatus suffers from two serious difficulties: firstly, the inability to measure sample temperature, and secondly, the requirement that the sample support itself to maintain ohmic heating. In the induction furnace facility, to be discussed in this section, both of these limitations of the wire-burning apparatus are overcome.

Induction heating was chosen rather than resistance heating for the investigation for three primary reasons: firstly, because only the load within the work coil is heated during an experiment, heating and cooling rates of several hundred Celsius degrees per minute are attainable; thus furnace down time for cooling is negligible. Secondly, because of the present state of the art in materials, resistance furnaces are limited to temperatures considerably below 2000^{o}C. In induction furnaces, however, again because only the load is heated, much higher temperatures are attainable. Finally, in certain experiments to be discussed in Chapter VII, extremely accurate temperature control is desired. Induction furnaces which are characterized by very low thermal lags are highly superior to resistance furnaces in this last category. The disadvantages of the use of induction heating in ignition experiments will be elucidated by some of the

experimental results and will be discussed in Chapter VII.

a. Apparatus Description

The complete induction furnace facility is shown in Fig. 19: the RF generator is shown at the right of the photograph, the pressure vessel housing the work coil and its control panel is at the left, and the instrumentation rack is in the center. Each of these components will now be discussed separately.

The radio frequency power supply used in the investigation was built by McDowell Electronics, Inc., of Metuchen, New Jersey. Its model number was 10KW-2DFCT/LA and its serial number was 4862. The output power of the unit was continuously variable from 1.2 to 12 KW. Two no load frequency ranges were available: 0.5 to 0.7 and 2.0 to 5.0 Mc/sec. For all of the experiments, the low frequency circuit was used.[2]

This model was equipped with a Leeds and Northup Speedomax H AZAR (adjustable zero, adjustable range) strip chart potentiometric recorder and Three Action Series 60 Control Unit. When used in the automatic control mode, this control system is specified to give automatic temperature control of $\pm$ 0.5°C at any chosen preset temperature; about $\pm$2°C was attained in the present investigation.

The design of the pressure vessel (20 atm maximum operating pressure) and its control system was

---

[2] In the higher frequency range dielectric heating becomes important and would have led to difficulties with the teflon-insulated current feedthroughs at the rear of the chamber. Also, the so-called skin effect, that is, depth of penetration of heating in the load, is inversely proportional to the square root of output frequency in use (260). Thus in order to maximize the area of heating within the samples, the low frequency RF generator was used.

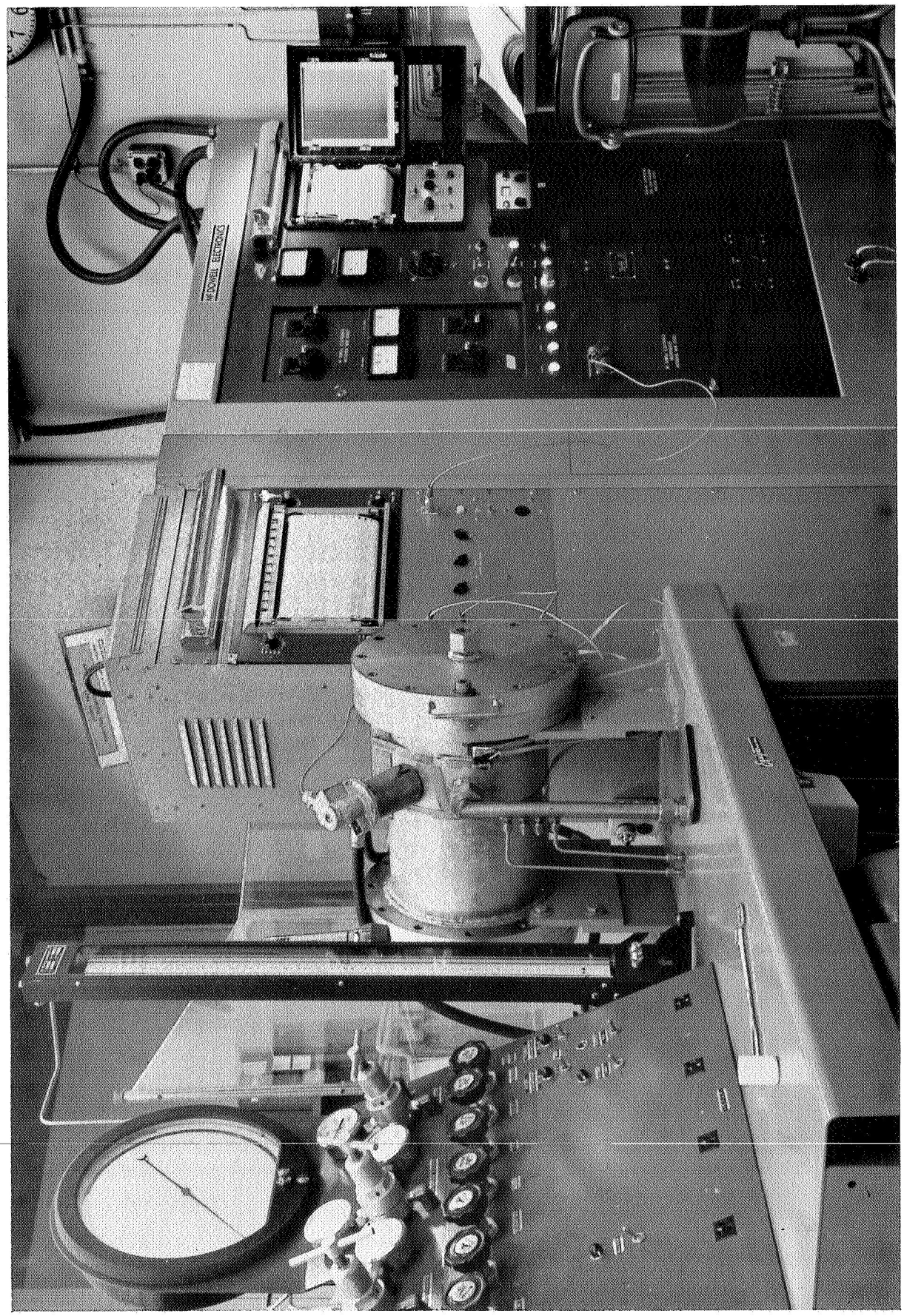

FIGURE 19

based on that of the wire-burning apparatus. A schematic is shown in Fig. 20. The test vessel, inside of which was the work coil, was larger than the vessel comprising the wire-burning apparatus so that a RF current transformer for use with a single turn work coil could be accomodated within the chamber. The cylindrical pressure chamber was of about 25 cm diameter and about 43 cm length, or about 21.3 volume. The chamber, which was contructed from steel, was lined with a 1.6 mm thick Al annulus in order to minimize coupling between the chamber and the work coil. Relatively severe coupling occurred in the area of the current feed-throughs in the back of the chamber; this and the convective and radiative heat transfer from the hot sample necessitated water cooling on the outside of the chamber to prevent overheating. The vessel leak rate was maintained low and did not affect the results. Similarly, firebrick outgasing was unimportant.

The top of the work coil was mounted in a plane 12.5 cm above the bottom of the chamber; the cylindrical coil was centered 12.5 cm from either side of the chamber, and 15 cm from the front door, in line with quartz windows on the side of the vessel. A photograph of the interior of the pressure vessel, work coil, and crucible inside the work coil is shown in Fig. 21. The thermocouple connections at the bottom of the chamber are visible in the picture.

For most of the experiments performed, a 5 1/2 turn, water cooled Cu coil was used. Depending on the particular experiment. the coil had inside diameters from 6 to 10 cm.

Two 2.54 cm diameter quartz windows were situated 15 cm from the front door on the top of the vessel, at 45° from the vertical. Upon one of these

FIGURE 20

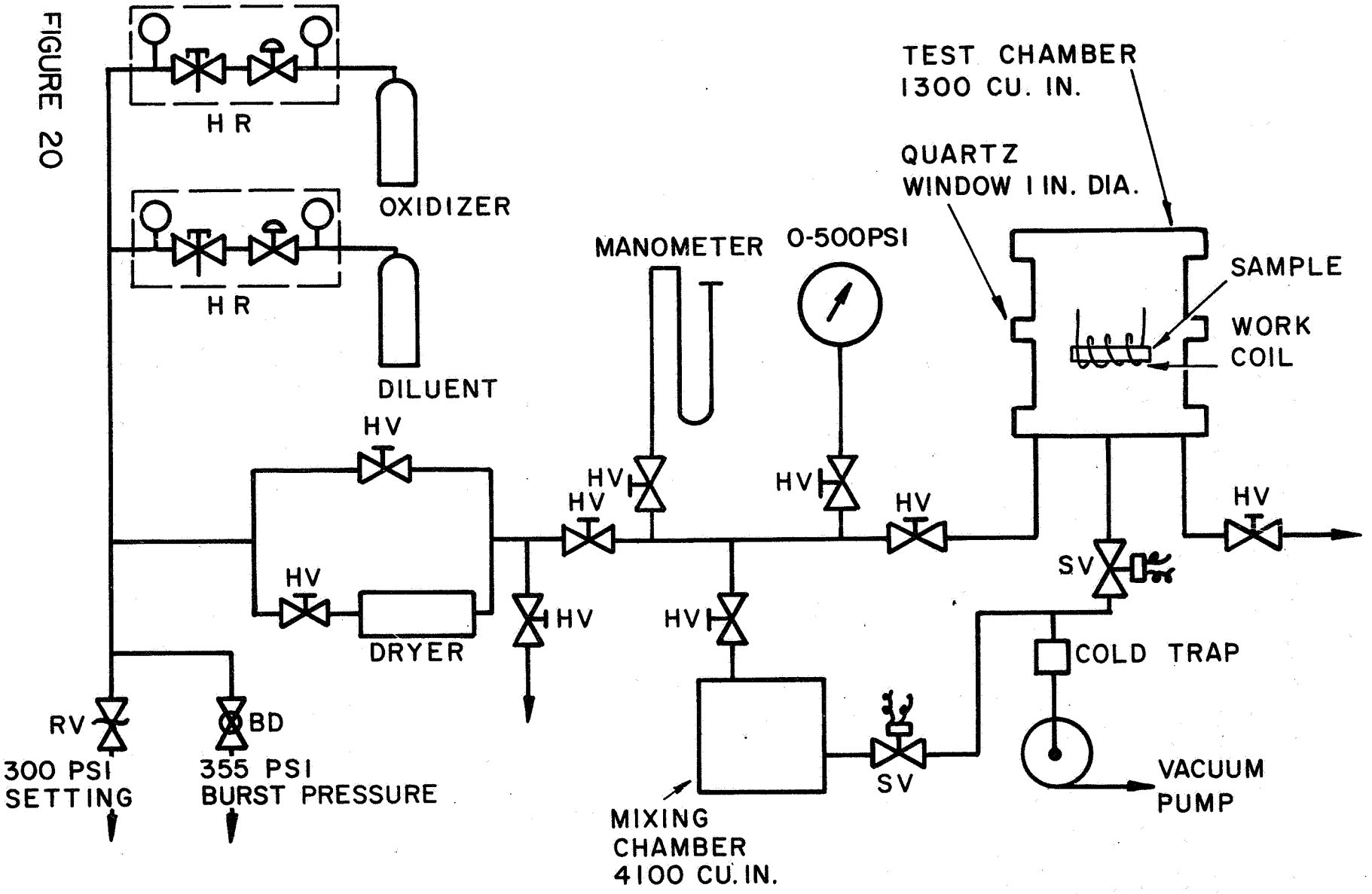

INDUCTION FURNACE FACILITY TEST APPARATUS SCHEMATIC

AP29-R4027-66

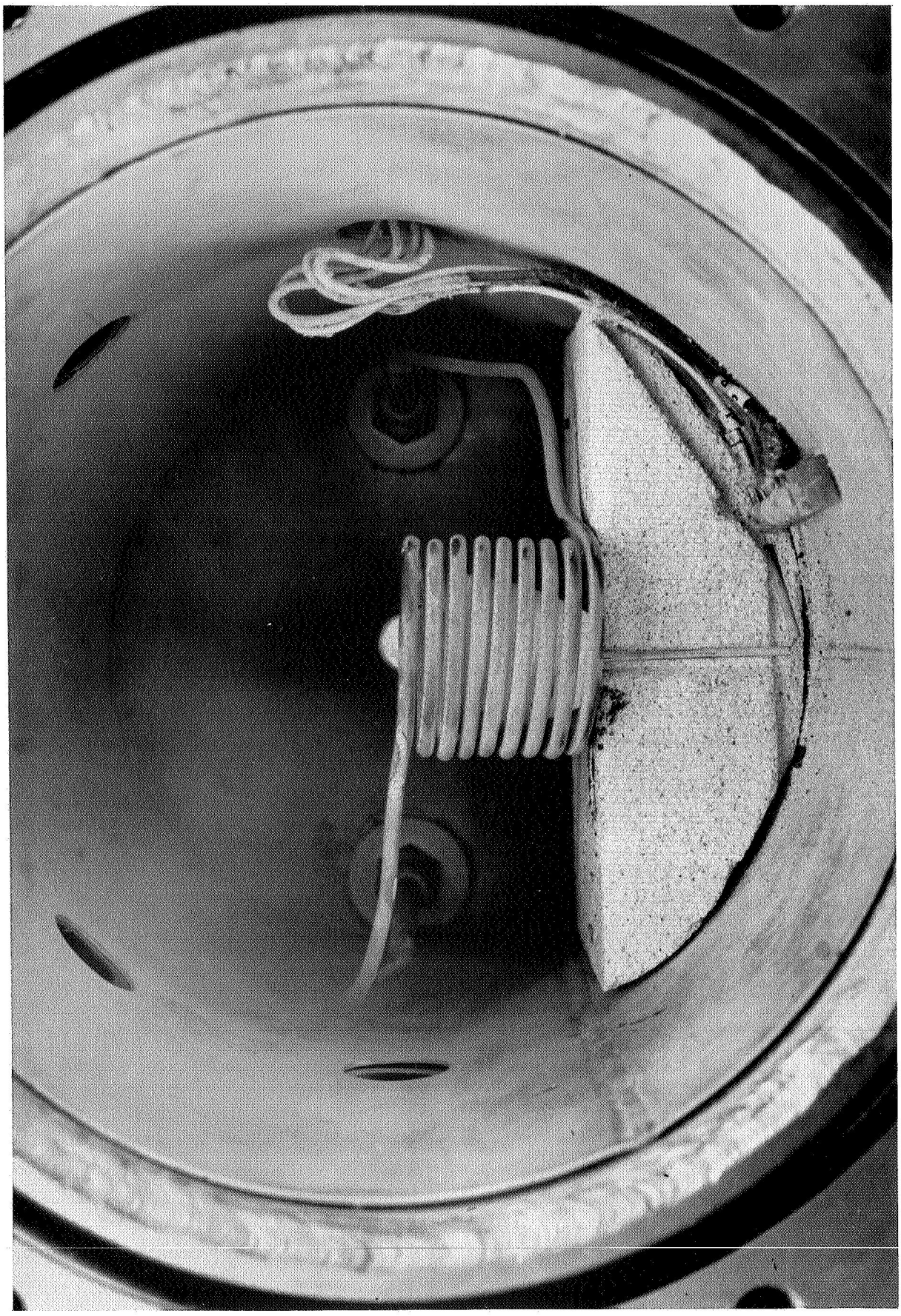

FIGURE 21

windows a Leeds and Northrup Rayotube temperature detector was mounted; the other window was used for visual observation. Windows were also placed at the center of the front and back plates.

As shown in Fig. 21, the metal sample to be heated was centered in the work coil by a suitable arrangement of fire bricks. Thermocouples mounted within the sample or to the crucible, and so forth, were connected to the appropriate type of lead wires within the chamber.

Included in the system was a mixing chamber of about 67.2 ℓ volume. When gas mixtures rather than pure gases were desired for the static test atmosphere, mixing was accomplished in the mixing chamber, which was filled to the desired pressure in the desired proportions. Mixing was accomplished by diffusion.

The schematic shown in Fig. 20 shows a gas dehumidifier in the feed system. It was a Matheson Co. Model 460 Gas Purifier. The cold trap also shown in the schematic was filled with liquid N_2 for certain of the experiments in which the test gas was removed from the chamber while hot. The cold trap served to protect the vacuum pump from any metal vapor entrained in the gas.

The primary data recording unit was a Model FSO2W6L Servo/Riter II Potentiometric Strip Chart Recorder built by Texas Instruments, Inc. Two data channels were used for recording the sample temperature as measured by a thermocouple and a Rayotube. The Rayotube was protected by a solenoid-actuated shutter which closed automatically whenever a temperature in excess of a preset value was recorded.

During the investigation of the ignition of Mg as performed in the induction furnace facility, it was

found that manual adjustment of the furnace output power in order to obtain a linear rate of rise of sample temperature (more properly, thermocouple millivolt output) was extremely difficult. Design of a differentiating circuit to be used in conjunction with the Leeds and Northrup control unit was then considered; rather than acting as a constant temperature controller, the control unit would provide a constant rate of change of temperature with time.

In principle, such a differentiating circuit would consist of simply a resistance and a capacitor (see for example Ref. (261)), but when the design specifications for the thermocouples in use, desired heating rates, and so forth were considered, it became apparent that such a circuit could not be used because capacitors in the necessary capacitance range are not available commercially. Rather, a differentiating circuit employing an operational amplifier was constructed. A block schematic of the control system is shown in Fig. 22, and the reader is referred to Ref. (261) and (262) for details of construction and operation of similar circuits.

In brief, the output voltage of a retransmitting slidewire connected to the Texas Instrument Recorder channel which was used to measure the sample temperature with a thermocouple was passed through a variable filter[3] to the differentiator. This voltage may be expressed as:

$$e_{in} = -\alpha t \qquad \text{(V-1)}$$

[3] Filtering was always necessary because of the radio frequency noise problem.

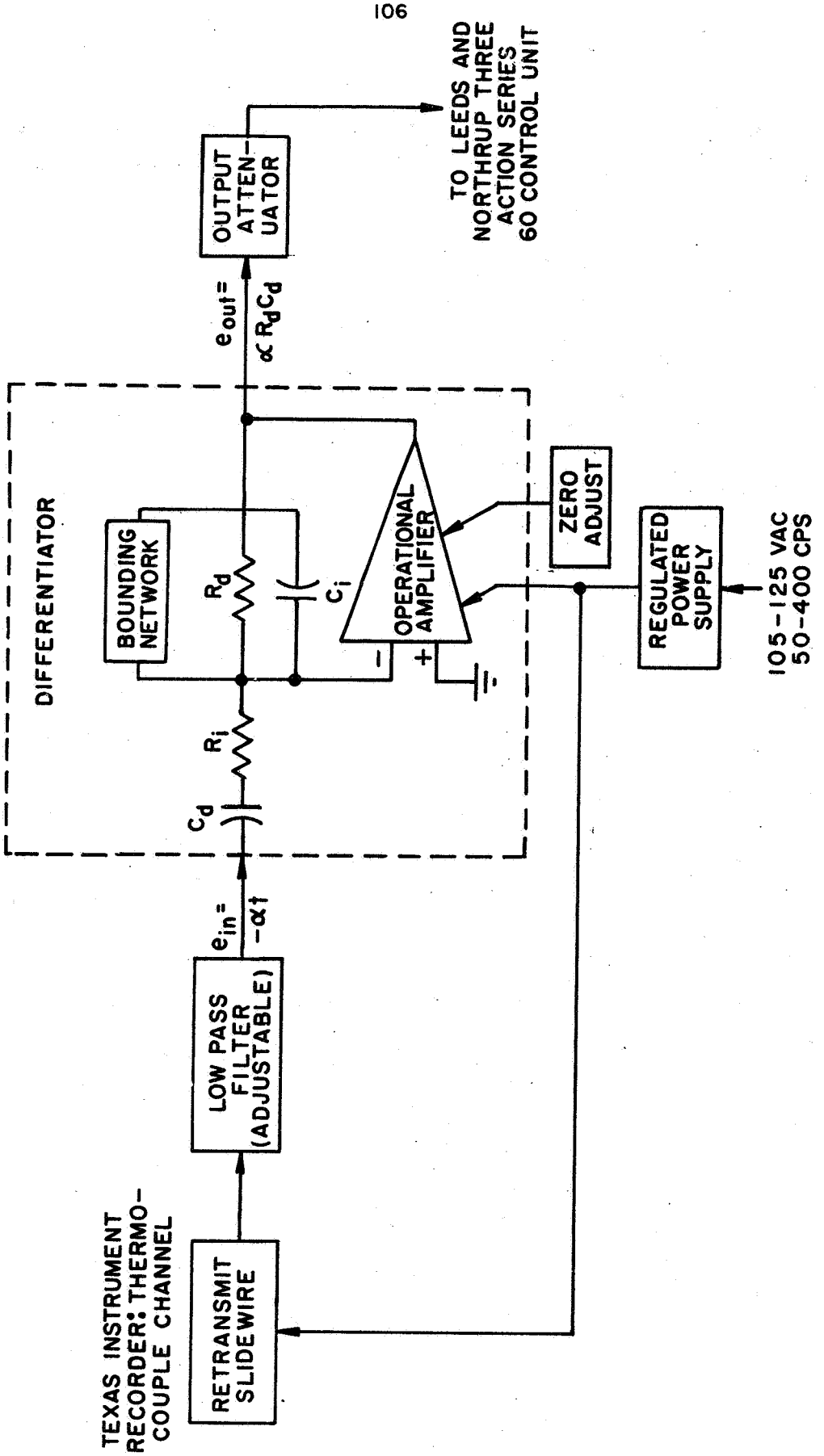

HEATING RATE CONTROL SYSTEM BLOCK DIAGRAM

FIGURE 22

AP29-4049-67

where α is the negative of the slope of the temperature-time curve. The output of the differentiator is then:

$$e_{out} = \alpha R_d C_d = -R_d C_d \frac{de_{in}}{dt} \qquad \text{(V-2)}$$

where R_dC_d is the time constant of the circuit. (The function of R_i and C_i is to provide further filtering; R_iC_i must be much less than R_dC_d to avoid allowing the circuit to act as an integrator, however.) The Leeds and Northrup controller was then used to maintain this signal constant during an experiment.

The design specifications of the unit were 0.0208 to 0.267 and 0.00865 to 0.267 percent of full scale per second on the Texas Instrument 20 and 50 mv scales, respectively. In terms of heating rates, these values represent rates at 200°C from about 10 to 200 °C/min for a chromel/alumel thermocouple, and from about 30 to 350 °C/min for a Pt/Pt13Rh thermocouple.

b. Experimental Procedure

The sample to be ignited was wiped clean and weighed. It was then placed in its crucible, and the crucible and sample were mounted within the work coil. The sample thermocouple was connected to the appropriate lead wires.

The front door of the chamber was closed and the chamber and feed system were evacuated. After a pressure on the order of 1 torr was attained in the system, the chamber was filled with the appropriate oxidizing gas or gas mixture to the desired pressure, directly from the gas cylinder or from the mixing chamber, respectively. The furnace was turned on and the experiment begun.

As soon as ignition had occurred, the furnace was turned off and the pressure vessel was purged with high pressure Ar in order to extinguish the metal fire as soon as possible. Because of this procedure, very few fires resulted in serious damage to the contents of the chamber. However, upon one occasion, in an experiment with large Mg samples in 5 atm of O_2, during the subsequent temperature rise after ignition the crucible melted, and molten Mg and/or crucible came into contact with the Cu work coil, which ignited and burned to the feedthroughs at the back of the chamber. Also, the thermocouple connectors and lead wires were destroyed. Slight redesigns including a larger inside diameter work coil and a different firebrick arrangement prevented a recurrence of this accident. Nevertheless, under the existing conditions inside of the test chamber, the furnace is not suitable for the study of metal combustion.

In an experiment after the metal fire was extinguished, the chamber was exhausted to 1 atm and opened. The sample, crucible, and the thermocouple were removed.

For convenience, the particular type of ignition experiments which were performed in the induction furnace facility will be discussed in the chapter on these experimental results, Chapter VII.

c. Auxiliary Apparatus

Throughout the Mg and Ca experiments, chromel-alumel thermocouples with an ice bath reference junction were used. When experiments were performed in which a susceptor[4] was used, the susceptor temperature was mon-

[4] A susceptor, as used in this investigation, is a hollow cylinder placed inside of the work coil, and within which the sample and crucible are placed. The susceptor couples preferentially with the magnetic field and heats the sample by conduction, convection, and radiation heat transfer.

itored with Pt/Pt13Rh thermocouples. Calibration of the thermocouples will be discussed in Chapter VII.

The Rayotube used in the Mg and Ca investigations was a Model 8893, which allows blackbody temperature measurements over the range from 450 to 1000°C. For these experiments, the Rayotube safety shutter circuit was set to trigger when a temperature in excess of 1000°C was measured.

Crucibles and double bore ceramic insulater tubing constructed from Alundum (predominantly Al_2O_3) were used for the Mg and Ca investigations. Al_2O_3 melts at 2030°C (6), and since these metals ignite at temperatures at or below 1000°C, this material was satisfactory provided that the metal fire which ensued after ignition was promptly put out.

The susceptors[4] for the Mg investigation, used in certain types of experiments to be discussed in Chapter VII, were constructed from Inconel W. The susceptors were hollow cylinders 5.1 cm long of 6.8 cm outside diameter, with 0.8 cm wall thickness. For the Ca experiments, SiC susceptors (with which higher temperatures could be obtained) 6.5 cm long, of 7 cm outside diameter,and of 0.7 cm wall thickness were used.

Finally, the firebricks upon which the sample crucible (and susceptor) rested were Type HW-30LI insulating firebricks, supplied by Harbison-Walker Refractories Co., Pittsburgh. These firebricks are adequate at temperatures up to about 1500°C.

Preliminary experimentation on the ignition of Al was conducted with W/Re, Ir/Ir60Rh, and Pt/Pt13Rh thermocouples. Better results were obtained with the latter two, as would be expected in oxidizing atmospheres. Calibrations for the first two thermocouples were supplied by Engelhard Industries, Inc., Newark.

A Model 8890 Rayotube with blackbody temperature range from 975° to 2200°C was used in the Al experiments. The safety circuit was set to close the Rayotube shutter upon attaining this latter temperature.

SiC crucibles supplied by the Norton Company, Worcester, Mass., were used in the preliminary experiments with Al. As will be discussed in Chapter VII, this material was found to be inadequate at the required temperatures (about 2000°C; see Chapter IV). Finally, ZrO_2 firebricks also obtained from Norton were used.

4. Miscellaneous

Most of the still photographs in this report were taken with a 4x5 view camera upon which a Polaroid film holder was mounted. The film generally used was Polaroid Type P/N 55.

Flame spectrograms were obtained from a Bausch and Lomb 1.5 m grating spectrograph, Model No. 11, which in first order covers the spectrum from 3700 to 7400 Å with a linear dispersion of 15 Å/mm. Depending on the flame brightness, Kodak 1-N spectroscopic film, Royal-X Pan, or 2475 recording film was used. The negatives were analyzed on a Leeds and Northrup microdensitometer of the Knorr-Albers type.

5. Summary

Basically two types of experiments were performed: firstly, the qualitative wire-burning experiments, and secondly, the quantitative induction furnace experiments. The wire-burning studies of the ignition of Mg ribbons and Al wires will be described in Chapter VI. The induction furnace results with variously sized samples of Mg, Ca, and Al are given in Chapter VII. The combustion of Mg ribbons and Al wires in H_2O containing mixtures will be discussed in Appendix I.

As mentioned in Chapter IV, other studies conducted with the wire-burning apparatus (the ignition and combustion of wires of Ta and Mo, and improved ignition efficiency for Al) are reported elsewhere (247-249).

CHAPTER VI - QUALITATIVE STUDIES OF THE IGNITION OF MAGNESIUM RIBBONS AND ALUMINUM WIRES

The experimental results obtained in this and earlier investigations on the ignition of Mg ribbons and Al wires are divided into two sections: early experimental results on the ignition of Mg ribbons and Al wires in O_2-Ar and O_2-CO_2 mixtures (7, 9, 19, 20), and the original development of the physical model of metal ignition (21); and subsequent qualitative investigations of the ignition of Mg ribbons and Al wires in H_2O-containing atmospheres. These findings are reviewed in the present chapter. A description of the combustion of Mg ribbons and Al wires in H_2O-containing gas mixtures is given in Appendix III.

1. The Ignition of Magnesium and Aluminum in Oxygen-Argon and Oxygen-Carbon Dioxide Mixtures and the Original Model of Metal Ignition

It was stressed in Chapter V that the information obtained from the wire-burning apparatus with respect to ignition is necessarily qualitative. Thus the interpretation of the ignition results is based primarily on visual observation and on a relative experimental datum, the total power at ignition. This power is relative because it includes many extraneous factors due to the electrodes, and so forth. Nevertheless, as the original version of the physical model of metal ignition was based on this type of data, the wire-burning apparatus can yield meaningful information on the ignition process.

The first investigation in the wire-burning apparatus was that of Brzustowski (7, 9). He studied the combustion of Mg ribbons and of unanodized and anodized Al wires in O_2-Ar mixtures over wide ranges of pressure and

and composition. In a corollary investigation, Mellor studied the combustion of these same metals in O_2-CO_2 and CO_2-Ar mixtures over a smaller pressure range (19, 20). Several important observations on the ignition characteristics were made in both of these investigations.

a. Magnesium

In both of the investigations, the Mg ribbons were mounted horizontally between the brass electrode blocks. In O_2-Ar mixtures (7, 9), ignition generally occurred in a cylindrical vapor-phase flame before the ribbon broke. Under some circumstances, flame spread along the ribbon occurred at the speed of several cm/sec. Where flame spread did not occur, the initial vapor-phase ignition flame collapsed when the metal melted and the ribbon broke.

Several differences in the ignition of Mg ribbons in O_2-CO_2 and CO_2-Ar mixtures were noted (19, 20). Firstly, Mg ignited over a much more limited range of pressure and composition in O_2-CO_2 mixtures, and could not be ignited in CO_2-Ar mixtures. Secondly, in the no ignition regime (or, more properly, in the regime in which flame spreading did not occur), rather than appearing as a cylindrical vapor-phase flame before the ribbon broke, the initial ignition flame seemed to take place in the gas phase near the metal exposed when the ribbon broke. This significant difference between the mode of ignition in O_2-Ar and O_2-CO_2 mixtures was attributed to the formation of a protective product film on the surface of the ribbon in O_2-CO_2 mixtures.

Furthermore, two observations indicated that the ignition temperature of Mg is higher in O_2-CO_2 mixtures than in O_2-Ar mixtures: as is seen in Table 32, which is

TABLE 32.

AVERAGE EXPERIMENTAL POWERS AT IGNITION (FROM REF. (21))

Metal	Atmosphere	Average Power at Ignition, watts	Reference
Mg	O_2-Ar	23.1	(263)
	O_2-CO_2	30.2	(19)
Anodized Al	O_2-Ar	145.3	(263)
	O_2-CO_2	174.1	(19)
	CO_2-Ar	125.1	(19)
	H_2O-Ar	131.3	
	H_2O-CO_2	131.6	
Unanodized Al	O_2-Ar	195.4	(263)
	O_2-CO_2	193.3	(19)
	CO_2	106.5	(19)

repeated from Ref. (21), the average total power at ignition was higher in the former case; secondly, for those cases for which ignition did not occur in the former atmosphere, part of the ribbon had been observed to melt.

To conclude, two important observations were made on the ignition of Mg ribbons. In O_2-Ar mixtures, ignition occurred below the metal melting point in a cylindrical vapor-phase flame over the ribbon; in O_2-CO_2 mixtures, vapor-phase ignition occurred at or above the metal melting point near the clean metal surfaces exposed upon the ribbon's breaking. These observations are consistent with the Mg ignition temperatures listed in Table 14.

b. Aluminum

Brzustowski concluded that ignition of either unanodized or anodized Al wires in O_2-Ar mixtures, above a

total pressure of 300 torr, occurred at the melting point of Al_2O_3 (7, 9). This observation was independent of whether the wire was mounted horizontally or in the "L" configuration. Ignition occurred when molten Al was exposed to the oxidizing atmosphere at the melting point of the oxide.

At and below total pressures of 300 torr, the anodized wire ignited at somewhat lower temperatures, and the unanodized wire generally did not ignite.

In general, over the entire pressure range, it was noted that the anodized wires were characterized by a lower total power at ignition (7), as is shown in Table 32. On this basis, Brzustowski concluded that the anodic oxide film impeded oxidation during the pre-ignition heating period, and that at ignition a thicker oxide film was present on the unanodized wire (7).

No significant differences between the ignition of either unanodized or anodized Al wires in O_2-Ar and O_2-CO_2 atmospheres was found (19, 20). However, it was observed that unanodized Al wires could not be ignited in CO_2-Ar mixtures. Again, the total power at ignition in O_2-CO_2 mixtures was considerably lower for the anodized wire, which indicated the presence of a thinner oxide coat at ignition.

In CO_2-Ar mixtures at total pressures below about 500 torr, a new type of ignition was observed with the anodized Al wires (19, 20). Before the wire broke, a cylindrical vapor-phase ignition flame was observed to appear over the wire surface. Such an ignition flame is shown in Fig. 23, which is reproduced from Ref. (19) and (20).

It was originally concluded that the anodized Al coating was porous to Al vapor diffusion, even after

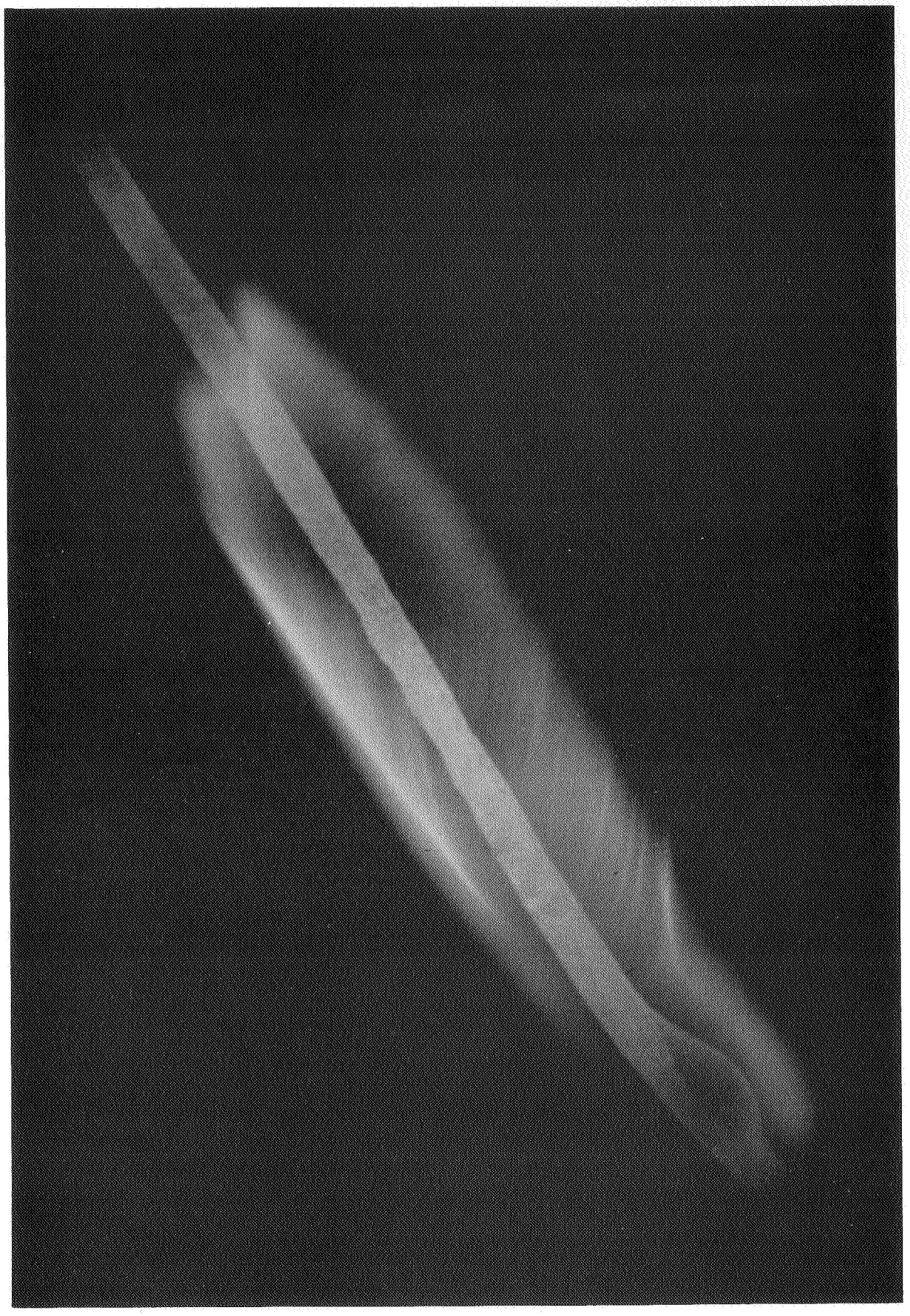

FIGURE 23

the pre-ignition heating period in CO_2-Ar atmospheres (19). When it was later learned that the anodized film was indeed porous, as was described in Chapter V, this conclusion was substantiated, and it was argued that in O_2-containing atmospheres these pores were filled by the oxidation process during the ohmic heating period (21). In other words, at ignition in O_2-CO_2 mixtures the structure of the anodized and thermal Al_2O_3 films was similar, but on the basis of the total power required for ignition, the latter was a thicker film; in CO_2-Ar mixtures, the unanodized wires could not be ignited because insufficient oxide formed below the metal melting point to support the molten Al. A sufficiently thick film already existed on the surface of the anodized wire to allow ohmic heating to continue above the metal melting point, but because most of this anodized coating was porous and because little oxidation occurred during the pre-ignition period in CO_2, ignition occurred in a cylindrical vapor-phase flame, before the wire broke at the melting point of the oxide.

In a later paper (21), it was suggested that even in this latter case, the ignition temperature was equal to the melting point of Al_2O_3, but that only the thin barrier layer between the outer porous layer and the metal substrate (see Chapter V) was required to melt before ignition could occur. Because the total power at ignition for the anodized wire was lower in CO_2-Ar mixtures than in O_2-Ar or O_2-CO_2 mixtures (see Table 32), the requirement that only the thin barrier layer melt before ignition was further substantiated.

To summarize, ignition in O_2-containing atmospheres for both the unanodized and anodized Al wires occurred on metal freshly exposed at the melting point

of the oxide. The higher ignition power requirement of the unanodized wire was taken to indicate the presence of a thicker oxide film in this case.

Only the anodized Al wires could be ignited in CO_2-Ar mixtures because insufficient oxide formed on the unanodized wire during the ohmic heating period to mechanically support the molten Al above its melting point. For these anodized wires, ignition in the form of a cylindrical vapor-phase flame before the breaking of the wire was due to the porous nature of the anodized film. The lower power requirement over that in O_2-containing atmospheres indicated that a thinner oxide film was melting prior to ignition, and it was surmised that this thinner film was the non-porous barrier layer film present next to the metal substrate on the anodized wire, that is, even in CO_2 atmospheres the transition temperature equals the melting point of Al_2O_3.

The results on the ignition of Al in O_2-Ar mixtures are consistent with those of Kuehl (17, 18), who also studied the ignition of Al wires in an apparatus similar to that developed at Princeton.
This investigator found that the ignition temperature of Al decreased below an oxygen partial pressure of about 50 torr (see Appendix I). However, he also found the appearance of the cylindrical vapor-phase ignition flame even in O_2-Ar atmospheres, but at total pressures less than about 250 torr.

Kuehl associated the appearance of this type of ignition flame in O_2-Ar mixtures at low pressures with those pressures at which the boiling point of Al is less than or equal to the melting point of Al_2O_3; these temperatures are equal at a pressure of about 250 torr (17, 18). Thus it is interesting to note that the appearance

of this flame in CO_2-Ar atmospheres before the breaking of the wire, which was observed at pressures of 300 torr and below (19, 20), may also be a result of the melting point of Al_2O_3 exceeding the boiling point of Al,[1] in addition to resulting from the porosity of the surface coating. Thus the transition temperature may decrease with decreasing pressure below about 300 torr.[2]

c. The Original Model of Metal Ignition

The experimental results obtained in the wire-burning apparatus discussed in Sections 1.a and 1.b of this chapter were the essential basis of the physical model of metal ignition as originally developed for bulk samples (21). As mentioned in Chapter I, these results were summarized in Fig. 1, which is taken from Ref. (21). Data obtained in H_2O-containing atmospheres will be discussed in detail in Section 2 of this chapter.

As can be seen from Fig. 1, the mode of ignition (that is, the cylindrical vapor-phase ignition flame appearing before breaking of the metal sample versus the ignition flame near the fresh metal surface exposed by the breaking of the sample) was correlated with the Pilling and Bedworth ratio (V_f/V_m) of the product film present on the surface of the sample during the pre-ignition heating period. In the former case, for Mg ribbons in O_2-Ar atmospheres and for anodized Al wires in mixtures not containing O_2, the value of this ratio was thought to be less than one, that is, the product film was thought to be non-protective.

---

[1] Gordon (264) originally offered this explanation of the cylindrical vapor-phase ignition flame in CO_2-Ar mixtures at low pressures.

[2] Recent experimental studies at Princeton have favored this second interpretation (265).

In the latter case, for Mg ribbons in O_2-CO_2 mixtures and for both types of Al wires in O_2-containing atmospheres, the Pilling and Bedworth ratio was thought to be greater than one, thus indicating a protective product film.

Since the total power at ignition was characteristically lower for the cylindrical vapor-phase mode of ignition (Table 32), the presence of a non-protective product film with a Pilling and Bedworth ratio less than one was concluded to indicate that ignition would occur more readily for those metal-oxidizer systems forming this type of film.

However, when the oxidation literature for the Mg-O_2 system was examined, it was learned that even though the room-temperature Pilling and Bedworth ratio of MgO is less than one, the oxide film is protective (as indicated by the so-called protective rate laws) up to temperatures on the order of 400°C (as has been shown in Chapter III). Furthermore, even though the majority of the anodic film on the anodized Al wires was porous and thus non-protective, ignition was not thought to occur until the non-porous barrier layer melted. Thus the elementary concept of the Pilling and Bedworth ratio as indicating a non-protective oxide film could be misleading, and the concept of the transition temperature, at which any product film becomes non-protective regardless of its room-temperature Pilling and Bedworth ratio, was introduced and correlated with the bulk ignition temperatures of Mg, Al, Ca, and Mo in O_2, as measured by other investigators.

This was essentially the development of the ignition criterion based on early wire-burning results, as reported in Ref. (21). As has been seen in the previous chapters of the present report, the model has been de-

veloped to a much greater extent since that time, and now is in a position to explain metal pyrophoricity (that is, the size effect in ignition) and to predict means of improving the ignition of metals characterized by high transition temperatures. Furthermore, the literature verification of the model has been extended to many other metal-oxidizer systems.

Since this development of the original model, further experimentation has been conducted with Mg ribbons and unanodized and anodized Al wires in H_2O-containing atmospheres, in order to verify the conclusions based on the ignition of these metals in O_2-Ar, O_2-CO_2, and CO_2-Air mixtures. These later results will be discussed in the next section of this chapter.

2. The Ignition of Magnesium and Aluminum in Atmospheres Containing Water Vapor[3]

These experiments were performed primarily because it was felt that if the conclusions reached on the ignition of Mg and Al in CO_2 were valid, then similar results would be obtained in H_2O, as opposed to O_2-containing mixtures.

As was stated in Chapter V, the maximum partial pressure of H_2O obtained conveniently in the wire-burning apparatus was 100 torr; thus the test points of interest were somewhat different than in the dry gas mixtures. For Mg ribbons and Al wires, the wet atmospheres which were used were as follows: pure H_2O at 50 and 100 torr, and 50 volume percent-50 volume percent mixtures of H_2O-O_2, H_2O-CO_2, and H_2O-Ar at total pressures of 50, 100, and 200 torr.

---

[3]Brief descriptions of the combustion of these metals in H_2O are given in Appendix III.

a. Magnesium

It is shown in Appendix II see in particular Table 14) that the ignition temperature of bulk Mg samples in O_2 and H_2O is slightly below the metal melting point of 650°C (6), whereas that in CO_2 is considerably above the metal melting point. Thus in the wire-burning apparatus, in which the sample must support itself in order to maintain ohmic heating, some irreproducibility in ignition would be expected in H_2O and in O_2 atmospheres, and ignition in CO_2 atmospheres would be expected to be difficult or even impossible.[4] These expectations were borne out in the present experiments as is shown in Table 33, in which the Mg ignition reproducibility in the various H_2O mixtures is given.

In H_2O-Ar and H_2-O_2 mixtures the ribbons generally ignited before they broke, as expected; the ignition and breaking events could not be distinguished in H_2O-CO_2 mixtures. All of these results are consistent with the ignition criterion and with the results of other investigators as cited in Appendix II and Chapter IV.

The average total power at ignition or breaking for Mg in the three gas combinations is shown in Table 34. The breaking power in H_2O-CO_2 mixtures exceeds the ignition power in the other gas combinations, as was the case in O_2-CO_2 mixtures as compared to O_2-Ar mixtures (see Table 32). Note that the powers listed in Table 34 are low compared with those in Table 32. Part of this discrepancy no doubt results from the different apparatus used in the two

[4] In experiments involving gas mixtures not cited in Appendix II, Darras et al. (211) showed that in even slightly humid CO_2 the Mg ignition temperature is lowered considerably and becomes on the order of the Mg melting point. Thus in the H_2O-CO_2 mixtures used in the present investigation some ignitions were expected.

TABLE 33.

REPRODUCIBILITY OF MAGNESIUM IGNITION

Atmosphere	Total Pressure, torr	Number of Experiments	Percent Ignited
H_2O	50	5	60
	100	5	80
H_2O-Ar	50	5	60
	100	16	75
	200	5	20
H_2O-O_2	50	7	71
	100	8	88
	200	3	100
H_2O-CO_2	50	5	40
	100	5	0
	200	5	0

TABLE 34.

AVERAGE EXPERIMENTAL POWERS AT IGNITION OR BREAKING

Metal	Atmosphere	Average Power at Ignition or Breaking, watts
Mg	H_2O-O_2	16.7
	H_2O-Ar	24.4
	H_2O-CO_2	25.8*
Unanodized Al	H_2O-O_2	59.5*
	H_2O-Ar	45.8*
	H_2O-CO_2	44.4*
	Ar	44.8*
Anodized Al	H_2O-O_2	109.5
	H_2O-Ar	69.4
	H_2O-CO_2	72.2

* Breaking power.

investigations, and especially from the different power supplies and voltage rise rates. Another effect, however, is that the H_2O experiments were conducted only at pressures of 200 torr and less, whereas the earlier experiments were conducted over a larger pressure range. Since the total power at ignition or at breaking increases with increasing pressure because of increasing convective heat losses, lower powers are obtained at lower pressures.

b. Aluminum

Both unanodized and anodized Al wires were tested in the wet atmospheres listed in Section 2.a; results obtained with the former will be discussed first.

The behavior of the unanodized samples during the ohmic heating period was the same in pure H_2O, pure Ar, in the H_2O-Ar and H_2O-CO_2 mixtures, and at 50 torr total pressure in the H_2O-O_2 mixture. As the wire was heated, near the center of the wire length the metal melted and the wire broke. The wire glowed only slightly if at all. Upon examination at the termination of an experiment, the wire was found to have retained its metallic luster in all cases. As is seen in Table 34 , the average total power at breaking for atmospheres not containing O_2 was essentially equivalent.

In H_2O-O_2 mixtures at 100 and 200 torr total pressure, the wire glowed quite brightly before it broke. No ignition, however, was ever observed. Although the sample was found to have retained its metallic luster, a greater length of the wire appeared to have melted. Note that the average total power at breaking was slightly higher for O_2-containing atmospheres (Table 34).

These results are interpreted as follows, in direct analogy to the CO_2 results discussed previously:

in atmospheres not containing O_2 the surface film formed during the ohmic heating period was not sufficiently thick to support the Al once it had melted. When the wire broke and exposed molten metal, the mean metal temperature was below the appropriate critical temperature, and thus ignition was impossible.

In O_2-containing atmospheres, a similar explanation applies, except that a higher mean temperature was attained due to the higher oxidation rate, and thus thicker oxide film in the presence of O_2. The critical temperature was not exceeded before the wire broke, however.

These results are exactly equivalent to those obtained previously in O_2 and in CO_2: in the former case, the unanodized wire could not be ignited reproducibly at total pressures of 200 torr or less (7, 9), and in the latter case ignition was never observed (19, 20).

It was predicted that in H_2O mixtures not containing O_2 anodized Al wires would ignite in the cylindrical vapor-phase ignition flame previously observed in CO_2 atmospheres (21) and shown in Fig. 23. This prediction was completely substantiated as this type of ignition flame was observed in pure H_2O, H_2O-Ar, and H_2O-CO_2 mixtures at total pressures from 50 to 200 torr.

In H_2O-O_2 mixtures, however, this type of ignition flame was not observed: ignition occurred when the wire broke at the exposed metal ends. As is seen in Table 34, the average total power at ignition is considerably higher in this latter case.

The two different types of ignition were observed under the circumstances expected on the basis of the earlier experiments with O_2 and CO_2. Furthermore, similar trends in total power at ignition were obtained.

c. Summary

On the basis of the ignition criterion and the ignition literature, it was expected that the ignition of Mg in H_2O would be similar to that in O_2. CO_2 was expected to elevate the ignition temperature in combination with H_2O. The experimental results obtained with Mg ribbons in the wire-burning apparatus in various H_2O-containing atmospheres substantiated these predictions insofar as possible.

Since, like CO_2, H_2O dissociates to yield O_2 only at temperatures high compared to those below the Al ignition temperatures, the ignition of both types of Al wire in wet atmospheres was expected to be exactly equivalent to that in the various CO_2 combinations. Such was found to be the case, as unanodized Al wires could not be ignited in pure H_2O or in H_2O-Ar or H_2O-CO_2 mixtures (as in CO_2-Ar mixtures). In these three atmospheres, the cylindrical vapor-phase ignition flame was observed with the anodized Al wire (as in CO_2-Ar mixtures), but in H_2O-O_2 mixtures the anodized wires broke and then ignited (as in O_2-CO_2 mixtures).

Trends observed in total power at ignition were consistent between the earlier O_2 and CO_2 investigations and the present H_2O investigation for both the Mg ribbon and anodized Al wire. The absolute values, however, were not comparable because of the different equipment used in the investigations and because of the lower pressures of interest in the H_2O experiments.

To conclude, in this chapter some of the necessarily qualitative experimental results obtained in the wire-burning apparatus have been discussed. The early development of the model of metal ignition was demonstrated and subsequent results on the ignition of Mg ribbons and anodized and unanodized Al wires in H_2O mixtures were described.

In the next chapter is given a discussion of results obtained in the induction furnace, an experimental apparatus designed to give quantitative results and thus test the metal ignition criterion. Mg and Ca received the most study, and some experiments were performed with Al. The difficulties which curtailed the Al investigation are described in Chapter VII.

CHAPTER VII - QUANTITATIVE STUDIES OF THE IGNITION OF MAGNESIUM AND CALCIUM

1. Introduction

Qualitative results obtained in the wire-burning apparatus on the ignition of Mg ribbons and Al wires were described in the preceding chapter. Although such results can be intrepreted in terms of the physical model of metal ignition, and although these results were responsible for the original development of the model, quantitative experimentation is necessary in order to examine in detail the validity of the model. This chapter is concerned with these latter studies.

Quantitative ignition results were obtained in the induction furnace facility which was described in Chapter V. Three basic types of experiments were performed to measure ignition and critical temperatures for Mg and Ca. Preliminary experimentation with Al was accomplished.

(1) Ignition temperature experiments in which the sample and crucible were placed directly within the work coil of the induction furnace by means of an appropriate firebrick arrangement. The furnace output power was varied in such a way to give as linear a rate of change of sample temperature with respect to time as possible. Ignition was defined as the sample temperature just prior to temperature runaway, and values so obtained were compared with the thermocouple ignition temperature at the appearance of the flame, as determined by the Rayotube. The independent variables of interest in the ignition temperature experiments were the oxidizing gas composition and total pressure, sample surface area to volume ratio, and applied heating rate.

Two types of isothermal furnace or critical temperature experiments were performed; in both types a sus-

ceptor, which couples preferentially with the magnetic field of the work coil, was orientated just inside of the coil. These hollow cylindrical susceptors, within which the sample and crucible were placed, were held at a predetermined temperature in the automatic furnace control mode, to provide the isothermal furnace environment for the sample. The different types of critical temperature experiments were as follows:

(2) A critical temperature experiment in which the sample was heated in the oxidizing gas to a predetermined temperature below the ignition temperature as determined in Experiment (1) above. The susceptor temperature was maintained constant, and, after equilibrium had been attained by the sample (time zero), the variation of sample temperature was monitored. If the sample was at or above its critical temperature initially, self-heating and eventual ignition were observed. Thus ignition delay times as a function of initial sample temperature were measured.

(3) Another critical temperature experiment in which the sample was heated to initial equilibrium in an inert gas (Ar). When equilibrium was established, the chamber was evacuated and then filled with the desired oxidizing gas. Unfortunately, during the evacuation process the furnace had to be turned off in order to avoid electrical arcing between the work coil and the susceptor or sample at low pressures, and thus the sample cooled somewhat during this evacuation and refill. Furthermore, because of the differing heat transfer coefficients between the Ar and the oxidizing gas, the second sample equilibrium temperature, obtained in the oxidizing gas, was in general not equal to that attained in the inert. Further details are given later in the chapter. Again, if at this second equilibrium temperature the sample was at or above its critical temperature, it would eventually ignite.

The major difference between critical temperature experiments (2) and (3) is the thickness of oxide present at the start of the experiment at equilibrium in the oxidizing gas. In (2), since the sample was heated in the oxidizer, in principle the oxide thickness for the initial sample temperature is present. However, in (3), ideally only the room-temperature thickness is present when the oxidizer is admitted at temperature. Thus the dependence on oxide thickness of critical temperature (and ignition temperature as determined in these experiments) was examined.

Because of the time consuming nature of the critical temperature experiments, the independent variables were not varied over as wide ranges as in the ignition temperature experiments, as will be discussed further in the following sections. The applied furnace heating rate was standardized to give a sample temperature rise rate of about $50^{o}C/min$. Also, once equilibrium was established in the oxidizing gas in either type of experiment, the experiment was terminated after 1 hr. If the sample had not ignited, it was considered to be below its critical temperature; that is, the critical temperatures measured in the present experiments were defined in terms of a 1 hr ignition delay time.

Before discussing the experimental results which have been obtained on the ignition of Mg, Al, and Ca, a brief discussion will be given of the trends expected on the basis of the physical model of metal ignition for variations of the experimental parameters. To repeat, the independent variables are gas pressure and composition, metal sample size, and applied furnace heating rate. The effect of induction heating will also be examined.

The intersection of the $\dot{q}_{chem}$ and $\dot{q}_{loss}$ curves which occurs at the critical temperature is in the low

temperature regime, in which the reaction rate is kinetically controlled. The pressure dependence of this intersection may be examined as follows:

$$(\dot{q}_{chem})\big|_{T_s=T_{crit}} = (\dot{q}_{loss})\big|_{T_s=T_{crit}} \tag{VII-1}$$

$$\dot{q}_{chem} = \dot{m}Q = a(T_s)P_{ox}^{n} \tag{VII-2}$$

$$\dot{q}_{loss} = (\dot{q}_{cond,f} + \dot{q}_r) + \dot{q}_{cond,g} \tag{VII-3}$$

$$= b(T_s) + c(T_s)P_{tot}^{m} \tag{VII-4}$$

$$= b(T_s) + c(T_s)(P_{dil} + P_{ox})^{m} \tag{VII-5}$$

$$\therefore a(T_{crit})P_{ox}^{n} = b(T_{crit}) + c(T_{crit})(P_{dil} + P_{ox})^{m} \tag{VII-6}$$

where it has been assumed that the conduction heat loss into the sample, $\dot{q}_{cond,f}$, and radiation heat loss, $\dot{q}_r$, are independent of gas pressure, and where

- $\dot{m}$ = chemical reaction rate, mole fuel/cm^{2}sec;
- Q = chemical energy release, cal/mole fuel;
- $a(T)$, $b(T)$, and $c(T)$ = functions of temperature independent of pressure, cal/cm^{2}sec torr^n, cal/cm^{2}sec, and cal/cm^{2}sec torr^m, respectively;
- T_s = metal surface temperature, ^{o}K;
- $\dot{q}_{cond,g}$ = conduction heat loss into the gas (g), cal/cm^{2}sec;

p_i = total pressure (tot), or partial pressure of oxidizer (ox) or diluent (dil), torr;

n, m = pressure dependence exponents, dimensionless.

The complicated nature of the functions a, b, and c, and the uncertainty in the numerical values of the parameters which they involve preclude any further progress with Eqn. (VII-6), which gives the oxidizer pressure dependence of the critical temperature. However, the pressure dependence of the ignition temperature may also be examined.

For $T_{crit} > T_{trans}$, the equation defining the ignition temperature is Eqn. (II-55):

$$\left(\frac{\partial \dot{q}_{chem}}{\partial T_s}\right)\Big|_{T_s=T_{ign}} = \left(\frac{\partial \dot{q}_{loss}}{\partial T_s}\right)\Big|_{T_s=T_{ign}} \qquad \text{(II-55)}$$

$$\frac{\partial \dot{q}_{chem}}{\partial T_s} = \frac{\partial a}{\partial T_s} P_{ox}^n = A(T_s) P_{ox}^n \qquad \text{(VII-7)}$$

$$\frac{\partial \dot{q}_{loss}}{\partial T_s} = \frac{\partial b}{\partial T_s} + \frac{\partial c}{\partial T_s}(P_{dil} + P_{ox})^m = B + C(P_{dil} + P_{ox})^m \qquad \text{(VII-8)}$$

$$\therefore A(T_{ign}) P_{ox}^n = B(T_{ign}) + C(T_{ign})(P_{dil} + P_{ox})^m \qquad \text{(VII-9)}$$

where A(T), B(T), and C(T) are functions of temperature independent of pressure, cal/cm^{2}sec^{o}K torr^n, cal/cm^{2}sec^{o}K, and cal/cm^{2}sec^{o}K torr^m, respectively.

Again, A, B, and C cannot be calculated, but by comparison of Eqn. (VII-6) and (VII-9) it is seen that in any case the pressure dependences of the critical and ignition temperatures may be similar for metals whose bulk

ignition is controlled by the former.

The pressure dependence of the transition temperature is available only from examination of the pertinent literature on the oxidation of the particular metal-oxidizer system. Such estimates have been made in cases for which sufficient data are available and are presented in Table 13.

Other than oxidizer pressure and mole fraction, a second independent variable in the experiments is the metal sample size, or more precisely, the surface area to volume ratio of the sample. It has been shown in Chapter II that the critical temperature decreases with decreasing sample size (increasing S/V), and that therefore the transition temperature, which is independent of size (Chapter III), will become controlling in ignition. Thus for Mg, whose bulk ignition is controlled by its critical temperature (as shown in Chapter IV), as the sample size is decreased, the ignition temperature is expected to decrease accordingly to its transition temperature.

For Al, however, because it is thought that its ignition is controlled by its transition temperature (see Chapters III and IV), no size effect in ignition temperature is expected.

Finally, for Ca in O_2, in Appendix IIit was concluded that its bulk ignition is controlled by its transition temperature; no conclusion was reached for the Ca-CO_2 system as no oxidation data are available in the literature. In Section 4 of this chapter, however, it will be seen that the bulk ignition of Ca in both gases is controlled by the appropriate critical temperatures.

The dependence of transition temperature and critical temperature on applied furnace heating rate is

difficult to predict. In the case of the former temperature, since it is estimated from isothermal oxidation experiments, in which equilibrium is established, these temperatures may possibly be upper limiting values, that is, for the case of zero heating rate. As the heating rate is increased from zero, it might be expected that the transition temperature will decrease somewhat as a result of thermal gradients cracking the film at a lower temperature. However, this trend with applied heating rate is exactly the opposite of that indicated by literature studies of this effect, as discussed in Section o.c of Chapter III. As noted there, insufficient experimental evidence is available to come to a definite conclusion.

Also, the critical temperature dependence on applied furnace heating rate is not clear. Several simple cases may be imagined: for temperatures above the transition temperature, $\dot{q}_{chem}$ should be independent of applied heating rate, that is, of oxide thickness. If it is assumed that the rate of heat loss from the sample surface is independent of the heating rate at any given surface temperature, then the only effect of the increases heating rate will be to increase the magnitude of the heat input rate ($\dot{q}_{chem} + \dot{q}_{applied}$) at that T_s. Under this assumption, because the $\dot{q}_{chem}$ curve is displaced upwards and because the $\dot{q}_{loss}$ curve remains the same on the heating curve diagram (see Fig. 3c), the critical temperature intersection will move to lower temperatures as the applied heating rate is increased.

In actuality, $\dot{q}_{loss}$ will increase with increasing applied heating rate, because the central sample temperature will lag further behind the surface temperature as the heating rate is increased. Thus both $\dot{q}_{chem}$ and $\dot{q}_{loss}$, and consequently T_{crit} and T_{ign}, may increase with increasing heating rate.

For temperatures below the transition temperature, the $\dot{q}_{chem}$ curve is a function of oxide thickness (or time), and thus also of applied furnace heating rate. As can be seen from Fig. 6a, the faster the heating rate, the less will be the value of $\dot{q}_{chem}$ at a given value of T_s, and this trend may tend to cancel the increase in $\dot{q}_{applied}$.

In the more realistic case, however, in which $\dot{q}_{loss}$ increases with increasing heating rate, the trend is unclear and may go in either direction, depending on the relative displacements of the $\dot{q}_{input}$ and $\dot{q}_{loss}$ curves as functions of applied furnace heating rate.

To reiterate, the important independent variables in the ignition and critical temperature experiments performed in the induction furnace facility with Mg, Ca, and Al are oxidizer mole fraction, total pressure, sample size, and furnace heating rate. When the critical temperature controls in ignition, the oxidizer pressure trend of the critical and ignition temperatures is thought to be the same, according to the model. For the case of Mg, the ignition temperature is predicted to decrease to the limiting value of the transition temperature at a particular pressure as the sample S/V is increased. The Al ignition temperature is expected to equal the transition temperature irrespective of sample size. The latter trend is also expected for Ca in O_2 on the basis of the literature review.

If the critical temperature controls in ignition, then both $\dot{q}_{chem}$ and $\dot{q}_{loss}$ are expected to increase with increasing applied heating rate. Therefore, both T_{crit} and T_{ign} will increase with this parameter. Since below the transition temperature, however, $\dot{q}_{chem}$ decreases with increasing heating rate, and since this decrease may tend to cancel the increase in $\dot{q}_{applied}$ with increasing heating

rate, trends with heating rate are unclear in cases for which the ignition is controlled by T_{trans}.

The final experimental characteristic which must be examined before considering the experimental results is the use of induction heating. As was mentioned briefly in Chapter V, radio-frequency heating is characterized by the so-called skin effect, that is, the eddy currents which are induced in the sample by the alternating magnetic field of the work coil (and which are primarily responsible for the heating of the sample through ordinary ohmic heating) tend to concentrate near the outer edge of the sample. In the geometry used in the present investigation (a cylindrical work coil), the majority of the heating will take place near the outer circumference of the cylindrical or circular samples.

The skin effect is characterized by the depth of penetration δ, which is the depth (measured from the circumference of the sample) at which the value of eddy current per unit area has declined to 1/e of its value at the surface (260):

$$\delta = 1/2\pi\sqrt{10^{-9}\mu_r \sigma f} \qquad \text{(VII-10)}$$

where μ_r is the relative magnetic permeability, σ is the conductivity (mho/cm^3), and f is the frequency of the heating current (cps). Eqn. (VII-10) is applicable to large samples in large cylindrical coils, as the heat distribution is a strong function of the relation between axial coil length and axial sample length (266).

For the non-ferrous metals studied in the present investigation, the relative magnetic permeability will be

on the order of one; as mentioned in Chapter V, the no load frequency range of the low-frequency oscillator of the ratio-frequency generator is 500 to 700 kilocycles per second. Taking a frequency of 5×10^5 cps and a conductivity of 2×10^5 mho/cm^3 (typical for Mg, Al, or Ca at room temperature; obtained from resistivity data listed in Ref. (5)), the depth of penetration δ may be calculated from Eqn. (VII-10) to be on the order of 0.1 or 0.2 mm. Thus in the induction furnace experiments in which the sample is heated directly within the work coil, the heating is applied in a region extremely close to the outer edge of the sample. The effect of this type of heating on the measured ignition and critical temperatures will be discussed further in the following sections of this chapter.

2. Magnesium

Mg was chosen for study in the induction furnace for several reasons: firstly, as indicated in Chapter IV, this metal ignites at relatively low temperatures and thus would present no materials problems; secondly, the wealth of experimental values of ignition and critical temperatures in the literature allows comparison with the results of the present method; and finally, transition temperatures for both the Mg-O_2 and Mg-CO_2 systems are well-defined.

The ignition of Mg samples of four sizes was studied in the dry gas combinations of interest listed in Chapter V. In Table 35, the specifications for the particular samples are listed; impurity analyses of the source materials may be found in Chapter V.

The largest samples consisted of Mg cylinders of 2.38 cm diameter and 3.81 cm length and were of average S/V equal to 0.202 mm^{-1}. These cylindrical samples are

TABLE 35.

MAGNESIUM SAMPLE DESIGNATIONS

Designation	Sample Geometry	Average S/V, mm^{-1}	Source	Sample Dimensions	Thermocouple Position
MGII	cylinder	0.202	2.38 cm rod	2.38 cm diam by 3.81 cm	center of bottom
MGIV	cylinder	0.202	2.38 cm rod	2.38 cm diam by 3.81 cm	6.3 mm from top on centerline
MGV	cylinder	0.202	2.38 cm rod	2.38 cm diam by 3.81 cm	25 mm from top on centerline
MGVI	wafer	0.772	2.38 cm rod	2.38 cm diam by 1.59 mm	center of top
MGVII	0.254 mm foil	7.74	0.254 mm foil	3.34 cm diam by 0.254 mm	center of top
MGIII	0.127 mm foil	15.02	0.127 mm foil	3.34 cm diam by 0.127 mm	center of top

designated MGII, MGIV, or MGV, depending on the placement of the sample thermocouple. For the MGII samples, the chromel-alumel thermocouple extended through the bottom of the containing crucible and just touched the bottom of the sample. For the MGIV samples, a hole was drilled along the centerline of the cylinder, and the thermocouple, encased in Al_2O_3 tubing, was mounted about 6.3 mm from the top surface of the cylinder. Finally, for the MGV samples, the thermocouple was mounted about 25 mm from the top of the sample on the centerline. In all cases, the bottom edge of the samples was beveled slightly to assure that the bottom surface was in contact with the crucible.

For purposes of the S/V calculation, it was assumed that the bottom surface of the cylinder was not exposed to the oxidizing gas, and that the reaction surface

thus consisted only of the side (of 3.81 cm length) and the top surface (of 2.38 cm diameter) of the cylinder. Note that this geometrical surface area was assumed even for cases in which the sample melts before ignition, that is, for all correlations with respect to the surface area to volume ratio of a particular sample, the room-temperature value of S/V was used.

The volume of the samples was obtained by weighing each sample before an experiment and dividing by the room-temperature density of Mg, which was taken as 1.74 g/cm^3 (5).

Because of poor thermocouple contact with the sample, very few experiments were performed with the MGII samples. For those cases in which ignition occurs above the metal melting point (CO_2-containing mixtures), MGV samples were used, and for those cases in which ignition occurs at or below the metal melting point, MGIV samples were used.

A few ignition temperature experiments were performed with MGIV and MGV cylindrical samples in which two Pt/Pt13Rh thermocouples were mounted in the sample, one on the centerline and one halfway between the centerline and the outer edge, im order to examine the temperature distribution within the sample. For an MGIV sample in O_2 at a total pressure of 300 torr heated at an average initial rate of 61 $^oC/min$, a typical discrepancy during heating between the two thermocouples was 20^oC, with the side thermocouple indicating the higher value. Both thermocouples indicated ignition simultaneously as the metal sample was melting, with the centerline thermocouple recording an ignition temperature of 641^oC and the side thermocouple indicating 643^oC.

For an MGV sample in CO_2 at a total pressure of 300 torr heated at an average initial rate of 53 ^{o}C/min, a typical discrepancy during the heating below the metal melting point was 30^{o}C. During the melting of the metal, the maximum discrepancy between the two thermocouples occurred initially and was equal to 11^{o}C. Both thermocouples indicated ignition simultaneously; the centerline temperature was 788^{o}C and the side value was 786^{o}C. It was thus concluded that in terms of measuring the ignition temperature for the large Mg cylinders, placing the thermocouple on the centerline of the sample introduced an error in the measurement less than or on the order of experimental error.[1]

The RF skin effect is thought to be unimportant in cases in which the Mg samples are melting at or have melted before ignition, because reasonably uniform temperatures are expected in melting or molten Mg. Note that the smallness of the depth of penetration of the skin effect (on the order of 0.1 mm) precludes accurate temperature measurement in the zone where eddy currents are predominant.

The second type of sample, designated MGVI and of average S/V equal to 0.772 mm^{-1}, consisted of Mg wafers of 2.38 cm diameter and 1.59 mm thickness (Table 35). Again, for purposes of the geometrical surface area calculation, it was assumed that only the top and side of the wafer were exposed to the oxidizing gas. Two small holes were drilled through these samples and their crucibles, and the chromel-alumel thermocouples were mounted on the center of the top surface of the sample.

[1]Estimates of experimental error are discussed shortly.

Finally, the ignition of foils of two thicknesses, 0.127 and 0.254 mm, was investigated. The circular samples were of 3.34 cm diameter and were designated MGIII and MGVII, respectively. Because the foils were not perfectly flat, and because their curvature increased as they were heated, to calculate their surface area it was assumed that both top and bottom surface were exposed to the oxidizer. Average S/V for the 0.127 and 0.254 mm foils were 15.02 and 7.74 mm^{-1}, respectively. As for the wafers, the sample thermocouples extended through the crucible and sample and were in contact with the center of the top surface of the foil.[2]

In order to examine the surface temperature distribution on the foil and wafers, an ignition temperature experiment was conducted with a 0.127 mm foil, with Pt/Pt13Rh thermocouples mounted on the top of the sample, one in the center and one halfway between the center and the outer edge. In O_2 at a total pressure of 300 torr with a sample heating rate of 59°C, the side thermocouple led the centerline thermocouple by about 5 °C during the initial heating. Ignitions were simultaneous: the side thermocouple indicated an ignition temperature of 450 °C, and the centerline 431 °C. Experimentation was continued with one thermocouple mounted in the center of the sample.

For the wafer and foil samples, the axial work coil thickness was much greater than the thickness of the sample (the ratio was about 63 for the wafers, the thickest samples). In a geometrical situation of this type, the zone of heating of the magnetic field will not be limited to the outer circumference of the sample; rather,

[2] In preliminary experiments the thermocouples extended only through the crucibles and touched the foils on their bottom surface. When the induction furnace was turned on, the starting transient was sufficient to flip the foil out of the crucible. Thus the above method of anchoring the samples was necessary.

the top and bottom surfaces will also be heated, and the maximum heating will occur at the outer radius on the top and bottom edges of the sample (266). Thus there will be some discrepancy between the temperature in this zone of maximum heating and that indicated by the thermocouple centered on the top surface of the sample. Estimates of this error may be obtained by varying the applied heating rate, as will be discussed in later sections of this chapter. However, as ignition was taken to be that temperature just prior to the spreading flame enveloping the thermocouple, the errors in ignition temperature due to the skin effect should be slight.

All thermocouples were calibrated in situ whenever possible by observation of the metal melting point, either during the initial heating or subsequent to ignition. In some cases, a metal freezing point was also determined; for each specific size both temperatures were compared with the Mg melting point of 650^{o}C (6), and an average temperature error for each size was deduced. Note that this type of calibration includes all possible extraneous sources of error, such as induction heating of the thermocouple, lack of contact between the thermocouple and the sample, errors in recorder reading, and so forth. Throughout the Mg investigation, the average experimental error was on the order of 5 to 10 ^{o}C.

a. Ignition Temperature Experiments

For the large Mg cylinders (MGII, MGIV, and MGV), the experimental results are shown in Fig. 24: the datum from each ignition temperature experiment is plotted versus total pressure on a logarithmic scale. At least two experiments were performed at each test point, which are listed in the figure and in Chapter V. Results are

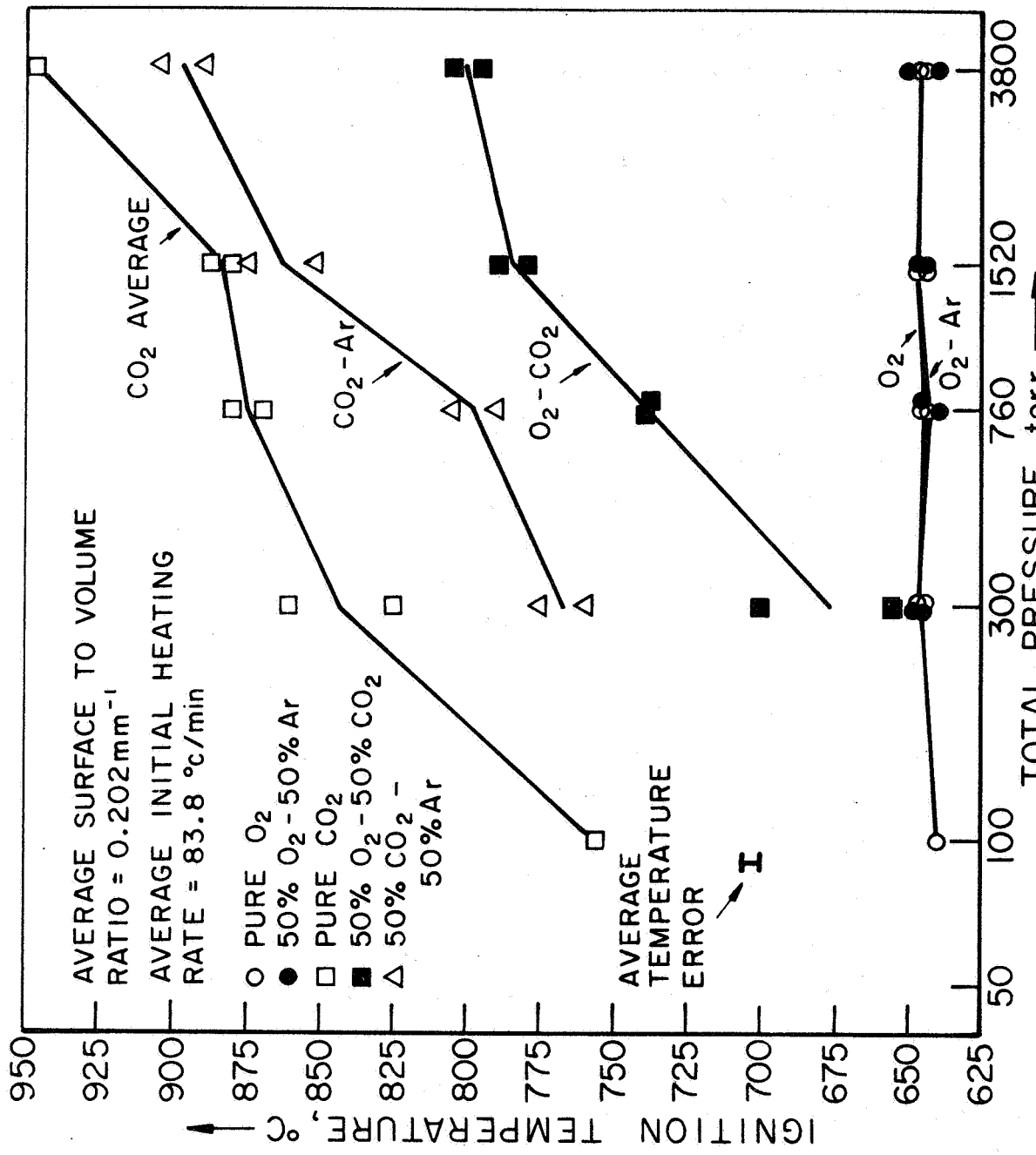

FIGURE 24

MAGNESIUM IGNITION TEMPERATURE IN VARIOUS OXIDIZING GASES VS TOTAL PRESSURE (CYLINDERS, MG II, MG IV, MG V)

AD29-R405-66

missing in some cases at total pressures of 50 and 100 torr, because arcing occurred between the turns of the work coil before the sample ignited. Also, occasionally arc-induced ignitions were observed; these data are not included in the figure.

The heavy solid lines in Fig. 24 are the average ignition temperatures as a function of total pressure in the various gas compositions, connected for convenience by straight lines between the test points. From the figure it is seen that the average temperature error (as determined by measurement of the metal melting and freezing points) for the large Mg cylinders was about 5 ^{o}C.

The average initial heating rate which is given in Fig. 24 was obtained as follows:[3] in the approximate temperature range from 50 to 300^{o}C, the sample thermocouple output was taken as linear over one minute of the heating period. Such a measurement was made for each experiment. The value reported in the figure is the average of the individual values for all the experiments performed with a sample S/V equal to 0.202 mm^{-1}. The influence of heating rate on ignition temperature will be described below.

It is seen from Fig. 24 that for the large Mg cylinders in all the oxidizing gases several well-defined trends are evident. The ignition temperature in O_2 or O_2-Ar is independent of pressure, a result of ignition

[3]The temperature differentiating circuit described in Chapter V, which when used with the furnace automatic control gave a constant rate of change of temperature, was not completed until after the completion of the Mg investigation. Thus for the Mg experiments, the temperature output was kept as linear with respect to time over the entire temperature range of interest as was possible manually.

occurring at the metal melting point of 650°C (6). It was observed that the Mg samples began to melt on their outer surface, due to the radio-frequency skin effect. Ignition generally occurred in this region, and the subsequent flame spread enveloped the sample. As the center portion of the sample near the thermocouple had not yet melted, the thermocouple indicated a somewhat lower ignition temperature. As was shown in Appendix II the fact that the ignition temperature of bulk Mg is equal to the metal melting point has not been stressed in the literature.

In CO_2-containing mixtures, ignition occurred above the metal melting point, and the ignition temperature is a strong function of pressure. This is not a result of diffusional dependence of the ignition temperature, for if the data are plotted versus the CO_2 partial pressure rather than versus the total pressure, the CO_2 and CO_2-Ar results are essentially equivalent, as is shown in Fig. 25. (The average ignition temperatures, that is, the heavy solid lines in Fig. 24, are shown in Fig. 25.) Note the inhibiting effect that CO_2 has upon the Mg-O_2 ignition, as indicated by the O_2-CO_2 results in Fig. 24.

It was noted that there was poor correlation between the thermocouple ignition temperature trends and those of the brightness ignition temperature, as measured by the Rayotube; this disagreement was observed for the other sample sizes as well. The lack of correlation is attributed to several causes: firstly, it is not possible to focus the Rayotube until the target is at a brightness temperature of 450°C; at the low temperatures encountered in the ignition of Mg, focusing was extremely

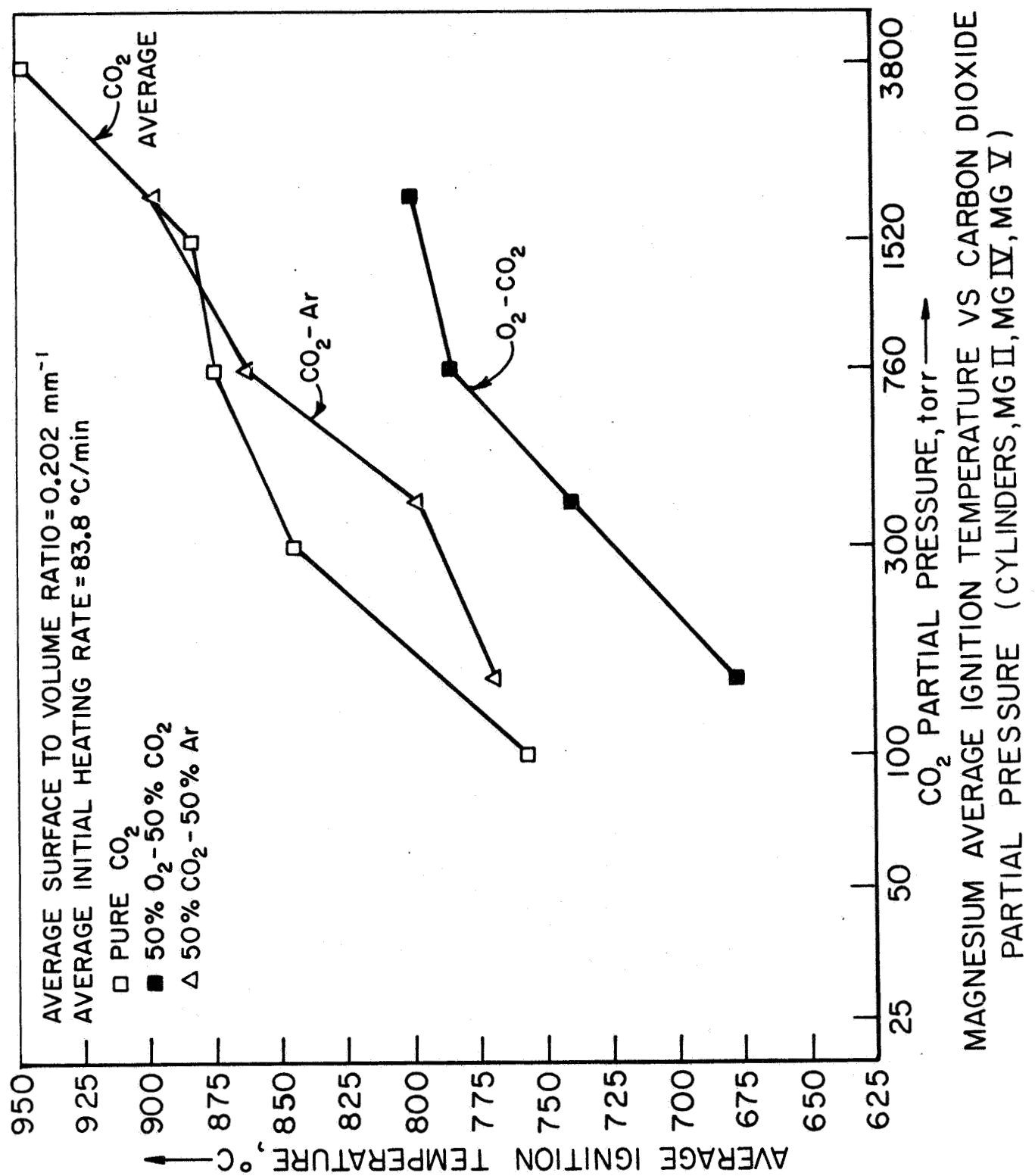

MAGNESIUM AVERAGE IGNITION TEMPERATURE VS CARBON DIOXIDE PARTIAL PRESSURE (CYLINDERS, MG II, MG IV, MG V)

FIGURE 25

AP29-4032-66

difficult. Furthermore, the placement of the sample in the work coil is critical, and although it was maintained as constant as possible, slight variations from experiment to experiment gave large variations in Rayotube viewing area, and thus brightness temperature. The nature of the metal surface near the ignition event was generally extremely unsmooth, and large oxide pustules were observed to grow in isolated areas. Thus the emissivity of the surface varied from experiment to experiment. For these reasons, little value was placed on the brightness ignition temperatures, and no attempt was made to calculate a mean emissivity for the sample surface. Therefore, for the Mg investigation, the primary use of the Rayotube was to define ignition in terms of the appearance of a flame (that is, in terms of maximum rate of change of light intensity emitted by the sample).

The thermocouple reading at this ignition temperature (flame appearance) was compared with the thermocouple ignition temperature defined by maximum rate of change of sample temperature.[4] For Mg samples of any size in any of the gas combinations over the entire pressure range of interest, the ignition temperatures as obtained by these two definitions were equivalent, within experimental error. Occasionally, with the large Mg cylinders a discrepancy was observed, but was invariably a result of the initial flame appearing out of view of the Rayotube.

The ignition temperature of the MGVI wafers in O_2 or O_2-Ar is also equal to the melting point of the metal, although the temperatures shown in Fig. 26 are somewhat lower than those for the Mg cylinders, as ignition

[4]Recall that these two definitions are those generally used to define ignition experimentally (see Chapter II).

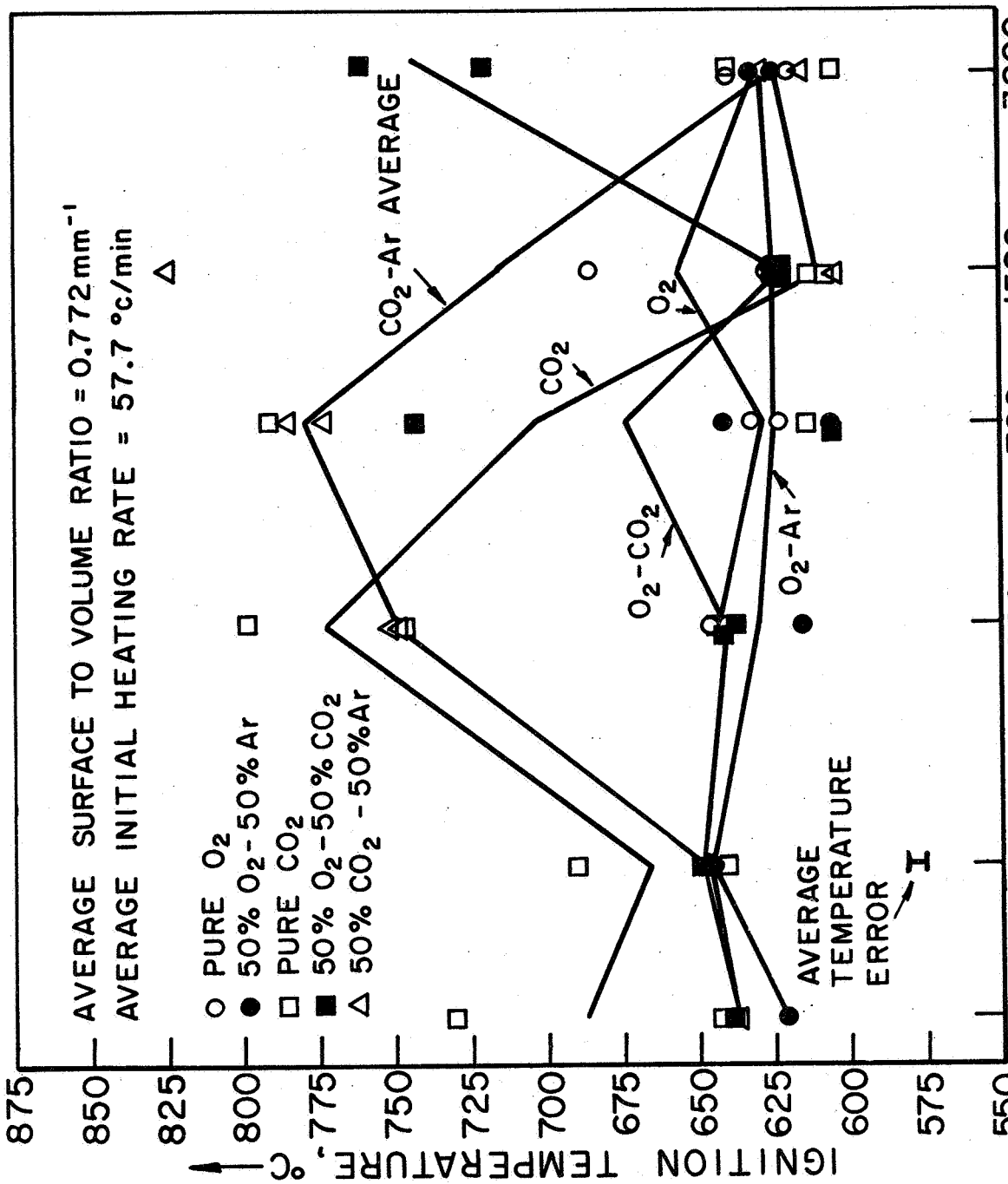

MAGNESIUM IGNITION TEMPERATURE IN VARIOUS OXIDIZING GASES VS TOTAL PRESSURE (WAFERS, MG VI)

FIGURE 26

AP29-R4028-66

occurred somewhat earlier in the melting process. Considerable scatter is evident in those results obtained in CO_2-containing mixtures, which is a result of the mode of ignition.

In pure CO_2, 50%CO_2-50%Ar, and 50%O_2-50%CO_2, during the melting of the metal occasionally bright white flashes were observed on isolated sections of the sample. In some cases, these flashes led immediately to flame spread and combustion, but in other cases, predominantly at the lower pressures investigated, ignition did not occur until well after the metal had melted. Since self-sustaining combustion must follow ignition, and since the initial occurrence of the isolated flashes did not always lead to flame, considerably more scatter was observed in the wafer results than in the cylinder results.

If the average ignition temperature for the wafers as measured in the CO_2-containing mixtures was graphed versus the CO_2 partial pressure, the same result as shown in Fig. 25 was obtained. Thus, for the wafers also the measured ignition temperatures are in the kinetically controlled regime of reaction rate.

In Fig. 27, the ignition temperatures for the 0.254 mm foil as obtained in the various oxidizing gases are plotted versus the total gas pressure. Considerable scatter is seen in the CO_2 and 50%CO_2-50%Ar results, while those of the other gas mixtures are more self-consistent. Again, the CO_2 behavior results from the anomalous type of ignition which was observed.

In CO_2 or CO_2-Ar, on some experiments the following phenomena were observed: during the initial heating process, isolated flashes and glows were observed on the outer sections of the sample surface at temperatures 50

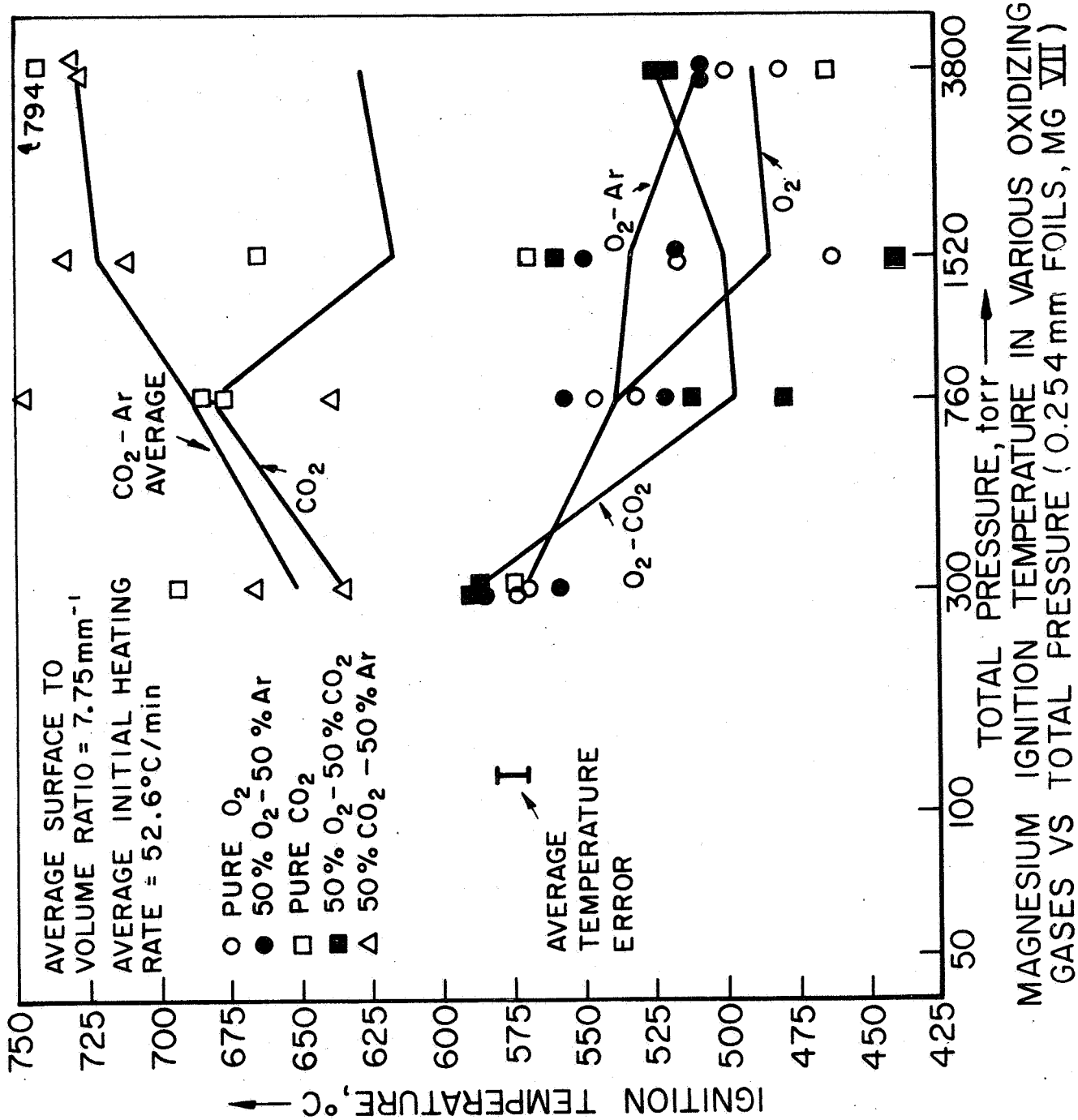

MAGNESIUM IGNITION TEMPERATURE IN VARIOUS OXIDIZING GASES VS TOTAL PRESSURE (0.254 mm FOILS, MG VII)

FIGURE 27

or 100°C below the metal melting point (Table 36). As indicated by the sample thermocouple, the temperature of the sample then dropped from a temperature roughly equal to the melting point to a temperature some 200°C below the metal melting point. As heating was continued, again flashes were observed, but over a temperature range, starting below the melting point and corresponding roughly to the temperature at which flashes were observed initially. Finally, if heating was continued further, the entire sample surface was enveloped by a self-sustaining flame at a temperature generally higher than the metal melting point (Table 36).

The occurrence of the flashes may be correlated with the attainment of the critical temperature, but only on that section of the sample at which the flash appeared. The characteristic temperature drop can be attributed to several causes: firstly, during the initial flashing, possibly enough metal was consumed that the coupling between the metal and the magnetic field of the work coil was substantially decreased; secondly, the sample may have moved during the flashing in such a way to decrease the coupling; thirdly, during the flashing the thermocouple may have moved out of contact with the sample, but the calibration with the metal melting point (Table 36) and the consistent nature of the temperature drop indicate that this explanation is unlikely.

In the critical temperature experiments to be discussed in the following section, the susceptor provided a magnetic shield for the sample, and this characteristic flashing and temperature drop phenomenon was never observed. Thus this behavior is attributed either to consumption of the metal by the rapid reaction during the flashing, or to movement of the melting Mg. This

TABLE 36.

CO_2 CONTAINING MIXTURES: FLASHING PHENOMENON

0.254 mm Mg FOILS, MGVII (AVERAGE S/V = 7.75 mm^{-1})

Mixture	Total Pressure	Run Number	Heating Rate, °C/min	Initial Flashing Temperature, °C	Sample Thermocouple Drop, °C From	To	Flashing Range, °C	Flame Ignition Temperature, °C	Metal Melting Point, °C
Pure CO_2	300 torr	1	55	586	605	522	560-667	693	---
		2	34	574	---	---	---	574	---
		3	14	576	646	540	593	724	636
		4	110	608	624	580	594-653	706	632
	1 atm	1	54	575	633	558	605-655	672	635
		2	47	555	635	589	589-634	684	646
	2 atm	1	49	540	610	437	440-487	569	645
		2	45	545	628	522	525-628	664	---
		3	13	547	619	575	593-646	776	646
		4	96	551	635	558	595-635	696	---
	5 atm	1	58	531	694	394	378-429	462	576
		2	47	494	621	593	621-628	792	---
50% CO_2-50% AR^2	300 torr	1	66	583	643	566	610	635	635
		2	75	618	621	561	---	671	---
		3	16	607	---	---	---	607	---
		4	113	652	681	619	616-628	645	652
	1 atm	1	71	578	637	548	589-710	747	659
		2	95	546	640	561	587-605	633	---

TABLE 36, concluded

Mixture	Total Pressure	Run Number	Heating Rate, °C/min	Initial Flashing Temperature, °C	Sample Thermocouple Drop, °C From	To	Flashing Range, °C	Flame Ignition Temperature, °C	Metal Melting Point, °C
	2 atm	1	65	555	635	503	575-605	605	647
		2	55	558	671	530	546-581	711	668
		3	9	560	640	546	569-677	709	619
		4	142	534	665	520	546-588	602	---
	5 atm	1	41	538	629	558	558-628	730	645
		2	47	544	655	551	539-579	731	653
50% O_2- 50% CO_2	300 torr	1	48	586	---	---	---	586	645
		2	60	587	---	---	---	587	---
		3	193	532	---	---	---	532	---
		4	7	560	---	---	---	560	652
	1 atm	1	44	513	630	388	392-511	511	667
		2	53	479	---	---	---	479	---
	2 atm	1	66	559	---	---	---	559	---
		2	55	539	659	389	392-416	437	---
		3	15	537	---	---	---	537	---
		4	130	516	---	---	---	516	---
	5 atm	1	26	526	---	---	---	526	---
		2	39	541	639	538	450-506	511	---

phenomenon will be discussed further in the section concerned with the effect of applied heating rate on ignition temperature.

The average ignition temperature obtained in the O_2-containing gas mixtures is plotted versus the O_2 partial pressure in Fig. 28. The correlation is excellent, again indicating that the portion of the appropriate $\dot{q}_{chem}$ curve at which ignition occurs is in the kinetically controlled regime. In Fig. 29 a similar plot is shown for the CO_2-containing mixtures; the indicated disagreement between the CO_2 and CO_2-Ar results may be attributed to the anomalous nature of the ignitions as discussed previously, rather than to a diffusional dependence of ignition temperature.

Finally, ignition temperature results for the MGIII 0.127 mm foils are shown in Fig. 30. Reproducibility is excellent, and consistent results are obtained with the other sample sizes, particularly with respect to oxidizer partial pressure dependence.

Observation of the combustion of all sizes of Mg samples was cursory because, as noted in Chapter V, it was desirable to extinguish the fires as soon as possible after ignition in order to avoid damage to the interior of the test vessel. Generally, however, in O_2, O_2-Ar, and O_2-CO_2 mixtures, the samples burned with a white flame which was too brilliant to resolve any structure with the naked eye. In CO_2 and CO_2-Ar mixtures, the flame was much more dim and sometimes orange-colored. Flame-spreading was much slower in this case, and at times several well-defined flamelets occupied the surface simultaneously.

The products of combustion in the O_2-containing mixtures were predominantly white, and great quantities of white smoke were produced during the reaction. In the

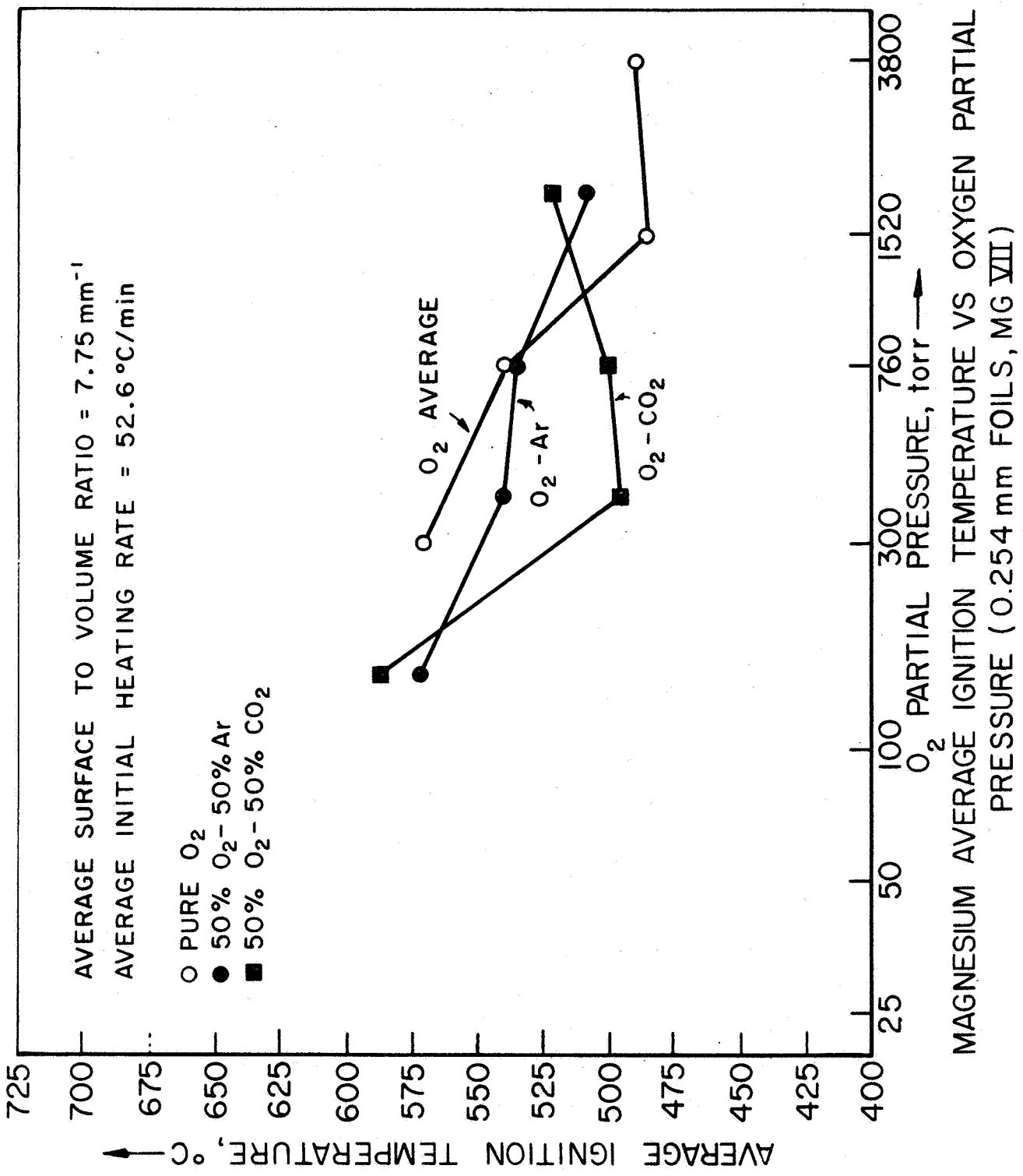

FIGURE 28

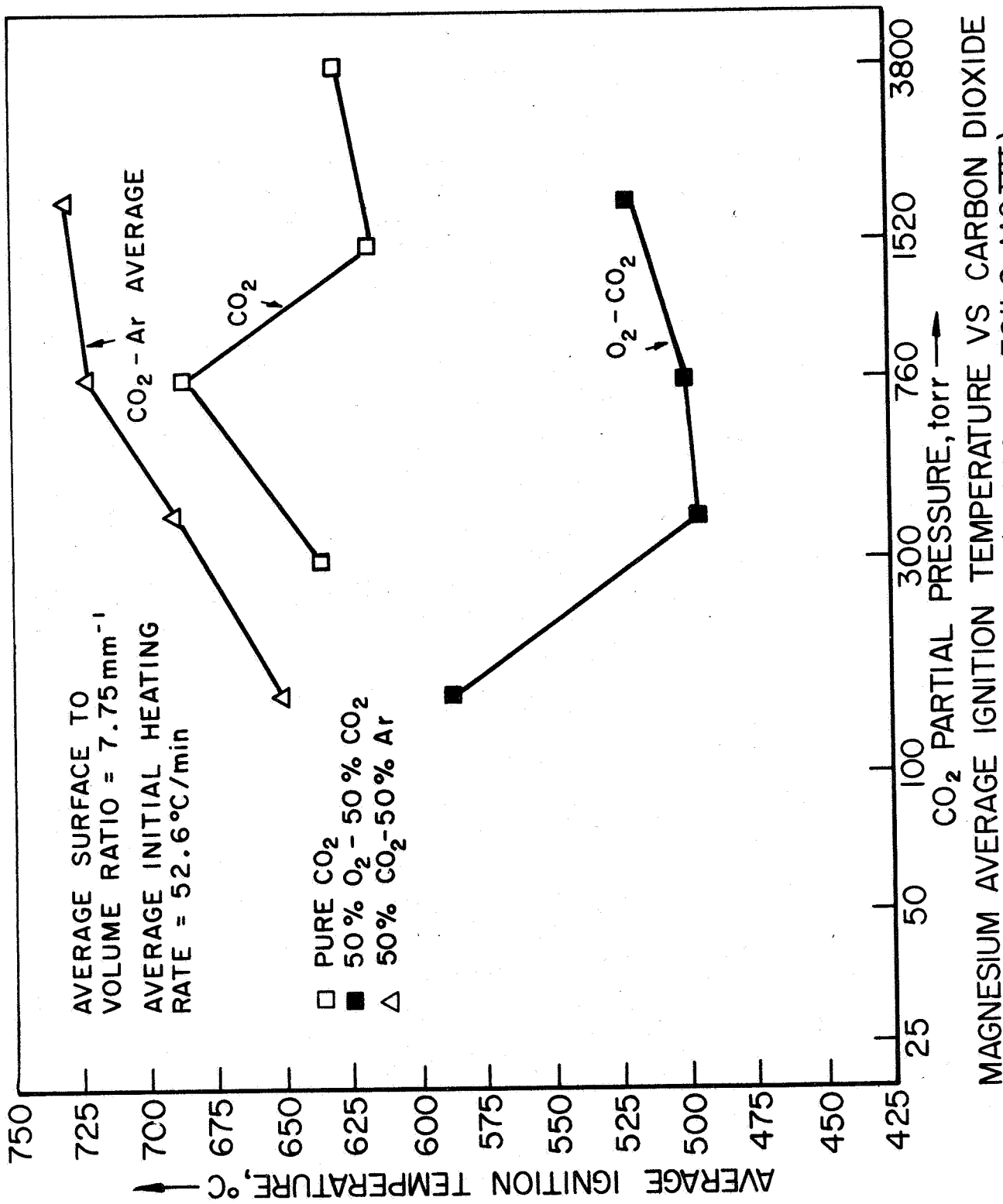

MAGNESIUM AVERAGE IGNITION TEMPERATURE VS CARBON DIOXIDE PARTIAL PRESSURE (0.254 mm FOILS, MG VII)

FIGURE 29

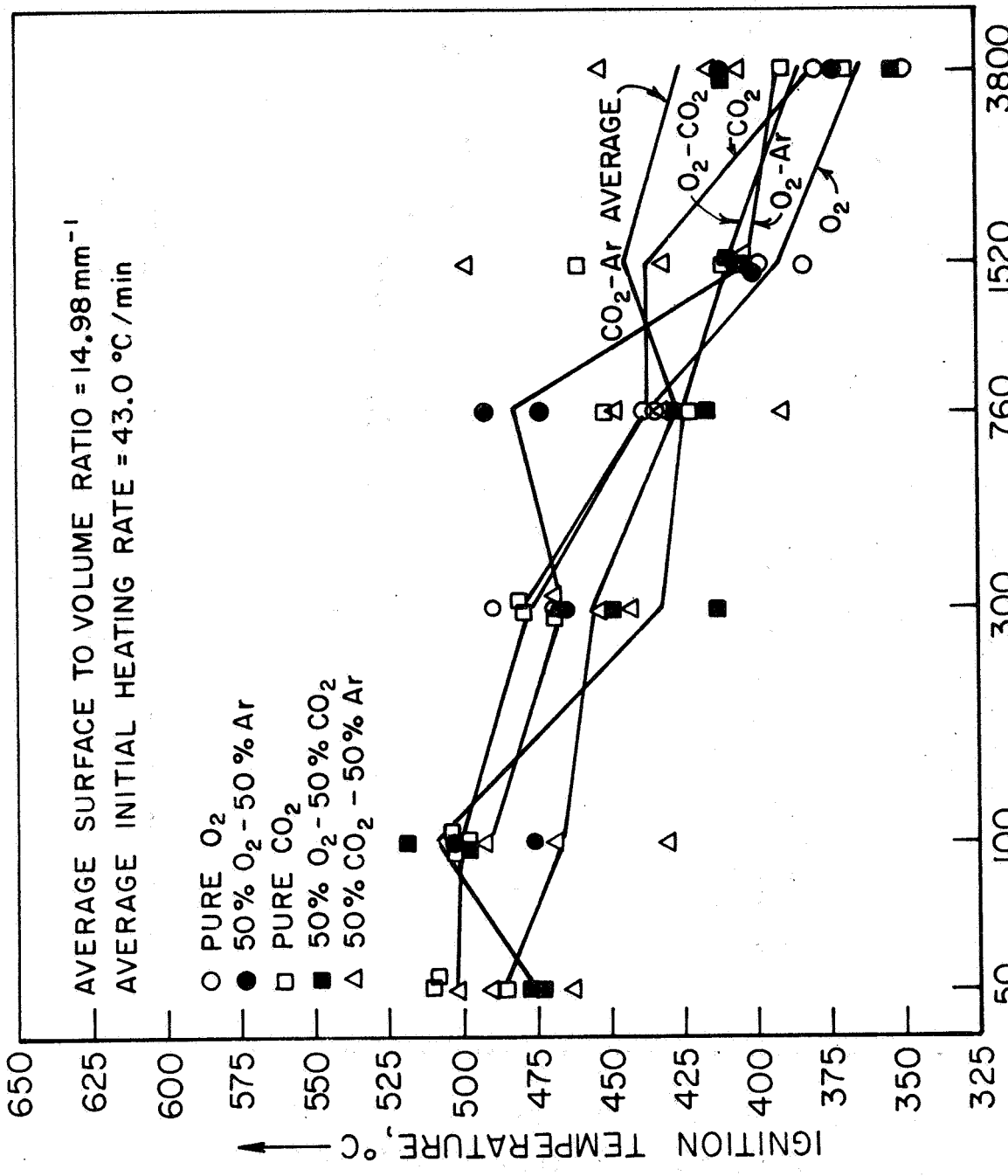

MAGNESIUM IGNITION TEMPERATURE IN VARIOUS OXIDIZING GASES VS TOTAL PRESSURE (0.127 mm FOILS, MG III)

FIGURE 30

AP24-4034-44

carbonaceous gases much less smoke was produced, and the powdery products found in the crucible contained great amounts of black deposits, probably C. In all gas compositions, the brilliance of the flame was observed to increase with increasing oxidizer pressure.

It is interesting to note the correspondence of the Mg-O_2 ignition temperature for the larger samples and the appearance of the flashes in the experiments involving Mg in CO_2-containing mixtures with the melting point of the metal. This connection can be explained by an examination of Eqn. (II-44) and (II-38), which are repeated here for convenience:

$$\dot{q}_{chem} = \frac{K\beta}{K+\beta} c\left\{\sum_i n_i \Delta H_{i,T_s} - \sum_j n_j \Delta H_{j,T_s}\right\} \qquad \text{(II-44)}$$

$$\Delta H_{\ell,T_s} = \Delta H_{f,\ell}^{298} + (H_{T_s} - H_{298}) \qquad (\ell = i,j) \qquad \text{(II-38)}$$

where subscript i indicates reactants and j products.

Because of the definition of enthalpy, as given by Eqn. (II-38), it is noted that upon attainment of the melting point of the metal, the total enthalpy of the Mg reactant will increase by the heat of fusion. Therefore, by virtue of Eqn. (II-44), at the metal melting point $\dot{q}_{chem}$ will also increase discontinuously by the heat of fusion. This increase will appear as a vertical jump in the $\dot{q}_{chem}$ curve at the metal melting point on the $\dot{q}$ versus surface temperature diagram and accounts for the noted correspondence between ignition temperature and metal melting point.

(1) The Effect of Total Oxidizer Pressure

By comparison of Fig. 24, 26,27, and 30, a well-defined pressure trend with respect to sample size is observed: for the largest samples (Fig. 24), the CO_2 ignition temperatures increase with increasing pressure, and for the wafers (Fig. 26), the CO_2 ignition temperatures first increase, and then decrease with increasing pressure. (Because of the correspondence of the Mg-O_2 ignition temperature with the metal melting point for these two sample sizes, no pressure dependence is indicated in O_2.) Finally, for the foil samples, the ignition temperatures decrease with increasing pressure for all gas compositions (Fig. 27 and 30). In other words, by merely changing the sample surface area to volume ratio, the ignition temperature reverses its dependence on pressure: for the cylindrical samples, it increases with pressure, while for the wafers, it increases and then decreases with increasing pressure; for the smallest samples, it decreases uniformly with increasing pressure. This result can be explained by an examination of Eqn. (VII-9).

As shown in Chapter II, according to the model the term which depends most strongly on sample size is the conduction heat loss into the fuel, which is included in $B(T_{ign})$ in Eqn. (VII-9). This term has been shown to increase in magnitude as the physical size of the sample is increased. Thus for large samples this term may overpower the other heat loss terms (conduction into the gas and radiation losses to the surroundings) included in the second term on the right hand side of Eqn. (VII-9). If this second term is neglected with respect to the first, then for the ignition of large samples the energy equation

(VII-9) may be approximated

$$A P_{ox}^{n} \cong B \qquad \text{(VII-11)}$$

Any pressure dependence will thus be given only by the chemical reaction rate and should be a function only of partial pressure of the oxidizer. Such a dependence was observed for both the Mg cylinders and wafers in CO_2-containing mixtures, and is shown for the former samples in Fig. 25.

As the surface area to volume ratio of the samples is increased, the magnitude of $B(T_{ign})$ will decrease, and therefore for small samples, the energy equation governing ignition may be approximated

$$A P_{ox}^{n} \cong C[P_{dil} + P_{ox}]^{m} = C P_{tot}^{m} \qquad \text{(VII-12)}$$

Here a much more complicated pressure dependence is predicted, and as shown in Fig. 28 and 29 was observed for the smaller samples.

The result that for large samples only the conduction loss into the sample is the important heat loss term is also substantiated by the experimental results of Reynolds (220). This investigator found excellent correlation between a theory developed for calculation of ignition temperatures of large samples and experimental values of ignition temperature for similar samples only if the heat loss term involving convection to the gas atmosphere was neglected in the calculation (see Section 12.c of Appendix II).

(2) The Effect of Sample Size

In Fig. 31 through 34, the average ignition temperature is plotted versus the surface area to volume ratio for the various Mg samples; each graph is for a particular value of total pressure. The estimated transition temperatures for pure O_2 and pure CO_2 are shown as dashed horizontal lines, since the transition temperature is independent of sample size, as was shown in Chapter III.

The pressure dependence of the transition temperature was obtained as follows: in Table 13, for the $Mg-O_2$ and $Mg-CO_2$ systems it is noted that transition temperatures are available at two pressures. For purposes of the figures, it was assumed simply that the transition temperature is a linear function of oxidizer pressure, and extrapolation or interpolation yielded the transition temperatures for the two systems at the total pressures of interest, 300 torr, and 1, 2, and 5 atm.

Also shown in Fig. 31 through 34 are comparable ignition temperature results from the literature. It is seen that the bulk results of Fassellet al. (201) for the $Mg-O_2$ system are in excellent agreement with the present results. The quiescent pile results of Freeman and Campbell (214) in Fig. 32 do not agree with the bulk results of the present investigation, as expected for reasons discussed in Chapter IV. Finally, the bulk result of Darras et al. (211, 212) for the $Mg-CO_2$ system is in disagreement with the present results, but this discrepancy is most likely a result of differing methods of calculation of the value of S/V for the molten samples (recall that in CO_2 large Mg samples ignite above the metal melting point).

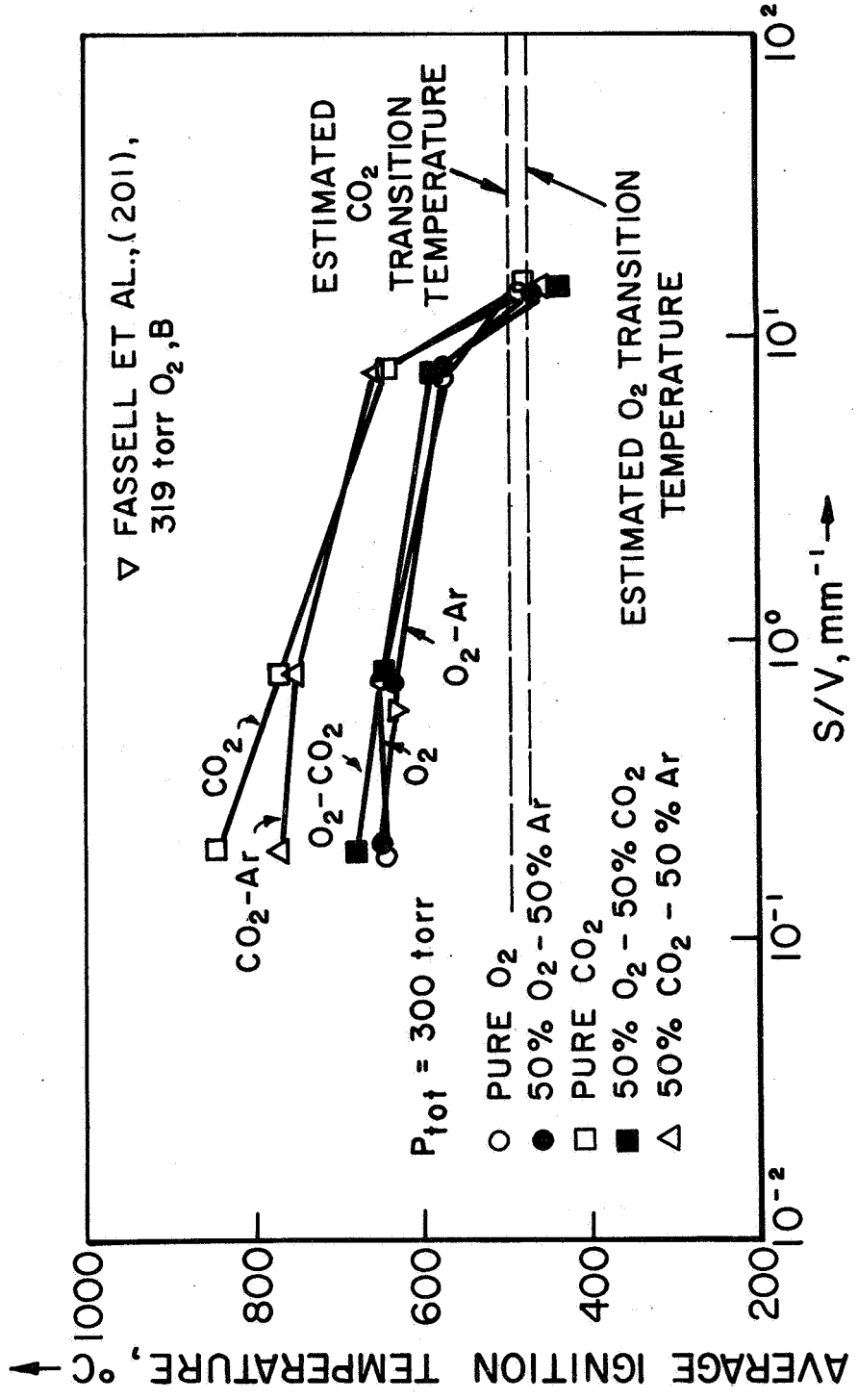

MAGNESIUM AVERAGE IGNITION TEMPERATURE IN VARIOUS OXIDIZING GASES VS SURFACE TO VOLUME RATIO (TOTAL PRESSURE = 300 torr)

FIGURE 31

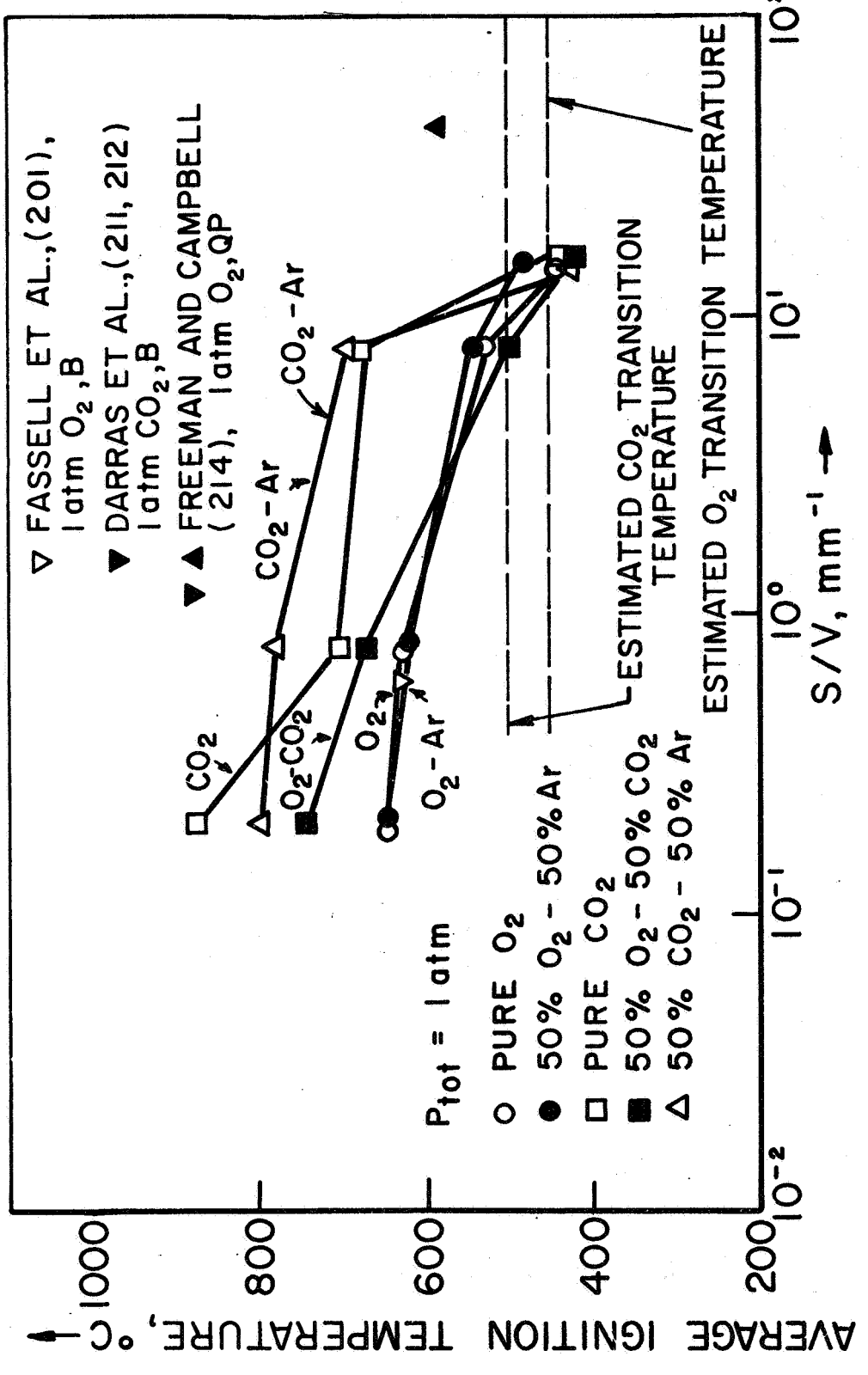

MAGNESIUM AVERAGE IGNITION TEMPERATURE IN VARIOUS OXIDIZING GASES VS SURFACE TO VOLUME RATIO (TOTAL PRESSURE = 1atm)

FIGURE 32

AP24-R 4038a-66

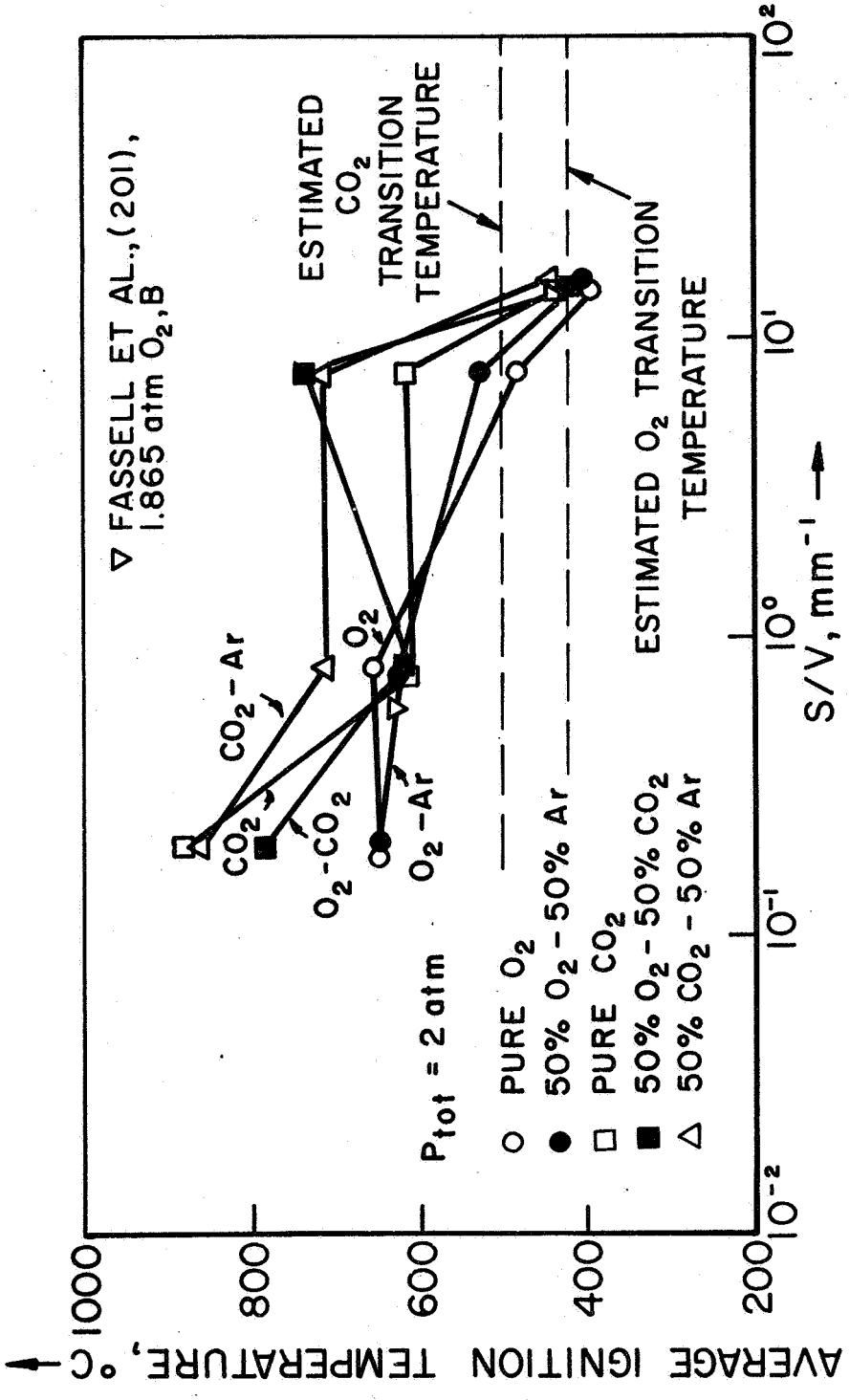

MAGNESIUM AVERAGE IGNITION TEMPERATURE IN VARIOUS OXIDIZING GASES VS SURFACE TO VOLUME RATIO (TOTAL PRESSURE = 2 atm)

FIGURE 33

AP29-R4040466

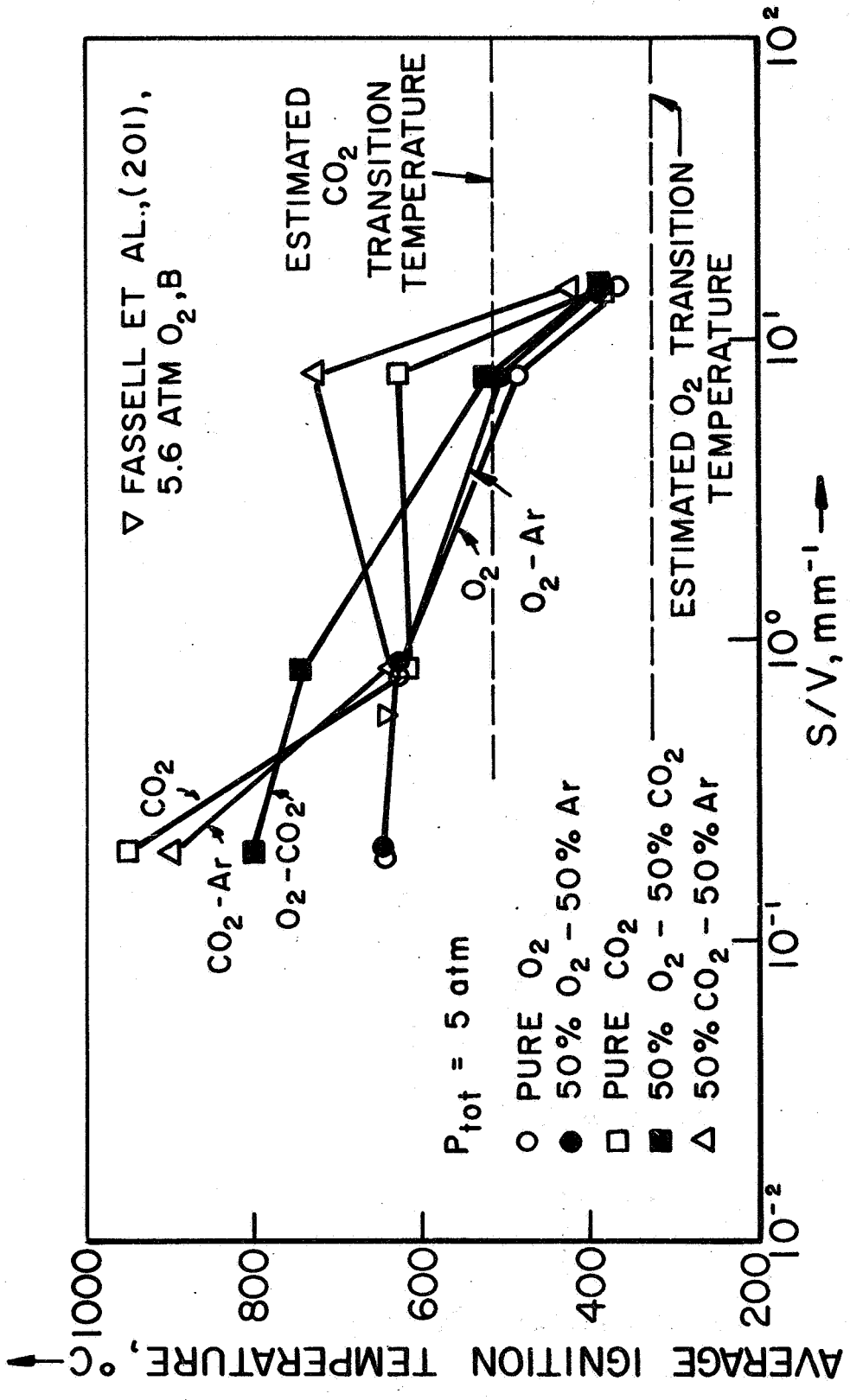

FIGURE 34

MAGNESIUM AVERAGE IGNITION TEMPERATURE IN VARIOUS OXIDIZING GASES VS SURFACE TO VOLUME RATIO (TOTAL PRESSURE = 5 atm)

AD-A036266

Some of the expected size trends are seen in the figures. For the larger samples (smaller S/V), the ignition temperature is relatively independent of size; this is the S/V range where the critical temperature is relatively independent of size. As the sample size is decreased (increasing S/V), the ignition temperature decreases (as the critical temperature decreases), and for the smallest samples the ignition temperature is approximately equal to the appropriate estimated transition temperature.

At the higher pressures (2 and 5 atm, Fig. 33 and 34), however, it is seen that a large discrepancy exists between the CO_2 ignition temperatures and the estimated CO_2 transition temperature; the former, in fact, is some 100°C below the latter. If the ignition model is correct, then the estimated transition temperature for the Mg-CO_2 system is incorrect. It is interesting to note that this hypothesis is consistent with the observations of McIntosh and Bagley (50) and of Salesse (51), both of whom indicated that the product film formed in the Mg-CO_2 reaction becomes non-protective at about 450°C (See Section 1 of Appendix I). Their remarks are contrasted with the results of Darras et al. (42, 45), which indicate a higher transition temperature and from which the Mg-CO_2 transition temperature was estimated.

According to the ignition model, experiments with Mg samples with larger surface to volume ratios than the 0.127 mm foil should give ignition temperatures independent of sample size, because for the 0.127 mm foils (S/V equal to about 15 mm^{-1}) the transition temperature has become controlling in ignition. To this end it was attempted to find a source for Mg foil thinner than the 0.127 mm foil.

It was learned in this process that for purely mechanical reasons, Mg cannot be rolled to thicknesses less than 0.1 mm. Alloys Unlimited, Inc., of Melville, New York, attempted to roll Mg foil to the required thickness and found it virtually impossible because of lateral tearing in the samples (267). Thus the possibility of investigating the ignition of bulk samples with surface area to volume ratios larger than 15 mm^{-1} was discarded.

It is also interesting to note that according to the present results (that is, Fig. 32), the critical temperatures of samples of this thickness may be only slightly above room temperature; thus such samples may be pyrophoric.

Experimentation with quiescent piles of Mg powder was not attempted because the literature results discussed in Appendix II and the result of Freeman and Campbell (214) shown in Fig. 32 demonstrate that the results of such experiments are not comparable with those of experiments with single pieces of Mg.

Vapor plating Mg samples for experimentation was not attempted because per plating process a film of thickness on the order of only 1 can be deposited (268). Films of this thickness would oxidize substantially during the pre-ignition reactions, and the labor involved in making thick films of Mg by vapor deposition precluded the use of this process.

Thus, unfortunately, although the Mg ignition temperature results are consistent with the ignition criterion as far as they go, it appears impossible to test the criterion further by investigating the ignition of smaller sample sizes. Perhaps the literature verification indicated in Table 25 for the Mg-O_2 and Mg-CO_2 systems with small Mg samples is sufficient to demonstrate the validity of the hypothesis that the minimum possible ignition temperature is the appropriate transition temperature.

(3) The Effect of Applied Heating Rate

Results demonstrating the influence of initial heating rate on ignition temperatures for the four sizes

of Mg samples are shown in Tables 37 through 40. These experiments were conducted in the various gas combinations only at total pressures of 300 torr and 2 atm.

It is seen from Tables 37 through 39 that for the three largest sample sizes the effect of heating rate on ignition temperature is very slight, although some increase in ignition temperature with increasing heating rate is apparent. As was developed in the introductory section of this chapter, such a trend may indicate that the critical temperature controls in ignition for these particular sample sizes, and this conclusion was also reached on the basis of variation of ignition temperature with sample S/V. One also concludes that the ignition temperature for these sample sizes is relatively independent of oxide thickness.

For the smallest samples (Table 40), however, a reasonably well-defined trend is evident: the ignition temperature decreases with increasing heating rate. The appearance of this dependence for the smallest samples may suggest that the ignition of these samples is controlled by the transition temperature rather than by the critical temperature, as also indicated by the T_{ign} versus S/V graphs.

However, there is another interpretation of the ignition temperature results for the smallest samples, the 0.127 mm foils. One notes from Fig. 30 through 34 that these ignition temperatures are relatively independent of gas composition and are primarily a function of total gas pressure. As already noted, this independence on the oxidizer present in the atmosphere may result from the importance of heat losses to the atmosphere in the ignition of small samples, as demonstrated by Eqn. (VII-12). This independence could also result from magnetic effects peculiar to the induction furnace, however, as discussed below.

TABLE 37.

EFFECT OF HEATING RATE ON IGNITION TEMPERATURE:
Mg CYLINDERS, MGII, MGIV, AND MGV (AVERAGE S/V = 0.202 mm^{-1})

Gas	Total Pressure	Time Average Initial Heating Rate, °C/min	Ignition Temperature, °C
O_2	300 torr	10	646
		77	645
		87	647
		198	646
	2 atm	24	643
		74	647
		84	645
		197	648
50% O_2- 50% Ar	300 torr	27	648
		89	647
		93	649
		97	642
		120	647
	2 atm	22	647
		94	648
		95	645
		147	645
CO_2	300 torr	28	799
		61	863
		≈90	825
		105	787
	2 atm	32	880
		≈90	879
		92	881
		174	896
50% CO_2- 50% Ar	300 torr	25	769
		82	759
		112	776
		159	817
	2 atm	43	833
		≈90	874
		133	852
		141	837
50% O_2- 50% CO_2	300 torr	36	622
		79	700
		91	658
		100	655
		143	672
	2 atm	18	730
		79	789
		79	780
		96	795
		106	801

TABLE 38.

EFFECT OF HEATING RATE ON IGNITION TEMPERATURE:
Mg WAFERS, MGVI (AVERAGE S/V = 0.772 mm^{-1})

Gas	Total Pressure	Time Average Initial Heating Rate, °C/min	Ignition Temperature, °C
O_2	300 torr	22	606
		40	641
		71	645
		111	630
	2 atm	6	661
		59	685
		63	627
		91	636
50% O_2-50% Ar	300 torr	62	615
		66	645
		119	641
	2 atm	12	630
		52	626
		69	626
		121	640
CO_2	300 torr	11	764
		34	798
		50	747
		87	816
	2 atm	18	798
		39	607
		64	613
		152	829
50% CO_2-50% Ar	300 torr	17	745
		51	751
		79	748
		133	810
	2 atm	11	637
		76	605
		81	825
		141	781
50% O_2-50% CO_2	300 torr	17	647
		47	642
		47	637
		186	697
	2 atm	21	728
		48	621
		56	621
		120	752

TABLE 39.

EFFECT OF HEATING BATE ON IGNITION TEMPERATURE:
0.254 mm Mg FOILS, MGVII (AVERAGE S/V = 7.75 mm^{-1})

Gas	Total Pressure	Time Average Initial Heating Rage, °C/min	Ignition Temperature, °C
O_2	300 torr	5	561
		38	573
		56	568
		169	549
	2 atm	5	540
		42	517
		54	462
		160	537
50% O_2- 50% Ar	300 torr	7	560
		54	558
		70	586
		186	513
	2 atm	15	542
		36	551
		48	516
		162	557
CO_2	300 torr	14	725
		34	574
		55	693
		110	710
	2 atm	13	776
		47	665
		49	569
		96	698
50% CO_2- 50% Ar	300 torr	16	607
		66	635
		75	667
		113	645
	2 atm	9	709
		55	712
		65	733
		142	602
50% O_2- 50% CO_2	300 torr	7	560
		48	586
		60	587
		193	532
	2 atm	15	537
		55	440
		66	559
		130	518

TABLE 40.

EFFECT OF HEATING RATE ON IGNITION TEMPERATURE: 0.127 mm Mg FOILS, MGIII (AVERAGE S/V = 14.98 mm^{-1})

Gas	Total Pressure	Time Average Initial Heating Rate, °C/min	Ignition Temperature, °C
O_2	300 torr	7	449
		37	469
		48	490
		98	425
	2 atm	10	444
		35	386
		68	399
		138	429
50% O_2- 50% Ar	300 torr	8	465
		35	466
		41	469
		193	380
	2 atm	10	420
		29	403
		36	405
		129	380
CO_2	300 torr	6	500
		29	470
		34	481
		35	483
		136	452
	2 atm	8	671
		27	413
		46	463
		106	376
50% CO_2- 50% Ar	300 torr	5	519
		28	444
		30	453
		61	471
		195	454
	2 atm	15	422
		31	433
		43	499
		44	406
		125	395
50% O_2- 50% CO_2	300 torr	17	451
		26	414
		40	457
		216	430
	2 atm	12	534
		29	412
		39	412
		154	362

Suppose that because of the RF skin effect through which maximum heating occurs at the outer edge of the sample, ignition actually occurs in this region, and consequently the ignition temperatures as indicated by the thermocouple located in the center of the sample are low. If this were the case, then the ignition temperatures would be expected to decrease with increasing heating rate, because as the heating rate is increased, the discrepancy between the centerline temperature (given by the thermocouple) and the temperature at the outer edge of the sample will increase. This is exactly the trend observed with the smallest samples. Recall, however, that ignition is defined to occur upon flame spreading to the thermocouple; thus, the discrepancy between the ignition temperatures at the center and edge should be slight.

Another effect could account for some discrepancy: experiments were performed in pure Ar with these smallest samples. At temperatures about 100 to 150^{o}C below the metal melting point glows were observed near the outer edge of the sample. These glows were not self-sustaining and were not a result of chemical reaction; rather, they indicated local hot spots where non-uniform heating was occurring in the magnetic field. Apparently the Mg had begun to melt at the outer edge and surface tension had drawn the Mg into drops near to the previous position of the outer edge.

Similar experiments were performed with small samples of Al in Ar, as will be discussed in Section 3 of this chapter, and glows were also observed with this metal at comparable temperatures below the metal melting point. Upon termination of the experiments with the smallest Al samples, most of the Al was observed to have

formed a ring of metal surrounding the position of the thermocouple and roughly of the original radius of the sample; within the ring was a thin layer of metal. Similar experiments could not be performed with Ca in Ar, because of glow discharges and arcs resulting from the high vapor pressure of this metal.

Because the eddy currents induced in the metallic sample by the magnetic field flow in a direction opposite to the current within the work coil (266), there will be a $\vec{j} \times \vec{B}$ force acting on the metal which will point radially inward in the present cylindrical geometry. This force will oppose any tendency of the melting metal to draw into a hollow ring. Nevertheless, for the smallest samples (for which the smallest magnetic field and thus smallest induced current will be required to heat the sample to its melting point), the effect of surface tension becomes relatively stronger than the opposing $\vec{j} \times \vec{B}$ force, and upon melting, the samples tend to form an annulus in their crucibles.

Such behavior would of course not allow a thermocouple mounted in the center of the crucible to give an accurate value of ignition temperature, and because the magnetic field, eddy currents, and surface tension phenomena are independent of the oxidizing gas, indicated ignition temperatures will also be independent of oxidizer.

This magnetic field-surface tension interaction and the meaning of the measured ignition temperatures can be interpreted more clearly in view of the ignition temperatures measured in the critical temperature experiments, which were performed with the susceptor and which will be discussed in Section 2.b of this chapter. It is seen, however, that the ignition temperature results in CO_2 must be regarded with caution.

It is noted that the flashing and temperature

drop behavior observed with the 0.254 mm samples in CO_2-containing atmospheres may be a result of exactly the same interaction. Such phenomena were not observed in O_2 atmospheres because ignition occurs upon the first melting of the sample at the outer edge.

The desirability of performing experiments with Mg samples thinner than the 0.127 mm foils becomes even more clear at this point. If ignition temperatures of the same magnitude as those for the 0.127 mm foils are observed, then the first explanation of the decrease in ignition temperature with increasing applied heating rate (that the transition temperature has become controlling in ignition) is appropriate; if the measured ignition temperatures are below the ignition temperatures for the 0.127 mm foils (and thus below the estimated transition temperatures), then the latter explanation based on the interaction between the $\vec{j} \times \vec{B}$ force and the surface tension acting on the molten part of the samples is correct. Unfortunately, as was discussed previously, such foil is not available commercially and cannot be rolled by conventional processes.

To summarize, for the Mg cylinders, wafers, and 0.254 mm foils any dependence of ignition temperature on applied heating rate is slight, but a small increase in ignition temperature with increasing heating rate may indicate that the critical temperature controls in the ignition of samples in this S/V range. For the 0.127 mm foils, the opposite trend was observed: the ignition temperature decreases with increasing heating rate. Such a dependence may indicate either that the transition temperature controls in the ignition of these samples or that the measured ignition temperatures are low because of a thermal lag between the temperature in the zone of maximum heating and that

indicated by the thermocouple.

For these latter samples, characterized by a ratio of depth of penetration of heating (the skin effect) to sample thickness on the order of one, magnetic field-surface tension interactions may be important, and thus ignition temperatures measured for these smallest samples must be interpreted with care.

On the basis of the experiments determining ignition temperature as a function of heating rate, it is concluded that the ignition temperatures for the three largest Mg sample sizes are valid, but for the 0.127 mm foils may be somewhat low.

In the next section the results of the critical temperature experiments performed with the Mg samples are described. As mentioned above, because the susceptor used in these experiments to provide a constant temperature environment for the sample effectively shields the sample from the magnetic field of the work coil, and thus eliminates the problem of magnetic interactions and the RF skin effect, some further light can be shed on the interpretation of the results of the ignition temperature experiments.

b. Critical Temperature Experiments

As noted previously, because of the duration and difficulty of the critical temperature experiments, the range of variation of the experimental parameters was curtailed as compared to the ignition temperature experiments. In particular, the initial sample heating rate was standardized to about 50 ^{o}C/min, only pure O_2 and pure CO_2 were used as oxidizers, and only at pressures of 300 torr and 2 atm, and, finally, experiments were conducted only with the large Mg cylinders (MGIV and MGV) and the

two Mg foils (MGIII and MGVII).

Examples of experimental traces as obtained in both types of critical temperature experiments discussed at the beginning of this chapter are shown in Fig. 35 and 36. In Fig. 35 the type II critical temperature experiment with initial heating and equilibration in oxidizer is demonstrated, for the particular case of a large Mg cylindrical sample in 300 torr of O_2 with average initial heating rate equal to 33°C/min.

Both the sample and susceptor thermocouple readings are presented in the figure (the hollow susceptor which surrounds the sample is held at constant temperature automatically after equilibration). Recall that chromel-alumel thermocouples were used to measure the sample temperature, and Pt/Pt13Rh thermocouples to measure the susceptor temperature. Also, because different recorder scales were used for these two temperatures, the relative values of temperature shown in Fig. 35 and 36 have no meaning.

Approximately 10 min into the experiment the susceptor reached equilibrium at its set point of 740 °C. Some time later, the sample temperature leveled off; time zero is indicated in the figure, at which the initial sample temperature was 602°C.

In Fig. 35, sample self-heating after time zero is observed clearly as the sample temperature runaway. Although difficult to see in the figure, the sample temperature rose abruptly (and a flame appeared) 4.3 min later at a sample temperature of 639 °C.

Immediately after this ignition, the furnace was turned off and the Mg-O_2 fire was extinguished by means of a high pressure Ar purge. Not all of the metal was consumed in the fire, as a definite metal freezing

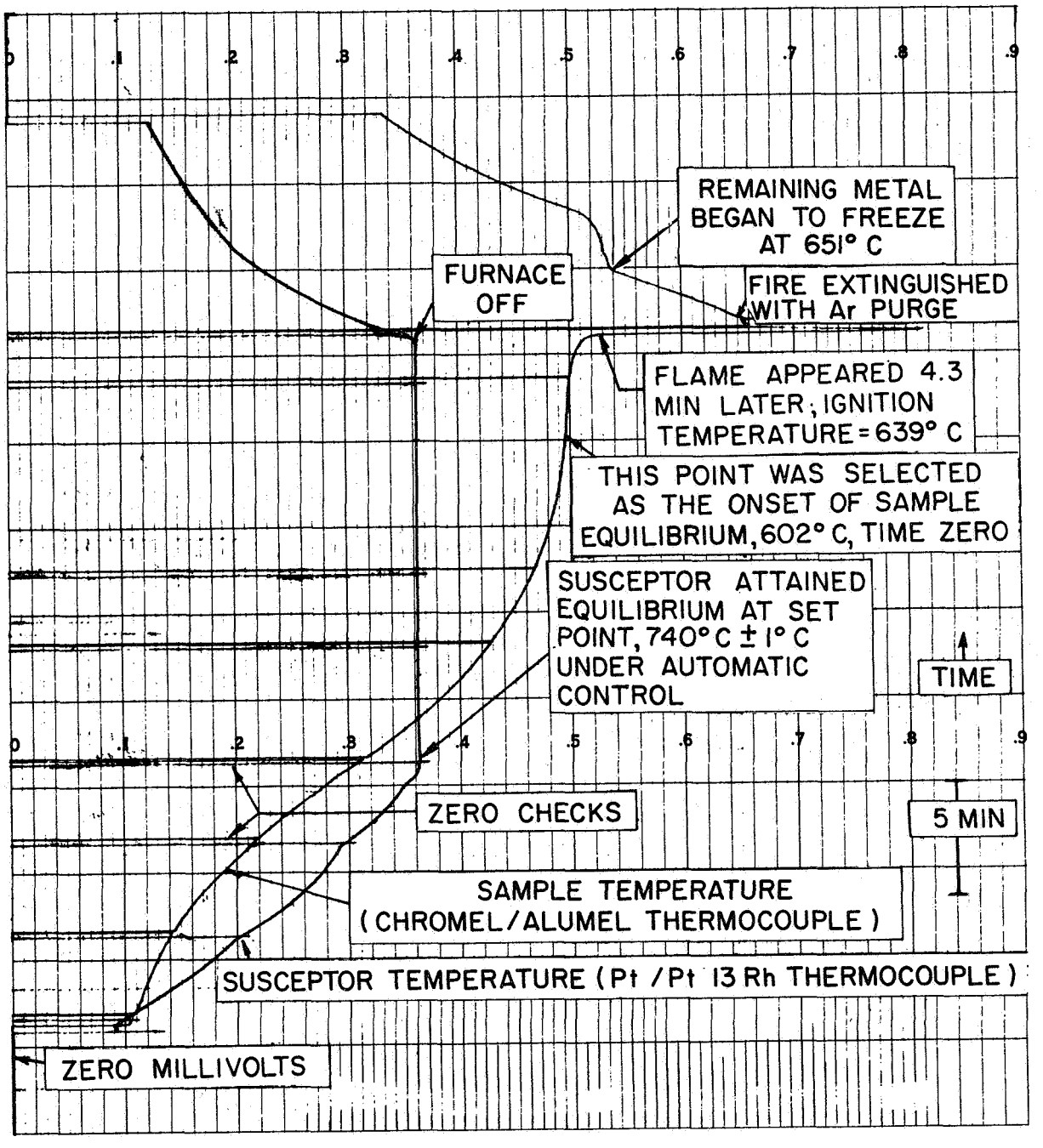

CRITICAL TEMPERATURE EXPERIMENT (TYPE II)
(INITIAL HEATING IN OXIDIZER)
MG IV SAMPLE (S/V = 0.201 mm^{-1}); 300 TORR O_2
INITIAL AVERAGE SAMPLE HEATING RATE = 33° C/MIN

FIGURE 35

AP29-4042-66

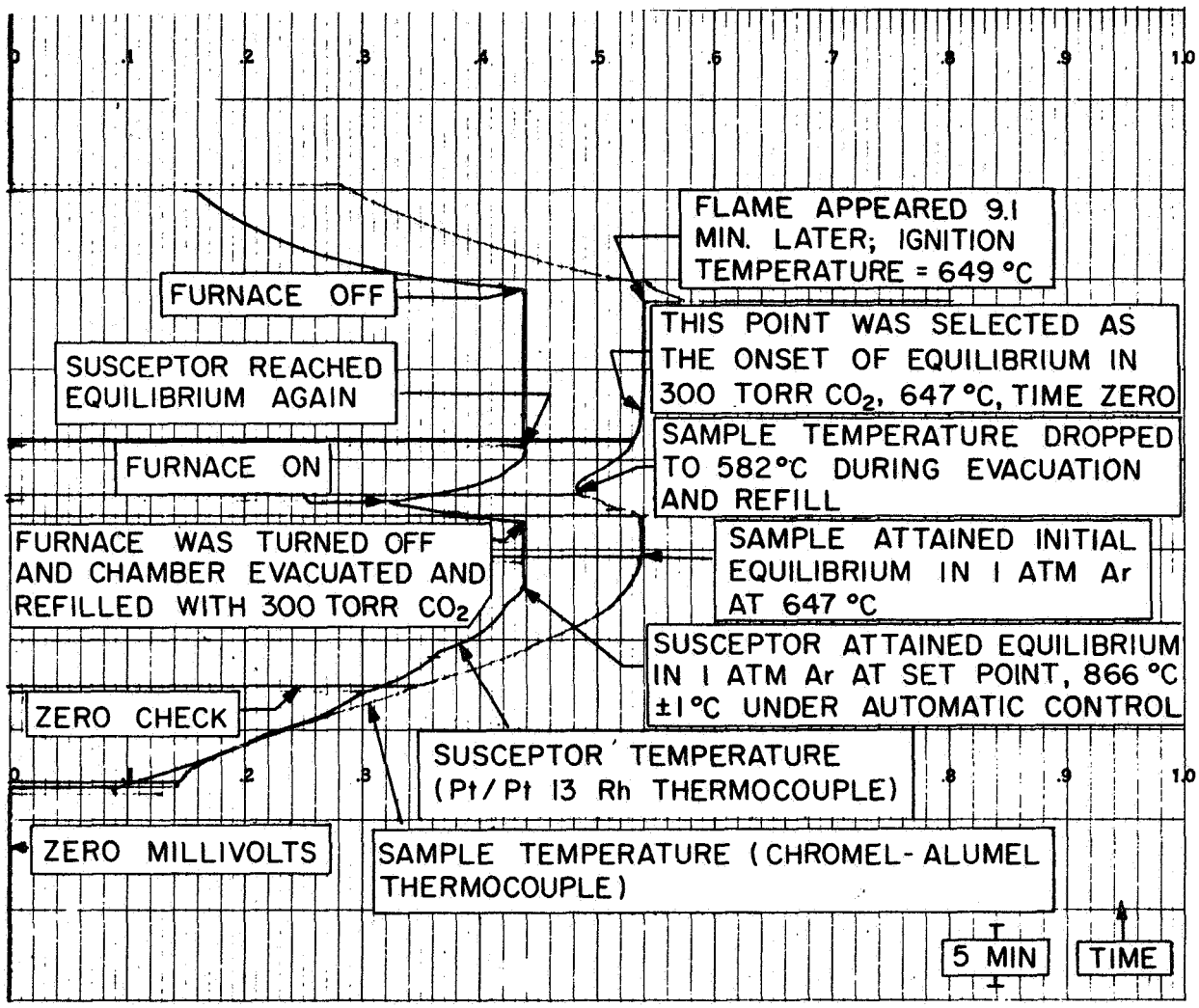

CRITICAL TEMPERATURE EXPERIMENT (TYPE I)
(INITIAL HEATING IN ARGON)
Mg III SAMPLE (S/V = 15.68 $m\,m^{-1}$); 300 TORR CO_2
INITIAL AVERAGE SAMPLE HEATING RATE = 37°C/MIN

FIGURE 36

point was observed at 651 ^{o}C (to be compared with the literature value of 650 ^{o}C)).

Under these test conditions it was concluded that the critical temperature was less than 602 ^{o}C, the initial sample temperature in this experiment.

In experiments of this type (that is, with initial heating and equilibration in the oxidizer of interest), below the appropriate critical temperature no ignition was observed within the one hour limit (after equilibration) of the experiment, although in general sample self-heating occurred.

The method of defining time zero essentially by eye while in the process of the particular experiment is extremely arbitrary. In fact, in Fig. 35 the choice was premature, and probably time zero should have been taken some 2 or 3 min later when the sample thermocouple was at 0.5 on the scale in the figure. As a rule, however, estimated initial sample temperatures and measured ignition delay times were roughly self-consistent: the lower the initial temperature, the longer the ignition delay.[5]

In general, very few ignition delay times between 15 and 60 min were found, which may indicate that the estimation of sample equilibrium was conservative. It is felt that the 60 min cut-off on the experiments served to define the lower limiting critical temperature quite concretely (the upper limit was, of course, the ignition temperature), but little confidence is placed

[5]Some thought was given to using the temperature differentiating circuit to define time zero in terms of a minimum rate of change of sample temperature. However, as noted previously, the construction of this apparatus was not complete until after the Mg investigation was finished.

in the absolute value of ignition delay time for a specific initial sample temperature.

An experimental trace from the other type of critical temperature experiment (with initial heating and equilibration in Ar, removal of the inert, and admission of the appropriate oxidizer) is shown in Fig. 36. Recall that because of the low pressure arcing problem, the furnace had to be turned off during the chamber evacuation and refill. In the figure, again the sample and susceptor temperatures are recorded, for the particular case of a 0.127 mm Mg foil in 300 torr of CO_2.

It was desired to accomplish the initial heating and equilibration in Ar at that pressure appropriate to the second part of the experiment, conducted in the oxidizer, so that the two equilibrium temperatures would be as close as possible. This was found impossible for pressures of 300 torr, however, because at the furnace power levels and work coil-susceptor spacing necessary to heat the susceptor at the desired rate, in 300 torr of Ar arcing invariably occurred. Thus if the oxidizer pressure in the second part of the experiment was to be 300 torr, initial heating was accomplished in Ar at 1 atm. For experiments involving an oxidizer pressure of 2 atm, 2 atm of Ar were used initially.

Rather than evacuation of the Ar and refilling with the oxidizer, the test chamber could have been flushed with the oxidizing gas after attainment of the initial equilibrium, so that the furnace could have been left on during the gas changeover and thus ideally the equilibrium maintained. However, in view of the strong dependence of ignition temperature on oxidizer partial pressure, as demonstrated in the previous section, this method was rejected because it was felt that the unknown oxidizer

partial pressure during the flushing process (and actually throughout the remainder of the experiment) would increase the irreproducibility of the results.

The only justification of the method which was used in the present experiments must result from comparison with experiments conducted in resistance furnaces, in which equilibrium can be maintained during evacuation and refill. Such comparison will be made shortly.

It is seen from Fig. 36 that during the gas changeover process the sample temperature dropped 65 ^{o}C. Throughout the experiments the temperature drop was typically on the order of 100 to 150 ^{o}C. In the particular case shown in the figure, the second equilibrium temperature was equal to the first, but this was the exception rather than the rule; generally, the differing heat transfer coefficients of the Ar and oxidizer (and the pressure difference in runs with oxidizer pressure equal to 300 torr) was sufficient to guarantee that these temperatures be different.

Sample self-heating is not as noticeable in Fig. 36 as in Fig. 35, and in general was not as noticeable in CO_2 as in O_2. Furthermore, the sample temperature increase observed upon the initial admission of oxidizer was less in CO_2 than in O_2; in the latter gas it was typically 10 or 15 ^{o}C and depended on the sample size and temperature. In Fig. 36 this temperature increase is obscured by zero checks and the slow recorder chart speed.

In general, to define a critical temperature under a given set of experimental conditions (sample size, oxidizer and oxidizer pressure, and initial heating in the oxidizer or in Ar), a series of experiments was performed under these experimental conditions in which the susceptor set point temperature was varied in order to vary the initial sample temperature. The results of such a series are presented in Table 41.

TABLE 41.

TYPICAL DATA FROM A SERIES OF CRITICAL TEMPERATURE EXPERIMENTS

(MGVII, 0.254 mm Mg foil in pure O_2 at 300 torr)

Initial Equilibration in 300 torr of O_2

Run Number	Susceptor Set Point, °C	Average Initial Heating Rate (Sample), °C/min	Initial Sample Temperature, °C	Ignition Delay Time, min	Ignition Temperature, °C	Self-heat in one hour, °C
1	---	43	---	---	646	---
2	---	47	---	---	610	---
4	826	44	---	0	603	---
3	831	58	606	1.5	609	---
6	822	50	605	2.7	609	---
7	814	58	600	4.0	609	---
10	786	47	594	>60	---	+ 7
9	794	40	592	7.8	602	---
8	794	44	588	>60	---	+ 7
11	774	52	581	>60	---	+15

Average Ignition Temperature = 613°C

Estimated Critical Temperature = 593°C

The first two experiments were conducted with the susceptor temperature increasing indefinitely, simply to measure the ignition temperature of the sample with the susceptor present. The remainder of the experiments were performed with the constant temperature environment for the sample provided by the susceptor. For those experiments beginning at initial sample temperatures below

the critical temperature (that is, experiments without ignition within the 60 min time limit), the change in sample temperature in the hour is recorded in the column at the right hand side of the table.

Several points are evident from the table: firstly, note the large range of observed ignition temperatures; this range made experimentation extremely difficult, because of unexpected ignitions at unusually low temperatures, as in runs number 4 and 9. Secondly, note that there is little correspondence between susceptor set points and initial sample temperatures; thus it was difficult to predict the initial sample temperature for a given susceptor temperature, and this problem placed the experiments in a hit-or-miss category. Finally, although in the series presented in the table the agreement between the ignition delay times and the initial sample temperatures is good, as noted previously most of the data were not as precise.

For these reasons, critical temperatures estimated from tables such as Table 41 are considered to be defined within ± 5 ^{o}C.

The results of such estimations for all of the various experimental conditions are presented in Table 42. Shown are the estimated critical temperatures and average ignition temperatures as determined under each set of conditions in critical temperature experiments. Also, in the table are listed the average ignition temperatures as determined in the ignition temperature experiments (that is, without the susceptor) discussed in the preceding section.

In Table 43 are given the important experimental parameters, averaged over the critical temperature experiments for a particular sample size. As before,

TABLE 42.

RESULTS OF THE MAGNESIUM CRITICAL TEMPERATURE EXPERIMENTS

Gas	Pressure	Estimated T_{trans}, °C	Sample	Average S/V, mm^{-1}	Initial Equilibration in Ar: T_{crit}, °C	Initial Equilibration in Ar: $(T_{ign})_{ave}$, °C	Initial Equilibration in O_2 or CO_2: T_{crit}, °C	Initial Equilibration in O_2 or CO_2: $(T_{ign})_{ave}$, °C	$(T_{ign})_{ave}$, as Measured in Ignition Temperature Experiments, °C
O_2	300 torr	472	cylinder	0.202	575	640	595	638	646
			0.254 mm foil	7.73	590	604	593	613	571
			0.127 mm foil	15.06	580	590	590	604	480
O_2	2 atm	420	cylinder	0.202	570	637	581	633	646
			0.254 mm foil	7.73	550	599	580	598	489
			0.127 mm foil	15.06	542	581	560	582	393
CO_2	300 torr	498	cylinder	0.202	683	718	655	712	844
			0.254 mm foil	7.73	625	645	625	654	634
			0.127 mm foil	15.06	638	654	623	645	478
CO_2	2 atm	504	cylinder	0.202	655	702	>619	---	880
			0.254 mm foil	7.73	620	623	648	669	617
			0.127 mm foil	15.06	>615	647	615	626	438

TABLE 43.

EXPERIMENTAL PARAMETERS FOR THE MAGNESIUM CRITICAL TEMPERATURE EXPERIMENTS

Sample	Designation	Average S/V, mm^{-1}	Average Initial Heating Rate, $^{o}C/min$	Sample Thermocouple Error, ^{o}C	Susceptor Deviation From Set Point, ^{o}C
cylinder	MGIV, MGV	0.202	36.1	3.6	1.4
0.254 mm foil	MGVII	7.73	52.2	2.9	2.6
0.127 mm foil	MGIII	15.06	45.0	8.2	1.7

the sample thermocouple error was estimated from observations of the indicated melting and freezing points of the Mg samples. The susceptor deviation from its set point was monitored only from time zero, as defined above, to the termination of the experiment, either upon ignition of the sample or at the end of 60 min.

Returning to the results of the critical temperature experiments listed in Table 42, comparison can be made with the results of other investigators for the Mg-O_2 system (Appendix II) in order to test the experimental method used in the present investigation. For Mg samples of S/V from 0.579 to 1.23 mm^{-1} in O_2 or air at 1 atm, the critical temperature was estimated as 575 or 580^{o}C on the basis of the results of Fassell et al.(201) and Darras et al. (211, 212). This estimate is consistent with the results shown in Table 42 for all of the Mg samples in O_2 at 300 torr and for the Mg cylinders in O_2 at 2 atm. Thus it is concluded that the experimental method which was used in the critical temperature experiments in the present investigation is valid.

Several other significant observations can be made on the basis of Table 42. Firstly, in all cases the measured critical temperatures are lower than the appropriate average ignition temperatures, in agreement with the metal ignition criterion. As discussed in Chapter II, the fact that the critical and ignition temperatures are not equal indicates that the experiments were not conducted at the ignition limit, at which the $\dot{q}_{chem}$ and $\dot{q}_{loss}$ curves are tangent.

Secondly, as predicted by the model, for a given gas and pressure, as the sample size is decreased (increasing S/V), both the critical and ignition temperatures decrease; since both of these temperatures exceed the appropriate transition temperatures, the observed size dependence was expected.

It is seen from the ignition temperatures as obtained in both types of critical temperature experiments that the ignition temperature is relatively independent of oxide film thickness, a finding which is consistent with the result of varying the heating rate in the ignition temperature experiments, as discussed in the previous section. However, there appears to be a relatively well-defined trend in critical temperature with oxide thickness: the critical temperature decreases with decreasing oxide film thickness, as it is generally lower for those samples heated initially in Ar. Ideally, this trend was not expected since the transition temperatures have been exceeded, but, as noted in Chapter II, in the real case $\dot{q}_{chem}$ will depend on the initial oxide thickness to some extent even above the transition temperature.

Both the critical and ignition temperatures are lower at 2 atm than at 300 torr; such a correspondence in

pressure dependences when the critical temperature exceeds the transition temperature was predicted earlier in this chapter.

A final, and most significant result is the lack of correspondence between the ignition temperatures as measured in the critical temperature and ignition temperature experiments. It is seen that although the predicted size dependence is observed in both experiments, the size dependence is not as marked in the critical temperature experiments.

The only difference between these two experiments is the presence of the susceptor,[6] which has the following effects: without the susceptor, the sample is heated by induction heating; at radio frequencies the majority of the heating occurs near the outer edges of the sample. This localized heating will tend to accentuate the conduction heat loss into the metal sample. Since this heat loss term is thought to be responsible for the size effect in ignition (see Section 4 of Chapter II), a strong size effect is expected and was obtained in the experiments without the susceptor, that is, the ignition temperature experiments.

However, it must be recalled that because the sample thermocouples were mounted near the center of the sample, and because the zone of maximum heating and of ignition were usually located on the outer circumference

---

[6] At the end of the Mg investigation, two experiments were conducted one after the other under exactly the same conditions, except that the susceptor was removed for the second test. The ignition temperature was 188°C lower without the susceptor, thus substantiating that the susceptor was completely responsible for the change in ignition temperature.

of the sample, ignition temperatures measured in the induction furnace environment will be somewhat low. The heating rate experiments indicated that this effect may be important for only the smallest samples, however, as only for these samples did the measured ignition temperature decrease with increasing heating rate.

Ideally, the function of the susceptor is to couple preferentially with the magnetic field of the work coil and thus to shield the sample from the field. The susceptor then heats the sample by ordinary conduction, convection, and radiation heat transfer and effectively provides an environment similar to a resistance furnace for the sample.

In this situation, the sample is heated much more uniformly, and the conduction heat loss into the sample becomes much smaller than in the induction furnace environment. Therefore, as observed in the former configuration, the size effect in ignition is much less pronounced.

In other words, in the environment provided the sample by the susceptor, the sample may be assumed to be completely shielded from the heat loss environment, that is,

$$\dot{q}_{cond,g} = \dot{q}_r = 0 \qquad \text{(VII-13)}$$

and therefore

$$\dot{q}_{loss} = \dot{q}_{cond,f} \qquad \text{(VII-14)}$$

However, as expected on the basis of the ignition model

and as indicated by the pressure dependence of the ignition temperature as measured in the ignition temperature experiments, for large samples in general

$$\dot{q}_{loss} = \dot{q}_{cond,f} \qquad \text{(VII-15)}$$

Thus with the susceptor acting as a magnetic and as an environmental heat loss shield, the observed ignition (and critical) temperatures are relatively independent of sample size and remain near the bulk ignition temperature rather than demonstrating the strong size effect.

As noted above, with the susceptor the metal sample is heated more uniformly (because there is no skin effect with the susceptor), and thus the heat loss into the sample should be of smaller magnitude with the susceptor. Consequently, the $\dot{q}_{loss}$ curve will shift downwards at any given value of surface temperature, and measured ignition temperatures should be lower with the susceptor. As can be seen from Table 42, this lowering of ignition temperature with the susceptor was observed with the large Mg cylinders in 300 torr and 2 atm of CO_2. The trend cannot be observed in O_2 because of the equivalence of ignition temperature and metal melting point.

These observations have several far-reaching implications: firstly, experiments designed to measure the size effect in metal ignition (either critical or ignition temperatures, provided that the former exceeds the transition temperature) must be conducted in a manner such that the metal sample is not heated uniformly; because of the radio frequency skin effect, induction

furnaces are greatly superior to resistance furnaces in this respect. In fact, under some circumstances, it may be impossible to measure any size effect in resistance furnaces. Thus for many of the metal-oxidizer systems discussed in Appendix III for which the critical temperature controls in "bulk" ignition, the independence of ignition temperature on sample size may have been a result of the use of a resistance furnace rather than of the critical temperature becoming independent of size (see Chapter II).

The results indicate the strong dependence of measured ignition and critical temperatures on the experimental environment, a dependence which is reflected in the ignition model in that both of these temperatures are defined in terms of the $\dot{q}_{chem}$ and $\dot{q}_{loss}$ curves, the latter of which depends strongly on the environment. (It is again assumed that the critical temperature exceeds the transition temperature, as for the bulk Mg-O_2 system.) The fundamental question is then raised as to the possibility of assigning an absolute ignition temperature for a given metal-oxidizer system.

On the basis of the experiments with Mg in the induction furnace facility, it is concluded tentatively that there are two absolute ignition temperatures characteristic of a given metal-gas system; these are the bulk ignition and the transition temperatures (in cases which the transition temperature exceeds the critical temperature, the transition temperature and bulk ignition temperatures are equal; thus there is only one absolute ignition temperature for this type of system). The former may be considered absolute for several reasons: firstly, the agreement between the Mg cylinder and wafer ignition temperatures in O_2 observed in the induction furnace, which

is characterized by the accentuated size effect; secondly, the agreement of the present results with the bulk results of other investigators (but both of these arguments may result from the correspondence between the ignition temperature and the (absolute) metal melting point, as noted above); and finally, for other metal-gas systems in the $T_{crit} > T_{trans}$ category, the agreement in bulk ignition temperatures as measured by different investigators (Appendix II). The absolute nature of the bulk ignition temperature will be examined further in the section of this chapter concerned with the ignition of Ca.

The transition temperature is considered an absolute quantity because, as indicated in Chapter III, it is relatively independent of the experiment, and for transitions which are a result of melting of the oxide or of a phase change in metal or oxide it should be completely independent of experimental configuration since it is then a physical property of the metal or oxide.

Thus it is concluded that it is only possible to assign an ignition temperature for Mg in O_2 between 650 ^{o}C (for large samples, the bulk ignition temperature) and 450 ^{o}C (for small samples, the transition temperature); all other ignition temperatures measured for this system in any experiment should fall between these values.

c. Summary

Several conclusions can be drawn on the basis of quantitative ignition results obtained in the induction furnace facility with Mg samples of various sizes in O_2, CO_2, and combinations of these gases with each other and with Ar. The more important findings can be listed as follows:

(1) That the minimum possible ignition temperature is the appropriate transition temperature was verified in both the ignition temperature and critical temperature experiments. For the Mg-O_2 system in the pressure range from 300 torr to 5 atm, the lowest observed ignition temperatures were commeasurate with the estimated transition temperatures. However, for the Mg-CO_2 system at 2 and 5 atm the agreement was not good, but may be a result of an incorrect choice in transition temperature. Experiments on the effect of applied heating rate indicated that the ignition temperatures measured for the smallest samples may have been somewhat low.

(2) In the critical temperature experiments, under all circumstances the observed ignition temperatures exceeded both the measured critical temperatures and the estimated transition temperatures, in complete agreement with the metal ignition criterion.

(3) Comparison of the ignition temperatures measured in the ignition temperature experiments (induction heating, without a susceptor) and the critical temperature experiments (environment of a resistance furnace, with a susceptor) indicates that the size effect is lessened in resistence furnaces or in any other environment in which the sample is heated uniformly throughout its volume.

(4) Therefore, for metals such as Mg, for which the critical temperature exceeds the transition temperature for bulk samples, the only absolute ignition temperatures of merit are those for large samples (the bulk ignition temperature) and for small samples (the transition temperature). Any other ignition temperatures are functions of the experimental environment rather than the chemistry, and are thus not comparable with results obtained in differing experimental situations.

Several other conclusions particularly appropriate to the ignition of Mg have been discussed in the preceding sections; only the most significant results have been listed here. However, it is concluded that the ignition model and criterion as applied to the ignition of Mg have been verified both in general and in detail.

In the next section of this chapter, a preliminary investigation of the ignition of Al as conducted in the induction furnace facility is reported.

3. Aluminum

Al was chosen for study in the induction furnace facility primarily because of its wide application in propulsion systems and because of its ignition and combustion inefficiency observed in such systems. Also, as discussed in Appendix II, the ignition of Al is thought to be controlled by its transition temperature, and thus is in contrast to that of Mg, which as has been shown is controlled by the critical temperature in the case of large samples.

The transition temperature of Al in O_2 is thought to equal the melting point of Al_2O_3 (see Chapter III), which is equal to 2030°C (6). Attainment of this temperature in a furnace will of course present several problems, the most obvious of which is materials. For this and other reasons to be discussed below, in the present investigation only preliminary experimentation with this metal was accomplished.

Al samples of two geometries were used in the investigation (Table 44): wafers of 2.54 cm diameter by 1.59 mm thickness and foils of 3.34 cm diameter by 0.254 mm; impurity analyses of the source materials are given in Chapter V. In both cases, the most satisfactory re-

TABLE 44.

ALUMINUM SAMPLE DESIGNATIONS

Designation	Sample Geometry	Average $S/V, mm^{-1}$	Source	Sample Dimensions	Thermocouple Position
ALI	wafer	0.764	2.54 cm rod	2.54 cm diam by 1.59 mm	center of bottom
ALII	0.254 mm foil	7.30	0.254 mm foil	3.34 cm diam by 0.254 mm	center of bottom

sults were obtained if the thermocouple bead was placed in the center of the containing crucible in contact with the bottom of the Al sample.

Only ignition temperature experiments were conducted with this metal. In the course of these experiments, five difficulties, some of which are unique to the induction furnace, became apparent.

The first problem involved measuring the temperature of the sample. As was noted in Chapter V, three types of thermocouples were tested, W/Re, Ir/Ir60Rh, and Pt/Pt13Rh thermocouples. The first type was found inadequate in both O_2 and CO_2 atmospheres because of oxidation of the W. Thermocouple wires of 0.51 mm diameter failed consistently at temperatures on the order of 1000°C in both of these gases in the pressure range of interest (300 torr through 5 atm).

Better results were obtained with the other two types of thermocouples, also using 0.51 mm diameter wire. In general, most of the experiments which were performed were limited by one of the other difficulties to be discussed below, but in the event of a thermocouple failure the following method was used to estimate the sample temperature.

The Leeds and Northrup Rayotube appropriate to the temperatures of interest in the Al investigation is calibrated at and above brightness temperatures of 975°C (see Chapter V). The thermocouples, on the other hand, could be used in most cases to temperatures on the order of 1500°C. Thus there is an overlapping of data from these two methods of temperature measurement.

If a mean emissivity of the Rayotube target was calculated according to Eqn. (VII-16):

$$\epsilon = (T_{RT}/T_{TC})^4 \qquad \text{(VII-16)}$$

where T_{TC} is the temperature measured by the thermocouple and T_{RT} is the grey body temperature registered by the Rayotube, then this mean emissivity, which was used to calculate the true temperature of the sample on the basis of the Rayotube temperature after the thermocouple had failed, was found to be relatively constant in any given experiment throughout the region of overlap (from about 1100 to 1500°C).

Values of emissivity so calculated are not comparable to literature values of the emissivity of Al, Al_2O_3, or the SiC crucibles because, firstly, the viewing area of this particular Rayotube, Model 8890, is large (6.54 square cm), secondly, the Rayotube may not have been in focus in a particular experiment, and finally, the actual position of the molten Al and crucible with respect to the Rayotube viewing area varied from experiment to experiment.

Crucible materials were the source of the second problem which curtailed the Al investigation. As noted

in Chapter V, the preliminary experimentation was conducted with ignition dishes constructed from SiC, which was found to be completely unsatisfactory. At heating rates of about 60°C/min, in many of the individual experiments these crucibles were observed to crack and in some cases explode at temperatures in excess of 1000°C.

Because SiC couples with the magnetic field of the work coil, it is subject to the RF skin effect which was discussed in the preceding section of this chapter. The skin effect creates large thermal gradients in the crucible, and these gradients are thought to be responsible in part for the observed failure of the crucibles. The hole which was drilled in the center of the bottom of the crucible to accomodate the thermocouple also presented a source of mechanical stresses. Many of the cracks which destroyed the crucibles appeared to emanate from these holes.

The materials problem may possibly be circumvented by use of other high temperature materials such as ZrO_2 or SiO_2N_2; crucibles of these compounds were not available at the time of the present investigation.

The other three difficulties which were encountered in the Al investigation are all unique to the induction furnace; these are electrical arcing, power-limited experiments, and the magnetic field-surface tension interaction. The former was observed generally at the lower pressures of interest and occurred between the work coil and the sample or crucible. In several cases it was impossible to ascertain whether arcing or explosion of the crucible occurred first. Preliminary experiments in which a transformer was used in order to decrease the potential drop across the coil indicated that the efficiency of the transformer severely limited

the maximum power available. Increasing the spacing between the crucible and the coil, by using a larger diameter work coil, had the same effect. Most likely the high temperature Al experiments can be conducted only at pressures higher than atmospheric, where arcing was not observed.[7]

Recall that an induction furnace is power-limited rather than temperature-limited. Some of the experiments with the large Mg cylinders in 5 atm of CO_2 were power-limited, and similar difficulties were found in some experiments with Ca. Even for the small Al samples, this problem occasionally appeared.

Since the power input to the sample within the work coil is proportional to the square root of frequency in use (260), higher sample power inputs could be attained with the present 10 KW generator by using the high frequency oscillator circuit rather than the low frequency circuit. However, as was mentioned in Chapter V, in the frequency range of the high frequency generator dielectric heating becomes important and would bring about heating of the insulators surrounding the current feedthroughs entering the test vessel. Also, the arcing problem would be expected to increase with use of the higher frequency. Thus use of the high frequency oscillator circuit in conjunction with the present design of the pressure vessel is unfeasible.

The final problem which limited the Al experiments is the magnetic field-surface tension interaction which was explained in the preceding section of this chapter. For the ALII samples (of thickness 0.254 mm) most of the metal formed an annulus after the metal had

[7] As will be shown later, arcs were not observed at 2 or 5 atm.

melted; only a thin film of metal remained in the interior. Thus the thermocouple readings will not indicate the true metal temperature. This interaction was not observed with the ALI samples, however, and successful experimentation could be conducted with samples of this thickness (1.59 mm) or larger.

As noted previously, only ignition temperature experiments were attempted in the present investigation. These were done primarily with the ALII samples, and only in pure O_2 or CO_2. The results of these experiments are shown in Table 45. In the table are listed the maximum temperature attained in the particular experiment, either as measured by the thermocouple or as estimated from the mean emissivity calculation for the particular experiment, and the cause of termination or failure of the experiments. The first values listed in these columns were obtained in experiments using Pt/Pt13Rh thermocouples and the second using Ir/Ir60Rh. The legend for failure mode is an follows: P indicates a power-limited experiment; A indicates arcing; and C indicates a crucible cracking or exploding. All of the experiments with the ALII samples were also subject to the surface tension problem.

The highest temperature attained in the experiments with no ignition observed was 1586°C. Two ignitions were observed, in O_2 and in CO_2 at 5 atm, at temperatures of 1329 and 1170°C, respectively. However, because the thermocouple was not in contact with all of the molten metal sample (due to the surface tension effect), these ignition temperatures are definitely low. Also, it was not definitely ascertained that the Al ignited; in other

TABLE 45.

RESULTS OF PRELIMINARY Al EXPERIMENTS

0.254 mm FOILS, ALII (Average S/V = 7.30 mm^{-1})

Gas	Total Pressure	Average Initial Heating Rate, °C/min*	Ignition Temperature, °C*	Failure Mode*
O_2	300 torr	61,60	>1318, >1515	P,P
	1 atm	67,60	>1321, >1120	A,A
	2 atm	58,80	>1424, >1315	C,P
	5 atm	58,70	1329, >1040	C or A,C
CO_2	300 torr	--,95	>1182, >1527@	C or A,C
	1 atm	66,85	>1586@, >1210	P,C or A
	2 atm	66,--	>1437, >1315	P,P
	5 atm	54,70	>1433,1170	P,C

*First value listed is from an experiment with Pt/Pt13Rh thermocouple, and second value with Ir/Ir60Rh thermocouple.
P denotes experiment power-limited.
A denotes experiment terminated by an arc.
C denotes experiment terminated by explosion of SiC crucible.
@This temperature was estimated from the Rayotube mean emissivity calibration. The thermocouple failed at a lower temperature.

words, the SiC crucible may have ignited first, and then heated the Al to ignition.[8] As is seen from the table, these ignitions were unreproducible.

With the ALI samples similar temperatures were attained before the onset of the difficulties noted above, but in one experiment in O_2 at 1 atm, a temperature of 1720°C was reached with no ignition in a power-limited experiment.

It is felt that most of the difficulties encountered in the preliminary experiments with Al can be

[8]A blank run, without the Al sample, could not be conducted because the thermocouple would immediately couple with the field and burn out. Thus any ignition temperature of the SiC crucibles could not be measured.

circumvented: temperatures may be estimated after failure of the thermocouple through use of the Rayotube brightness temperature and the mean emissivity calculation; ZrO_2 or SiO_2N_2 crucibles may withstand the thermal stresses in the temperature range of interest; the arcing problem may be eliminated by experimentation at 2 and 5 atm; redesign of the current feedthroughs at the rear of the test vessel may allow use of the high frequency oscillator circuit of the RF generator and thus permit higher power inputs to the sample; and use of ALI and larger samples will guarantee that the interaction between the magnetic field and the surface tension of the molten metal is unimportant.

The results which were obtained in the present investigation do not contradict the conclusions reached on the basis of the literature review, that the ignition and transition temperatures of Al in O_2 and CO_2 equal the melting point of Al_2O_3.

4. Calcium

When the various problems associated with the study of the ignition of Al were discovered, an investigation of the ignition of Ca was begun. This metal was chosen for study for primarily the following reasons: firstly, literature values of bulk ignition temperature in O_2 equal 550°C (22, 196, 200), and this low temperature could present no problems of the nature encountered in the Al investigation; secondly, the literature review indicated that the ignition of this metal was controlled by the transition temperature (see Chapter IV), and thus the ignition of Ca and Al were thought to be similar; and finally, the O_2 ignition temperature for Ca, 550°C, given by other investigators (22, 196, 200), is well below the metal melting point of 850°C (6), and thus the interaction

between the magnetic field and the surface tension acting on the molten metal should not occur in the temperature range associated with the ignition of this metal. As will be seen in this section, however, under the experimental conditions of the present investigation ignition of Ca occurred at a higher temperature than that listed in the literature and for large samples is controlled by the critical temperature.

The investigation of the ignition of Ca was conducted by exactly the same methods and procedures used with Mg; that is, ignition temperature experiments and critical temperature experiments with initial equilibration either in Ar or in the oxidizing gas of interest were performed. The only important differences were the use of a SiC rather than Inconel W susceptor in the critical temperature experiments and heating by means of the constant rate of change of temperature control unit described in Chapter V.

Sample specifications for the three sample sizes which were used are given in Table 46. (The impurities contained within the source materials are listed in Chapter V.) For the purpose of calculation of the surface areas of the three types of samples, it was assumed that the top and side of the cylinders and all surfaces of the two foil sizes were exposed to the oxidizing gas.

Thermocouple calibrations in situ were accomplished during the experiments by observation of the metal melting and freezing point of 850°C (6). The thermocouple error throughout the Ca investigation was 10°C or less. Chromel-alumel thermocouples were found satisfactory except in certain experiments in which the thermocouple was exposed to molten Ca for times longer than about 10 min; upon such exposure the thermocouples usually failed.

TABLE 46.

CALCIUM SAMPLE DESIGNATIONS

Designation	Sample Geometry	Average $S/V, mm^{-1}$	Source	Sample Dimensions	Thermocouple Position
CAI	cylinder	0.201	2.34 cm rod	2.34 cm diam by 1.90 cm	6.3 mm from top on centerline
CAII	0.889 mm foil	2.30	0.889 mm foil	3.34 cm diam by 0.889 mm	center of top
CAIII	0.508 mm foil	4.08	0.508 mm foil	3.34 cm diam by 0.508 mm	center of top

a. Ignition Temperature Experiments

Results of the ignition temperature experiments for the Ca cylinders and foils are shown in Fig. 37 through 39. As before, ignition temperature is plotted versus total pressure on a logarithmic axis, and the average ignition temperature in a particular gas combination, average initial heating rate, average surface to volume ratio, and average temperature error are indicated in the figures.

From these figures it is seen that only with the smallest samples in 5 atm of O_2 were ignition temperatures observed commeasurate with the literature value of 550°C (22, 196, 200). However, the literature value is presumably for bulk ignition in O_2 at 1 atm; unfortunately, none of these investigators gave the surface area to volume ratio of the samples used in their experiments (Table 16).

However, these investigators used resistance furnaces to measure their ignition temperatures (22, 196, 200), whereas the present investigation makes use of an induction furnace for the ignition temperature experiments. As was

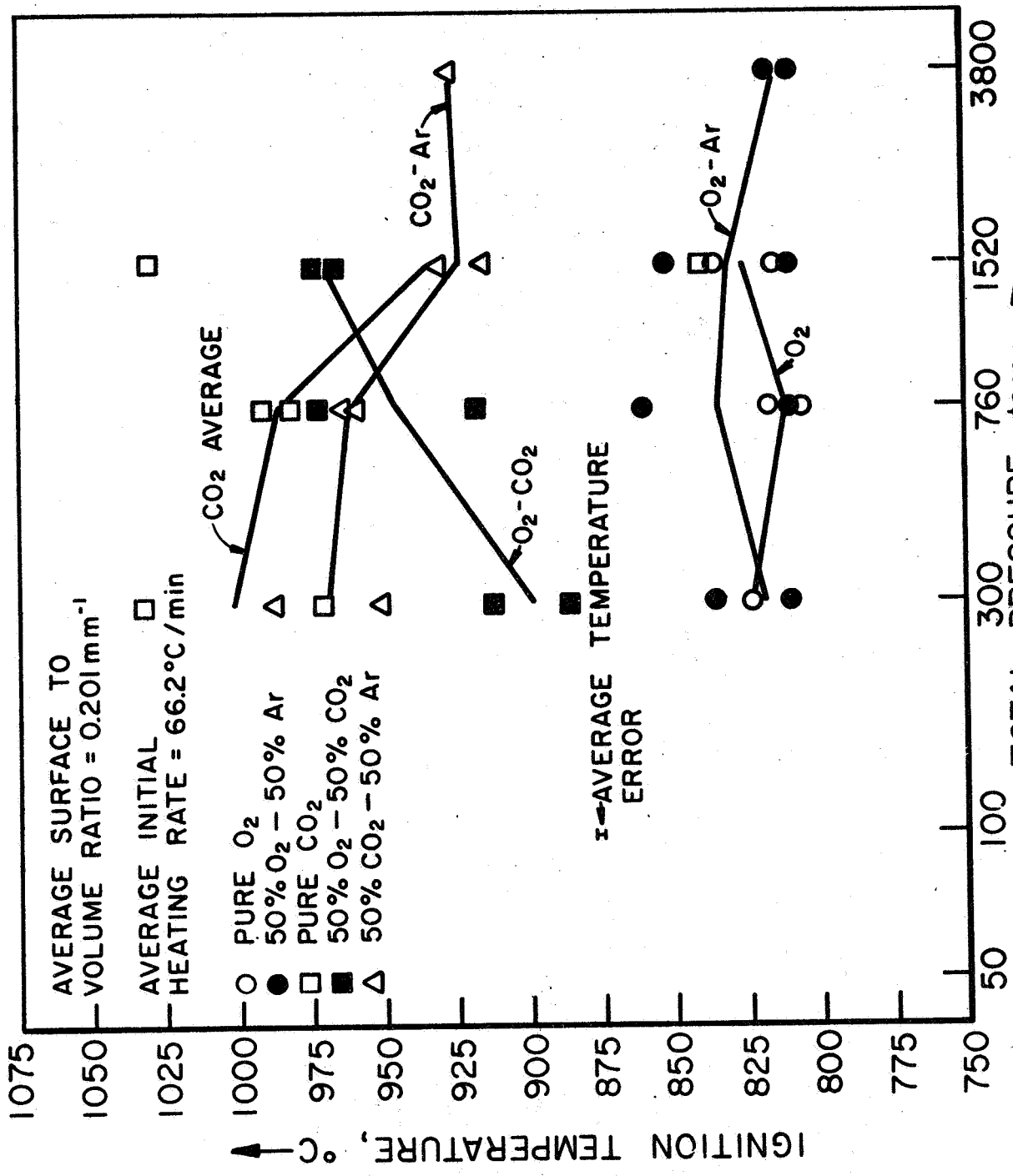

CALCIUM IGNITION TEMPERATURE IN VARIOUS OXIDIZING GASES VS TOTAL PRESSURE (CYLINDERS, CA I)

FIGURE 37

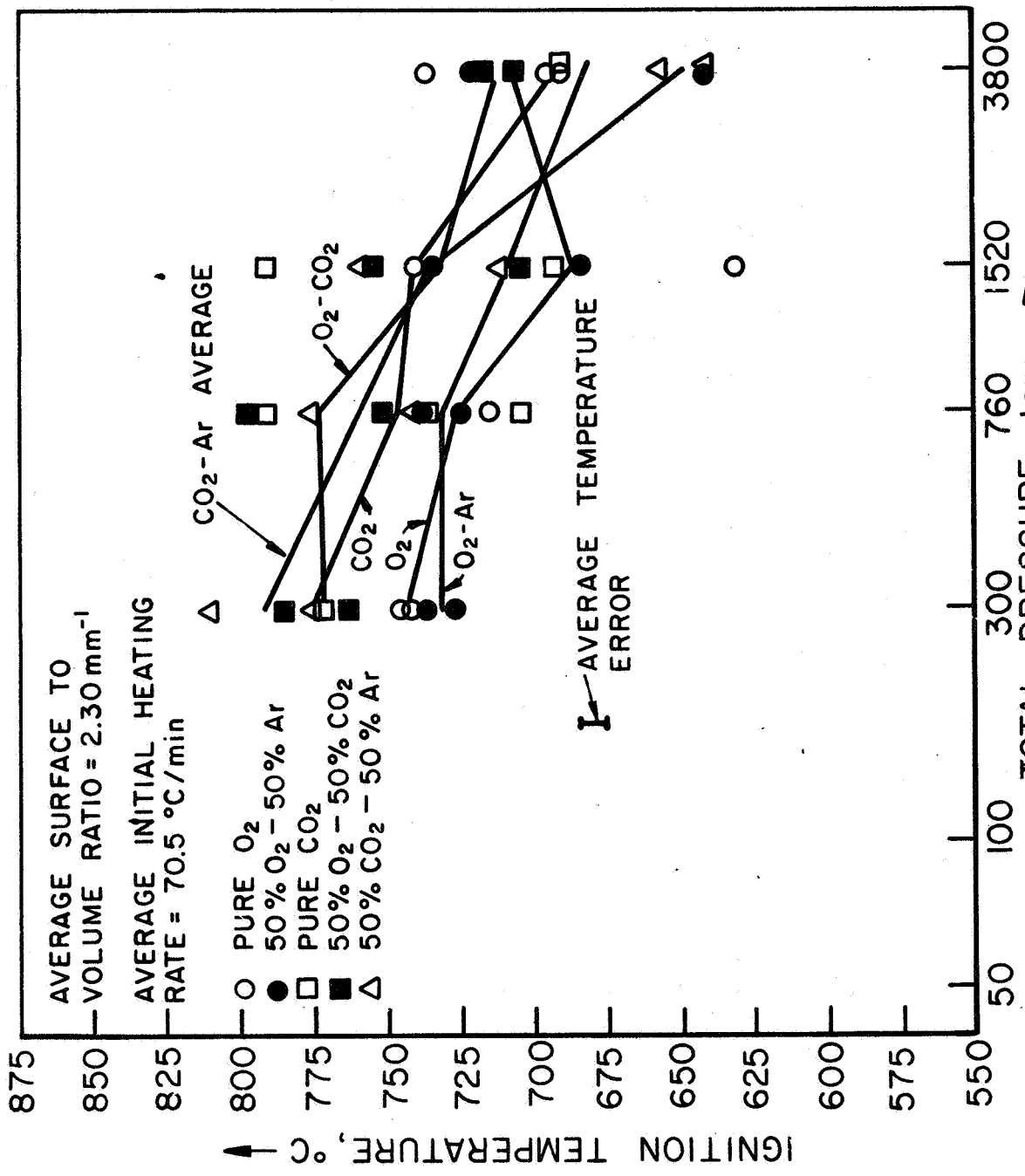

CALCIUM IGNITION TEMPERATURE IN VARIOUS OXIDIZING GASES VS TOTAL PRESSURE (0.889 mm FOILS, CA II)

FIGURE 38

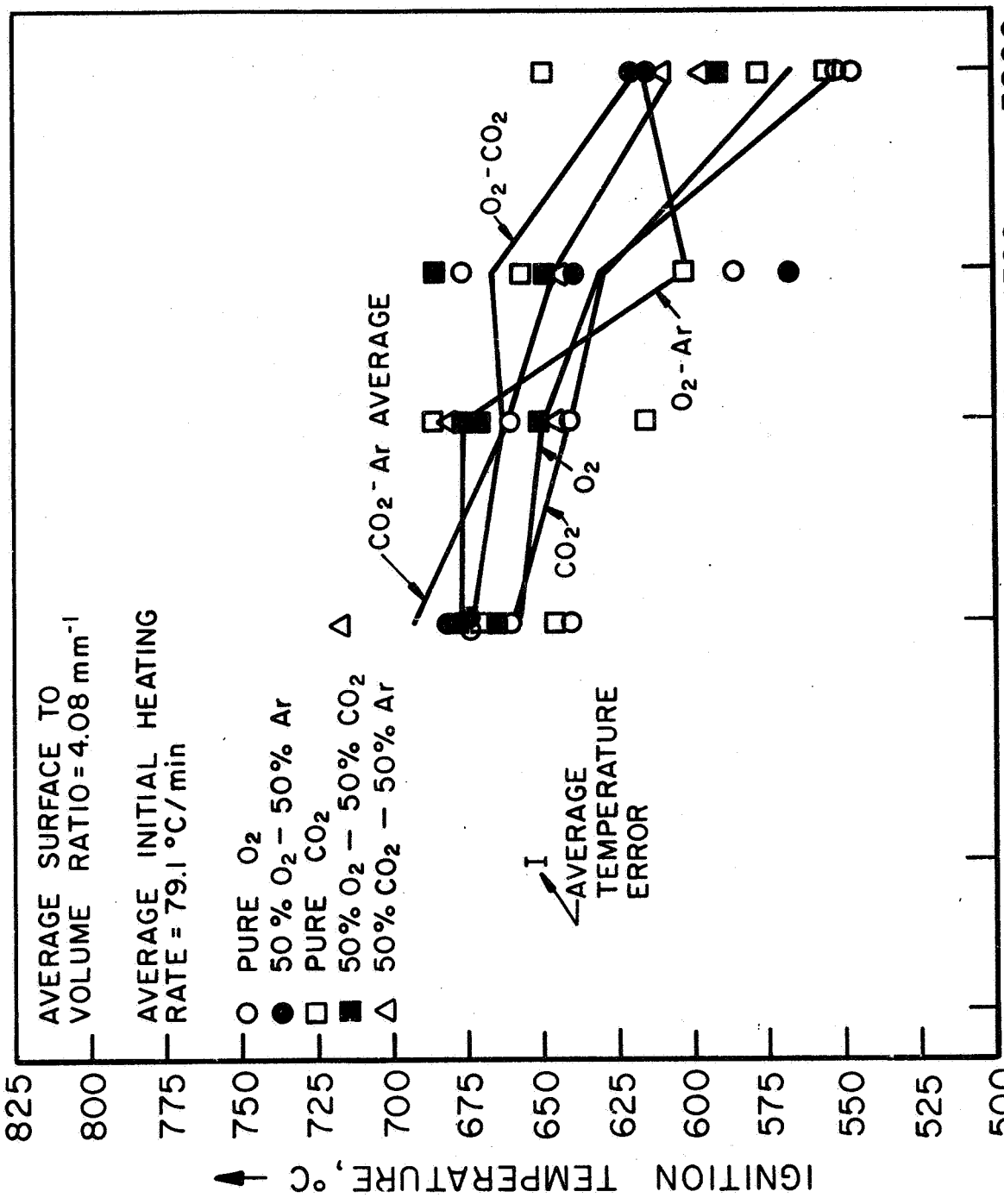

CALCIUM IGNITION TEMPERATURE IN VARIOUS OXIDIZING GASES VS TOTAL PRESSURE (0.508 mm FOILS, CA III)

FIGURE 39

noted in Section 2, in the environment provided by the latter type of furnace, a large conduction heat loss into the sample is expected because of the radio frequency skin effect. Thus the $\dot{q}_{loss}$ curve will shift upwards on the $\dot{q}$ versus T_s diagram, and higher ignition (and critical) temperatures will be measured in an induction furnace for metals whose bulk ignition is controlled by the critical temperature.[9]

As was the case for Mg, the Ca cylinders ignited at the metal melting point (850°C (6)) in O_2 and the O_2-Ar combination and above the metal melting point in CO_2, CO_2-Ar, or O_2-CO_2 mixtures (Fig. 37). As expected on the basis of the ignition model, for the smaller samples lower ignition temperatures were observed (Fig. 38 and 39). In all cases, the thermocouple ignition temperatures defined by maximum rate of change of sample temperature and of light intensity emitted by the sample were essentially equivalent, except in a few cases where the Rayotube viewed an area different from the thermocouple position.

Combustion of all sample sizes in O_2, CO_2, or the various gas mixtures occurred in a brilliant white flame with traces of orange coloring (emission from either atomic Ca or molecular CaO (269)); only at the lower pressures in CO_2 and the CO_2-Ar mixture did several flamelets occupy the sample surface simultaneously. The products of combustion in all of the oxidizers consisted of white smoke and white, brown, and black powders and deposits; in the CO_2-containing mixtures a strong scent of C_2H_2 emanated from the massive products after an experiment and indicated that CaC_2 had been formed in the reaction. Occasionally a similar smell was observed with the products of combus-

[9] See Section 4.b.

tion in O_2 and the O_2-Ar mixture, probably as a result of incomplete washing of the mineral oil (under which the samples had been stored) from the sample during its preparation.

(1) The Effect of Total Oxidizer Pressure

By comparison of Fig. 37, 38, and 39, the total pressure trend in ignition temperature as a function of sample size can be seen. One major difference from that observed with Mg is apparent: for Ca the ignition temperature for the cylinders in CO_2 and 50%CO_2-50%Ar decreases with increasing total pressure. (Recall that for the large Mg cylinders the ignition temperature increased with increasing pressure.) As one would suspect from examination of Fig. 37, the Ca ignition temperatures in CO_2 and in the CO_2-Ar mixture are more a function of total pressure than of partial pressure of CO_2.

Although it is possible that the lack of correlation of these ignition temperatures with the partial pressure of CO_2 indicates that the reaction is diffusion controlled, it is felt that the disagreement is simply a result of the large scatter in the measured ignition temperatures which are shown in Fig. 37 because, firstly, the opposite trend observed in the O_2-CO_2 mixture suggests a kinetic effect, and secondly, the ignition temperatures for the smaller samples appeared to be functions only of the CO_2 partial pressure. In the case of these smaller samples the ignition temperature in O_2 or 50%O_2-50%Ar was a function only of the O_2 partial pressure; the results obtained in the O_2-CO_2 mixture correlated with the CO_2 partial pressure.

The decrease in ignition temperature with increasing total pressure found for the two foil samples

(Fig. 38 and 39) indicates that heat losses to the environment are the important mechanisms of heat transfer from the reaction surface, as was the case for the small Mg samples as well (see Section 2.a.(1)).

(2) The Effect of Sample Size

For a total pressure of 300 torr, the average ignition temperatures for the various Ca samples in the various gas combinations are plotted versus surface area to volume ratio in Fig. 40. As the plots for total pressures of 1, 2, and 5 atm were exactly similar except for a slight lowering of ignition temperature with increasing pressure, only the single figure is presented.

The estimation of the Ca-O_2 transition temperature as 400°C in the pressure range from 100 to 760 torr has been discussed in Appendix I. As no reaction rate data are available in the literature for the oxidation of Ca in CO_2, no estimate of the Ca-CO_2 transition temperature can be made. Also, no comparable ignition temperatures are available in the literature (Table 16), because in the oxidizing gases of interest other investigators neglected to give the surface-volume ratio of their samples.

For the three sample sizes used in the present investigation, no bulk ignition regime, in which the ignition temperature is expected to become independent of sample size, is apparent. However, the definite lowering of ignition temperature with increasing S/V and the magnitude of the discrepancy between the ignition temperature in O_2 and the appropriate transition temperature suggest that the ignition of Ca in all of the gases studied is controlled by the critical temperature rather than the transition temperature under the conditions of the present

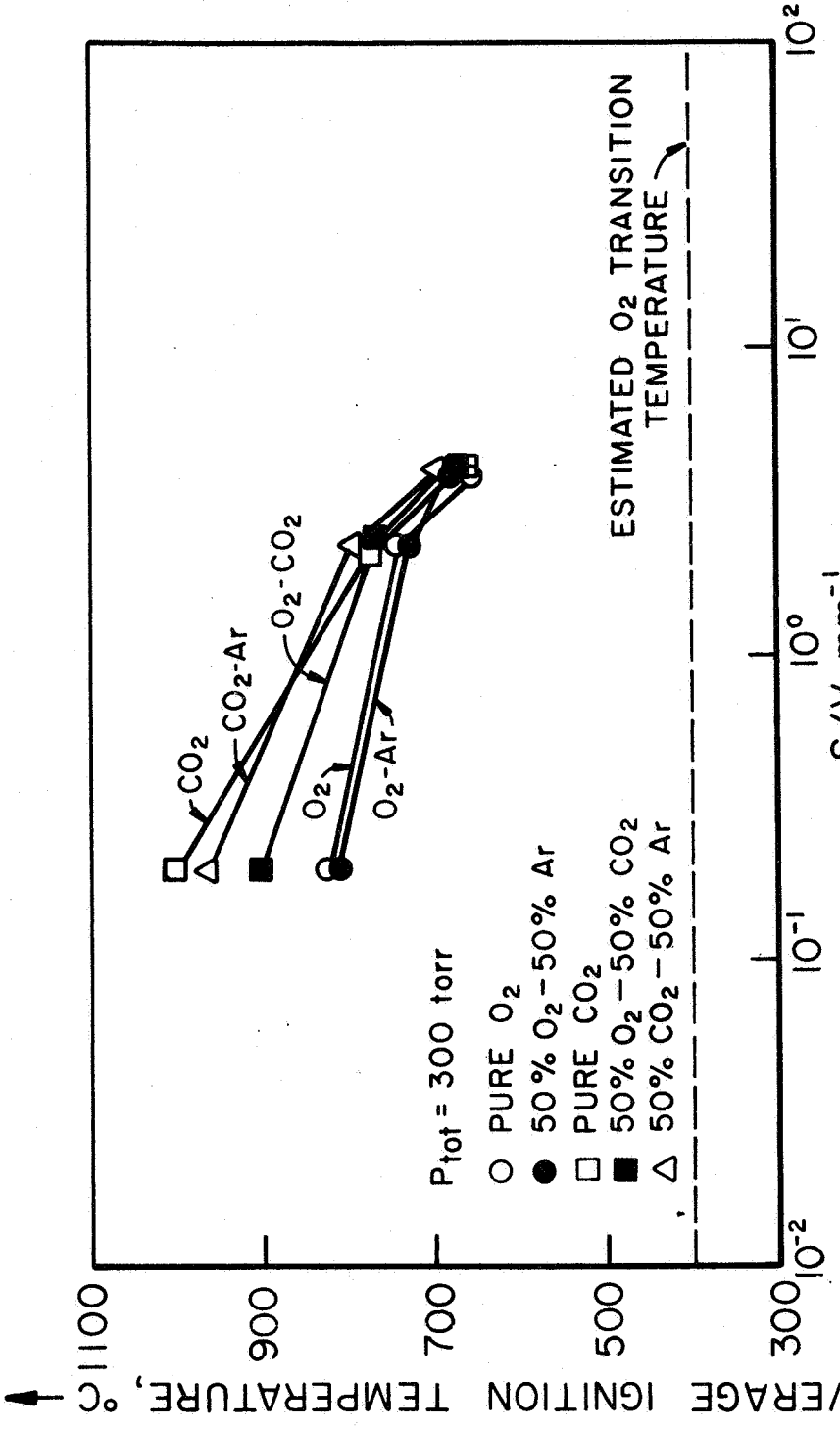

CALCIUM AVERAGE IGNITION TEMPERATURE IN VARIOUS OXIDIZING GASES VS SURFACE TO VOLUME RATIO (TOTAL PRESSURE = 300 torr)

FIGURE 40

AP 24 E 4053 C7

experiments. This conclusion will be substantiated further in the section which follows dealing with the measured critical temperatures for Ca.

(3) The Effect of Applied Heating Rate

Ignition temperature as a function of applied heating rate is shown in Tables 47 through 49. In general, for all three sample sizes any dependence on heating rate is slight except in two isolated cases: for the large Ca cylinders in O_2 at 300 torr or 2 atm, and for the smaller foils in 50%O_2-50%CO_2 also at these total pressures, the ignition temperature decreases with increasing heating rate. The former trend may be explained as follows: since ignition occurs at the melting point of the metal for the large cylinders in O_2, and since the metal melting point of 850°C is the value which would be obtained in an melting experiment only for extremely slow heating rates, but in actuality will occur over a wider and wider temperature range as the applied heating rate is increased, ignition occurs at lower temperatures with increasing heating rate. Note, however, that this trend is not clearly defined in the O_2-Ar mixture, as would be expected.

Because of the general independence of ignition temperature on heating rate and because no anomalous glows or flashes were observed with this metal during the heating process, it is concluded that the magnetic force-surface tension effect which was important with the smaller samples of both Mg and Al had no influence on the measured ignition temperatures, probably as a result of the larger thickness of the Ca samples (0.508 mm) as compared to the depth of penetration or skin effect (on the order of 0.15 mm). Therefore, at least in terms of the present experimental environment of the induction furnace, these igni-

TABLE 47.

EFFECT OF HEATING RATE ON IGNITION TEMPERATURE:

Ca CYLINDERS, CAI (AVERAGE S/V = 0.201 mm^{-1})

Gas	Total Pressure	Time Average Initial Heating Rate, ^{o}C/min	Ignition Temperature, ^{o}C
O_2	300 torr	8	863
		83	823
		104	803
	2 atm	9	832
		44	836
		81	815
		179	803
50% O_2- 50% Ar	300 torr	8	837
		76	836
		93	810
		162	839
	2 atm	10	827
		38	852
		60	810
		157	832
CO_2	300 torr	9	1020
		82	1032
		87	970
		187	997
	2 atm	9	909
		70	839
		71	1029
		170	968
50% CO_2- 50% Ar	300 torr	7	958
		67	987
		76	950
	2 atm	8	967
		66	930
		83	915
		151	>935
50% O_2- 50% CO_2	300 torr	10	924
		74	912
		79	886
		172	929
	2 atm	9	939
		55	964
		63	973
		122	828

TABLE 48.

EFFECT OF HEATING RATE ON IGNITION TEMPERATURE:

0.889 mm Ca FOILS, CAII (AVERAGE S/V = 2.30 mm^{-1})

Gas	Total Pressure	Time Average Initial Heating Rate, $^{o}C/min$	Ignition Temperature, ^{o}C
O_2	300 torr	11	764
		71	746
		96	742
		132	758
	2 atm	57	739
		66	632
		174	752
50% O_2- 50% Ar	300 torr	8	723
		38	727
		81	736
		131	730
	2 atm	13	739
		38	733
		92	683
		131	761
CO_2	300 torr	7	697
		39	772
		80	779
		167	758
	2 atm	10	680
		80	790
		83	692
		181	748
50% CO_2- 50% Ar	300 torr	9	767
		57	811
		94	773
		191	771
	2 atm	11	710
		75	758
		91	711
		182	765
50% O_2- 50% CO_2	300 torr	9	787
		86	779
		93	763
		114	757
	2 atm	9	761
		69	757
		73	705
		171	778

TABLE 49.

EFFECT OF HEATING RATE ON IGNITION TEMPERATURE:

0.508 mm Ca FOILS, CAIII (AVERAGE S/V = 4.08 mm^{-1})

Gas	Total Pressure	Time Average Initial Heating Rate, °C/min	Ignition Temperature, °C
O_2	300 torr	11	689
		55	640
		61	661
		68	673
		197	684
	2 atm	12	661
		76	674
		78	585
		186	632
50% O_2- 50% Ar	300 torr	10	700
		78	673
		84	680
		181	646
	2 atm	8	671
		84	567
		93	633
		188	655
CO_2	300 torr	11	705
		70	645
		99	670
		165	642
	2 atm	12	645
		78	601
		81	655
		171	605
50% CO_2- 50% Ar	300 torr	9	687
		81	667
		100	717
		183	677
	2 atm	7	632
		77	643
		98	646
		174	603
50% O_2- 50% CO_2	300 torr	9	711
		72	664
		90	678
		193	620
	2 atm	13	702
		86	683
		90	647
		151	626

tion temperatures are "real".

In the next section of this chapter the results of the critical temperature experiments with Ca are described and discussed.

b. Critical Temperature Experiments

The only significant differences between the procedure and apparatus of the Mg and Ca critical temperature experiments were the use of the temperature differentiating unit to assist in definition of sample equilibrium (that is, time zero of the experiments) and use of a SiC rather than Inconel W susceptor. As was noted in Chapter V, higher initial sample temperatures could be attained with the former susceptor.

In spite of these higher temperatures, it was found necessary to conduct experiments at 300 and 760 torr rather than at 300 torr and 2 atm as in the Mg investigation, because in both O_2 and CO_2 at 2 atm the Ca critical temperature experiments were invariably power-limited; radiation and convective heat losses from the outside of the large susceptor were responsible for this difficulty.

Critical temperature experiments were performed with only the Ca cylinders and 0.508 mm foils in pure O_2 and pure CO_2 at the aforementioned pressures. The results are listed in Table 50, and the experimental parameters and errors are given in Table 51. Several observations can be made on the basis of Table 50; most of these are expected on the basis of the Mg investigation or of the Ca T_{ign} versus S/V graphs.

The first and differing result is the correspondence of the ignition and critical temperatures for both sample sizes at both total pressures in O_2. Extensive

TABLE 50.

RESULTS OF THE CALCIUM CRITICAL TEMPERATURE EXPERIMENTS

Gas	Pressure	Estimated T_{trans}, °C	Sample	Average S/V, mm^{-1}	Initial Equilibration in Ar: T_{crit}, °C	Initial Equilibration in Ar: $(T_{ign})_{ave}$, °C	Initial Equilibration in O_2 or CO_2: T_{crit}, °C	Initial Equilibration in O_2 or CO_2: $(T_{ign})_{ave}$, °C	$(T_{ign})_{ave}$, as measured in Ignition Temperature Experiments, °C
O_2	300 torr	400	cylinder	0.204	801	801	801	801	823
			0.508 mm foil	4.02	760	760	763	763	668
O_2	1 atm	400	cylinder	0.204	799	799	798	798	812
			0.508 mm foil	4.02	777	777	816	816	649
CO_2	300 torr	---	cylinder	0.204	870	874	885	935	1001
			0.508 mm foil	4.02	796	---*	799	844	658
CO_2	1 atm	---	cylinder	0.204	850	919	850	884	986
			0.508 mm foil	4.02	760	793	770	798	640

* This datum is missing because of failure of the chromel-alumel thermocouples upon prolonged exposure to molten Ca. In such cases ignition and ignition delay times were defined with the Rayotube.

TABLE 51.

EXPERIMENTAL PARAMETERS FOR THE CALCIUM CRITICAL TEMPERATURE EXPERIMENTS

Sample	Designation	Average S/V_{-1} mm	Average Initial Heating Rate, ^{o}C/min	Sample Thermocouple Error, ^{o}C	Susceptor Deviation From Set Point, ^{o}C
cylinder	CAI	0.204	52.4	6.6	5.5
0.508 mm foil	CAIII	4.02	58.6	9.2	3.8

experimentation was performed at these test points, but in no case was sample self-heating observed; the samples either ignited before equilibrium was established or did not ignite (or self-heat) within the one hour time limit of the experiments. Thus the ignition and critical temperatures could not be distinguished and have been taken as equal in Table 50.

The explanation of this phenomenon that immediately comes to mind is that the experiments were performed at the ignition limit at which these two temperatures are equal (see Chapter II). However, it is extremely unlikely that coincidence with the ignition limit could occur over such a wide range of the independent experimental variables: increasing the total pressure should increase the reaction rate and thus $\dot{q}_{chem}$ and decreasing the sample size should decrease the magnitude of heat losses into the sample and thus $\dot{q}_{loss}$.

Rather, it is thought that this coincidence of critical and ignition temperatures results from ignition

occurring at the metal melting point (850°C (6)) at all of the O_2 test points. This conclusion is substantiated by the experimental observation of the levelling of the temperature traces in the temperature range of the ignition temperatures in O_2. In other words, the intersection of the $\dot{q}_{chem}$ and $\dot{q}_{loss}$ curves which represents the critical temperature occurs at the metal melting point in the particular experimental situation used in the present investigation. Ignition also occurs at this temperature because of the increase in enthalpy of the Ca at its melting point (that is, addition of the heat of fusion), as was also the case for the large Mg samples in O_2.

As the critical (and ignition) temperatures in O_2 given in the table far exceed the Ca-O_2 transition temperature of 400°C, it is concluded that the critical temperature controls in the ignition of Ca in O_2. Thus all of the trends which were observed with the Mg results should appear in the Ca results as well.

Although no estimate of transition temperature for the Ca-CO_2 system can be made, the appearance of the size effect in ignition temperature indicates that the critical temperature controls in CO_2 as well.

As for the Mg investigation, the following observations can be made (Table 50): firstly, the ignition temperatures in both O_2 and CO_2 are relatively independent of oxide film thickness, as little difference in the values measured in the two types of critical temperature experiments is seen[10] (as expected in cases for which the critical temperature exceeds the transition temperature). The lack of any effect of applied heating rate for all sample sizes in the ignition temperature ex-

[10]Note, however the anamolous behavior of the data for the large samples in CO_2 and the small samples in O_2 at 1 atm.

periments is consistent with this observation, and the discrepancies shown in Table 50 are generally within the experimental scatter.

Secondly, in CO_2 at 300 torr where the critical and ignition temperatures are distinguishable, the pressure trend of these two temperatures is similar. At 1 atm, since the critical temperature is approximately equal to the metal melting point, no pressure trend in critical temperature is observed.

Thirdly, the size effect in ignition is not as pronounced in the experiments using the susceptor, which is characterized by more uniform heating of the sample and shielding of the sample from heat losses to the environment.[11]

Finally, for the large Ca cylinders measured ignition temperatures are lower with the susceptor, because the magnitude of the heat loss into the interior of the sample is decreased (relative to the environment using induction heating). That is, for the large Ca (and Mg) samples in the susceptor, more uniform heating of the sample occurs since there is no skin effect; thus this heat loss term is diminished by the susceptor.[12] For the smaller samples, however, which are shielded from heat losses to the environment by the susceptor,

---

[11] Recall that because the effect of heating rate on ignition temperature in ignition temperature experiments was slight, it was concluded that the thermocouple errors due to the skin effect and to any surface tension phenomena were unimportant in these experiments.

[12] Also, of course, since ignition temperatures with the susceptor are measured in experiments generally starting at equilibrium (that is, critical temperature experiments), temperature gradients into the sample should be very small or, in the limit, zero.

higher ignition temperatures are observed with the susceptor environment. See Section 2.b os this chapter.

Again the importance of experimental environment on measured critical and ignition temperatures is demonstrated for cases in which the critical temperature exceeds the transition temperature. Recall, however, that it was concluded tentatively on the basis of the Mg results that a bulk ignition temperature exists, at which the heat losses into the sample and thus the ignition (and critical) temperatures become relatively independent of size. This conclusion must now be questioned because of the lack of correspondence between literature values of Ca-O_2 ignition temperature (550°C (22,196, 200)) and those obtained in the present investigation, even with the susceptor in the critical temperature experiments. It was noted at the beginning of this section that lower ignition temperatures measured in resistance furnaces can be explained by the model in terms of reduced heat losses into the metal sample; the fact that high ignition temperatures were observed also using the SiC susceptor must then reflect incomplete shielding of the sample from the magnetic field of the work coil. However, it is possible that a region of bulk behavior exists in a given experimental situation and, that in differing experiments, bulk ignition temperatures may not be comparable.

Apparently, then, the only absolute value of ignition temperature for any metal-oxidizer system is the appropriate transition temperature. Since this temperature is also the lowest possible ignition temperature, only a lowering limiting value can be placed on ignition temperature, both for cases in which the critical temperature is larger than the transition temperature and vice versa. The value of ignition temperature as compared to the transition temperature will then reflect the sample size, method of sample heating, and heat losses from the sample to the environment, that is, the particular nature of the experimental environment.

c. Summary

Although Ca was selected for study in the induction furnace because literature values of transition and ignition temperatures in O_2 indicated that the latter was controlled by the former, the present results have shown that in the experimental apparatus used the critical temperature controls in ignition, both in O_2 and in CO_2. Thus the ignition of Mg and Ca are similar. The more significant conclusions are as follows:

(1) Although the samples used in the present investigation were too large to have ignition temperatures on the order of the transition temperatures, the expected size trend was observed, as the ignition temperature decreased as the surface area to volume ratio of the sample was increased. In CO_2 under all conditions the ignition temperature exceeded the measured critical temperatures.

(2) Unlike the case of Mg, however, in O_2 the ignition and critical temperatures could not be distinguished, probably because both occurred within the temperature range of melting of the metal.

(3) The lack of correspondence between the bulk ignition temperatures measured in the present investigation and those reported in the literature indicates that the bulk ignition temperature also cannot be considered an absolute ignition temperature independent of the particular experimental environment; use of an induction furnace with its associated skin effect gives large conduction losses into the interior of the metal sample and thus high ignition temperatures and emphasizes the relative nature of ignition and critical temperatures.

(4) It is therefore concluded that only the transition temperature is actually an absolute reference temperature. For metals such as Mg or Ca, one can expect ignition temperatures greater than or equal to the appropriate transition temperatures; for a metal such as Al, ignition will always occur at the transition temperature.

In this chapter quantitative data on ignition temperatures and critical temperatures for Mg and Ca, obtained in the induction furnace facility, have been discussed. Although experimentation with metals whose ignition is thought to be controlled by the transition temperature was not conducted, because of experimental difficulties encountered in the study of Al, and because unexpected results were found in experiments with Ca, the ability of the metal ignition criterion to correlate ignition data has been demonstrated both in general and in particular.

CHAPTER VIII - CONCLUSIONS

Metal ignition and metal combustion have gained widespread attention in recent years because of several modern applications, including the addition of the light metals to solid propellant rocket fuels. In situations of this type fast and efficient ignition and combustion are necessary to guarantee attainment of theoretical specific impulse. However, for reasons not clearly understood, the desired performance is usually not fully realized.

Fundamental studies of metal ignition and combustion are needed in order to shed light on those processes which are important in propulsion applications; the present investigation has concerned itself with the problem of metal ignition in such a manner.

A physical model of metal ignition has been developed in Chapter II. This model is based on the classical thermal theories of heterogeneous ignition, but distinguishes between the spontaneous ignition and ignition temperatures: the former, named the critical temperature, is introduced as that intersection of the curves of rate of heat release by the chemical reaction and of rate of heat loss from the reaction surface which is unstable with respect to perturbations of surface (or reaction) temperature. The ignition temperature, on the other hand, is that surface temperature at which immediate inflammation or temperature runaway (ending in steady, self-sustained combustion) occurs. Other than a numerical difference between these two temperatures, an ignition delay time separates them. Since such delays are undesired, in propulsion applications it is of interest to see that the metallic additives are heated to their ignition temperatures by the reaction of the solid propellant.

However, there is one further complication arising in the problem of metal ignition. This complication is the formation of a solid-phase product film on the reaction surface through ordinary low-temperature oxidation reactions. Study of the metal oxidation literature has revealed that in general at low temperatures such oxidation product films may be classified as protective and as non-protective at higher temperatures (but below the ignition temperatures). The distinction between a non-protective and protective product film is defined by the temporal dependence of the reaction rate describing its formation: the low-temperature, or protective rate laws are inversely proportional to some function of time, whereas the higher temperature, non-protective rate law is independent of time (the linear rate law).

As noted, the different types of rate laws occur in different temperature regimes; on this basis, a third temperature, called the transition temperature, is introduced into the physical model of metal ignition. At and above this transition temperature, the oxide film is non-protective in the sense that a linear rate law is observed for its formation in ordinary low-temperature metal oxidation experiments.

Since the critical and ignition temperatures are defined in terms of heat losses from the reaction surface, these temperatures are expected to depend strongly on the environment experienced by the metal sample; the transition temperature, however, is postulated to be relatively independent of environment.

A criterion for metal ignition is then postulated: the ignition temperature, defined by the appearance of a flame, must be greater than both the critical tem-

perature, at and above which sample self-heating is possible, and the transition temperature, at and above which the oxide film formed in the low temperature pre-ignition reactions is non-protective. A more restrictive statement can be made because of the absolute nature of the transition temperature: the minimum possible ignition temperature is the transition temperature appropriate to the product film formed on the reaction surface.

Study of the effect of size of the metallic sample in ignition indicates that above some large size the ignition and critical temperatures will be relatively independent of sample size, because for further increases in size the conduction heat loss from the reaction surface to the interior of the sample changes little in magnitude. As the size of the sample is decreased, the relative importance of this heat loss term decreases, and the ignition and critical temperatures also decrease.

Because of the postulate of the metal ignition criterion, however, the ignition temperature can be no lower than the transition temperature, which is postulated to be independent of sample size.

In Appendix I and Chapter III, with the help of the metal oxidation literature transition temperatures are estimated as a function of oxidizing gas pressure for twenty metal-gas systems involving eleven metals, which were selected because of their use in propulsion applications or characteristic properties of the metal or product formed in the oxidation reaction. Examination of the influence of sample size and surface pretreatment on transition temperature indicates little effect of these parameters. However, sample purity and non-isothermal situations may have some effect on transition temperature.[1]

[1] Transition temperatures are in most cases estimated on the basis of the usual isothermal metallurgical experiments.

The metal oxidation and metal ignition literatures are reviewed in Appendix II and Chapter IV and critical temperatures and ignition temperatures for the metal-gas systems under study are listed. Certain types of ignition experiments, in which observation of sample self-heating is difficult or impossible and thus in which confusion between the critical and ignition temperatures is possible, are interpreted in view of the physical model of metal ignition. The ignition criterion, that the ignition temperature will be greater than the critical and transition temperatures, is obeyed in the case of eleven metal-gas systems. Eight systems cannot be tested against the criterion because of insufficient data, and in only one case is the criterion not followed.

The stronger statement that the minimum ignition temperature is the transition temperature is satisfied in fourteen of the sixteen metal-gas combinations for which sufficient data are available in the literature, if those types of experiments are neglected in which sample self-heating can interfere with measured ignition temperatures; otherwise, ten of sixteen combinations satisfy the statement.

Those systems which consistently disobey the criterion are characterized by high solubilities of the particular oxidizing gas in the metal (the Zr-O_2 and Ti-O_2 systems). This high solubility may account for discrepancies between the initial gas concentrations in the metal samples used in the various experiments, upon which estimates of transition and critical temperatures and measurements of ignition temperatures were based.

On the basis of the literature review, it is concluded that the transition temperature controls (that is, is greater than the critical temperature) in the ignition of at least four of the twelve metal-gas systems for which sufficient data are available to make a prediction.

The predicted size effect, that the critical and ignition temperatures decrease with decreasing sample size in cases for which the ignition temperature is controlled by the critical temperature, is observed for many of the metal-gas systems which were studied.

Other theories of metal ignition are reviewed in Appendix II. Three basic difficulties are observed with all of those quantitative theories developed for the ignition of single metal pieces: no size effect or the wrong size effect in ignition is predicted; ignition and critical temperatures are predicted to be independent of oxidizer pressure; and quantitative calculations are impossible for zero oxide thicknesses. Although the mathematical statement of the present model is too complicated for quantitative calculations (for reasons to be discussed below), none of these difficulties associated with the other theories occur. Also, the concept of the transition temperature is unique to the present model.

The failure of all other metal ignition theories to predict the observed and important size dependence is attributable to simplification of the heat loss terms chosen for the various theories. The physical model of metal ignition avoids this problem by considering exact heat loss terms in its formulation, but such a complication prevents quantitative calculation.

It is concluded on the grounds of the review of the metal oxidation and ignition literatures that the physical model of metal ignition presented in this report is more general than other theories of ignition and correlates ignition data more successfully over wide ranges of independent variables. Agreement with the single quantitative aspect of the model, the transition temperature,

is surprisingly good in view of its rather simple definition.

Two general types of experiments were performed in the present investigation in order to further verify the validity of the model and criterion. The first type was a relatively qualitative experiment involving the ignition of metal wires heated ohmically. Al and Mg received the most study in these experiments, and in Chapter VI the original development of the model on the basis of such studies, and more recent experiments with these metals in H_2O atmospheres are reported. In the latter experiments observations are consistent with expectations based on the model, but as noted above, no quantitative data were obtained. Other studies of the ignition and combustion of Ta and Mo wires and of improved ignition efficiency for Al are, because of space limitations, reported elsewhere (247, 248, 249).

Quantitative data were obtained in an induction furnace facility designed and constructed for this purpose (Chapter VII). Detailed experimental measurements of critical and ignition temperatures for Mg and Ca in O_2, CO_2, and mixtures of these gases with each other or with Ar were accomplished and used to probe the validity of the model and criterion of metal ignition. Although experimentation with Al was attempted, various experimental difficulties which may require some redesign of the facility curtailed the investigation.

With Mg and Ca, however, many important observations were made which demonstrate the applicability of the model. In all cases measured ignition temperatures equaled or exceeded measured critical and estimated transition temperatures. Trends in critical and ignition temperatures for variations in metal sample size, oxidizing gas pressure,

and experimental environment were consistent with the model. Most importantly, lack of agreement between bulk ignition temperatures for Ca in O_2 from literature studies and from the present investigation indicate that the bulk ignition temperature cannot be considered an absolute quantity, but also varies as a function of the experimental environment (or more properly, the method of sample heating).

It is thus concluded that the transition temperature is the only absolute index of ignition temperature for any metal-oxidizer system; depending on the relative magnitudes of the critical temperature for the particular sample environment in use and the (absolute) transition temperature, the ignition temperature will vary as follows: if the critical temperature exceeds the transition temperature, then the ignition temperature will be greater than both of these temperatures. As the size of the metal sample is decreased, the ignition temperature will decrease to the transition temperature and become independent of further reductions in size. In other words, if the critical temperature exceeds the transition temperature, then any measured ignition temperature will be greater than or equal to the transition temperature, depending on the sample size, experimental configuration, and so forth.

If the transition temperature exceeds the critical temperature appropriate to the ambient conditions, then the ignition temperature will always equal the transition temperature.

The transition temperature, then, becomes an important design parameter which can in most cases be estimated easily from the metal oxidation literature. The

rocket designer must insure that the flame temperature of the non-metallic propellants is equal to or exceeds the transition temperature of the metal additive in order to guarantee efficient ignition and fast combustion of the metallic fuel. Should this important design criterion of a metallized propellant system be met, most likely theoretical performance of the system will be approached more closely.

Future studies should include the ignition of a metal such as Al for which the ignition process is controlled by the transition temperature.[2] Also, quantitative data can be obtained in the induction furnace facility on the promising methods of lowering the transition and ignition temperatures of Al by coating clean surfaces of this metal with other metals such as Mg and Ca (249), which have low transition temperatures. Such pretreatments of metal additives of Al (or Be) should assist in performance improvements for chemical propulsion systems.

Finally, efforts should be made to determine experimentally the transition temperatures of metals like Al and Be, which are of propulsion interest, in combustion gases and gas mixtures likely to be encountered in solid propellant and hybrid rockets. Such data are not currently available in the metal oxidation literature.

---

[2]Ca was selected for study for this reason on the basis of the literature review, but in the course of the investigation it was learned that in the present experimental facility the critical temperature controlled in its ignition.

LIST OF REFERENCES

1. Glassman, I. (1959), "Metal combustion processes," Amer. Rocket Soc. Preprint 938-59.

2. Glassman, I., "Combustion of metals. Physical considerations," 253-258, Solid Propellant Rocket Research, Summerfield, M., Editor, Academic Press, New York, 1960.

3. Brzustowski, T. A. and Glassman, I., "Spectroscopic investigation of metal combustion," 41-74, Heterogeneous Combustion, Wolfhard, H. G., Glassman, I., and Green, L., Jr., Editors, Academic Press, New York, 1964.

4. JANAF Thermochemical Tables, The Dow Chemical Co., Midland, Mich., March 31, 1965.

5. Hodgman, C. D., Editor, Handbook of Chemistry and Physics, 46th Edition, Chemical Rubber Publishing Co., Cleveland, 1964.

6. Kubaschewski, O. and Hopkins, B. E., Oxidation of Metals and Alloys, Second Edition, Butterworths, London, 1962.

7. Brzustowski, T. A., "Vapor-phase diffusion flames in the combustion of magnesium and aluminum," Ph. D. Thesis, Princeton Univ., Dept. of Aeronautical Engineering, 1963.

8. Brzustowski, T. A. and Glassman, I., "Vapor-phase diffusion flames in the combustion of magnesium and aluminum: I. Analytical developments," 75-115, Heterogeneous Combustion, Wolfhard, H. G., Glassman, I., and Green, L., Jr., Editors, Academic Press, New York, 1964.

9. Brzustowski, T. A. and Glassman, I., "Vapor-phase diffusion flames in the combustion of magnesium and aluminum: II. Experimental observations in oxygen atmospheres," 117-158, Heterogeneous Combustion, Wolfhard, H. G., Glassman, I., and Green, L., Jr., Editors, Academic Press, New York, 1964.

10. Markstein, G. H. (1963), "Combustion of metals," AIAA J. 1, 550-562.

11. Christensen, H. C., Knipe, R. H., and Gordon, A.S. (1965), "Survey of aluminum particle combustion," Pyrodynamics 3, 91-119.

12. Wolfhard, H. G., Glassman, I., and Green, L., Jr., Editors, Heterogeneous Combustion, 3-307, Academic Press, New York, 1964.

13. Bahn, G. S., Editor (1965), Pyrodynamics 3, 29-168.

14. Preprints of the 1966 Spring Meeting of the Western States Section, The Combustion Institute, Denver, 1966.

15. Friedman, R. and Macek, A. (1962), "Ignition and combustion of aluminum particles in hot ambient gases," Combust. Flame 6, 9-20.

16. Friedman, R. and Macek, A., "Combustion studies of single aluminum particles," 703-712, Ninth Symposium (International)on Combustion, Academic Press, New York, 1963.

17. Kuehl, D. K. (1965), "The ignition and combustion of small diameter aluminum wires," Pyrodynamics 3, 65-79.

18. Kuehl, D. K. (1965), "Ignition and combustion of aluminum and beryllium," AIAA J. 3, 2239-2247.

19. Mellor, A. M., "The combustion of aluminum and magnesium in carbon dioxide - oxygen and carbon dioxide - argon mixtures," B.S.E. Thesis, Princeton Univ., Dept. of Aeronautical Engineering, 1963.

20. Mellor, A. M. and Glassman, I., "Vapor-phase diffustion flames in the combustion of magnesium and aluminum: III. Experimental observations in carbon dioxide atmospheres," 159-176, Heterogeneous Combustion, Wolfhard, H. G., Glassman, I., and Green, L., Jr., Editors, Academic Press, New York, 1964.

21. Mellor, A. M. and Glassman, I. (1965), "A physical criterion for metal ignition," Pyrodynamics 3, 43-64.

22. Pilling, N. B. and Bedworth, R. E. (1923), "The oxidation of metals at high temperatures," J. Inst. Met. 29, 529-591.

23. Frank-Kamenetskii, D. A., Diffusion and Heat Exchange in Chemical Kinetics, Thon, N., Translator, Princeton Univ. Press, Princeton, 1955.

24. Semenoff, N. (1928), "Zur Theorie des Verbrennungsprozesses," Z. Physik 48, 571-582.

25. Fristrom,, R. M. and Westenberg, A. A., Flame Structure, McGraw-Hill, New York, 1965.

26. Hauffe, K., Oxidation of Metals, Plenum Press, New York, 1965.

27. Bénard, J., Oxydation des Métaux, Vol. I and II, Gauthier-Villars, Paris, 1962.

28. Gulbransen, E. A. (1949), "Kinetic and structural factors involved in oxidation of metals," Ind. Eng. Chem. 41, 1385-1391.

29. Sleppy, W. C. (1961), "Oxidation of molten high-purity aluminum in dry oxygen," J. Electrochem. Soc. 108, 1097-1102.

30. Alymore, D. W., Gregg, S. J., and Jepson, W. B. (1960), "The high temperature oxidation of beryllium," J. Nucl. Mater. 2, 169-175.

31. Cubicciotti, D. (1950), "The oxidation of beryllium at high temperatures," J. Amer. Chem. Soc. 72, 2084-2086.

32. Carslaw, H. S. and Jaeger, J. C., Conduction of Heat in Solids, Second Edition, Oxford, London, 1959.

33. Smith, R. B. (1956), "Pyrophoricity - a technical mystery under vigorous attack," Nucleonics 14 (12), 28-33.

34. Gulbransen, E. A. (1947), "The kinetics of oxide film formation on metals and alloys," Trans. Electrochem. Soc. 91, 573-604.

35. Gulbransen, E. A. (1945), "The oxidation and evaporation of magnesium at temperatures from 400° to 500°C," Trans. Electrochem. Soc. 87, 589-599.

36. Baur, J. P., Bridges, D. W., and Fassell, W. M., Jr., (1955), "High pressure oxidation of metals - Oxidation of metals under conditions of a linear temperature increase," J. Electrochem. Soc. 102, 490-496.

37. Terem, H. N. (1948), "Sur la cinètique de l'oxydation du magnésium," Comptes Rendus Acad. Sci., Paris 226, 905-906.

38. Gregg, S. J. and Jepson, W. B. (1959), "The high-temperature oxidation of magnesium in dry and moist oxygen," J. Inst. Met. 87, 187-203.

39. Aylmore, D. W., Gregg, S. J., and Jepson, W. B. (1959), "The formation of porous oxides on metals," J. Electrochem. Soc. 106, 1010-1013.

40. Leontis, T. E. and Rhines, F. N. (1946), "Rates of high-temperature oxidation of magnesium and magnesium alloys," Trans. AIME 166, 265-294.

41. Sthapitanonda, P. and Margrave, J. L. (1956), "Kinetics of nitridation of magnesium and aluminum," J. Phys. Chem. 60, 1628-1633.

42. Caillat, R. and Darras, R. (1958), "Corrosion of magnesium and some of its alloys in gas-cooled reactors," Proc. Second United Nations Int. Conf. on Peaceful Uses of Atom. Energy, Geneva, 5, 220-233.

43. Boussion, M. L., Grall, L., and Caillat, R. (1957), "L'oxydation du magnésium par l'air entre 350 et 500°C," Rev. Metall. 54, 185-188.

44. Grall, L. (1955), "Formation et exploitation sur le magnésium de figures orientées obtenues par sublimation," Rev. Metall. 52, 603-611.

45. Boussion, M. L., Darras, R., and Leclercq, D. (1959), "Comportement du magnésium et de deux alliages de magnésium chauffés dans le gaz carbonique," Rev. Metall. 56, 61-67.

46. Gibbs, D. S. and Svec, H. J. (1956), "Kinetics of the reaction between magnesium and water vapor," ISC 779.

47. Svec, H. J. and Gibbs, D. S. (1957), "Metal-water reactions. V. Kinetics of the reaction between magnesium and water vapor," J. Electrochem. Soc. 104, 434-439.

48. Eyring, H. and Zwolinski, B. J. (1947), "The foundations of reaction rate theory and some recent applications," Record Chem. Prog. 8, 87-102.

49. Castle, J. E., Gregg, S. J., and Jepson, W. B. (1962), "The effect of gaseous impurities on the high-temperature oxidation of magnesium," J. Electrochem Soc. 109, 1018-1023.

50. McIntosh, A. B. and Bagley, K. Q. (1956), "Selection of canning materials for reactors cooled by sodium/potassium and carbon dioxide," J. Inst. Met. 84, 251-270.

51. Salesse, M. (1958), "Safety of magnesium canning for CO_2-cooled reactors," Nucleonics 16(2), 123-124.

52. McFarlane, E. F. and Tompkins, F. C. (1962), "Kinetics of oxidation of lithium," Trans. Farad. Soc. 58, 1177-1186.

53. Irvine, W. R. and Lund, J. A. (1963), "The reaction of lithium with water vapor," J. Electrochem. Soc. 110, 141-144.

54. Chandrasekharaiah, M. S. and Margrave, J. L. (1961), "The kinetics of oxidation and nitridation of lithium, calcium, strontium, and barium," J. Electrochem. Soc. 108, 1008-1012.

55. Deal, B. E. and Svec, H. J. (1953), "Metal-water reactions. II. Kinetics of the reaction between lithium and water vapor," J. Amer. Chem. Soc. 75, 6173-6175.

56. Cubicciotti, D. (1952), "The oxidation of calcium at elevated temperatures," J. Amer. Chem. Soc. 74, 557-558.

57. Svec, H. J. and Apel, C. (1957), "Metal-water reactions. IV. Kinetics of the reaction between calcium and water vapor," J. Electrochem. Soc. 104, 346-349.

58. Hart, R. K. (1956), "The oxidation of aluminum in dry and humid oxygen atmospheres," Proc. Roy. Soc. 236A, 68-88.

59. Dignam, N. J. (1962), "Oxide films on aluminum. II. Kinetics of formation in oxygen," J. Electrochem. Soc. 109, 192-198.

60. Smeltzer, W. W. (1956), "Oxidation of aluminum in the temperature range 400-600°C," J. Electrochem. Soc. 103, 209-214.

61. Gulbransen, E. A. and Wysong, W. S. (1947), "Thin oxide films on aluminum," J. Phys. Coll. Chem. 51, 1087-1103.

62. Alymore, D. W., Gregg, S. J., and Jepson, W.B. (1960), "The oxidation of aluminum in dry oxygen in the temperature range 400-650°C," J. Inst. Met. 88, 205-208.

63. Cochran, C. N. and Sleppy, W. C. (1961), "Oxidation of high-purity aluminum and 5052 aluminum-magnesium alloy at elevated temperatures," J. Electrochem. Soc. 108, 322-327.

64. Dignam, M. J., Fawcett, W. R., and Böhni, H. (1966), "The kinetics and mechanism of oxidation of super-purity aluminum in dry oxygen. I. Apparatus description and the growth of 'amorphous' oxide," J. Electrochem. Soc. 113, 656-662.

65. Dignam, M. J. and Fawcett, W. R. (1966), "The kinetics and mechanism of oxidation of superpurity aluminum in dry oxygen. II. The growth of crystallites of γ-alumina," J. Electrochem. Soc. 113, 663-671.

66. Jackson, D. A. and Leidheiser, H. (1964), "The very rapid oxidation of aluminum at room temperature when in contact with mercuric iodide," J. Electrochem. Soc. 111, 652-656.

67. Dillon, R. L. and Troutner, V. H. (1957), "Observations on the mechanisms and kinetics of aqueous aluminum corrosion," HW-51849.

68. Haycock, E. W. (1959), "Transitions from parabolic to linear kinetics in scaling of metals," J. Electrochem. Soc. 106, 771-775.

69. Heyn, A. N. J. (1961), "An ultrastructure study of the corrosion of aluminum in the presence of mercury," J. Electrochem. Soc. 108, 482-483.

70. Gregg, S. J., Hussey, R. J., and Jepson, W. B. (1961), "The high temperature oxidation of beryllium. Part III. In carbon dioxide, carbon monoxide, and carbon monoxide-carbon dioxide mixtures," J. Nucl. Mater. 3, 175-189.

71. Beach, J. G. (1964), "Electrodeposited, electroless, and anodized coatings on beryllium," DMIC Memorandum 197.

72. Cubicciotti, D. (1952), "The reaction between uranium and oxygen," J. Amer. Chem. Soc. 74, 1079-1081.

73. Loriers, J. (1952), "Sur l'oxydation de l'uranium métallique," Comptes Rendus Acad. Sci., Paris, 234, 91-93.

74. Adda, Y. (1958), "Etude cinetique de l'oxydation, de la nitruration et de l'hydruration de l'uranium," CEA-757.

75. Leibowitz, L., Schnizlein, J. G., Mishler, L. W., and Vogel, R. C. (1961), "A microscopic study of oxide films on uranium," J. Electrochem. Soc. 108, 1153-1155.

76. Leibowitz, L., Schnizlein, J. G., Bingle, J. D., and Vogel, R. C. (1961), "The kinetics of oxidation of uranium between 125° and 250°C," J. Electrochem. Soc. 108, 1155-1160.

77. Adda, Y. (1956), "La regle de Pilling et Bedworth et les phénomènes d'attaque de l'uranium par l'oxygène, l'hydrogène, et l'azote," Comptes Rendus Acad. Sci., Paris, 242, 126-127.

78. Loriers, J. (1952), "Contribution à l'étude des métaux pyrophoriques. L'oxydation du cérium et de l'uranium," Rev. Metall. 49, 801-810, 883-905.

79. Schnizlein, J. G., Woods, J. D., Bingle, J. D., and Vogel, R. C. (1960), "Identification of the diffusing species in uranium oxidation," J. Electrochem. Soc. 107, 783-785.

80. Mallett, M. W. and Gerds, A. F. (1955), "Reaction of nitrogen with uranium," J. Electrochem. Soc. 102, 292-296.

81. Stobbs, J. J. (1965), "The oxidation mechanism of pure uranium in carbon dioxide between 350° and 650°C," J. Electrochem. Soc. 112, 916-921.

82. Schroeder, J. B., Vaughan, D. A., and Schwartz, C. M. (1959), "Aqueous uranium corrosion at 100°C," J. Electrochem. Soc. 106, 486-489.

83. Hopkinson, B. E. (1959), "Kinetics of the uranium-steam reaction," J. Electrochem. Soc. 106, 102-106.

84. Waber, J. T., O'Rourke, J. A., and Kleinberg, R. (1959), "Oriented dioxide films on uranium," J. Electrochem. Soc. 106, 96-102.

85. Schnizlein, J. G., Pizzolato, P. J., Porte, H. A., Bingle, J. D., Fischer, D. F., Mishler, L. W., and Vogel, R. C. (1959), "Ignition behavior and kinetics of oxidation of the reactor metals, uranium, zirconium, plutonium, and thorium, and binary alloys of each," ANL 5974.

86. Bagley, K. Q. and Oliver, D. S. (1953), "The oxidation of uranium in air," R&DB(C)TN-32.

87. Gulbransen, E. A. and Andrew, K. F. (1949), "Kinetics of the reactions of zirconium with O_2, N_2, and H_2," J. Metals 1, 515-525.

88. Gulbransen, E. A. and Andrew, K. F. (1949), "Reactions of zirconium, titanium, columbium, and tantalum with the gases, oxygen, nitrogen, and hydrogen at elevated temperatures," Trans. Electrochem. Soc. 96, 364-376.

89. Mackay, T. L. (1963), "Oxidation of single-crystal and polycrystalline zirconium," Trans. AIME 227, 1184-1187.

90. Charles, R. G., Barnartt, S., and Gulbransen, E. A. (1958), "Prolonged oxidation of zirconium at 350° and 450°C," Trans. AIME 212, 101.

91. Sense, K. A. (1962), "On the oxidation of zirconium," J. Electrochem. Soc. 109, 377-382.

92. Hussey, R. J. and Smeltzer, W. W. (1964), "The oxidation kinetics of zirconium in the temperature range 400°-600°C," J. Electrochem. Soc. 111, 564-568.

93. Gulbransen, E. A. and Andrew, K. F. (1957), "Oxidation of zirconium between 400° and 800°C," J. Metals 9, 394-400.

94. Hussey, R. J. and Smeltzer, W. W. (1964), "The mechanism of oxidation of zirconium in the temperature range 400°-850°C," J. Electrochem. Soc. 111, 1221-1224.

95. Porte, H. A., Schnizlein, J. G., Vogel, R. C., and Fischer, D. F. (1960), "Oxidation of zirconium and zirconium alloys," J. Electrochem. Soc. 107, 506-515.

96. Belle, J. and Mallett, M. W. (1954), "Kinetics of the high temperature oxidation of zirconium," J. Electrochem. Soc. 101, 339-342.

97. Dravnieks, A. (1950), "The oxidation of several metals in activated oxygen at high temperatures," J. Amer. Chem. Soc. 72, 3761-3767.

98. Westerman, R. E. (1964), "High-temperature oxidation of zirconium and zircaloy-2 in oxygen and water vapor," J. Electrochem. Soc. 111, 140-147.

99. Debuigne, J. and Lehr, P. (1962), "Sur l'oxydation du zirconium," Comptes Rendus Acad. Sci., Paris, 254, 3710-3712.

100. Cubicciotti, D. (1950), "The oxidation of zirconium at high temperatures," J. Amer. Chem. Soc. 72, 4138-4141.

101. Kofstad, P. (1958), "Oxidation of metals: determination of activation energies," Acta Chem. Scand. 12, 701-707.

102. Bradhurst, D. H., Draley, J. E., and Van Drunen, C. J. (1965), "An electrochemical model for the oxidation of zirconium," J. Electrochem. Soc. 112, 1171-1177.

103. Perdereau, M. and Bardolle, J. (1963), "Étude cinétique de l'oxydation de zirconium aux températures élevées," Comptes Rendus Acad. Sci., Paris, 256, 4665-4668.

104. Wallwork, G. R. and Jenkins, A. E. (1959), "Oxidation of titanium, zirconium, and hafnium," J. Electrochem. Soc. 106, 10-14.

105. Sainfort, G. (1959), "Les mécanismes et les lois d'oxydation du zirconium a haute temperature," Rev. Metall. 56, 704-712.

106. Osthagen, K. and Kofstad, P. (1962), "Oxidation of zirconium and zirconium-oxygen alloys at 800°C," J. Electrochem. Soc. 109, 204-207.

107. Pemsler, J. P. (1965), "Studies on the oxygen gradients in oxidizing metals. III. Kinetics of the oxidation of zirconium at high temperatures," J. Electrochem. Soc. 112, 477-484.

108. Dravnieks, A. (1950), "The kinetics of the zirconium-nitrogen reaction at high temperature," J. Amer. Chem. Soc. 72, 3568-3571.

109. Mallett, M. W., Belle, J., and Cleland, B. B. (1954), "The reaction of nitrogen with, and the diffusion of nitrogen in, beta zirconium," J. Electrochem. Soc. 101, 1-5.

110. Korobkov, I. I., Ignatov, D. V., Evstyukhin, A. I., and Emelyanov, V. S. (1958), "Electron diffraction and kinetic investigations of the oxidation reactions of zirconium and some of its alloys," Proc. Second United Nations Conf. on Peaceful Uses of Atom. Energy, Geneva, 5, 60-68.

111. Phalnikar, C. A. and Baldwin, W. M., Jr. (1951), "The scaling of zirconium in air," Proc. ASTM 51,1038-1060.

112. Herenguel, J., Whitwham, D., and Boghen, J. (1956), "Étude de l'oxydation à chaud du zirconium Kroll dans l'air," Comptes Rendus Acad. Sci., Paris, 243, 2060-2063.

113. Kendall, L. F. (1955), "Reaction kinetics of zirconium and zircaloy-2 in dry air at elevated temperatures," HW-39190.

114. Kendall, L. F., Wheeler, R. G., and Bush, S.H. (1958), "Reaction kinetics of zirconium and zircaloy-2 in dry air at elevated temperatures," Nucl. Sci. Eng. 3, 171-185.

115. Hussey, R. J. and Smeltzer, W. W. (1965), "The reaction of zirconium with carbon dioxide and carbon monoxide at 850°C," J. Electrochem. Soc. 112, 554-560.

116. Cox, B. (1960), "An investigation of the mechanism of oxide film growth and failure on zirconium and zircaloy-2," TID-7587, 116-120.

117. Mallett, M. W., Albrecht, W. M., and Bennett, R. E. (1957), "Reaction of zirconium with water vapor at subatmospheric pressures," J. Electrochem. Soc. 104, 349-352.

118. Dravnieks, A. (1951), "Action of hot ionized gases upon zirconium and copper," J. Phys. Coll. Chem. 55, 540-549.

119. Polling, J. J. and Charlesby, A. (1954), "The influence of anodic oxide films on the thermal oxidation of zirconium," Acta Metall. 2, 667-674.

120. De Boer, J. H. and Fast, J. S. (1936), "The influence of oxygen and nitrogen on the α-β transition of zirconium," Rec. Trav. Chim. 55, 459-467.

121. De Boer, J. H. and Fast, J. D. (1940), "Electrolysis of solid solutions of oxygen in metallic zirconium," Rec. Trav. Chim. 59, 161-167.

122. Perdereau, M. and Bardolle, J. (1963), "Étude micrographique de l'oxydation ménagée du zirconium," Comptes Rendus Acad. Sci., Paris, 257, 2477-2480.

123. Hayes, E. T. and Roberson, A. H. (1949), "Some effects of heating zirconium in air, oxygen, and nitrogen," Trans. Electrochem. Soc. 96, 142-151.

124. Guldner, W. G. and Wooten, L. A. (1948), "Reactions of zirconium with gases at low pressure," Trans. Electrochem. Soc. 93, 223-235.

125. Fast, J. D. (1938), "Ausserordentlich grosse Löslichkeit von Stickstoff und Sauerstoff in einigen Metallen; studiert an Zirkon und Titan," Metallwirkschaft 17, 641-644.

126. Debuigne, J. and Lehr, P. (1962), "Sur la dissolution d'oxygène dans le réseau métallique au cours de l'oxydation du zirconium à hautes températures," Comptes Rendus Acad. Sci., Paris, 254, 4168-4170.

127. Schnizlein, J. G., Porte, H. A., Pizzolato, P. J., Bingle, J. D., Fischer, D. F., Mishler, L. W., Martin, P., Bayens, C. A., Leibowitz, L., and Vogel, R. C. (1958), "Metal oxidation - ignition kinetics", ANL-5959.

128. Mallett, M. W., Baroody, E. M., Nelson, H. R., and Papp, C. A. (1953), "The diffusion and solubility of nitrogen in beta zirconium," J. Electrochem. Soc. 100, 103-106.

129. Wanklyn, J. N., Britton, C. F., Silvester, D. R., and Wilkins, N. J. M. (1963), "Influence of environment on the corrosion of zirconium and its alloys in high-temperature steam," J. Electrochem. Soc. 110, 856-866.

130. Cox, B. (1960), "Oxidation and corrosion of zirconium and its alloys," Corrosion 16, 380t-384t.

131. Thomas, D. E. (1954), "Corrosion of zirconium in high-temperature water," Nucl. Eng., Part II, Chem. Eng. Prog. Sym. Ser. No. 12, 16-22.

132. Pemsler, J. P. (1966), "Studies on the oxygen gradients in oxidizing metals. V. The oxidation of oxygen-saturated zirconium," J. Electrochem. Soc. 113, 1241-1244.

133. Alexander, W. A. and Pidgeon, L. M. (1950), "Kinetics of the oxidation of titanium," Can. J. Res. 28B, 60-72.

134. Gulbransen, E. A. and Andrew, K. F. (1949), "Kinetics of the reactions of titanium with O_2, N_2, and H_2," J. Metals 1, 741-748.

135. Kofstad, P., Hauffe, K., and Kjöllesdal, H. (1958), "Investigation on the oxidation mechanism of titanium," Acta Chem. Scand. 12, 239-266.

136. Hauffe, K. (1959), "Über die unzureichende Oxydationsbeständig von Titan, Zirkon, Niob, und Tantal bei höheren Temperaturen," Z. Elektrochem. 63, 819-824.

137. Hurlen, T. (1960), "Oxidation of titanium," J. Inst. Met. 89, 128-136.

138. Menard, R. C. (1962), "Optical measurement of oxide thickness on titanium," J. Opt. Soc. Amer. 52, 427-431.

139. Jenkins, A. E. (1955), "A further study of the oxidation of titanium and its alloys at high temperatures," J. Inst. Met. 84, 1-9.

140. Davies, M. H. and Birchenall, C. E. (1951), "Oxidation of titanium," J. Metals 3, 877-880.

141. Richardson, L. S. and Grant, N. J. (1954), "Reaction of oxygen and nitrogen with titanium from 700° to 1050°C," J. Metals 6, 69-70.

142. Pfeiffer, H. and Hauffe, K. (1952), "Über die Beeinflussung der Oxydationsgeschwindigkeit von Nickel und Titan durch Legierungszusätze und durch Behandlung mit Metalloxyddampf," Z. Metallk. 43, 364-369.

143. Kinna, W. and Knorr, W. (1956), "Über die Oxydation von Titan," Z. Metallk. 47, 594-598.

144. Simnad, M., Spilners, A., and Katz, O. (1955), "Oxidation of oxygen-saturated titanium," J. Metals 7, 645-646.

145. Kofstad, P., Anderson, P. B., and Krudtaa, O. J. (1961), "Oxidation of titanium in the temperature range 800-1200°C," J. Less-Common Met. 3 89-97.

146. Stringer, J. (1960), "The oxidation of titanium in oxygen at high temperatures," Acta Metall. 8, 758-766.

147. Stringer, J. (1960), "The effect of pressure on the second stage parabolic rate in the oxidation of titanium," Acta Metall. 8, 810-811.

148. Wasilewski, R. J. and Kehl, G. L. (1954), "Diffusion of nitrogen and oxygen in titanium, " J. Inst. Met. 83, 94-104.

149. Kofstad, P. and Hauffe, K. (1956), "Oxydation von Titan," Werkstoffe u. Korrosion 7, 642-649.

150. Jenkins, A. E. (1953), "The oxidation of titanium at high temperatures in an atmosphere of pure oxygen," J. Inst. Met. 82, 213-221.

151. Basseches, H. (1962), "The oxidation of sputtered tantalum films," J. Electrochem. Soc. 109, 475-479.

152. Gulbransen, E. A. and Andrew, K. F. (1950), "Kinetics of the reactions of columbium and tantalum with O_2, N_2, H_2," J. Metals 2, 586-599.

153. Kofstad, P. (1963), "Oxidation of tantalum in oxygen at 300-550°C," J. Inst. Met. 91, 209-216.

154. Cathcart, J. V., Bakish, R., and Norton, D. R. (1960), "Oxidation properties of tantalum between 400° and 530°C," J. Electrochem. Soc. 107, 668-670.

155. Kofstad, P. (1962), "Oxidation of tantalum in the temperature range 500-700°C," J. Inst. Met. 90, 253-264.

156. Peterson, R. C., Fassell, W. M., Jr., and Wadsworth, M. E. (1954), "High pressure oxidation of metals: tantalum in oxygen," J. Metals 6, 1038-1044.

157. Albrecht, W. M., Klopp, W. D., Koehl, B. G., and Jaffee, R. I. (1961), "Reaction of pure tantalum with air, nitrogen, and oxygen," Trans. AIME 221, 110-117.

158. Stringer, J. (1965), "The effect of nitrogen on the oxidation of tantalum at high temperatures," J. Electrochem. Soc. 112, 1083-1091.

159. Cowgill, M. G. and Stringer, J. (1960), "The effect of oxygen pressure on the high-temperature oxidation of tantalum," J. Less-Common Met. 2, 233-240.

160. Kofstad, P. (1963), "The oxidation behavior of tantalum at 700°-1000°C," J. Electrochem. Soc. 110, 491-501.

161. Gebhardt, E. and Seghezzi, H. D. (1959), "Untersuchungen im System Tantal-Sauerstoff. I. Über den Mechanismus der Sauerstoffaufnahme bei hohen Temperaturen," Z. Metallk. 50, 248-257.

162. Gebhardt, E. and Seghezzi, H. D. (1957), "Lösung und Oxydation im System Tantal-Sauerstoff," Z. Metallk. 48, 503-508.

163. Kofstad, P. (1963), "Studies of the oxidation of tantalum at 1000°-1300°C," J. Less-Common Met. 5, 158-170.

164. Kofstad, P. (1964), "Low-pressure oxidation of tantalum at 1300°-1800°C," J. Less-Common Met. 7, 241-266.

165. Waber, J. T., Sturdy, G. E., Wise, E. M., and Tipton, C. R., Jr., (1951), "A spectrophotometric study of the oxidation of tantalum," AECU 1355.

166. Waber, J. T., Sturdy, G. E., Wise, E. M., and Tipton, C. R., Jr., (1952), " A spectrophotometric study of the oxidation of tantalum," J. Electrochem. Soc. 99, 121-129.

167. Vaughan, D. A., Stewart, O. M., and Schwartz, C. M. (1961), "Determination of interstitial solid-solubility limit in tantalum and identification of the precipitate phases," Trans. AIME 221, 937-946.

168. Gebhardt, E., Seghezzi, H. D., and Stegherr, A. (1957), "Über die Diffusion von Sauerstoff in Tantal," Z. Metallk. 48, 624-627.

169. Gebhardt, E. and Preisendanz, H. (1955), Über die Löslichkeit von Sauerstoff in Tantal und die damit verbunden Eigenschaftsänderungen," Z. Metallk. 46, 560-568.

170. Kofstad, P. and Krudtaa, O. J. (1963), "High temperature metallographic microscope studies on the initial oxidation of tantalum," J. Less-Common Met. 5, 477-492.

171. Andrews, M. R. (1932), "Reaction of gases with incandescent tantalum," J. Amer. Chem. Soc. 54, 1845-1854.

172. Wasilewski, R. J. (1953), "The solubility of oxygen in, and the oxides of, tantalum," J. Amer. Chem. Soc. 75, 1001-1002.

173. Vermilyea, D. A. (1958), "The oxidation of tantalum at 50-300°C," Acta Metall. 6, 166-175.

174. Cathcart, J. V., Campbell, J. J., and Smith, G. P. (1958), "The microtopography of oxide films on niobium," J. Electrochem. Soc. 105, 442-446.

175. Pawel, R. E. and Campbell, J. J. (1966), "The effect of anodic films on the gaseous oxidation of tantalum," J. Electrochem. Soc. 113, 1204-1209.

176. Gulbransen, E. A. and Wysong, W. S. (1948), "Thin oxide films on molybdenum," Trans. AIME 175, 628-647.

177. Simnad, M. and Spilners, A. (1955), "Kinetics and mechanism of the oxidation of molybdenum," J. Metals 7, 1011-1016.

178. Gulbransen, E. A., Andrew, K. F., and Brassart, F. A. (1963), "Oxidation of molybdenum 550° to 1700°C," J. Electrochem. Soc. 110, 952-959.

179. Berkowitz-Mattuck, J. B., Büchler, A., Engelke, J. L., and Goldstein, S. N. (1963), "Mass-spectrometric investigation of the oxidation of molybdenum and tungsten," J. Chem. Phys. 39, 2722-2730.

180. Bartlett, R. W. (1965), "Molybdenum oxidation kinetics at high temperatures," J. Electrochem. Soc. 112, 744-746.

181. Nachtigall, E. (1952), "Eigenschaften von Molybdän und Wolfram bei niedrigen und mittleren Temperaturen," Z. Metallk. 43, 23-26.

182. Jones, E. S., Mosher, J. F., Speiser, R., and Spretnak, J. W. (1958), "The oxidation of molybdenum," Corrosion 14, 2t-8t.

183. Lustman, B. (1950), "Oxidation of molybdenum in air at 1100 to 1600°F," Met. Prog. 57, 629-630, 674.

184. Ligenza, J. R. and Spitzer, W. G. (1960), "The mechanisms for silicon oxidation in steam and oxygen," J. Phys. Chem. Solids 14, 131-136.

185. Law, J. T. (1957), "The high temperature oxidation of silicon," J. Phys. Chem. 61, 1200-1205.

186. Deal, B. E. (1963), "The oxidation of silicon in dry oxygen, wet oxygen, and steam," J. Electrochem. Soc. 110, 527-533.

187. Brodsky, M. B. and Cubicciotti, D. (1951), "The oxidation of silicon at high temperatures," J. Amer. Chem. Soc. 73, 3497-3499.

188. Atalla, M. M., Tannenbaum, E., and Scheibner, E. J. (1959), "Stabilization of silicon surfaces by thermally grown oxides," Bell Sys. Tech. J. 38, 749-783.

189. Evitts, H. C., Cooper, H. W., and Flaschen, S. S. (1964), "Rates of formation of thermal oxides of silicon," J. Electrochem. Soc. 111, 688-690.

190. Claussen, B. H. and Flower, M. (1963), "An investigation of the optical properties and the growth of oxide films on silicon," J. Electrochem. Soc. 110, 983-987.

191. Evans, J. W. and Chatterji, S. K. (1958), "Kinetics of the oxidation and nitridation of silicon at high temperatures," J. Phys. Chem. 62, 1064-1067.

192. Archer, R. J. (1957), "Optical measurement of film growth on silicon and germanium surfaces in room air," J. Electrochem. Soc. 104, 619-622.

193. Ligenza, J. R. (1962), "Oxidation of silicon by high-pressure steam," J. Electrochem. Soc. 109, 73-76.

194. Dean, L. E. and Thompson, W. R. (1961), "Ignition characteristics of metals and alloys," ARS J. 31, 917-923.

195. Loriers, J. (1950), "Loi d'oxydation du cérium mètaux," Comptes Rendus Acad. Sci., Paris, 231, 522-524.

196. Grosse, A. V. and Conway, J. B. (1958), "Combustion of metals in oxygen," Ind. Eng. Chem. 50, 663-672.

197. Kofstad, P. (1957), "Oxidation of metals: determination of activation energies," Nature 179, 1362-1363.

198. Bahn, G. S. (1965), "On pyrophoricity of metals, and of fine metal powders in particular," Pyrodynamics 3, 29-41.

199. White, E. L. and Ward, J. J. (1966), "Ignition of metals in oxygen," DMIC Report 224.

200. Conway, J. B. and Kirshenbaum, M. S. (1954), Ninth Progress Report Contract N9-onr-87301, Res. Inst. Temple Univ., AD-45,649.

201. Fassell, W. M., Jr., Gulbransen, L. B., Lewis, J. R., and Hamilton, J. H. (1951), "Ignition temperatures of magnesium and magnesium alloys," J. Metals 3, 522-528.

202. Kubaschewski, O. and Ebert,H.(1947), "Notiz über das Reaktionsvermögen von Wasserdampf und Wasserstoffsuperoxyd mit Leichtmetallen bei höheren Temperaturen," Z. Metallk. 38, 232-235.

203. Jacobson, M., Cooper, A. R., and Nagy, J. (1964), "Explosibility of metal powders," Bureau of Mines RI 6516.

204. Hartmann, I., Nagy, J., and Brown, H. R. (1943), "Inflammability and explosibility of metal powders," Bureau of Mines RI 3722.

205. Hartmann, I. (1948), "Recent research on the explosibility of dust dispersions," Ind. Eng. Chem. 40, 752-758.

206. Constantinides, G. (1952), "Sulla temperatura di autoaccensione di polveri metalliche," Ann. Chim. Roma 42, 383-390.

207. Hartmann, I. and Nagy, J. (1944) "Inflammability and explosibility of powders used in the plastics industry," Bureau of Mines RI 3751.

208. Fairbairn, A. (1965), "The fire hazard of metallic beryllium," AHSB(S)R80.

209. Rhein, R. A. (1965), "Ignition and combustion of powdered metals in the atmospheres of Venus, Earth, and Mars," Astronautica Acta 11, 322-327.

210. Rhein, R. A. (1965), "The combustion of powdered metals in nitrogen and carbon dioxide," Pyrodynamics 3, 161-168.

211. Darras, R., Baque, P., and Leclercq, D. (1959), "Influence de faibles concentrations en vapeur d'eau dans l'air et le gaz carbonique sur l'inflammabilite du magnesium dans ces milieux," Comptes Rendus Acad. Sci., Paris, 249, 1647-1649.

212. Darras, R., Baque, P., and Leclercq, D. (1959), "Inflammabilite du magnesium et de l'uranium chauffes dans divers milieux gazeux," NP-9715.

213. Hill, P. R., Adamson, D., Foland, D. H., and Bressette, W. E. (1956), "High-temperature oxidation and ignition of metals," NACA RM L55L23b.

214. Freeman, E. S. and Campbell, C. (1963), "Kinetics of the high-temperature reaction between magnesium powder and oxygen," Trans. Farad. Soc. 59, 165-175.

215. Cassel, H. M. and Liebman, I. (1959), "The cooperative mechanism in the ignition of dust dispersions," Combust. Flame 3, 467-475.

216. Brown, C. R. (1934), "The determination of the ignition temperatures of solid materials," D. Sc. Thesis, Cath. Univ. of Amer.

217. Cassel, H. M. and Liebman, I. (1963), "Combustion of magnesium particles. II. Ignition temperatures and thermal conductivities of ambient atmopheres," Combust. Flame 7, 79-81.

218. Tammann, G. and Boehme, W. (1934), "Die Entzündungstemperaturen in Abhängkeit von der Grösse der Metallteilchen," Z. anorg. allge. Chem. 217, 225-236.

219. Markowitz, M. J. and Boryta, D. A. (1962), "Lithium metal-gas reactions. Interaction of lithium metal with air and its component gases," J. Chem. Eng. Data 7, 586-591.

220. Reynolds, W. C. (1959), "Investigation of ignition temperatures of solid metals," NASA TN D-182.

221. Smolenski, D. and Seweryniak, M. (1963), "Combustion of aluminum dust in a burner in oxygen, carbon monoxide, carbon dioxide, nitrous oxide, and steam," Biul. Wojskowej. Acad. Tech. 12 (5), 37-50. (Chemical Abstracts 60, 1529, (1964)).

222. Smolenski, D. and Seweryniak, M. (1963), "Combustion of aluminum dust in various oxidizing gases," Biul. Wojskowej. Acad. Tech. 12 (4), 43-64. (Chemical Abstracts 60, 1529, (1964)).

223. Cassel, H. M. (1964), "Some fundamental aspects of dust flames," Bureau of Mines RI 6551.

224. Higgins, H. M. and Schultz, R. D. (1957), "The reaction of metals with water and oxidizing gases at high temperatures," IDO-28000.

225. Gordon, D. A., "Combustion characteristics of metal particles," 271-278, Solid Propellant Rocket Research, Summerfield, M., Editor, Academic Press, New York, 1960.

226. Macek, A., Friedman, R., and Semple, J. M., "Techniques for the study of combustion of beryllium and aluminum particles," 3-16, Heterogeneous Combustion, Wolfhard, H. G., Glassman, I., and Green, L., Jr., Editors, Academic Press, New York, 1964.

227. Leibowitz, L., Bingle, J. D., and Homa, M. (1964), "An X-ray study of oxidized uranium surfaces," J. Electrochem. Soc. 111, 248-249.

228. Hartmann, I., Nagy, J., and Jacobson, M. (1951), "Explosive characteristics of titanium, zirconium, thorium, uranium, and their hydrides," Bureau of Mines RI 4835.

229. Leibowitz, L., Baker, L., Schnizlein, J. G., Mishler, L. W., and Bingle, J. B. (1963), "Burning velocities of uranium and zirconium in air," Nucl. Sci. Eng. 15, 395-403.

230. Leibowitz, L., Schnizlein, J. G., and Mishler, L. W. (1963), "The effect of halogenated hydrocarbons on the burning of uranium and zirconium," Nucl. Sci. Eng. 15, 404-410.

231. Schnizlein, J. G., Baker, L., and Vogel, R. C. (1960), "Selections from ANL 6231. Metal oxidation and ignition kinetics and metal-water reactions," ANL-RCV-SL-1781.

232. Schnizlein, J. G., Porte, H. A., Pizzolato, P. J., Bingle, J. D., Fischer, D. F., Mishler, L. W., Martin, P., and Vogel, R. C. (1958), "Metal oxidation-ignition kinetics," ANL-5924.

233. Tetenbaum, M., Mishler, L., and Schnizlein, G. (1962), "Uranium powder ignition studies," Nucl. Sci. Eng. 14, 230-238.

234. Katz, J. J. and Rabinowitch, E., Chemistry of Uranium, Dover, New York, 1961.

235. Beal, J. L., Brown, W. R., and Vassallo, F. A. (1965), "Oxidation and explosion of drops of molten zirconium metal," Pyrodynamics 3, 135-160.

236. Anderson, H. C. and Belz, L. H. (1953), "Factors controlling the combustion of zirconium powders," J.Electrochem. Soc. 100, 240-249.

237. Gulbransen, E. A. and Andrew, K. F. (1958), "Oxidation of zircaloy-2 and -3A at 300 to 850°C, "Trans. AIME 212, 281-286.

238. Anonymous (1956), "Zirconium fire and explosion hazard evaluation," TID 5365.

239. Littman, F. E., Church, F. M., and Kinderman, E. M. (1961), "A study of metal ignitions. II. The spontaneous ignition of zirconium," J. Less-Common Met. 3, 379-397.

240. Hickman, J. W. and Gulbransen, E. A. (1948), "Oxide films formed on titanium, zirconium, and their alloys with nickel, copper, and cobalt," Analyt. Chem. 20, 158-165.

241. Littman, F. E., Church, F. M., and Kinderman, E. M. (1961), "A study of metal ignitions. I. The spontaneous ignition of titanium," J. Less-Common Met. 3, 367-378.

242. Riehl, W. A., Key, C. F., and Gayle, J. B. (1963), "Reactivity of titanium with oxygen," NASA TR R-180.

243. Cowgill, M. G. and Stringer, J., "The effect of oxygen pressure on the high temperature oxidation of tantalum," 190-197, Niobium, Tantalum, Molybdenum, and Tungsten, Quarrell, A. G., Editor, Elsevier, Amsterdam, 1961.

244. Schryer, D. R. and Walberg, G. D. (1966), "A theoretical and experimental investigation of the oxidation of molybdenum at temperatures at which its trioxide is volatile," NASA TR R-232.

245. Talley, C. P., "The combustion of elemental boron," 279-285, Solid Propellant Rocket Research, Summerfield, M., Editor, Academic Press, New York, 1960.

246. Nagy, J. and Surincik, D. J. (1966), "Thermal phenomena during ignition of a heated dust dispersion," Bureau of Mines RI 6811.

247. Mellor, A. M. and Glassman, I., "Combustion reactions of the refractory metals tantalum and molybdenum," Preprint No. 66-33, Spring Meeting, Western States Section/The Combustion Institute, April 1966.

248. Hansel, J. G., Mellor, A. M., and Sullivan, H. F., "The Combustion of Metals, Final Report - 1 July 1964 to 30 June 1966," SC-CR-67-2611, May 1967.

249. Mellor, A. M. and Glassman, I., "Augmented ignition efficiency for aluminum and beryllium," Report No. 791, Dept. Aero. Mech. Sci., Princeton University, Princeton, N. J., May 1967.

250. Young, L., Anodic Oxide Films, Academic Press, New York, 1961.

251. Renshaw, T. A. (1961), "A study of pore structures on anodized aluminum," J. Electrochem. Soc. 108, 185-191.

252. Hunter, M. S. and Towner, P. F. (1961), "Determination of the thickness of thin porous oxide films on aluminum," J. Electrochem. Soc. 108, 139-144.

253. Franklin, D. W. and Stirland, D. J. (1963), "Studies on the structure of anodic oxide films on aluminum, II," J. Electrochem. Soc. 110, 262-267.

254. Paolini, G., Masoero, M., Sacchi, F., and Paganelli, M. (1965), "An investigation of porous anodic oxide films on aluminum by comparitive adsorption, gravimetric, and electronoptical measurements," J. Electrochem. Soc. 112, 32-38.

255. Dorsey, G. A., Jr. (1966), "The characterization of anodic aluminas. I. Composition of films from acidic anodizing electrolytes," J. Electrochem. Soc. 113, 169-172.

256. MacLennan, D. F. (1959), "Impedance characteristics of isolated aluminum oxide films," Corrosion 15, 283t-285t.

257. Spooner, R. C. (1956), "Water sealing of detached aluminum oxide anodic film," Nature 178, 1113-1114.

258. Kerr, I. S. (1956), "The origin of the hydrated oxide formed when anodic aluminum oxide films are 'sealed' in boiling water," Proc. Phys. Soc. 69B, 1055-1056.

259. Burwell, R. L., Jr., Smudski, P. A., and May, T. P. (1947), "Ethylene adsorption isotherms at -183°C," J. Amer. Chem. Soc. 69, 1525-1529.

260. Cage, J. M., Theory and Application of Industrial Electronics, McGraw-Hill, New York, 1951.

261. Malmstadt, H. V., Enke, C. G., and Toren, E. C., Jr., Electronics for Scientists, Benjamin, New York, 1963.

262. Philbrick Researches, Inc., Applications Manual for Computing Amplifiers for Modeling, Measuring, Manipulating, and Much Else, Second Edition, Nimrod, Boston, 1966.

263. Brzustowski, T. A., Personal communication to A. M. Mellor, Princeton University, June 1964.

264. Gordon, A. S., Discussion of Ref. (20) at the AIAA Heterogeneous Combustion Conference, West Palm Beach, Florida, December 1963.

265. Laurendeau, N. M., "Renewed experimentation on anodized aluminum in carbon dioxide-argon atmospheres," Internal memorandum, Princeton University, March 1967.

266. Curtis, F. W., High-Frequency Induction Heating, First Edition, McGraw-Hill, New York, 1944.

267. Bialek, S., Personal communication to A. Bozowski, Princeton University, January 1967.

268. Holland, L., Vacuum Deposition of Thin Films, Wiley, New York, 1958.

269. Pearse, R. W. B. and Gaydon, A. G., The Identification of Molecular Spectra, Third Edition, Wiley, New York, 1963.

270. Glassman, I., Discussion of Ref. (16), 709-711, Ninth Symposium (International on Combustion, Academic Press, New York, 1963.

271. Rosner, D. E. (1959), "Steady-State Surface Temperatures in Dissociated High-Speed Gas Flows," J. Aerospace Sci. 26, 384-385.

272. Rosner, D. E. (1966), "Effects of the Stefan-Nusselt Flow on the Apparent Kinetics of Heterogeneous Chemical Reactions in Forced Convection Systems," Int. J. Heat Mass Transfer 9, 1233-1253.

APPENDIX I - LITERATURE REVIEW OF TRANSITION TEMPERATURES

Transition temperatures for the various metal-gas systems listed in Chapter III are estimated in this appendix by means of a comprehensive review of the metal oxidation literature. A summary of the review may be found in Chapter III.

1. Magnesium

Selected oxidation data from the metal oxidation literature for Mg in O_2, N_2, air CO_2, and H_2O are shown in Table 2. Each gas is discussed separately, in the order just given. In as much as possible, the data are ordered with respect to temperature. Also included in the table are test pressure, experiment duration, and sample geometry and surface preparation. An "m" in this last column denotes mechanical abrasion, a "c" chemical polishing, and an "e" electrochemical polishing. Annealing pretreatments, which are generally also included in oxidation experiments, are not listed. In order to avoid over-complication the table, only the sample geometry and not the sample dimensions is given.

Throughout this appendix the experimental data discussed have been obtained in general by gravimetric or manometric measurements. The reader is referred to Ref. (6), (26), or (27), or to the individual references cited in this section for discussions of the method of oxidation rate measurement.

On the basis of the data listed in Table 2, the transition temperatures of Mg in N_2, air, and H_2O may be estimated as 300°C (41), 450°C (44), and less than or equal

TABLE 2.

SELECTED OXIDATION DATA FOR MAGNESIUM

Reference	Temperature Range, °C	Gas Pressure	Experiment Duration	Sample Geometry	Surface Preparation	Rate	Remarks
Oxygen							
(28),(34)	<400	2.64 atm	2 hr	foil	various	protective	
(35)	<450	2-200 torr	<20 hr	foil	m[1]	linear→ protective	
(36)	417-584	6.7 atm	---	---	---	slight	furnace temperature increasing linearly; ignition at 591°C
(28),(34)	>400	2.64 atm	2 hr	foil	various	non-protective	
(37)	400-530	---	<6 hr	ribbon or powder	---	linear	
(35)	>475	2-200 torr	<20 hr	foil	m	linear	
(38)	450	flowing	<90 hr ≈90 hr	foil	various	protective non-protective	
(39)	525	1 atm	---	foil	m	linear	mechanical stress cracking at critical thickness
(38)	500-575	flowing	---	foil	various	linear	two linear branches, the second from complete cracking to the substrate due to oxide crystallization
(40)	503-575	1 atm	70 hr	foil	m	linear	mechanical stress cracking at critical thickness
Nitrogen							
(41)	<300	20-200 torr	40 min	cylinder	m	---	no significant reaction
	300-500					linear	no pressure effect

TABLE 2. (concluded)

Reference	Temperature Range, °C	Gas Pressure	Experiment Duration	Sample Geometry	Surface Preparation	Rate	Remarks
Air							
(42)	350-400	flowing	<1000 hr	plates or cog-shaped	c[2]	protective	
(43)	350-400	flowing	>1000 hr	foil	m and c	protective	
(44)	350	---	15 hr	sublimed film	---	protective	
	450		2 hr			non-protective	
	500		16 hr			non-protective	
(42)	500	flowing	<1000 hr	plates or cog-shaped	c	non-protective	
(43)	500	flowing	>1000 hr	foil	m and c	non-protective	
(40)	550-575	1 atm	70 hr	foil	m	linear	mechanical stress cracking at critical thickness
Carbon Dioxide							
(42)	400-500	1 atm	<1000 hr	plates or cog-shaped	c	protective	MgO+C in film
(42),(45)	400-550	15 atm	<3000 hr	plates or cog-shaped	c	protective	MgO+C in film
(40)	550	1 atm	70 hr	foil	m	negligible	
Water Vapor							
(46), (47)	425-575	31-208 torr	16 hr	cylinder	c	linear	MgO only in film

[1] m denotes mechanical abrasion.

[2] c denotes chemical polishing.

to 425°C (46,47). Insufficient data are available, however, to examine any pressure effect. For the case of the Mg-O_2 system, T_{trans} may be taken as 475°C in the pressure range 2-200 torr (35) and as 400°C at 2.64 atm (28, 34). In CO_2, the Mg transition temperature is greater than or equal to 500°C at 1 atm (42) and increases to at least 550°C at 15 atm (42,45). The effect of sample size and surface preparation are discussed in Chapter III. In the case of the Mg-O_2 system, Eyring and Zwolinski (48) took 450°C as the temperature which distinguishes between protective and non-protective oxidation regimes.

The physical cause of the transition in O_2 has been cited as mechanical stress cracking at a critical oxide thickness (39,40), mechanism (f) as discussed in Chapter II, and as oxide crystallization (38), mechanism (c). If mechanism (f) mechanical stress cracking were responsible for the transition, then a decrease in T_{trans} with increasing oxidizer pressure is not unexpected: at a higher pressure, the oxide will grow to its critical thickness in a shorter time at a given experimental temperature; effectively, then, the transition temperature will be attained at a lower temperature. However, mechanism (c) mechanical stress cracking would not be expected to show a pressure effect unless crystallization also occurred when a critical oxide thickness was reached.

Not included in the table are the data of Castle et al. (49). At an oxygen pressure of 100 torr in the temperature range 500-550°C these investigators obtained a protective oxidation rate if extremely pure oxygen was used. The resulting oxide film was observed to be protective for at least 300 hr at 525°C. They were able to show that slight amounts of hydrocarbon impurities in the test oxygen give rise to the non-protective rate generally observed in this

temperature range. This surprising observation has not been further investigated in the literature, and for the present purposes, the Mg-O_2 transition temperature will be taken as those values listed above in the appropriate pressure regimes.

The higher transition temperature which is observed in CO_2 results from the presence of C in the MgO film (42,43,50) rather than from carbonate or carbide films. The value of 550°C for Mg-CO_2 may be slightly high however, as McIntosh and Bagley (50) stated that "the protective value of the oxide film appears to be much reduced above 450°C," and Salesse (51) remarked that the film is protective to 450°C.

Since only MgO is formed upon reaction in H_2O (46,47), it is not surprising that the Mg-H_2O transition temperature is close to that of Mg-O_2. The slightly lower value in the former case may be due to the formation of H_2, which in escaping from the scale lowers its protective ability.

2. Lithium

As can be seen from Table 3, very little oxidation data is available for Li. Although McFarlane and Tompkins (52) indicated that the transition temperature of the Li-O_2 system is 27°C and results from type (f) mechanical stress cracking, in experiments at a much higher pressure Irvine and Lund (53) found that no reaction occurs in O_2 at a slightly higher temperature. This anomaly could be due to the presence of H_2O in the experiments of the former, as will be shown below. The inverse logarithmic rate law mentioned by Ref. (52) is another example of a protective rate law. It may be written:

TABLE 3.

SELECTED OXIDATION DATA FOR LITHIUM

Reference	Temperature Range, °C	Gas Pressure	Experiment Duration	Sample Geometry	Surface Preparation	Rate	Remarks
Oxygen							
(52)	-195-+27	10^{-4}-10^{-2} torr	100 min	evaporated film	---	logarithmic or inverse logarithmic	breakaway at 27°C due to mechanical stress cracking at critical thickness
(53)	40	1 atm	16 hr	wafer	freshly cut	none	dry oxygen
Nitrogen							
(54)	239-310	110-200 torr	2 hr	foil	m	exponential	rate possibly due to sample self-heating
Water Vapor							
(53)	25-42	2.5-12.6 torr	~24 hr	wafer	freshly cut	linear	carrier gas either Ar or O_2 with no difference in rate; three stage linear rate with mechanical stress cracking at critical thickness; rate increases with H_2O pressure
(55)	45-75	50-100 torr	1 hr	cylinder	freshly cut	logarithmic	rate increases with H_2O pressure

$$\frac{1}{x} = c_3 - K_3 \ln t \qquad \text{(A1-1)}$$

where x is the thickness of oxide formed at time t, and c_3 and k_3 are constants.

The exponential rate observed in N_2 (54), of the form:

$$x = c_4 \exp\{K_4 t\} + c_5 \qquad \text{(A1-2)}$$

where k_4, c_4, and c_5 are constants, was attributed by the authors to non-isothermal conditions during the experiments due to sample self-heating, that is, these experiments were performed above the Li-N_2 critical temperature. This result will be discussed further in Appendix II.

Deal and Svec (55) observed the Li-H_2O reaction rate by a manometric method based on the equation

$$Li + H_2O = LiOH + \frac{1}{2}H_2 \qquad \text{(A1-3)}$$

These authors obtained a logarithmic reaction rate, as is shown in Table 3. Irvine and Lund (53), however, found a monohydrate in the reaction products:

$$Li + 2H_2O = LiOH \cdot H_2O + \frac{1}{2}H_2 \qquad \text{(A1-4)}$$

Using a gravimetric method, they obtained a linear reaction rate, and attributed the difference between their results and those of Deal and Svec to the manometric method based on the incorrect reaction (A1-3)

Taking the results of Irvine and Lund to be correct, the transition temperature of the Li-H_2O system lies below room temperature; type (f) mechanical stress

cracking (at a critical oxide thickness), is cited as the physical mechanism (53).

3. Calcium

Selected oxidation data for calcium are shown in Table 4. In O_2, Ca may exhibit a linear oxidation rate at as low a temperature as 300°C (22,53). However, both of these investigators acknowledged the possibility of sample self-heating during their experiments. Cubicciotti (56) did not mention self-heating and did not observe a linear rate until about 435°C. Thus this discrepancy may possibly result from critical temperature interference with the oxidation experiments.

Another possibility, however, is that the Ca-O_2 transition temperature is a function of pressure: the transition temperature may equal 300°C from 100 to 200 torr (53), 435°C at 200 torr (56), and 525°C at 1 atm (39). However, it should be noted that Pilling and Bedworth's experiments (22) were most likely conducted at 1 atm. Also, type (f) mechanical stress cracking (39) is expected to show the opposite pressure trend, as was discussed in the section on Mg. Until more experimental evidence is available, the transition temperature of the Ca-O_2 system is taken to be close to the value indicated by Cubicciotti (56), namely 400°C, over the approximate pressure range 100 torr-1 atm.

Svec and Apel (57) obtained breakaway[1] after 100 min in H_2O in the temperature range 20-70°C; thus the transition temperature of the Ca-H_2O system may be only slightly above 70°C.

The comparison of the three metals Mg, Li, and Ca,

[1]Breakaways are sudden discontinuous jumps observed in the oxidation rate, which may or may not be followed by a linear rate law, depending on the ability of the oxide film to self-heal.

TABLE 4.

SELECTED OXIDATION DATA FOR CALCIUM

Reference	Temperature Range, °C	Gas Pressure	Experiment Duration	Sample Geometry	Surface Preparation	Rate	Remarks
Oxygen							
(22)	300-500	---	50 hr	wire	---	linear	possible sample self-heating
(54)	300-350	100-200 torr	2 hr	foil	m	~linear	small rates
(56)	330-385	200 torr	3.3 hr	cube	m	parabolic	
(54)	350-435	100-200 torr	2 hr	foil	m	exponential	rate possibly due to sample self-heating
(56)	435 435 435-475	200 torr	<5 min >5 min 3.3 hr	cube	m	parabolic linear linear	
(39)	525	1 atm	---	cylinder	m	linear	mechanical stress cracking at critical thickness
Water Vapor							
(57)	20-70	18-93 torr	<1.67 hr	cylinder	c	logarithmic	breakaway after 100 min; pressure dependent up to 70°C

and the extension of the metal ignition criterion to the other alkali and alkaline earth metals will be postponed until the respective critical and ignition temperatures are discussed in Appendix II.

4. Aluminum

Literature oxidation data for Al in O_2, N_2, air, and H_2O are shown in Table 5. By far the greatest amount of data is available for the Al-O_2 system, and that there is a linear oxidation regime in the temperature range 450°C to the metal melting point (660°C (6)) is extremely well documented. Gulbransen and Wysong (34,61) attributed the linear rate to slow, rate-determining ion formation at either the oxide-gas or metal-oxide interface, but other investigators (62,68) argued that a constant thickness layer situated between the metal and an outer porous layer is responsible for the linear rate. At least in this temperature range, gas pressure is a relatively unimportant parameter.

Sleppy (29) investigated the oxidation of molten Al in the range 660° through 835°C. For either as-rolled specimens, upon which only a thin oxide film was present at the start of an experiment, or for samples which were pre-oxidized at 600°C for one hour, protective rates were observed. The modified parabolic law with which Sleppy correlated his data is of the form

$$x^2 + K_5 x = K_6 t + K_7 \qquad \text{(Al-5)}$$

where, as before, x is the oxide thickness at time t and the k_i are constants (29).

TABLE 5.

SELECTED OXIDATION DATA FOR ALUMINUM

Reference	Temperature Range, °C	Gas Pressure	Experiment Duration	Sample Geometry	Surface Preparation	Rate	Remarks
Oxygen							
(58)	20	1 atm	168 hr	---	m and e[1]	inverse logarithmic	
(59)	250-350	150 torr	1000 hr	foil	e	protective	
(60)	350-475	1 atm	24 hr	foil	m	parabolic	
(28),(34)	400	1 atm	2 hr	foil	various	protective	
(61)	400-475	7.6 torr	2 hr	foil	c and m or m	parabolic	
(62)	400-650	7.6 torr	200 hr	foil	m	parabolic	linear first stage
(59)	450	150 torr	1000 hr	foil	e	linear	
(63)	450-640	50-150 torr	167 hr	foil	c	linear then stops	
(64),(65)	454-505	10 torr	<20 hr	foil	e	protective	carrier gas Ar with pressure 9 torr
(28),(34)	500	1 atm	2 hr	foil	various	linear	shift to linear independent of oxide film thickness and O_2 pressure
(61)	500-550	7.6 torr	2 hr	foil	c and m or m	linear	after about 20 min

TABLE 5. (concluded)

Reference	Temperature Range, °C	Gas Pressure	Experiment Duration	Sample Geometry	Surface Preparation	Rate	Remarks
(60)	500-600	1 atm	24 hr	foil	m	linear	
(29)	660-700	110-120 torr	1 hr	plate	as-rolled	logarithmic	
	750-835					modified parabolic	
	660-700			plate	pre-oxidized at 600°C for 1 hr	~parabolic	
	750-835					parabolic	
Nitrogen							
(41)	<530	20-200 torr	40 min	cylinder	m	---	no significant reaction
	530-580					linear	no pressure effect
	590-625					parabolic	
Air							
(66)	20	1 atm	<100 min	cylinder	amalgamated	linear	humid air
Water Vapor							
(67)	100-350	flowing	<1 yr	---	---	parabolic	
(63)	450-640	4.6 torr	167 hr	foil	c	linear then stops	rate slower than in O_2

[1] e denotes electrochemical polishing.

There appears to be no oxidation data available for temperatures greater than the range investigated by Sleppy, but for reasons to be discussed in Appendix II, in which the ignition of Al will be reviewed, the transition temperature of the Al-O_2 system is assigned as the melting point of Al_2O_3, 2030°C (6).[2] The physical mechanism responsible for the transition is then the melting of the oxide, mechanism (b) as discussed in Chapter II.

Note that a similar linear, then protective, rate behavior occurs in N_2 (41). The quoted air results are for amalgamated Al; this pretreatment is known to destroy the usually protective nature of the oxide film. The mechanism is not clearly understood, but is discussed by Jackson and Leidheiser (66) and by Heyn (69).

Insufficient data are available to estimate the transition temperature of Al in N_2, air, CO_2, or H_2O, but if the principle product formed in these last three reactions were Al_2O_3, the transition temperatures could be expected to be equal to the melting point of this oxide, as is the case in pure O_2.

5. Beryllium

The oxidation behavior of Be in O_2 appears to be very similar to that of Al, as can be seen from Table 6. At medium temperatures, a linear reaction rate is observed (30), but at higher temperatures a protective rate prevails (31). This reverse transition is most likely a result of self-healing of the cracks in the oxide film, as suggested by Alymore et al. (30).

---

[2] Recall that it is necessary that the oxidation rate be linear at all temperatures between the transition temperature and the ignition temperature (see Chapter II). Thus the transition temperature of the Al-O_2 system cannot be taken as 450°C.

TABLE 6.

SELECTED OXIDATION DATA FOR BERYLLIUM

Reference	Temperature Range, °C	Gas Pressure	Experiment Duration	Sample Geometry	Surface Preparation	Rate	Remarks
Oxygen							
(30)	500-700 700-750	100 torr	300 hr	foil	c	protective linear	transition due to mechanical stress cracking or chemical composition change
(31)	840-970 885	100 torr 100-720 torr	100 min	foil	m	parabolic parabolic	no pressure effect
Carbon Dioxide							
(70)	500-700 750	100 torr	300 hr	foil	c	paralinear linear	after about 200 hr

Not shown in Table 6 are the remarks of Beach (71), who stated that "beryllium metal resists attack by dry air, N_2, H_2, and CO_2 at temperatures up to 1500°F (816°C)." This description of the Be-CO_2 system is roughly consistent with the data of Gregg et al. (70) shown in Table 6. Beach also noted, however, that non-protective BeO coats are formed in the air oxidation of Be in the temperature range 482-815°C.

The paralinear rate observed by Gregg and co-workers (70) is of the form

$$k_8 x^2 + k_9 x = t \qquad \text{(A1-6)}$$

where the k_i are constants. This law is essentially the same as the modified parabolic law, Eqn. (A1-5), found in the oxidation of Al (29).

Because of the similarity between the oxidation and ignition of Al and Be,[3] the transition temperature of Be in O_2 will be taken as the melting point of BeO, 2530°C (6).

6. Uranium

Oxidation data for uranium are listed in Table 7. In the case of reaction with O_2 (or air), there is general agreement that linear rates are obtained over a wide pressure range above about 150°C, which is assigned as the transition temperature. Note, however, that paralinear rates have been observed above 150°C (73,74,78), which may indicate that the transition temperature is greater than 150°C. Some investigators regard mechanical stress cracking at a critical oxide thickness, mechanism (f), as the physical mechanism responsible (72,75-77), although Schnizlein and co-workers (85)

[3] See Appendix II.

TABLE 7.

SELECTED OXIDATION DATA FOR URANIUM

Reference	Temperature Range, °C	Gas Pressure	Experiment Duration	Sample Geometry	Surface Preparation	Rate	Remarks
Oxygen							
(72)	90-160	200 torr	100 min	cylinder	m	parabolic	
(73)	100-140	---	<8 hr	ingot	----	parabolic	UO_2 formed
(74)	120-150	200 torr	16 hr	plate	m and e	parabolic	UO_2 formed
(75),(76)	125-250	20-800 torr	20 hr	cube	e	linear	two linear stages; pressure effect in first stage; second stage from mechanical stress cracking at critical thickness
(77)	>125	---	---	plate	e	linear	mechanical stress cracking at critical thickness
(78)	<150	1 atm	<8 hr	plate	m	parabolic	UO_2 formed
(73)	150-240	---	<8 hr	ingot	----	paralinear	two layers, the outer cracked
(74)	150-265	200 torr	16 hr	plate	m and e	paralinear	U_3O_7 formed above 200°C
(78)	150-250	1 atm	<8 hr	plate	m	paralinear	$UO_2 + U_3O_7$ in film
(72)	165-215	200 torr	100 min	cylinder	m	linear	mechanical stress cracking at critical thickness
(79)	200	200 torr	---	cube	m	linear	UO_2 formed
(72)	>215	200 torr	100 min	cylinder	m	---	rate faster than linear
(39)	240	1 atm	---	foil	m	linear	mechanical stress cracking at critical thickness

TABLE 7, (concluded)

Reference	Temperature Range, °C	Gas Pressure	Experiment Duration	Sample Geometry	Surface Preparation	Rate	Remarks
(73)	240-360	---	<8 hr	ingot	---	linear	protective barrier layer; U_3O_8 formed
(78)	>250	1 atm	<8 hr	plate	m	linear	U_3O_8 formed
(74)	>265	200 torr	16 hr	plate	m and e	linear	
Nitrogen							
(74)	<350 350-650	200 torr	16 hr	plate	m and e	slight parabolic	
(77)	>350	---	---	plate	e	linear	mechanical stress cracking at critical thickness
(80)	550-900	1 atm	4.67 hr	cylinder	m	parabolic	$UN_2 \rightarrow U_2N_3$
(74)	>650	200 torr	16 hr	plate	m and e	linear	
Air							
(74)	150-220 250-450	200 torr	16 hr	plate	m and e	paralinear linear	U_3O_7 between 200 and 250°C; breakaways at temperatures greater than 400°C
Carbon Dioxide							
(81)	450-650	1 atm	150 hr	foil	m	parabolic	linear after 7 hr at 650°C; mostly UO_2 in scale
Water Vapor							
(82)	100	1 atm	24 hr	wafer	e, m, or m and c	linear	UO_2 formed
(83)	160-880	1 atm	<6.67 hr	foil or cylinder	m	linear	
(84)	400	5 torr	<1 hr	cylinder	---	logarithmic	
(83)	880-1060	1 atm	<6.67 hr	foil or cylinder	m	parabolic	linear after 1 or 2 hr

noted that "there is no clear indication that an oxide-cracking mechanism is applicable."

Another possibility is that a chemical composition change from UO_2 to U_3O_7 or U_3O_8 causes the transition (mechanism (d)), as this further oxidation of the dioxide is well documented (73,74,78).

The data shown for the N_2 reaction in Table 7 are in disagreement, perhaps because of the different pressures employed. Not shown in the table is the result of Bagley (86), who found very little reaction for this system in the temperature range 300-600°C.

Little information is available for the U-CO_2 reaction. Salesse (51) noted that U forms a protective film in 10 atm of CO_2 in the approximate range 650-800°C. The H_2O results are also few and in disagreement.

7. Zirconium

Selected oxidation data for Zr are shown in Table 8. As can be seen, the Zr-O_2 reaction is the subject of much controversy. Below about 800°C, parabolic, cubic, and paralinear rate laws have been used for correlation of the experimental results. The first linear rates are reported at temperatures equal to or greater than about 925°C and generally at pressures less than 1 atm (100,104,105), but other investigators have reported protective rates in this temperature range at higher O_2 pressures (101,107,132).

Part of this controversy no doubt results from the solubility of oxygen in the metal. Ref. (92), (96), (110), and (118) through (126) discuss this phenomenon in some detail. Perhaps the discrepancy between the experimental results is due to varying initial oxygen concentrations in the metal in the individual experiments.

TABLE 8.

SELECTED OXIDATION DATA FOR ZIRCONIUM

Reference	Temperature Range, °C	Gas Pressure	Experiment Duration	Sample Geometry	Surface Preparation	Rate	Remarks
Oxygen							
(87),(88)	200-425	0.76-76 torr	2 hr	foil	m	parabolic	pressure dependence
(89)	300-815	15 torr	4-6 hr	wafer	c	parabolic	
(90)	350-450	1 atm	200-500 hr	foil	m	cubic	
(91)	400 500	12-83 torr	16.7 min	foil or spheres	m or c	parabolic → cubic paralinear	
(92)	400-600	10-500 torr	200 hr	foil	m or c	~parabolic	no pressure effect
(93)	400-650	76 torr	6 hr	foil	m or c	cubic	
(94)	400-850	100 torr	<550 hr	foil	c	parabolic	
(95)	400-900	50-800 torr	500 hr	foil or block	m or c	cubic	little pressure dependence
(96)	575-900	1 atm	3 hr	cylinder	m	cubic	mechanical stress cracking observed
(97)	600	0.5-4 torr	13.3 hr	---	---	parabolic	
(98)	600-800	25 torr	16.7 hr	foil	c	cubic	
(99)	600-850	1 atm	<4.5 hr	---	c	~parabolic	
(100)	600-880	1-211 torr	1.67 hr	foil	none	parabolic	
(101)	650-950	---	---	---	---	cubic	furnace temperature increasing linearly
(102)	700	10-400 torr	5 hr	wafer	m and c	cubic	no pressure effect
(93)	700-750	76 torr	6 hr	foil	m or c	---	either cubic or parabolic
(103)	700-900	10 torr	3.3 hr	foil	m and c	cubic	rate decreases with increasing or decreasing pressure

TABLE 8, (continued)

Reference	Temperature Range, °C	Gas Pressure	Experiment Duration	Sample Geometry	Surface Preparation	Rate	Remarks
(104)	700-950	1 atm	24 hr	foil	---	---	linear after 24 hr
(105)	773-883	160 torr	1.25 hr	foil	c	cubic	
(106)	800	1 atm	5 hr	foil	none	cubic	
(107)	840	1 atm	< 80 hr	sphere	c	cubic	no pressure effect
			>150 hr			parabolic	below 1 atm
(132)	840-1300	---	100 hr	wafer or foil	---	parabolic	oxygen-free or oxygen-saturated Zr
(100)	920	1-211 torr	1.67 hr	foil	none	---	some linear, some parabolic; no pressure effect
(107)	910-975	1 atm	---	sphere	c	parabolic	no pressure effect below 1 atm
(105)	985	160 torr	1.25 hr	foil	c	linear	
(101)	950-1100	---	---	---	---	parabolic	furnace temperature increasing linearly
Nitrogen							
(87),(88)	400-825	1.5-76 torr	2 hr	foil	m	parabolic	
(108)	862-1043	10-300 torr	70 hr	foil	---	parabolic	linear at 70 hr at the higher temperatures due to expansion of the metal; little pressure dependence
(109)	975-1640	1 atm	3 hr	cylinder	m	parabolic	
Air							
(110)	300-400	---	60 hr	block	m	exponential	

TABLE 8, (concluded)

Reference	Temperature Range, °C	Gas Pressure	Experiment Duration	Sample Geometry	Surface Preparation	Rate	Remarks
(111)	400	---	400 hr	foil	c	parabolic	
(112)	400-500	---	0.5-24 hr	foil	---	≈protective	
(110)	500	---	60 hr	block	m	logarithmic	
	540					cubic	
(113),(114)	500-700	flowing	500 hr	foil or cylinder	c	protective	linear after 14 hr at 700°C; no effect of flow rate
(111)	500-800	---	400 hr	foil	c	parabolic	two stage parabolic rate; breakaways due to thermal expansion of the metal
(110)	575-800	---	60 hr	block	m	parabolic	transition due to oxide phase change
	>800					linear	
(111)	1050-1300	---	400 hr	foil	c	parabolic	
Carbon Dioxide							
(115)	850	100 torr	0.5-10 hr	foil	none	parabolic	rate decreases with decreasing pressure
Water Vapor							
(116)	250-450	---	---	---	m	cubic or logarithmic	becoming linear due to film cracking
(117)	300-600	33 torr	24 hr	foil or cylinder	m	cubic	
(98)	600-800	25 torr	16.7 hr	foil	c	cubic	

The linear oxidation rate observed at about 925°C has been attributed to several mechanisms: rate-controlling oxygen adsorption on the metal surface (100); various types of mechanical stress cracking of the oxide (119,127); mechanical stress cracking due to the α-β phase change in the oxide in the temperature range 700-800°C (110)[4]; and mechanical stress cracking caused by structural changes in the underlying Zr-O solid solution occurring at a solution value of 12 to 15 atomic percent (106). A final possibility is mechanical stress cracking caused by the α-β Zr phase change. De Boer and Fast (120) have noted that the presence of oxygen or nitrogen in the metal lattice alters the above transition from a sharp change at 865°C to a transition range; such a change could explain oxide cracking at a higher temperature.

On the basis of the literature, the Zr-O_2 transition temperature will tentatively be taken as 925°C in the O_2 pressure range 1-211 torr, with an error of ± 100°C in order to reflect the uncertainty in the literature. This estimate will be discussed further in Appendix II.

In N_2, the Zr transition temperature is apparently above 1640°C, as is seen from Table 8. This gas is also highly soluble in Zr (109,119-121,124,128). The upper limiting value of the Zr-N_2 transition temperature is 2980°C, the melting point of ZrN (6).

In air, as in O_2, the transition temperature is poorly defined, but, for the time being, will also be taken as 925°C ± 100°C.

In CO_2 insufficient data is available to estimate the transition temperature, and in H_2O in general protective rates are observed in the temperature range from 250-800°C.

[4] Kubaschewski and Hopkins (6), however, list this allotropic transition temperature as 1100°C.

Breakaways are found, however, (116), and have been attributed to film degradation by H_2 in the scale (129), mechanical stress cracking at metal grain boundaries (130), and mechanical stress cracking at a critical film thickness or resulting from the α-β ZrO_2 transition (131). Transition temperatures will not be assigned for Zr in either of these gases.

8. Titanium

As is the case for Zr, both O_2 (133,135,143,144, 146,149,150) and N_2 (148) are soluble in Ti. In general however, the oxidation regimes of Ti in O_2 (Table 9) are more clearly defined than are those of Zr. Breakaways were observed in O_2 in a temperature range as low as 300-500°C and were attributed to type (f) mechanical stress cracking at a critical oxide thickness (137). Linear oxidation rates have been found in the temperature range 650-1000°C at 1 atm after rather long induction periods (140), 850-1000°C in the pressure range 10^{-3}-760 torr for high purity Ti (135,136), 900-1000°C in a non-isothermal experiment with the furnace temperature rising linearly at 3.86 °C/min (101), and at 1000°C in 1 atm of O_2 (142). Mechanical stress cracking at a critical oxide thickness is generally cited as the cause of the transition (139,150).

On this basis the transition temperature for the Ti-O_2 system may be estimated as 900°C in the pressure range from 10^{-3}torr to 1 atm, but exceptions must be noted: parabolic rates were observed by Richardson and Grant (141) in this temperature and pressure range; in experiments of short duration, Simnad et al. observed a parabolic rate in the temperature regime 800-1200°C (144). These latter experiments, however, were conducted with oxygen saturated Ti, and the authors noted that faster rates were obtained with oxygen free Ti.

TABLE 9.

SELECTED OXIDATION DATA FOR TITANIUM

Reference	Temperature Range, °C	Gas Pressure	Experiment Duration	Sample Geometry	Surface Preparation	Rate	Remarks
Oxygen							
(133)	25-500	20-200 torr	21.3 hr	bar or powder	none	logarithmic	
(88),(134)	250-600	7.6-76 torr	2 hr	foil	m	parabolic	small pressure effect
(135),(136)	<300	10^{-3}-760 torr	5 hr	foil	m	logarithmic	
(137)	300-500	1-760 torr	<167 hr	foil	m	logarithmic	pressure effects and breakaways
(135),(136)	300-600	10^{-3}-760 torr	5 hr	foil	m	cubic	
(138)	482	flowing	5.67 hr	----	m	paralinear	
(137)	500	1-760 torr	<167 hr	foil	m	logarithmic or cubic	pressure effects and breakaways
	600-700					parabolic	no pressure effect; breakaways
(135),(136)	600-850	10^{-3}-760 torr	5 hr	foil	m	~parabolic	high or commercial purity
(139)	650-950	40-700 torr	8 hr	foil	c	parabolic	no pressure effect; breakaways
(140)	650-1000	1 atm	15 hr	foil	m	linear	100 min induction period
(101)	700-900	---	---	----	---	parabolic	furnace temperature increasing linearly
(141)	700-1050	380 torr	<2.5 hr	cylinder	m and c	parabolic	
(142)	800	1 atm	7 hr	----	---	parabolic	
(143)	800	10-1000 torr	<26 hr	cylinder	m	parabolic	no pressure effect
			26-72 hr			paralinear	

TABLE 9, (concluded)

Reference	Temperature Range, °C	Gas Pressure	Experiment Duration	Sample Geometry	Surface Preparation	Rate	Remarks
(144)	800-1200	---	< 2.5 hr	---	m	parabolic	
(145)	800-1200	1 atm	66.7 hr	foil	m	parabolic	linear after 15 min at 1000°C
(135),(136)	850-950	10^{-3}-760 torr	5 hr	foil	m	approaching linear	commercial purity; pressure dependence; mechanical stress cracking
	850-1000					approaching linear	high purity; pressure dependence; mechanical stress cracking
(146),(147)	850-1000	~1 atm	< 3 hr	foil	m and c	parabolic	eventually linear; two stage parabolic rate, second stage pressure dependent
(101)	900-1100	---	---	---	---	linear	furnace temperature increasing linearly
(136)	1000	10^{-3}-760 torr	5 hr	foil	m	parabolic	commercial purity; no pressure effect
(142)	1000	1 atm	7 hr	---	---	linear	
Nitrogen							
(88), (134)	550-850	.076-76 torr	2 hr	foil	m	parabolic	small pressure effect
(141)	700-1050	380 torr	< 2.5 hr	cylinder	m and c	parabolic	
(148)	800-1400	1 atm	---	cylinder	m	parabolic	

Furthermore, in a survey of the literature on the Ti-O_2 reaction, Kofstad and Hauffe have concluded that the oxidation is parabolic above 950°C (149).

In N_2 at 1 atm, the transition temperature lies between 1400°C (148) and 2930°C, the melting point of TiN (6).

9. Tantalum

Selected oxidation data for Ta in O_2, N_2, and air are shown in Table 10. Although O_2 is also soluble in Ta (152,153,155,156,160-162,167-173,175), as can be seen from the table it is generally agreed in the literature that Ta exhibits a linear rate in O_2 at and above 500°C. The appropriate pressure range is from 10 torr to 40 atm (156). At slightly lower pressures, the transition temperature may be higher than 500°C, as Dravnieks observed a parabolic rate at 500°C in the pressure range 0.5 to 4 torr (97). Usually type (f) mechanical stress cracking was cited as the appropriate physical mechanism (154,157,160,174). Stringer (158) found that the oxidation was inhibited by the addition of either N_2 or Ar to the test atmosphere; thus this investigator's experiments were conducted within the gas-phase diffusionally controlled regime. As can be noted from Table 10, in general the pressure dependence within the linear oxidation regime above 500°C is complicated.

The paralinear rates observed by Kofstad (160, 163) in the temperature range 800-1200°C were measured at the lower pressures used in the investigations, as at the higher pressures and temperatures, the rates were too fast to be measured (163). As will be discussed in , the ignition temperature of Ta in O_2 lies in this range

TABLE 10.

SELECTED OXIDATION DATA FOR TANTALUM

Reference	Temperature Range, °C	Gas Pressure	Experiment Duration	Sample Geometry	Surface Preparation	Rate	Remarks
Oxygen							
(151)	100-600	76 torr	2 hr	sputtered film	---	logarithmic	
(88), (152)	250-450	76 torr	2 hr	foil	m	parabolic	complicated pressure effects
(153)	300-450	1 atm	<75 hr	foil	m and c	logarithmic	
(136)	400-550	1 atm	2 hr	---	---	parabolic	no pressure effect from 500-600°C
(175)	425-455	1 atm	8.3 hr	foil	m and e	protective	
(153)	450-550	1 atm	<75 hr	foil	m and c	paralinear	
(154)	450	1 atm	<72 hr >72 hr	foil	m	parabolic linear	mechanical stress cracking
	475		<48 hr >48 hr			parabolic linear	
	500		<4 hr >4 hr			parabolic linear	
(36)	450-790	1-6.7 atm	---	---	---	linear	furnace temperature increasing linearly
(175)	480	1 atm	8.3 hr	foil	m and e	protective	breakaway after about 7 hr
	500					protective	breakaway after about 3 hr
	525					protective	breakaway after about 1 hr
(97)	500	0.5-4 torr	13.3 hr	---	---	parabolic	
(155)	500-575	0.1-760 torr	30 hr	foil	m and c	approaching linear	5 min induction period at 575°C; complicated pressure effect

TABLE 10. (continued)

Reference	Temperature Range, °C	Gas Pressure	Experiment Duration	Sample Geometry	Surface Preparation	Rate	Remarks
(156)	500-1000	10 torr-40 atm	2 hr	foil	m	linear	complicated pressure effects
(157)	500-1300	1 atm	2 hr	cylinder	m	linear	pressure dependent; mechanical stress cracking at critical oxide thickness
(136)	550-650	1 atm	2 hr	---	---	non-protective	rate increases with pressure, 600-800°C
(155)	600-700	0.1-760 torr	30 hr	foil	m or c	~linear	complicated pressure effects
(158)	600-925	360 torr	< 5 hr	foil	m and c	linear	rate inhibited by N_2 or Ar in atmosphere
(159)	610-1000	1-760 torr	---	foil	m	linear	complicated pressure effects
(160)	700-750	0.01-760 torr	5 hr	foil	m and c	linear	mechanical stress cracking
(161)	700-1420	2×10^{-2} torr	< 13 hr	wire	none	~linear	
(162)	800-1000	2×10^{-2} torr	< 1 hr	wire	none	linear	after oxygen saturation in Ta lattice
(160)	800-1000	0.01-760 torr	50 hr	foil	m and c	paralinear	
(163)	1000-1200 1200-1300	0.01-760 torr	< 5 hr	foil	m and c	paralinear linear	complicated pressure effects
(164)	1300-1800	10^{-4}-1 torr	4 hr	foil	m	linear	
(162)	1500	10^{-3} torr	< 1 hr	wire	none	linear	after oxygen saturation in Ta lattice

TABLE 10, (concluded)

Reference	Temperature Range, °C	Gas Pressure	Experiment Duration	Sample Geometry	Surface Preparation	Rate	Remarks
Nitrogen							
(157)	400-700	1 atm	2 hr	cylinder	m	cubic	no pressure effect
(88), (152)	500-800	76 torr	2 hr	foil	m	parabolic	small pressure effect
(157)	800-1475	1 atm	2 hr	cylinder	m	parabolic	no pressure effect
Air							
(165),(166)	220-350	1 atm	1400 hr	foil	m	logarithmic	
	350					---	logarithmic or parabolic
(157)	400-800 800-1400	1 atm	2 hr	cylinder	m	paralinear linear	mechanical stress cracking at critical oxide thickness

at pressures on the order of 1 atm; thus Kofstad most likely observed the combustion of Ta.

N_2 is also soluble in Ta (167,171) and protective rates were found at extremely high temperatures, similar to the behavior of Zr and Ti in N_2. The transition temperature of the Ta-N_2 system apparently lies between 1475°C at 1 atm (157) and the melting point of TaN, 3050°C (6).

In air, Ta exhibits a purely linear rate above 800°C at 1 atm (157). The raising of the transition temperature over that in pure O_2 probably results from the inhibition of the Ta-O_2 reaction by N_2.

10. Molybdenum

Oxidation data for Mo in O_2 and in air are reviewed in Table 11. The transition temperature in the former gas appears to be a strong function of pressure, changing from 725°C at 1 atm (177) to 600°C at 76 torr (178). The results of Dravnieks (97) indicate that it may again increase at lower pressures on the order of several torr. Type (f) mechanical stress cracking at a critical oxide thickness has been cited as the physical mechanism responsible for the appearance of the linear rate (177), but the volatility of the oxide MoO_3 may also play an important role through the mechanism (b) transition (the melting point of the trioxide is 795°C (6)).

The non-isothermal experiments of Baur et al. (36) are discussed in Chapter III.

In air, few data are available, and several investigators neglect to mention the pressure used in their experiments. On the basis of the results of Lustman (183), the transition temperature of the Mo-air system is taken

TABLE 11.

SELECTED OXIDATION DATA FOR MOLYBDENUM

Reference	Temperature Range, °C	Gas Pressure	Experiment Duration	Sample Geometry	Surface Preparation	Rate	Remarks
Oxygen							
(176)	300-450	.76-76 torr	7 hr	foil	m	parabolic	large pressure effect
(28),(34)	400	76 torr	2 hr	foil	various	parabolic	large pressure effect
(36)	450-790	6.7 atm	---	---	---	linear	furnace temperature increasing linearly
(177)	500-700	1 atm	16 hr	foil	m	parabolic	
(178)	600-700	76 torr	6 hr	cylinder	m	linear	corrected for MoO_3 volatization
(97)	690	0.5-4 torr	13.3 hr	---	---	parabolic	lowered rate with O atoms rather than O_2 molecules
(177)	725-750	1 atm	16 hr	foil	m	linear	mechanical stress cracking
(178)	1000	76 torr	6 hr	cylinder	m	~linear	large pressure effect, 800-1600°C
(179)	1500-2600	10^{-6}-10^{-4} torr	---	foil	---	linear	MoO_3(g) below 1477°C; MoO_2(g) above 1477°C
(180)	1380-2470	10^{-6}-760 torr	---	wire	---	linear	
Air							
(181)	500-700	---	2 hr	foil	none	linear	
(182)	524-938	---	60 hr	foil or wire	c	paralinear	
(183)	595	1 atm	63 hr	foil	c	linear	

TABLE 12.

SELECTED OXIDATION DATA FOR SILICON

Reference	Temperature Range, °C	Gas Pressure	Experiment Duration	Sample Geometry	Surface Preparation	Rate	Remarks
Oxygen							
(184)	700-1100	5-760 torr	---	foil	m	parabolic	
(185)	727-1027	10^{-3}-5×10^{-2} torr	2 hr	filament	c	parabolic	large pressure effect
(186)	900-1000	1 atm	4 hr	wafer	m	paralinear	
(187)	950	200 torr	1.67 hr	cube	m	logarithmic or parabolic	
(188)	1000	1 atm	---	---	---	parabolic	
(187)	1000-1100	200 torr	1.67 hr	cube	m	logarithmic	
(186)	1000-1200	1 atm	4 hr	wafer	m	parabolic	
(187)	1060	200 torr	1.67 hr	cube	m	parabolic	
(189)	1100-1300	1 atm	22 hr	---	c	parabolic	
(190)	1200	flowing	5.5 hr	wafer	m	parabolic	
(191)	1200-1400	1 atm	24 hr	block	m	parabolic	
Nitrogen							
(191)	1200-1400	1 atm	24 hr	block	m	---	erratic, perhaps breakaways
Air							
(192)	25	1 atm	24 hr	mirror	m and c	logarithmic	

TABLE 12, (concluded)

Reference	Temperature Range, °C	Gas Pressure	Experiment Duration	Sample Geometry	Surface Preparation	Rate	Remarks
Carbon Dioxide							
(191)	1200-1400	1 atm	24 hr	block	m	parabolic	
Water Vapor							
(193)	500-850	25-400 atm	7 hr	wafer	c	linear	
(184)	650	120 atm	---	foil	m	linear	
(186)	900-1000	1 atm	4 hr	wafer	m	paralinear	
(188)	1000	1 atm	---	---	---	parabolic	
(186)	1000-1200	1 atm	4 hr	wafer	m	parabolic	
(189)	1100-1300	1 atm	22 hr	---	c	parabolic	
(190)	1200	flowing	5.5 hr	wafer	m	parabolic	

as 595°C at 1 atm.

11. Silicon

In Table 12 some of the pertinent oxidation literature for Si is presented. In O_2 protective rate laws are observed up to the highest temperature investigated, 1400°C. Investigations at higher temperatures have most likely not been conducted because the metal melts at 1420°C (6). On the basis of the available data, the transition temperature of the Si-O_2 system most likely lies between 1400°C and 1610°C, the melting point of SiO_2 (6). It is possible, however, that the transition temperature lies above the melting point of the oxide because of the glassy, vitreous nature of SiO_2.

At high pressures in H_2O, the transition temperature lies at or below 500°C (193), but at pressures on the order of 1 atm it is much higher and may also be close to or equal the melting point of the oxide.

APPENDIX II - LITERATURE REVIEW OF CRITICAL AND IGNITION TEMPERATURES

The metal oxidation and ignition literatures are consulted in this appendix to, firstly, estimate and obtain literature values of critical and ignition temperatures for those metal-gas systems discussed in Appendix I and Chapter III, so that the metal ignition criterion can be tested by means of the literature, and secondly, review and compare with the present model other theories of metal ignition which have been presented in the literature. Specific discussions are given in this appendix; summaries may be found in Chapter IV.

Critical and ignition temperatures listed in this appendix have been obtained by thermal heating, that is, either by internal heating (ohmic or induction heating), or by external heating in a resistence furnace or flame. Thus other energy sources for ignition such as sparks and friction are not considered, as is also the case for samples broken in torsion, and so forth. Experiments of this latter type are not readily interpreted in terms of the model of metal ignition as developed in the present report.

The reader is referred to Ref. (10), (198), and (199) for details on these other methods of ignition. In particular Bahn (198) in his study of particle ignition included cases of mechanically induced ignition, ignition of metals other than those considered here, ignition of alloys, and ignition of non-metals. For O_2 as the oxidizer,

White and Ward (199) also have given a more general review of the metal ignition literature.

In this appendix, the method of thermal heating and applied heating rate will in general not be noted. The reader is referred to the individual references for this information. The applied heating rate varies over orders of magnitude from experiment to experiment, and only in those cases in which a particular investigator studied the effect of the variation of this parameter will it be mentioned.

In Chapter III the transition temperature was shown to be relatively independent of sample surface preparation; thus this detail of the individual experiments will in general be omitted here. Although sample purity is most likely an important parameter in ignition, because in many cases it is not given by the investigator, it also will not be considered except in isolated cases. Thus the main experimental independent variables of interest in the present appendix (for a given metal-oxidizer system) are oxidizer pressure, sample size, and sample condition. By the latter is meant a dispersion of particles, a bulk or massive sample, and so forth.

1. Magnesium

a. Critical Temperatures

The critical temperature is most frequently indicated in the literature as a spontaneous ignition temperature. Quite often ignition delay times are not given. (Recall that for zero ignition delay time, the initial sample temperature equals the ignition temperature.) The critical temperature is estimated where possible as the asymptotic initial sample temperature with infinite ignition delay time. The critical temperature is thought to be a strong function of sample size, experimental environment, and past history of the sample in that it may depend on the thickness of oxide present on the metal surface (see Chapter II).

Critical temperatures for Mg have been extremely well documented. In Fig. 8, sample initial temperature is plotted versus ignition delay time for bulk Mg with S/V of either 0.579 or 1.23 mm^{-1} in O_2 or air at 1 atm (201,211,212). The asymptotic critical temperature for Mg in this size range and in these oxidizers at 1 atm is seen to equal about 575 or 580°C.

Supplementary data also have been mentioned in the literature. Gregg and Jepson (38) noted difficulties with spontaneous ignition in their oxidation experiments with Mg foil in flowing O_2 at 575°C. Leontis and Rhines (40) observed that self-heating effects are important in the range 575-600°C for bulk Mg, S/V = 0.304 mm^{-1}, in O_2 at 1 atm. A Mg sample in air at 600°C or higher temperature will self-heat and ignite, according to Adda (74). Finally, Darras and

FIGURE 8

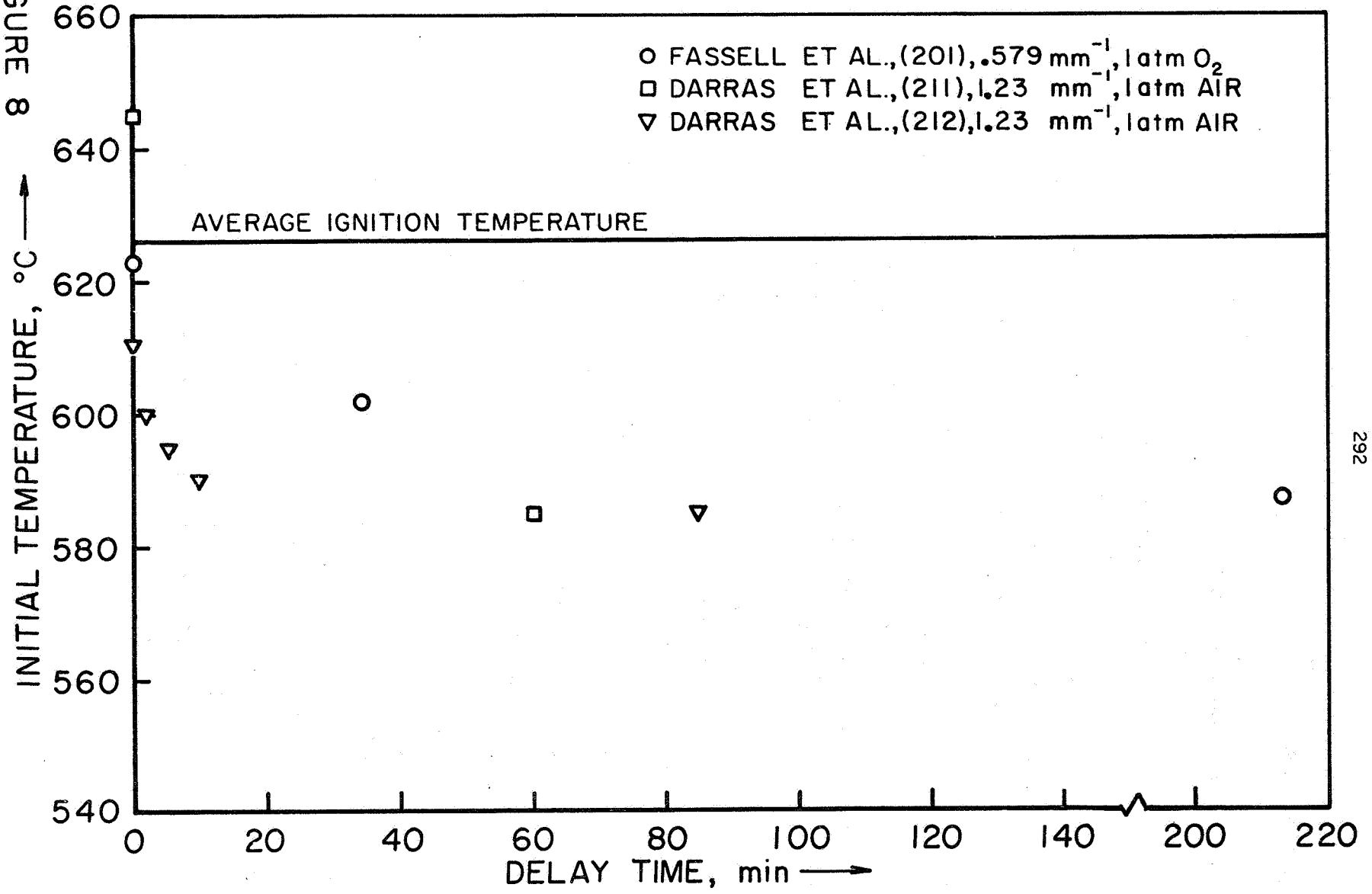

INITIAL TEMPERATURE vs DELAY TIME: BULK MAGNESIUM IN OXYGEN OR AIR.

co-workers (211) gave spontaneous ignition temperatures of bulk Mg in air at 1 atm as 615°C (ignition at 645°C) and in CO_2 at 15 atm as 790°C (ignition at 920°C), where the observed ignition delay times were less than 4 hr.

On the basis of the literature, one may conclude that a reasonably well-defined critical temperature exists for bulk Mg in O_2 or air at 1 atm, and is on the order of 575°C for samples with surface to volume ratios of about 0.1 to 1.0 mm^{-1}. Since the transition temperature at this pressure (on the order of 450°C, see Table 13) is lower than this critical temperature, one may further conclude that the ignition of bulk Mg in O_2 or in air will be controlled by the critical temperature, that is, the ignition temperature will be greater than or equal to 575°C. The results of Darras et al. (211) indicate that the ignition of large Mg samples in 15 atm of CO_2 is also controlled by the critical temperature, as the transition temperature equals at least 550°C.

b. Ignition Temperatures

All Mg ignition temperatures obtained from the literature survey are shown in Table 14 and in Fig. 9 and 10, correlated with respect to oxidizer, size, oxidizer pressure, and sample condition. As has been mentioned, surface treatment prior to experimentation, sample purity, and applied heating rate have been neglected for the purpose of the table and figures. The sample condition nomenclature which is used is as follows: DD indicates a dust dispersed in the gas of

TABLE 14.

LITERATURE IGNITION TEMPERATURES FOR MAGNESIUM

Reference	Stated Size	Gas Pressure	Sample Condition	Ignition Temperature, °C
Oxygen				
(196),(200)	~10 g	1 atm	B[1]	623
(201)	0.579 mm^{-1}	126 torr	B	645
		178		635
		277		628
		319		623
		441		623
		486		624
		523		622
		1.0 atm		623
		1.865		630
		2.75		631
		3.9		633
		4.25		645
		5.6		643
		5.95		648
		7.68		642
		7.95		643
		9.35		647
		10.0		639
(202)	---	flowing	B	649
(36)	---	6.7 atm	B	591
Nitrogen				
(203)	<53 μ	1 atm?	QP[2]	575
	<74 μ	1 atm?	QP	550
	<149 μ	1 atm?	QP	520
(204)	<149 μ	1 atm?	QP	530
Air				
(205)	---	1 atm?	DD[3]	520
(206)	<40 μ	1 atm?	DD	510
(209)	<44 μ	1 atm	QP	563
(208)	<53 μ	1 atm?	QP	510
(203)	<53 μ	1 atm?	QP	478

TABLE 14 (Concluded).

Reference	Stated Size	Gas Pressure	Sample Condition	Ignition Temperature, °C
(37)	53-62 μ	1 atm?	QP	470-500
(206)	40-66 μ	1 atm?	DD	551
(207)	<74 μ	1 atm?	DD	520
(203)	<74 μ	1 atm?	DD	620
			QP	490
(204)	<149 μ	1 atm?	DD	613
			QP	517
(203)	<149 μ	1 atm?	QP	520
Carbon Dioxide				
(210)	<44 μ	flowing	QP	749
(203)	<53 μ	1 atm?	QP	630
	<74 μ	1 atm?	QP	600
(204)	<149 μ	1 atm?	QP	630
(211),(212)	1.23 mm^{-1}	1 atm	B	880
		15 atm		920
(50)	---	11 atm	B	642
		flowing	B	>700
Water Vapor				
(202)	---	flowing	B	635

[1] B denotes a bulk or massive sample.

[2] QP denotes a quiescent pile experiment.

[3] DD denotes a dust dispersion experiment.

interest; QP indicates a quiescent pile of powder; B indicates a bulk, massive sample; and SP indicates a single particle dropped into the oxidizing gas. Although it is not expected a priori that correlations exist between the various sample configurations, it is hoped that data for each would be self-consistent. Wherever possible, some sizes in the table and all sizes in the figures are expressed in terms of the surface area to volume ratio, in units of reciprocal millimeters.

One notes from Table 14 that in general the measured ignition temperatures decrease with decreasing sample size. However, it must be remembered that in SP and DD experiments in which the particle or particles are dropped through the oxidizing gas, the temperature which is quoted is the temperature of the gas. Thus, if sample self-heating were important in these types of experiments, it could not be diagnosed, and the reported ignition temperature may actually be in many cases a critical temperature. (See Sections 4 and 5 for a discussion of this effect in SP experiments.)

DD experiments are expected to give somewhat lower ignition temperatures than SP experiments because of radiation heat transfer within the cloud of particles. Effectively, because of this radiation heat transfer between particles in dust dispersion experiments and because of the lack of it in single particle experiments, the critical temperature is lower in the former experiment than in the latter.

Also, one would expect that QP experiments would reveal lower ignition temperatures than DD exper-

AP24-4001a'65

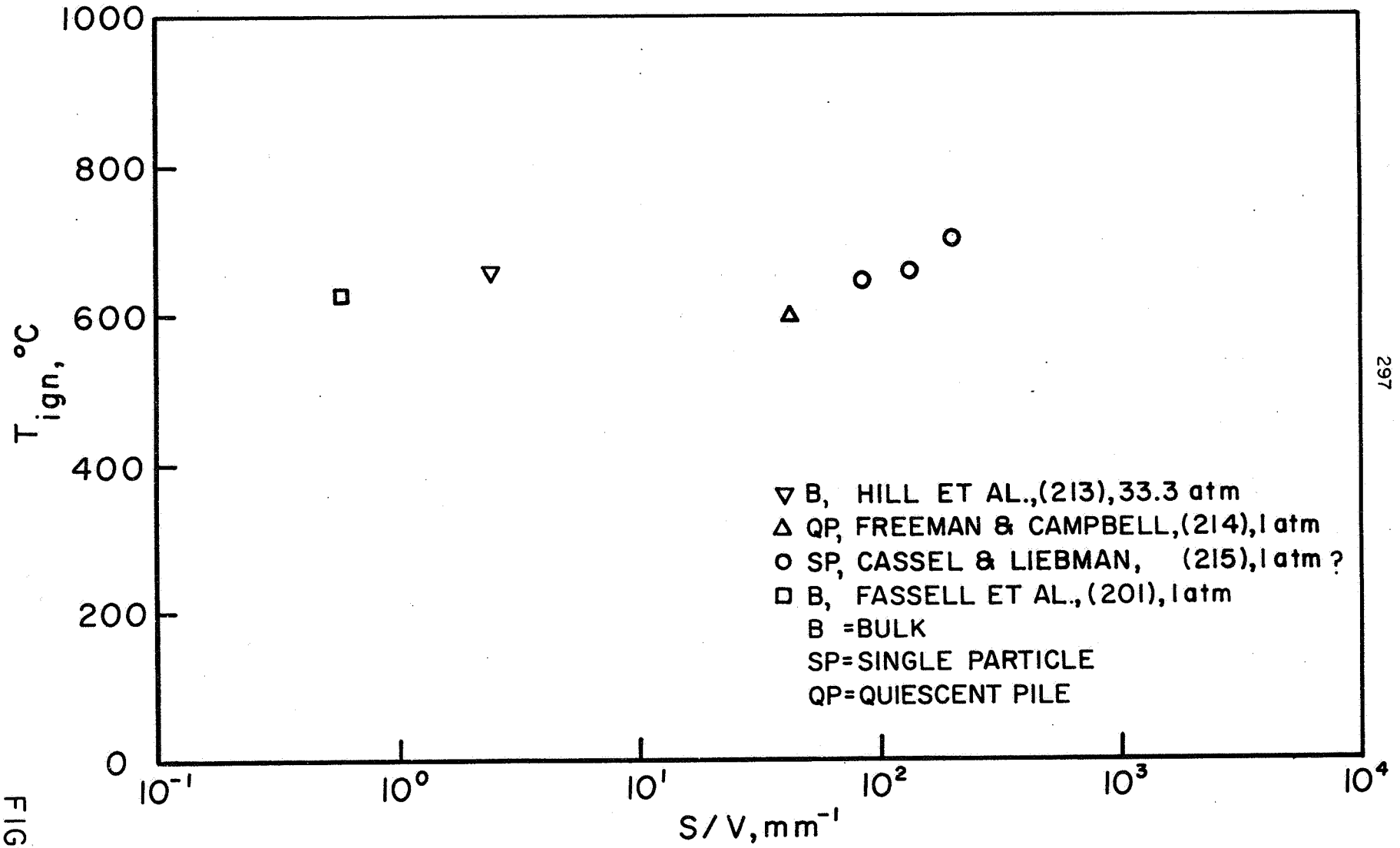

297

FIGURE 9

IGNITION TEMPERATURE vs SURFACE-VOLUME RATIO: MAGNESIUM IN OXYGEN

FIGURE 10

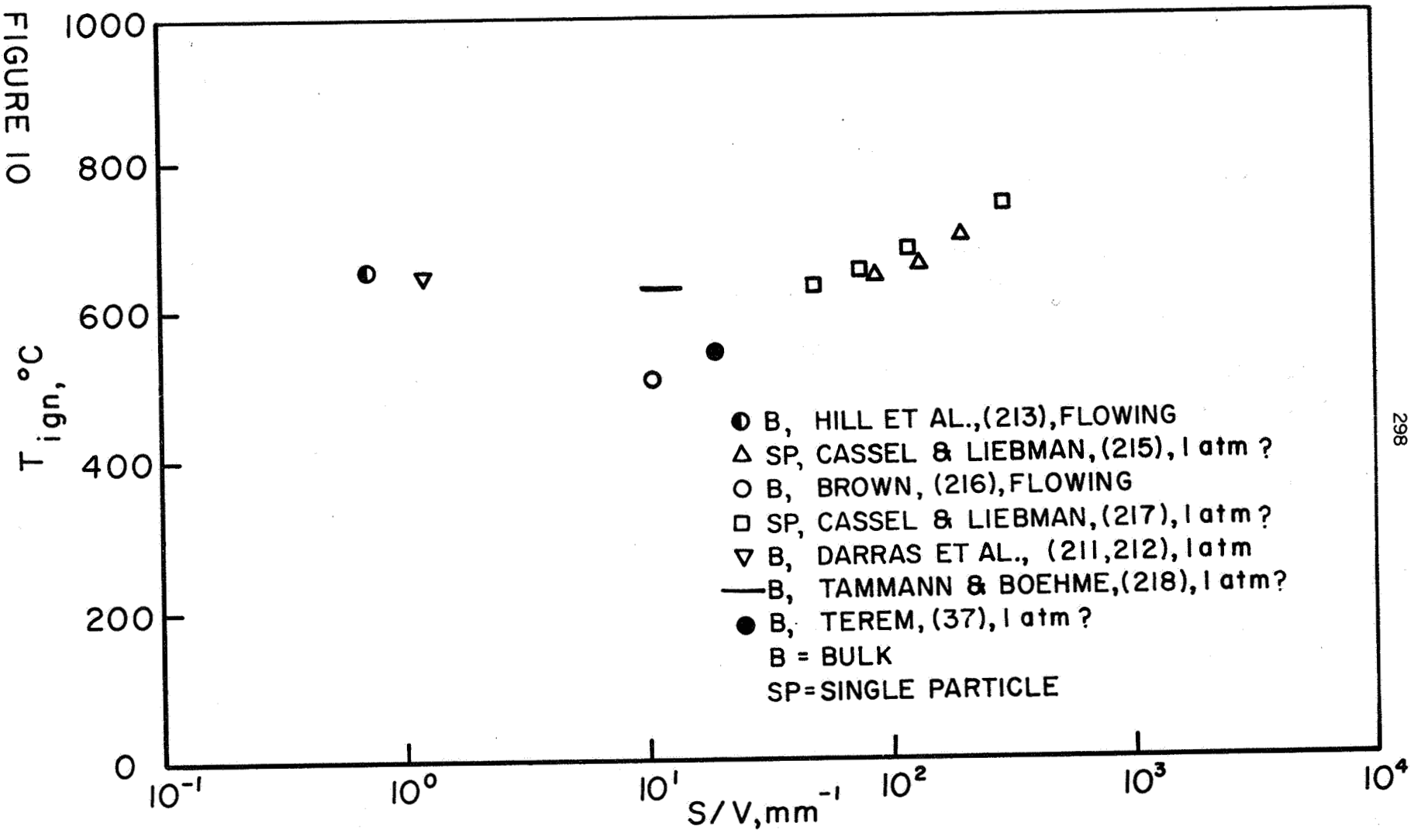

IGNITION TEMPERATURE vs SURFACE - VOLUME RATIO: MAGNESIUM IN AIR

iments. In the particular geometry of the former case, low critical temperatures will be encountered because of the high surface area available for chemical reaction compared to the low surface area available for heat loss to the surroundings. Furthermore, the S/V ratio is extremely large when averaged over the entire particle configuration.

As can be seen from the table and figures, all the reported ignition temperatures are greater than the appropriate transition temperatures for all the oxidizing gases given in Table 13. The large discrepancy between these temperatures in all the oxidizing gases listed indicates that the critical temperature may control in all cases in the ignition of Mg, that is, the critical temperature is greater than the transition temperature. This conclusion has already been drawn in Section 1.a above for the case of bulk Mg samples in O_2 or air at 1 atm and in CO_2 at 15 atm.

Furthermore, it is seen that in the case of Mg in air, lower ignition temperatures are measured in QP experiments than in DD experiments.

Certain qualitative data are not shown in Table 14 or Fig. 9 or 10. Schnizlein et al. (85) noted that bulk Mg ignites in O_2 "just below the (metal) melting point" and in CO_2 above 750°C. Hill et al. (213) could not ignite massive Mg of S/V = 0.736 mm^{-1} in an air wind tunnel with a Mach number of 5.2 and stagnation temperature of 332°C, even if the sample was preheated to 620°C. Finally, on the basis of a nuclear reactor accident, Salesse (51) concluded that the Mg ignition temperature in 10 atm of CO_2 is greater than 800°C. All of these data are consistent with the other literature

cited in this section.

In the SP experiments of Cassel and Liebman (215,217), the results of which are shown in Fig. 9 and 10, an anomalous trend is observed: the ignition temperature increases with decreasing sample size. These authors have explained their results in the following manner (217): from the classical theory of ignition for homogeneous systems, at ignition[1]

$$(\dot{q}_{chem})\Big|_{T_s=T_{ign}} = (\dot{q}_{loss})\Big|_{T_s=T_{ign}} \tag{A2-1}$$

$$\left(\frac{\partial \dot{q}_{chem}}{\partial T_s}\right)\Big|_{T_s=T_{ign}} = \left(\frac{\partial \dot{q}_{loss}}{\partial T_s}\right)\Big|_{T_s=T_{ign}} \tag{A2-2}$$

where as before, $\dot{q}_{chem}$ is the rate of generation of heat by the chemical reaction per unit area, $\dot{q}_{loss}$ is the rate of heat loss from the system per unit area, T_s is the surface temperature of the particle, and T_{ign} is the ignition temperature. The thermal conductivity of the gas, k_g, is assumed much smaller than that of the metal, and thus, neglecting convection and radiation, $\dot{q}_{loss}$ may be written:

$$\dot{q}_{loss} = k_g (T_s - T_g)/r \tag{A2-3}$$

where T_g is the gas temperature and r is the radius of the particle. Because their experimental results in-

[1] The authors actually use only Eqn. (A2-2) in the subsequent derivation. Thus their definition of ignition temperature is equivalent to that of the present investigation. If both Eqn. (A2-1) and (A2-2) are satisfied simultaneously, the ignition limit rather than ignition temperature is defined (23).

dicated that the experiments were performed in the chemically controlled regime, $\dot{q}_{chem}$ may be approximated:

$$\dot{q}_{chem} = Q_{chem} c_f c_g A e^{-E/RT_s} \qquad (A2\text{-}4)$$

where Q_{chem} is the molar heat of reaction, c_f and c_g are the concentrations of fuel and gas at the surface, respectively, A is the pre-exponential factor, E is the activation energy, and R is the universal gas constant.

When Eqn. (A2-3) and (A2-4) are substituted into Eqn. (A2-2) and two particle sizes are considered, Eqn. (A2-5) results:[2]

$$\ln\left(\frac{r_2}{r_1}\right) = 2\ln\left(\frac{T_{ign,2}}{T_{ign,1}}\right) - \left(\frac{E}{RT_{ign,1}} - \frac{E}{RT_{ign,2}}\right) \qquad (A2\text{-}5)$$

Making the approximation

$$\ln\left(\frac{T_{ign,2}}{T_{ign,1}}\right) \cong \frac{T_{ign,2}}{T_{ign,1}} - 1 \qquad (A2\text{-}6)$$

Eqn. (A2-5) may be written:

$$\ln\left(\frac{r_2}{r_1}\right) = \left(2 - \frac{E}{RT_{ign,2}}\right)\left(\frac{T_{ign,2} - T_{ign,1}}{T_{ign,1}}\right) \qquad (A2\text{-}7)$$

which explains the observed trend, that smaller particles ignite at a higher temperature than larger particles.[3]

---

[2] Cassel and Liebman included a ratio of thermal conductivies in this expression so that its influence on the ignition temperature of a single particle could be examined.

[3] $T_{ign,2}$ is always expected to be much smaller than E/2R.

To the best of the author's knowledge, these data are the only data which demonstrate this trend of ignition temperature with particle size, for all of the metals to be considered in this appendix. The theoretical agreement with the trend obtained by Cassel and Liebman results from the particular choice of Eqn. (A2-3) as the heat loss term; this choice is discussed in comparision with other theories in Chapter IV.

The experimental results may possibly be explained in the following manner: if the conditions of Cassel and Liebman's experiments were such that ignition temperatures were measured at the ignition limit (23), which is defined by the equations:

$$(\dot{q}_{chem})\Big|_{T_s = T_{ign,lim}} = (\dot{q}_{loss})\Big|_{T_s = T_{ign,lim}} \tag{A2-8}$$

$$\left(\frac{\partial \dot{q}_{chem}}{\partial T_s}\right)\Big|_{T_s = T_{ign,lim}} = \left(\frac{\partial \dot{q}_{loss}}{\partial T_s}\right)\Big|_{T_s = T_{ign,lim}} \tag{A2-9}$$

then it is possible that the reverse size trend could be obtained. Assume that $\dot{q}_{loss}$ can be separated into a size dependent and a size independent term:

$$\dot{q}_{loss} = a(T_s) + b(T_s) f(r) \tag{A2-10}$$

where f(r) is some function of sample size, and $a(T_s)$ and $b(T_s)$ are functions of temperature (and the other parameters involved in Eqn. (II-45) and are independent of sample size. Then Eqn. (A2-8) and (A2-9) may be

written:

$$\dot{m} Q_{chem} = a + bf(r) \tag{A2-11}$$

$$Q_{chem} \frac{\partial \dot{m}}{\partial T_s} = \frac{\partial a}{\partial T_s} + \frac{\partial b}{\partial T_s} f(r) \tag{A2-12}$$

where as before $\dot{m}$ is the molar reaction rate and Q_{chem} is the chemical energy release. It has been assumed for the purposes of this discussion that Q_{chem} may be approximated as temperature independent, which is a good assumption at the low temperatures associated with the ignition phenomenon. Since

$$\dot{m} = Ae^{-E/RT_s} \tag{A2-13}$$

where all symbols have their previous meanings, Eqn. (A2-11) and (A2-12) become

$$AQ_{chem} e^{-E/RT_{ign,lim}} = a + bf(r) \tag{A2-14}$$

$$\frac{E}{RT^2_{ign,lim}} AQ_{chem} e^{-E/RT_{ign,lim}} = \frac{\partial a}{\partial T_s} + \frac{\partial b}{\partial T_s} f(r) \tag{A2-15}$$

Combining Eqn. (A2-14) and (A2-15), one obtains:

$$[a+bf(r)] \frac{E}{RT^2_{ign,lim}} = \frac{\partial a}{\partial T_s} + \frac{\partial b}{\partial T_s} f(r) \tag{A2-16}$$

and it is possible that the size dependence indicated by Eqn. (A2-16) for the ignition limit is the opposite of that indicated by Eqn. (A2-12) for the ignition tempera-

ture. Unfortunately, only knowledge of the numerical values involved in these equations would confirm or negate this hypothesis.

In their simplified theory, Cassel and Liebman assumed that $a(T_s) = 0$, and thus Eqn. (A2-16) becomes:

$$\frac{E}{RT^2_{ign,lim}} b = \frac{2b}{2T_s} \qquad (A2-17)$$

and the ignition limit is independent of sample size.

Alternatively, in an experiment in which the metal sample is heated uniformly, the size effect resulting from the conduction loss to the interior of the sample will be unimportant. If this were the case in the experiments of Cassel and Liebman, then the size dependence of ignition temperature predicted by Eqn. (A2-3) could be observed. The dependence of ignition temperature on experimental environment in general is demonstrated here.

Experimental results on the ignition of Mg ribbons, obtained at Princeton by Brzustowski (7,9) and by Mellor (19,20), are reviewed in Chapter VI in order to facilitate comparison with the observations of the present investigation.

2. Lithium

No critical or spontaneous ignition temperatures have been reported in the literature for Li. The only mention of a possibility of sample self-heating is by Chandrasekharaiah and Margrave (54) in the nitridation of Li foil in the pressure range 110-220 torr and the temperature range 239-310°C. Thus the Li-N_2 critical temperature may lie at or below 239°C for samples with large S/V ratios. No estimate of the transition temperature for this system has been made, and thus no predictions regarding the Li-N_2 ignition can be made.

Literature ignition temperatures for Li are shown in Table 15. Because only the transition temperature for the Li-H_2O system and the critical temperature for the Li-N_2 system have been estimated, few conclu-

TABLE 15.

LITERATURE IGNITION TEMPERATURES FOR LITHIUM

Reference	Stated Size	Gas Pressure	Sample Condition	Ignition Temperature, °C
Oxygen				
(196),(200)	~10 g	1 atm	B	190
Nitrogen				
(210)	<100 μ	flowing	QP	399
(219)	125-149 μ	1 atm?	QP	170
Air				
(209)	<100 μ	1 atm	QP	374
Carbon Dioxide				
(210)	<100 μ	flowing	QP	330

sions may be drawn concerning the ignition of Li. As can be seen from Table 15, little information is available on the size effect in Li ignition. Not shown in the table is the Li-O_2 ignition temperature of 630°C given by Tyzack and Longton, quoted by Ref. (54), which is in complete disagreement with the result of Conway et al. (196,200).

The extension of the metal ignition criterion to the alkali and alkaline earth metals will be discussed at the end of Section 3.

3. Calcium

Like Li, few investigators have studied the oxidation and ignition of Ca. Consequently, only two

references to self-heating in oxidation or ignition experiments have been found. In 100-200 torr of O_2 in the temperature range 350 to 425°C (54), and in O_2 (probably at 1 atm) in the range 300 to 500°C (22), sample self-heating has been noted as possible in oxidation experiments. The transition temperature for the Ca-O_2 system has been estimated as 400°C in the pressure range 100-760 torr (Table 13). In spite of the scarcity of data on the critical temperature, however, because it is apparently less than the transition temperature, it may be concluded that the latter controls in Ca-O_2 ignition. Experimental studies performed in the present investigation shed more light on this conclusion; see Chapter VII.

In Table 16 it is noted that the ignition temperature of massive Ca in O_2 is 550°C (196, 200, 22), which is above the transition temperature and apparently above the critical temperature; thus the metal ignition criterion is satisfied in this case. The only conclusion that can be drawn from the remainder of the data shown in the table is that the expected size effect is demonstrated in air (209, 220).

Throughout the sections on the oxidation and ignition of Li and Ca in this and the previous chapter, the paucity of experimental results has been lamented. In the case of the other alkali and alkaline earth metals, the situation is worse. Thus it is of interest to generalize for the ignition of these other metals on the basis of the data on Mg, Li, and Ca reviewed here.

Most of the oxides formed by these metals have Pilling and Bedworth ratios less than unity (6).[4] As has been discussed in appendix I , however, the oxide

[4]Be does not fall in this category, and its ignition will be discussed in Section 5 of this appendix.

TABLE 16.

LITERATURE IGNITION TEMPERATURES FOR CALCIUM

Reference	Stated Size	Gas Pressure	Sample Condition	Ignition Temperature, °C
Oxygen				
(196),(200)	~10 g	1 atm	B	550
(22)	---	1 atm?	B	550
Nitrogen				
(210)	<44 μ	flowing	QP	327 360 671
Air				
(209)	<44 μ	1 atm	QP	229
(220)	0.227-0.25 mm^{-1}	flowing	B	730
Carbon Dioxide				
(210)	<44 μ	flowing	QP	293

films for Mg and Ca are protective at low temperature and become non-protective at higher temperature through mechanism (f) mechanical stress cracking at a critical oxide thickness. Most likely a similar mechanism will occur for the other alkali and alkaline earth metals, and thus their oxides are expected to also become non-protective at temperatures low compared with the melting point of their oxides, but above room temperature. (Recall that transitions due to mechanism (b), which occur at the oxide melting point, give an upper limit on the transition temperature.) Consequently, the ignition temperatures of the alkali and alkaline earth metals are expected to be low compared with the melting point of their oxides.

4. Aluminum

Friedman and Macek (15,16) have concluded that the ignition temperature of Al particles is equal to the melting point of Al_2O_3. They found a decrease in minimum ambient temperature required for ignition with increasing O_2 partial pressure in SP experiments (S/V = 171 mm^{-1}), but attributed this phenomenon to sample self-heating; that is, the critical temperature is below the melting point of the oxide. (See Section 12.e for further discussion of this result.)

Reported ignition temperatures for Al are shown in Table 17. For the various particle experiments, the trends expected on the basis of the relative critical temperatures are observed: high ignition temperatures are obtained in single particle (SP) experiments, medium ignition temperatures in dust dispersion (DD) experiments, and low ignition temperatures in quiescent pile (QP) experiments. In a given type of experiment, the ignition temperature decreases with decreasing particle size.

In the bulk experiments in O_2, ignition temperatures of 2030°C (the melting point of Al_2O_3) (17,18) and greater than 1000°C (196,200) have been reported.[5] Also, in SP experiments in various oxidizing gases, Al ignition temperatures of 2030°C (15,16) and greater than 1400°C (215,223) have been given. On the basis of these experiments (B and SP) in which the appropriate critical temperature will not be low as a

[5] In an earlier paper (21), the present author erroneously quoted Conway and co-workers as giving an ignition temperature for Al in O_2 as 1000°C, rather than as greater than 1000°C. This mistake resulted from a typographical error in Table VI of Ref. (196).

TABLE 17.

LITERATURE IGNITION TEMPERATURES FOR ALUMINUM

Reference	Stated Size	Gas Pressure	Sample Condition	Ignition Temperature, °C
Oxygen				
(221)	<44 μ	1 atm?	DD	663
(222)	3-200 μ	1 atm?	QP	590
(215),(223)	150 μ	1 atm?	SP?[1]	>1400
(17),(18)	7.8 mm^{-1}	0.067-66.7 atm	B	2030
(196),(200)	~10 g	1 atm	B	>1000
Nitrogen				
(203)	<44 μ	1 atm?	QP	750
	<74 μ	1 atm?	QP	800
(204)	<149 μ	1 atm?	QP	725
Air				
(205)	---	1 atm?	DD	645
(203)	<44 μ	1 atm?	DD	650
			QP	760 900
(207)	<74 μ	1 atm?	DD	645
(203)	<74 μ	1 atm?	QP	490
(204)	<149 μ	1 atm?	DD	673
			QP	585
(215),(223)	150 μ	1 atm?	SP?	>1400
(209)	$3x10^{5}$ mm^{-1}	1 atm	QP	538
Carbon Dioxide				
(203)	<44 μ	1 atm?	QP	900
(221)	44-60 μ	1 atm?	DD	1600
(203)	<74 μ	1 atm?	QP	540

TABLE 17, (concluded)

Reference	Stated Size	Gas Pressure	Sample Condition	Ignition Temperature, ^{o}C
(204)	$<149\mu$	1 atm?	QP	655
(222)	$3\text{-}200\mu$	1 atm?	QP	1030
(210)	2×10^{-5} mm^{-1}	flowing	QP	390
	760 mm^{-1}		QP	390
Water Vapor				
(224)	---	---	DD	1170
(221)	---	1 atm?	DD	None
(222)	$3\text{-}200\mu$	1 atm?	QP	1130
(17),(18)	7.8 mm^{-1}	---	B	<1427
Miscellaneous				
Natural gas/air Flame				
(225)	$<44\mu$	flowing	SP	~1500
C_3H_8/air Flame				
(15)	171 mm^{-1}	flowing	SP	2030
CO/air Flame				
(16)	171 mm^{-1}	flowing	SP	2030
(221)	---	1 atm?	DD	820

[1]SP denotes a single particle experiment.

result of cooperative heat transfer between particles (as in DD and QP experiments), it is concluded that the ignition temperature of Al is equal to the melting point of Al_2O_3, 2030°C (6). As was mentioned in Chapter III, the transition temperature is also thought to be the melting point of the oxide (mechanism (b)). This conclusion is reached because the ignition temperature of Al is independent of sample size over such a large range, 7.8 to 171 mm^{-1} (15 - 18), that is, the ignition temperature is apparently controlled by the transition temperature, which is independent of size. Recall that no evidence that the transition temperature is less than the melting point of Al_2O_3 is available in the oxidation literature.

The ignition temperatures which are below the oxide melting point measured in QP and DD experiments are thus thought to actually be critical temperatures. As has been mentioned previously, sample self-heating in these experiments is difficult to observe.

Two investigators were unable to ignite bulk Al below the metal melting point in O_2, CO_2, or 50%O_2-50%CO_2 at high pressures (194,213); these results are consistent with the conclusions reached here.

The lower ignition temperature of bulk Al in H_2O probably results from a lower transition temperature of the film formed. No conclusions can be reached for the Al-N_2 system, as no transition temperature can be estimated.

Kuehl (17,18) found that the ignition temperature of bulk Al in O_2-Ar mixtures decreases with decreasing pressure below an oxygen partial pressure of about 50 torr. At pressures on the order of 5 torr, the

ignition temperatures were as low as 1450°C. It was postulated that at these pressures a thinner oxide coat forms during the heating time; this coat is then not protective to its melting point. The results of Kuehl are discussed further in Chapter VI, in comparison with the results of Brzustowski (7,9) and of Mellor (19,20).

5. Beryllium

The only mention of Be self-heating in the literature is by Macek et al. (226), whose results are shown in Table 18. In an ammonium perchlorate/trioxymethylene flame, they observed that the ignition temperature of Be approached the melting point of BeO (2530°C (6)) as the O_2 partial pressure was decreased. In fact, as the O_2 partial pressure was decreased from 2 to 0.1 atm, the ignition temperature increased from 2100 to 2377°C. These authors suggested (similar to the case of Al, see Section 4) that this apparent decrease in the ignition temperature is a result of the Be particle temperature rising spontaneously above the ambient temperature to the melting point of BeO, due to increased reaction rates at the higher O_2 pressures. Thus the value of 2100°C measured at 2 atm of O_2 is actually a critical temperature.

Kuehl reached the conclusion that the ignition temperature of bulk Be in 66.7 atm of O_2 is equal to the melting point of the oxide. As is the case for Al, the ignition temperature is lower if H_2O is present (18).

Therefore, the ignition of Be is thought to be strictly analogous to the ignition of Al in O_2-con-

TABLE 18.

LITERATURE IGNITION TEMPERATURES FOR BERYLLIUM

Reference	Stated Size	Gas Pressure	Sample Condition	Ignition Temperature, °C
Air				
(209)	$<0.1\mu$	1 atm	QP	20
(208)	$<37\mu$	1 atm?	QP	635
	$500-2000\mu$	1 atm?	QP	780
(203)	6000 mm^{-1}	1 atm?	DD	910
			QP	540
Miscellaneous				
Ammonium perchlorate/trioxymethylene Flame (O_2 partial pressure listed)				
(226)	158 mm^{-1}	0.1 atm	SP	2377
		2 atm		2100
H_2/O_2 Flame, O_2 rich				
(225)	$<44\mu$	flowing	DD	>2000

taining gases. The ignition temperature is equal to the transition temperature, which results from mechanism (b), melting of the appropriate oxide. The critical temperature is below this value.

6. Uranium

a. Critical Temperatures

A graph of initial sample temperature versus ignition delay time is shown in Fig. 11 for bulk U in

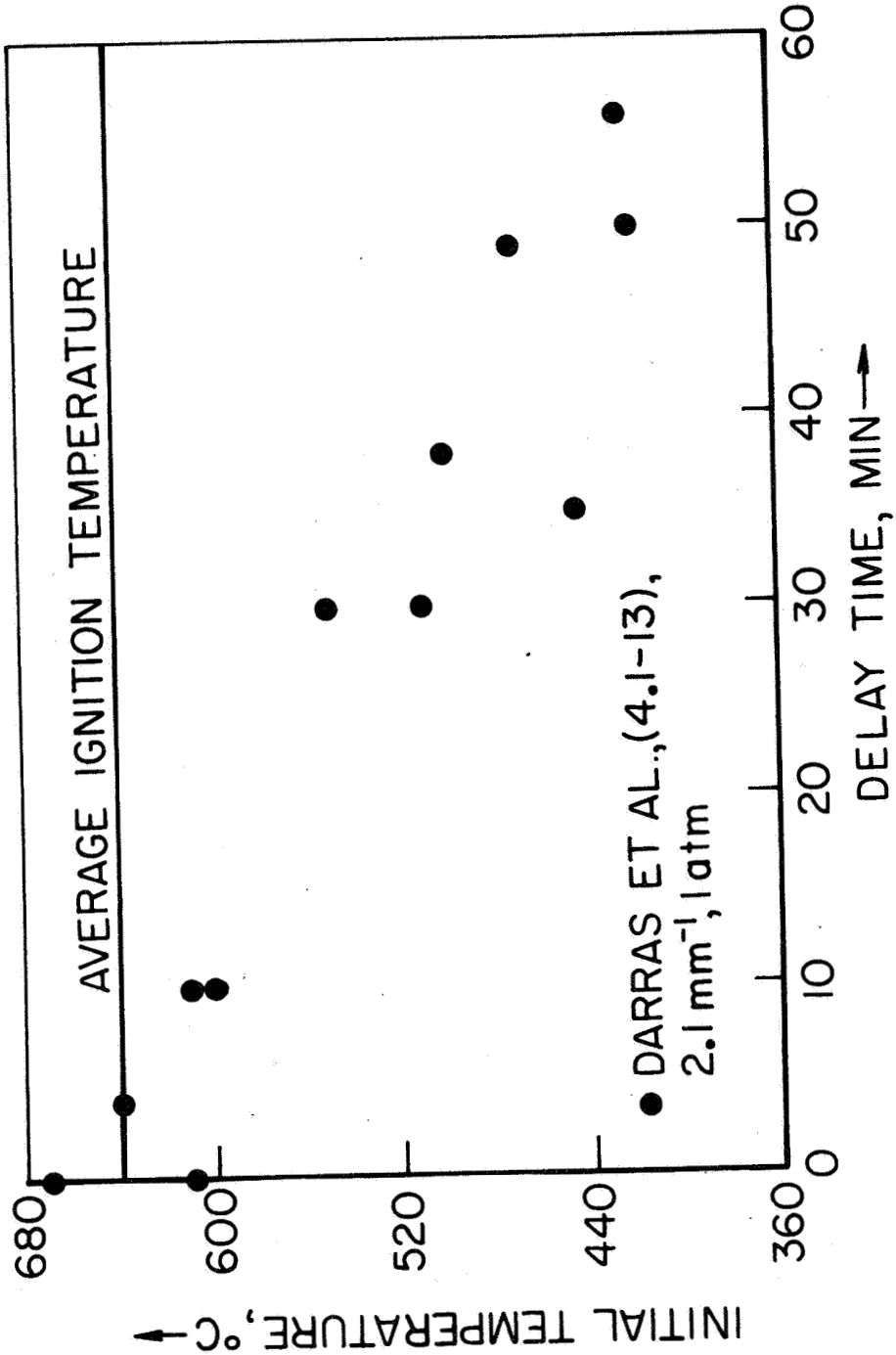

FIGURE 11

INITIAL TEMPERATURE vs DELAY TIME: BULK URANIUM IN AIR

APZ7-4048-67

air at 1 atm. The data are taken from Ref. (212). Although there is considerable scatter in the data, it is apparent that a critical temperature exists for U in this oxidizing gas. Darras and co-workers (212) estimated that infinite ignition delay time would be observed if the initial sample temperature were 400°C; this then is the critical temperature for bulk U ($S/V = 2.1\ mm^{-1}$) in air at 1 atm. Since the U-air transition temperature is probably about 150°C (see Chapter III), it is concluded that the ignition of bulk U in air is controlled by the critical temperature. It is interesting to note that Darras et al. (212) found that the spontaneous ignition temperatures shown in Fig. 11 are independent of applied heating rate.

Other investigators have reported the importance of sample self-heating in the oxidation of U: for U cubes in 200 torr of O_2 above 300°C (227); for U cubes in 20-800 torr of O_2 above 300°C (76); and for bulk U in 200 torr of air above 200°C (74). Adda (74) noted that the spontaneous ignition temperature decreases with increasing S/V, which verifies the prediction of such a trend made in Chapter II.

To summarize, on the basis of the literature, it is expected that the critical temperature will control the ignition of bulk U in either O_2 or air.

b. Ignition Temperatures

It was noted in Chapter II that the Atomic Energy Commission is concerned with the problem of U pyrophoricity, because of U fires and explosions in processing plants. The reader is referred to Ref. (234)

for further discussion of this problem.

Reported ignition temperatures for U in the various oxidizing gases of interest are shown in Table 19 and in Fig. 12 and 13. The excellent agreement shown in Fig. 12 and 13 results in part from the compilation of data from the various papers by the Argonne group (85,231-233).

TABLE 19.

LITERATURE IGNITION TEMPERATURES FOR URANIUM

Reference	Stated Size	Gas Pressure	Sample Condition	Ignition Temperature, °C
Oxygen				
(227)	---	200 torr	B	>300
Nitrogen				
(210)	<74 μ	flowing	QP	357
(228)	556 mm^{-1}	1 atm?	QP	410
Air				
(209)	<74 μ	1 atm	QP	145
(229)	---	flowing	B	397
(230)	---	flowing	B	355
Carbon Dioxide				
(210)	<74 μ	flowing	QP	235
(228)	556 mm^{-1}	1 atm?	DD	560
			QP	350
(212)	0.9 mm^{-1}	1 or 15 atm	B	800
(85)	0.778 mm^{-1}	flowing	B	>850

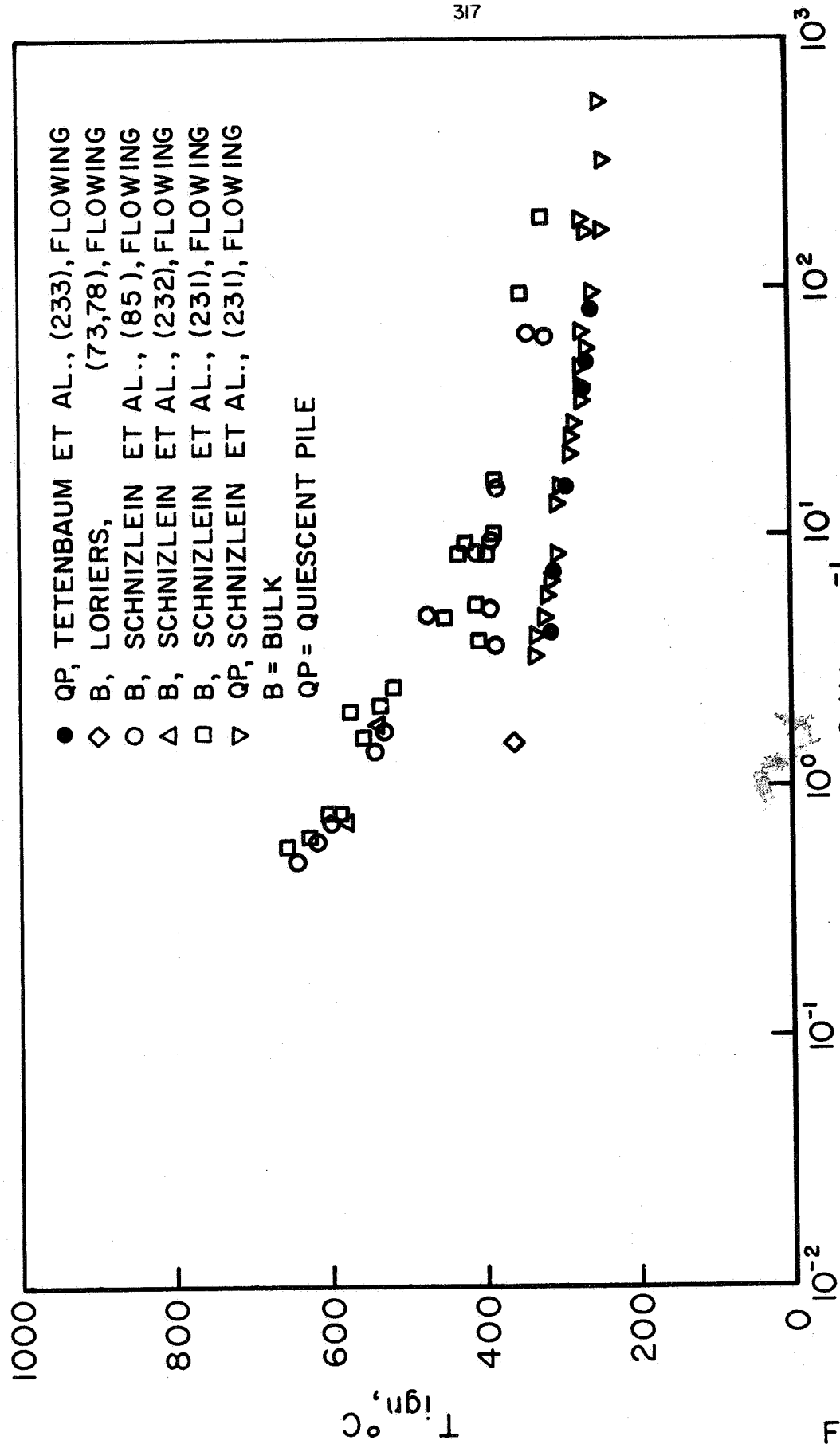

IGNITION TEMPERATURE vs SURFACE-VOLUME RATIO: URANIUM IN OXYGEN

FIGURE 12

FIGURE 13

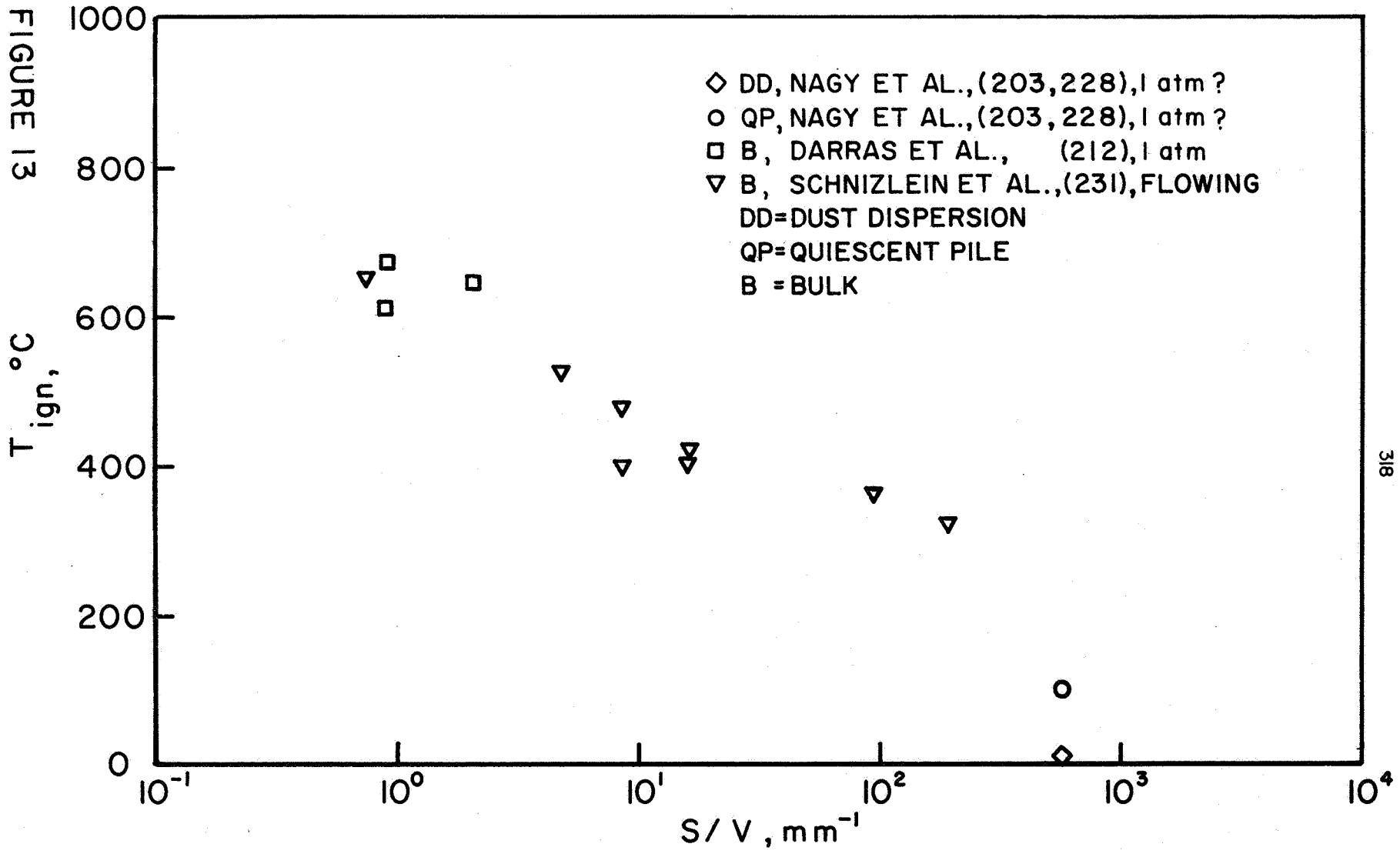

IGNITION TEMPERATURE vs SURFACE-VOLUME RATIO: URANIUM IN AIR

Throughout the table and figures, the expected trends are observed: the ignition temperature decreases with decreasing sample size, but in general in O_2 or air does not move below the transition temperature of 150°C (the exceptions are the DD and QP data of Jacobson and co-workers (203,228)), and measured ignition temperatures at a given S/V increase in QP, DD, and B experiments, respectively. The first trend is consistent with the explanation of pyrophoricity as given in Chapter II and as based on the model of metal ignition.

The data of Bagley and Oliver (86) are not shown in the table or figures: these investigators could not ignite bulk U (S/V = 0.3 mm^{-1}) in air below 600°C. Inspection of Fig. 13 shows agreement with the results presented there.

Schnizlein et al. (85) found that sample purity had little effect on the measured ignition temperature for bulk U in O_2, and two investigators reported that the U ignition temperature increases with increasing applied heating rate, for bulk U in air at 1 atm (212), and for a QP experiment in O_2 (233).

7. Zirconium

a. Critical Temperatures

Several investigators have noted difficulties with self-heating of Zr; however, as no ignition delay times are reported, no critical temperature may be estimated. For bulk Zr (S/V = 7.88 mm^{-1}) in O_2 at 76 torr, spontaneous ignition was encountered at 800°C (93,237);

for bulk Zr (S/V = 15.05 mm^{-1}) in 1 atm of O_2, at about 820°C (232); and for bulk Zr (S/V = 1.41 mm^{-1}) in O_2, at 1000°C (123). Note the general decrease in cited temperatures with increasing surface area to volume ratio, which may indicate a similar decrease in critical temperature.

Schnizlein and co-workers (85) noted that bulk Zr could not be ignited in flowing O_2 at temperatures less than 1300°C if the sample was initially heated in O_2. If however the initial heating was carried out in He, and O_2 was admitted at temperature, ignitions were observed at about 840°C. Their results were expressed in terms of the specific area as follows:

$$T_{ign} = 1070 - 208 \log (A/m) \qquad \text{(A2-18)}$$

where T_{ign} is in degrees Celsius and (A/m) is in cm^2/g (85).

This temperature of 840°C may correspond to the spontaneous ignition temperatures listed above, and thus Eqn. (IV-18) may define T_{crit} rather than T_{ign}. In any case, this temperature was observed to be independent of the method of sample surface pretreatment (85).

b. Ignition Temperatures

Literature ignition temperatures for Zr are reported in Table 20 and in Fig. 14. Turning first to the Zr-O_2 system,[6] the results of Beal et al. (235)

[6]The results of Littman et al.(239) on the ignition of Zr bars broken in torsion or tension will not be discussed in the present report.

TABLE 20.

LITERATURE IGNITION TEMPERATURES FOR ZIRCONIUM

Reference	Stated Size	Gas Pressure	Sample Condition	Ignition Temperature, °C
Oxygen				
(235)	9.19-23.6 mm^{-1}	flowing	B	855
Nitrogen				
(203)	<44 μ	1 atm?	QP	530
(204)	<149 μ	1 atm?	QP	530
(210)	2000 mm^{-1}	flowing	QP	508
(203),(228)	2000 mm^{-1}	1 atm?	QP	790
Air				
(205)	---	1 atm	DD	25
(203)	<44 μ	1 atm?	QP	210
(204)	<149 μ	1 atm?	DD	25
			QP	210
Carbon Dioxide				
(203)	<44 μ	1 atm?	QP	560
(204)	<149 μ	1 atm?	QP	560
(210)	2000 mm^{-1}	flowing	QP	365
(203),(228)	2000 mm^{-1}	1 atm?	QP	620
(228)	1820 mm^{-1}	1 atm?	DD	650
(203),(228)	330 mm^{-1}	1 atm?	QP	710
Water Vapor				
(224)	---	---	DD	2400

listed in the table were obtained in an experiment in which the sample was dropped into the hot oxidizing gas. Thus this experiment is subject to the difficulties in diagnosing sample self-heating that is common to SP experiments. On comparison of their ignition temperature of 855°C with the spontaneous ignition temperatures listed in Section 7.a, it is concluded that this value is not a true ignition temperature as defined in the present report.

Recall that in Appendix I the $Zr-O_2$ transition temperature was estimated to be 925 ± 100°C, and it was mentioned that protective oxidation rates have been observed at temperatures above this estimated transition temperature (101,107). The results of Schnizlein et al. (85) also indicate that the transition temperature may be substantially higher than 925°C, as they were unable to ignite Zr in O_2 below 1300°C if the sample was heated initially in O_2.

On the basis of the data of Schnizlein (85), Kofstad (101), and Pemsler (107), the transition temperature of 925 ± 100°C which was estimated in Appendix I is discarded. Evidently the $Zr-O_2$ transition temperature lies above 1300°C. Note, however, that this effect may actually be a result of the dependence of transition temperature on applied heating rate (see Chapter III).

Very recent data obtained by Pemsler (132) further substantiate the conclusion that the $Zr-O_2$ transition temperature is greater than or equal to 1300°C. For either oxygen-free or oxygen-saturated Zr, he observed parabolic rates in O_2 in the temperature range 840 - 1300°C. More rapid parabolic rates of film

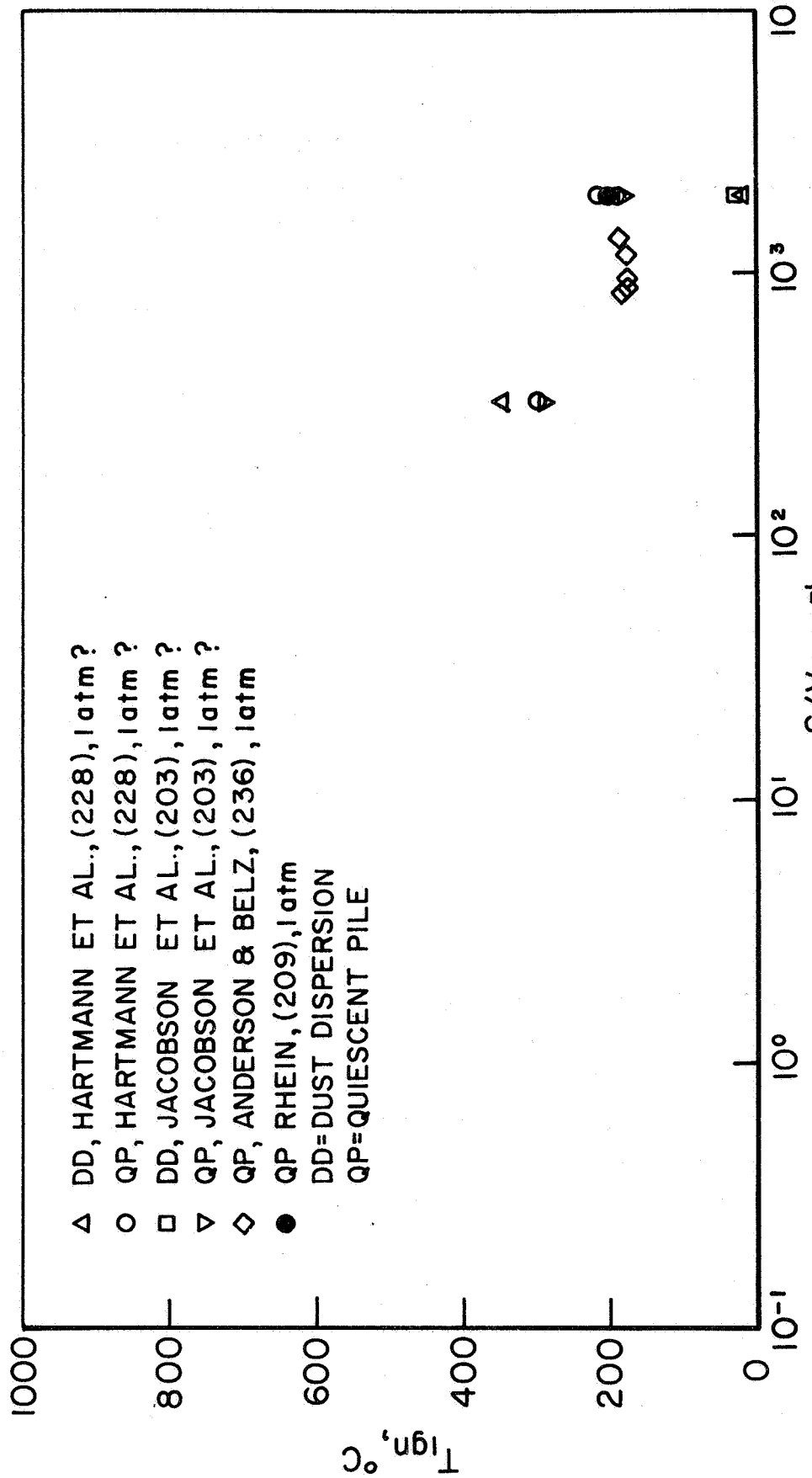

IGNITION TEMPERATURE VS SURFACE-VOLUME RATIO: ZIRCONIUM IN AIR

FIGURE 14

formation occurred with the oxygen-saturated metal. That the initial O_2 concentration in the metal is important in the experiment, as suggested in Chapter III, is demonstrated by the observation that adherent oxide films could not be obtained on oxygen-saturated Zr below 840°C (132).

Since the Zr-N_2 transition temperature is thought to lie above 1640°C, most likely critical temperature interference occurred in the QP experiments listed in Table 20.

That small Zr particles will ignite in air at room temperature is documented in both Table 20 and Fig. 14. For a discussion of this problem with respect to Zr fires and explosions, see Ref. (238). Also, Hickman and Gulbransen remarked that "at moderate temperatures finely powdered Zr will burst into flame when heated in air" (240). Because of the uncertainty in the Zr-O_2 transition temperature, the Zr-air transition temperature which was also estimated as 925 $\pm$ 100°C (Table 13) will also be rejected.

In CO_2, a decrease in ignition (or critical) temperature with increasing S/V is seen in Table 20.

To summarize, for Zr in the oxidizing gases of interest, spontaneous ignition apparently has led to reported ignition temperatures which are lower than the transition temperatures. Documentation of an O_2 critical temperature has been accomplished and has led to a revision in the transition temperature estimated on the basis of the oxidation literature. Furthermore, observed ignitions for dust dispersions of Zr in room-temperature air also indicate extremely low critical temperatures are involved, as there is no question that

protective oxidation rates are observed at low temperatures in the Zr-air reaction (see Table 8).

8. Titanium

a. Critical Temperatures

Hill et al. (213) measured spontaneous ignition temperatures for Ti in O_2 and in air. For bulk Ti samples of S/V = 2.56 mm^{-1}, the values are 1150°C in 33.3 atm of O_2 and 1592°C in 1 atm of air. Unfortunately, no ignition delay times are given.

The transition temperature of the Ti-O_2 system has only been estimated within the pressure range 10^{-3} through 760 torr, and was taken as 900°C. Subject to this large pressure difference and noting that a spontaneous ignition rather than critical temperature was reported by Hill et al. (213), it may be concluded that the critical temperature also controls in the ignition of bulk Ti in O_2.

b. Ignition Temperatures

Littman et al. (241) studied the ignition of Ti bars broken in tension in O_2; as has been mentioned previously, this experiment falls outside the scope of the present report.

Literature ignition temperatures are shown in Table 21 and Fig. 15. Few conclusions can be drawn for Ti in the various gases, as a transition temperature is available only in O_2. Some of the expected trends with respect to sample size and with respect to type of experiment are seen in the table and figure.

TABLE 21.

LITERATURE IGNITION TEMPERATURES FOR TITANIUM

Reference	Stated Size	Gas Pressure	Sample Condition	Ignition Temperature, °C
Oxygen				
(194)	2.25-7.88 mm^{-1}	3.3 atm	B	1315
		20 atm		815
Nitrogen				
(203)	<44 μ	1 atm?	QP	700
	<74 μ	1 atm?	QP	900
(228)	445 mm^{-1}	1 atm?	QP	760
(210)	1200-6000 mm^{-1}	flowing	QP	830
Air				
(205)	---	1 atm?	DD	480
(209)	1-5 μ	1 atm	QP	625
(206)	<40 μ	1 atm?	DD	401
(203)	<44 μ	1 atm?	QP	475
(206)	40-53 μ	1 atm?	DD	425
	<66 μ	1 atm?	DD	412
(203)	<74 μ	1 atm?	QP	460
(204)	<149 μ	1 atm?	DD	480
			QP	460
Carbon Dioxide				
(203)	<44 μ	1 atm?	QP	685
	<74 μ	1 atm?	QP	680
(204)	<149 μ	1 atm?	QP	680
(210)	1200-6000 mm^{-1}	flowing	QP	670
(228)	445 mm^{-1}	1 atm?	QP	550
(194)	2.25-7.88 mm^{-1}	20 atm	B	1520

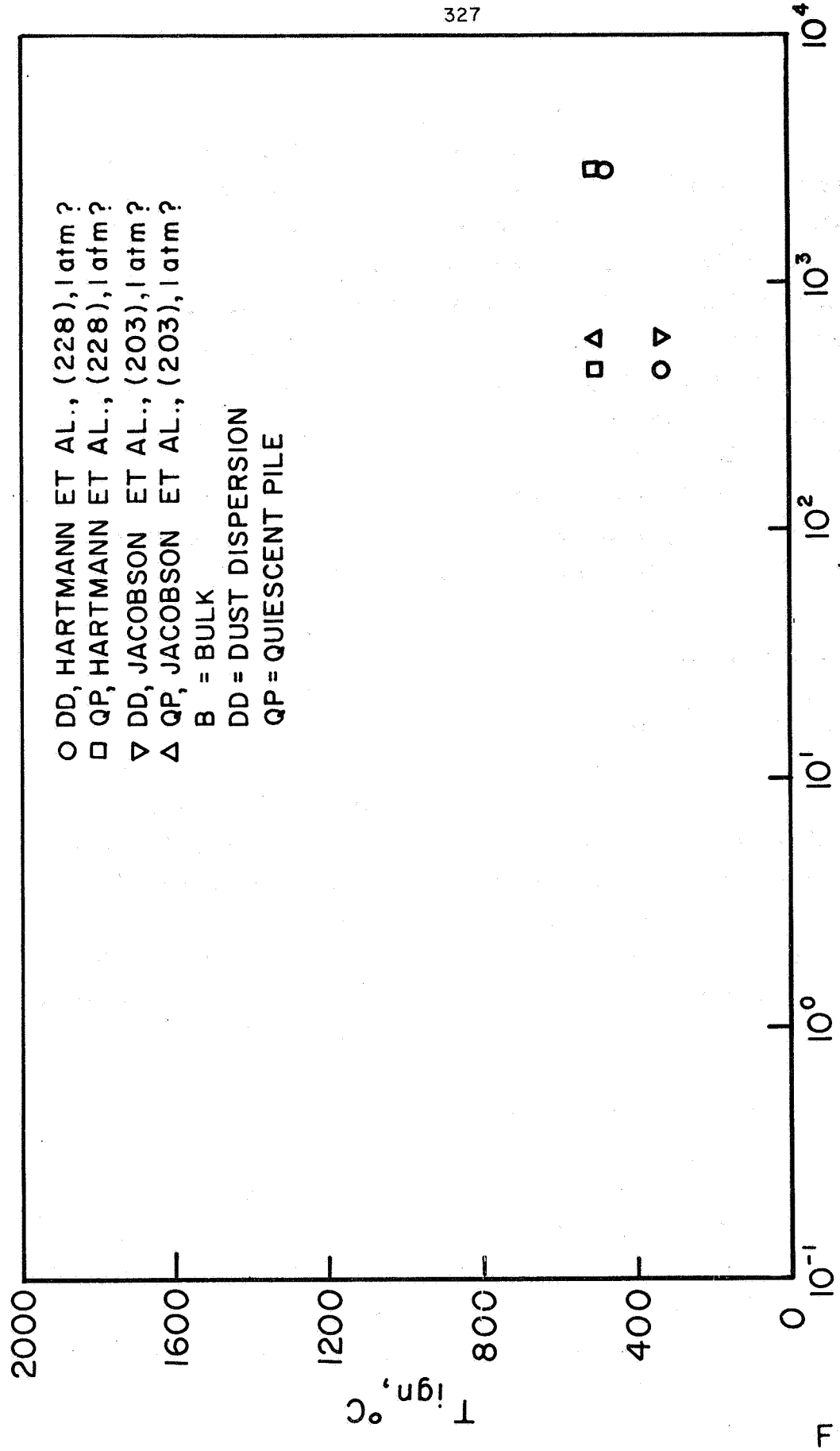

IGNITION TEMPERATURE vs SURFACE-VOLUME RATIO: TITANIUM IN AIR

FIGURE 15

Note that the results of Hill et al. (213) and of Dean and Thompson (194) on the ignition of bulk Ti in O_2 are in disagreement: according to these investigators, a spontaneous ignition temperature at 33.3 atm is 1150°C (213), and the ignition temperature at 20 atm is 815°C and at 3.3 atm is 1315°C (194), that is, an inconsistent pressure trend is reported. Perhaps a pressure dependence of the transition temperature has come into play here.

A final item is that Riehl and co-workers (242) could not ignite bulk Ti at a temperature less than 1200°C in a H_2/air flame at a pressure of about 1.67 atm.

9. Tantalum

a. Critical Temperatures

In oxidation experiments with bulk Ta (S/V = 0.845 mm^{-1}) in 1 atm of O_2, Albrecht et al. (157) reported an ignition delay time of 15 min at 1250°C. Ignition was instantaneous at 1300°C. Since the transition temperature is much below these values (500°C), it is concluded that the ignition of Ta in O_2 is controlled by the critical temperature.

b. Ignition Temperatures

Reported ignition temperatures for Ta in O_2 and air are shown in Table 22. Cowgill and Stringer (159,243) listed a value of 1000°C in O_2 for a slightly smaller sample than that used in Ref. (157). Since these authors noted that the sample burst into flame

TABLE 22.

LITERATURE IGNITION TEMPERATURES FOR TANTALUM

Reference	Stated Size	Gas Pressure	Sample Condition	Ignition Temperature, °C
Oxygen				
(159), (243)	4.2 mm^{-1}	---	B	1000
(157)	0.845 mm^{-1}	1 atm	B	1300
Air				
(203)	<44 μ	1 atm?	DD	630
			QP	300
(220)	4.32 mm^{-1}	1-7 atm	B	1238-1282[1]

[1] Brightness temperature.

when O_2 was admitted at 1000°C, this value may actually be a critical temperature as a result of sample self-heating during the transient filling period.

The bulk air results (220) are consistent with the air transition temperature of 800°C; lower ignition temperatures observed in DD and QP experiments are most likely a result of sample self-heating, as was the case for similar experiments with Zr and Ti.

10. Molybdenum

a. Critical Temperatures

Simnad and Spilners (177) investigated the oxidation of bulk Mo with S/V = 2.33 mm^{-1}. In O_2 at 1 atm, they found that ignition occurred at 750°C. However, if the sample was pre-oxidized at 725°C for more than 8 min, ignition was not observed below the melting point of MoO_3, 770°C. Since for a clean Mo surface ignition occurred instantaneously at 750°C, but at 725°C an ignition delay time of at least 8 min was observed, it may be concluded that the critical temperature of Mo in 1 atm of O_2 is on the order of 725 or 700°C. The transition temperature at this pressure is estimated as 725°C (Table 13); thus, because of the proximity of the critical and transition temperatures, either may control in the ignition of bulk Mo.

In a wind tunnel experiment with bulk Mo in 10.5 atm of air at a Mach number of 2.1, some samples, but not others, were observed to ignite for a stagnation point temperature greater than 1827°C (244). The authors noted that "also uncertain is the reason that some specimens which ignited did so under conditions apparently no more severe than those experienced by other specimens which did not ignite. . . Apparently the conditions employed in the present investigation lie in a transition regime between consistent normal oxidation and consistent ignition. In this region small differences in heat input and/or heat removal may determine whether a specimen ignites or behaves normally."

Evidently in this experimental environment the critical temperature of Mo is extremely high (perhaps due to large heat losses from the samples), and interferred with the oxidation experiments.

b. Ignition Temperatures

In Table 23 literature ignition temperatures for Mo in O_2 and air are listed. Excellent agreement is seen between the O_2 transition temperature of 725°C and the bulk ignition temperatures.

In air, the DD result is above the air transition temperature (595°C), but the QP datum is below this value, probably due to the low critical temperature associated with QP experiments.

TABLE 23.

LITERATURE IGNITION TEMPERATURES FOR MOLYBDENUM

Reference	Stated Size	Gas Pressure	Sample Condition	Ignition Temperature, °C
Oxygen				
(177)	2.33 mm^{-1}	1 atm	B	750
(196), (200)	~10 g	1 atm	B	750
(36)	---	6.7 atm	B	725
Air				
(203)	< 74 μ	1 atm?	DD	720
			QP	360

On the basis of the ignition temperature data, no further conclusion may be drawn as to which of the transition and critical temperatures controls the bulk ignition of Mo.

11. Silicon

No indications of Si self-heating or spontaneous ignition are present in the literature. Furthermore, very few ignition data are available for Si (Table 24). As transition temperatures have been estimated only for the $Si-O_2$ and $Si-H_2O$ systems, no conclusion can be drawn from the data listed in Table 24.

TABLE 24.

LITERATURE IGNITION TEMPERATURES FOR SILICON

Reference	Stated Size	Gas Pressure	Sample Condition	Ignition Temperature, °C
Nitrogen				
(203)	$<53\mu$	1 atm?	QP	1000
(204)	$<149\mu$	1 atm?	QP	1000
Air				
(203)	$<53\mu$	1 atm?	QP	950
	$<74\mu$	1 atm?	QP	790
(204)	$<149\mu$	1 atm?	QP	950
			DD	775
Carbon Dioxide				
(203)	$<53\mu$	1 atm?	QP	1000
(204)	$<149\mu$	1 atm?	QP	1000

12. Theories of Metal Ignition

Several theories of metal ignition have been given by various investigators in the literature; these will now be reviewed. In order to facilitate comparision, the defining equations for the critical and ignition temperatures in the present model are repeated:

$$(\dot{q}_{chem})|_{T_s = T_{crit}} = (\dot{q}_{loss})|_{T_s = T_{crit}} \qquad \text{(II-56)}$$

$$\left(\frac{\partial \dot{q}_{chem}}{\partial T_s}\right)\Big|_{T_s = T_{ign}} = \left(\frac{\partial \dot{q}_{loss}}{\partial T_s}\right)\Big|_{T_s = T_{ign}} \qquad \text{(II-57)}$$

Some of the theories to be discussed are appropriate to systems of any size, that is, are size independent, and others are for particular types of experiments such as those involving dust dispersions.

a. Bulk Ignition According to the Theory of Eyring and Zwolinski

The earliest theory of metal ignition is due to Eyring and Zwolinski (48). This theory, in terms of the present model, is a calculation for the critical temperature of a bulk system based on the Theory of Absolute Reaction Rates.

The temperature under consideration was defined by the following heat balance equation:

$$\dot{q}_{chem} = \dot{q}_{loss} \qquad \text{(A2-19)}$$

The $\dot{q}_{chem}$ term was expressed as:

$$\dot{q}_{chem} = \dot{m}\,\Delta H_f / N \qquad \text{(A2-20)}$$

where $\dot{m}$ is the reaction rate (number of metal atoms/cm^2 sec), ΔH_f is the heat of formation of the product (kcal/mole), and N is Avogadro's number.

It was stated that "the ignition of metal samples will occur when the conduction of heat through the oxide

film is inadequate for the removal of the heat produced at the metal-film interface as a result of corrosion". Radiation, conduction into the metal, and conduction into the ambient oxidizing gas are neglected, and thus $\dot{q}_{loss}$ was written:

$$\dot{q}_{loss} = K_{ox}(T_s - T_0)/d_{ox} \qquad (A2\text{-}21)$$

where k_{ox} is the thermal conductivity of the oxide (cal/^{o}C cm sec), T_s is the temperature at the metal-oxide interface, T_0 is the temperature at the oxide-gas interface (both in ^{o}K), and d_{ox} is the oxide film thickness (cm). Eqn. (A2-19) then becomes:

$$\dot{m}\Delta H_f/N = K_{ox}(T_s - T_0)/d_{ox} \qquad (A2\text{-}22)$$

The expression for the reaction rate was developed from the Theory of Absolute Reaction Rates and was written:

$$\dot{m} = (c_s K T_s F/h)e^{-E/KT_s} \qquad (A2\text{-}23)$$

where C_s is the number of adsorption sites or metal atoms per unit surface area, k is the Boltzmann constant (ergs/^{o}K), h is Planck's constant (erg sec), E is the activation energy (erg), and F is the ratio of the reaction surface area to the outer area of the oxide film. This rate expression is valid only for regimes of linear oxidation.

Eqn. (A2-22) and (A 2-23) may be rewritten:

$$T_0 = T_s[1 - (c_s K F d_{ox}\Delta H_f/K_{ox}hN)e^{-E/KT_s}] \qquad (A\,2\text{-}24)$$

Since ignition will occur when the heat balance represented by Eqn. (A2-22) is destroyed, T_s as calculated from Eqn. (A2-24) is the ignition temperature, which is seen to depend strongly on the oxide film thickness, d_{ox}. Note, however, that in terms of the present model, T_s as calculated from Eqn. (A2-24) is actually the critical temperature by virtue of Eqn. (II-56).

Upon comparison of temperatures calculated from Eqn. (A2-24) with ignition temperatures measured experimentally for Mg in O_2, Fassell et al. (201) noted the following difficulties with the theory: firstly, the experimental ignition temperature is independent of oxide thickness; secondly, self-heating below the temperature predicted by Eqn. (A 2-24) is impossible (that is, these authors recognized that self-heating below the ignition temperature is possible); and thirdly, the observed pressure dependence of the ignition temperature is not explained or predicted by the theory.

Recalling that the temperatures calculated by Eyring and Zwolinski are actually critical temperatures, two of the failures of the theory noted by Fassell and co-workers can be explained. It is possible that the critical temperature is a function of oxide film thickness (see Chapter VII), as was discussed in Chapter II, and self-heating is not only possible, but also expected above the critical temperature. A pressure dependence of ignition or critical temperature is predicted by a more complete theory.

Other difficulties with the theory of Eyring and Zwolinski are the independence of critical temperature with respect to sample size and the failure of the theory for zero oxide thicknesses. Also, the theory as

developed applies only to temperature regimes of linear oxidation.

In view of the difficulties noted with the theory of Eyring and Zwolinski, Higgins and Schultz proposed the following modifications, according to Ref. (199), in which T_s and T_0 were defined in terms of microscopic granules of metal: T_s is the mean temperature in the interior of a metallic granule at the metal-oxide interface; T_0 is a mean temperature at the external surface of the oxide film associated with the granule; and, allowing for non-uniformitities in the oxide film on the granule, d_{ox} is taken as a mean oxide thickness. It was then argued that for an aggregate of small granules, because of the near equality of T_s and T_0 from granule to granule, the temperature gradient $(T_s - T_0)/d_{ox}$ becomes vanishingly small and ignition occurs. However, no calculations were attempted.

b. Bulk Ignition According to the Theory of Hill, Adamson, Foland, and Bressette.

A second theory, also based on Eqn. (II-56), was proposed by Hill and co-workers (213). These authors, however, noted that the calculation provided an estimate of the spontaneous ignition temperature, rather than ignition temperature, and is thus consistent with the definitions of the present model.

These authors balanced a rate of chemical energy release with a convection and radiation heat loss:

$$\dot{q}_{chem} = \dot{q}_{conv} + \dot{q}_{rad} \qquad \text{(A2-25)}$$

A conduction term into the metal was neglected because in their experiments the samples were heated uniformly. Using engineering approximations to the three terms in Eqn. ($A2$-25), good agreement between calculated and measured spontaneous ignition temperatures was obtained for 1020 steel in air. The appropriate oxidation rate involved in $\dot{q}_{chem}$ was measured in their own experiments. The calculated values were dependent on the oxide thickness (as in the theory of Eyring and Zwolinski).

A major difficulty with the theory of Hill et al. is that the wrong size dependence of critical temperature is predicted. In their approximation of $\dot{q}_{conv}$ the sample size dependence enters as follows:

$$\dot{q}_{conv} \sim Re^{1/2}/d \qquad (A\ 2\text{-}26)$$

where d is now the characteristic size of the sample, and Re is the Reynolds number based on this size. Therefore, by virtue of the definition of Reynolds number:

$$\dot{q}_{conv} \sim d^{-1/2} \qquad (A\ 2\text{-}27)$$

That is, as the sample size is decreased, $\dot{q}_{conv}$ increases, and so does the critical temperature.

As in the theory of Eyring and Zwolinski, the theory of Hill et al. fails for clean metal surfaces, that is, for zero oxide thicknesses, because in this case the reaction rate is inversely proportional to oxide film thickness.

c. Bulk Ignition According to the Theory of Reynolds

A theory of metal ignition was advanced by

Reynolds (220), in which the temperature history of the metallic sample was described by the following energy equation, where conduction into the fuel is neglected:

$$\frac{C}{S}\frac{dT_s}{dt} = \dot{q}_{chem} - h(T_s - T_g) - \epsilon\sigma(T_s^4 - T_r^4) + \dot{q}_{input} \qquad \text{(A2-28)}$$

where C = total heat capacity of the sample, cal/^{o}K;
S = surface area of the sample, cm^2;
T_s = surface temperature of the sample, ^{o}K;
t = time, sec;
$\dot{q}_{chem}$ = chemical energy release rate per unit area, cal/cm^{2}sec;
h = heat transfer coefficient, cal/cm^{2}sec^{o}K;
T_g = sample recovery temperature, ^{o}K;
σ = Stefan-Boltzmann constant, cal/cm^{2}sec(^{o}K)^4;
ϵ = surface emissivity, dimensionless;
T_r = effective radiation temperature of the environment, ^{o}K;
$\dot{q}_{input}$ = any heat input independent of the body temperature, cal/cm^{2}sec.

According to Reynolds, "the ignition temperature is seen to be equivalent to the temperature at which the body temperature begins to increase at an increasing rate. This may be expressed mathematically as the temperature at which dT_s/dt is a minimum." Thus, at ignition:

$$\frac{d}{dT_s}\left(\frac{C}{S}\frac{dT_s}{dt}\right) = 0 \qquad \text{(A2-29)}$$

or, from Eqn. (IV-28):

$$\frac{d\dot{q}_{chem}}{dT_s} - h - 4\epsilon\sigma T_s^3 = 0 \qquad \text{(A2-30)}$$

Reynolds defined ignition to occur at an inflection point in the surface temperature-time curve; as no equilibrium positions (with respect to time) are indicated in his model and as the surface temperature is rising in time, by definition, the critical temperature has been exceeded. He then incorrectly indicated that dT_s/dt goes through a minimum at ignition, above the critical temperature.

In the present model ignition occurs at a maximum value of dT_s/dt above the critical temperature, which is indeed an experimental criterion for ignition. Mathematically, of course, there is no difference in the defining equation for ignition temperature, but the intuitive difference in approach to this equation is stressed.

Reynolds wrote $\dot{q}_{chem}$ as follows:

$$\dot{q}_{chem} = \dot{m} Q_{chem} \qquad \text{(A2-31)}$$

where $\dot{m}$ is the reaction rate (g $O_2/cm^2 sec$) and Q_{chem} is the heat of reaction (cal/g O_2). He considered both linear

$$w = K_l t = A_l t e^{-E_l/RT_s} \qquad \text{(A2-32)}$$

and parabolic regimes of oxidation

$$w^2 = K_p t = A_p t e^{-E_p/RT_s} \qquad \text{(A2-33)}$$

where the k_i are the appropriate rate constants, A_i are the appropriate pre-exponential factors, E_i are the appropriate activation energies, and R is the universal gas constant. w is the weight of O_2 per unit area that

has reacted with the metal at time t.

Since

$$\dot{m} = \partial w / \partial t \tag{A2-34}$$

then

$$\dot{m}_\ell = K_\ell = A_\ell e^{-E_\ell / RT_S} \tag{A2-35}$$

and

$$\dot{m}_p = K_p / 2w = K_p \gamma / 2\rho_{ox} d_{ox} \tag{A2-36}$$

Therefore:[7]

$$\dot{m}_p = (A_p \gamma / 2\rho_{ox} d_{ox}) e^{-E_p / RT_S} \tag{A2-37}$$

where ρ_{ox} is the oxide density, d_{ox} is the oxide thickness, and γ is the ratio of the mass of oxide to the mass of O_2 forming it. Multiplying by the heat release per gram O_2, Q_{chem}, the heat release rates are obtained:

$$\dot{q}_{chem,\ell} = A_\ell Q_{chem} e^{-E_\ell / RT_S} \tag{A2-38}$$

$$\dot{q}_{chem,p} = (A_p \gamma Q_{chem} / 2\rho_{ox} d_{ox}) e^{-E_p / RT_S} \tag{A2-39}$$

Substitution of Eqn. (A2-38) or (A2-39) into Eqn. (A2-30) yields:

$$e^{-1/T^*_{s,i}} = (T^*_{s,i})^5 / \eta_i + h^*_i (T^*_{s,i})^2 \tag{A2-40}$$

---

[7] Markstein (10) has shown that the placement of γ in the denominators of Eqn. (A2-36) and (A2-37) as in the original paper of Reynolds is in error.

where subscript i equals ℓ or p, and where

$$T^*_{s,i} = T_s R/E_i \qquad \text{(A2-41)}$$

$$\eta_\ell = A_\ell Q_{chem} R^4/4\epsilon\sigma E_\ell^4 \qquad \text{(A2-42)}$$

$$\eta_p = A_p \gamma Q_{chem} R^4/8\epsilon\sigma \rho_{ox} d_{ox} E_p^4 \qquad \text{(A2-43)}$$

$$h^*_\ell = hE_\ell/A_\ell Q_{chem} R \qquad \text{(A2-44)}$$

$$h^*_p = 2hE_p \rho_{ox} d_{ox}/A_p \gamma Q_{chem} R \qquad \text{(A2-45)}$$

The $T^*_{s,i}$ are dimensionless ignition temperatures, the h^*_i are dimensionless heat transfer coefficients, and the η_i are called pyrophoricities by Reynolds.

Reynolds noted that either an increase or decrease in the rate of convective heat transfer (and furthermore, when this term represents either heating or cooling) will increase the calculated ignition temperature.

Since the ignition temperature is expressed by the universal curve Eqn. (A2-40), all metal-oxidizer systems were expected to agree with this prediction. Reynolds calculated a family of curves of T^*_s versus η for various values of h*. He then measured ignition temperatures for various massive systems, some of which have been discussed in previous sections of this chapter. For the specific systems, the oxidation rate data were taken from the oxidation literature. Extremely good agreement between the curve of T^*_s versus η with h* equal to zero was obtained in all the cases investigated. Reynolds

argued that this agreement with the case of zero convective heat transfer was a result of his measuring the ignition temperatures in quiescent atmospheres. Experimentally, ignition was defined by "a sharp break in the temperature-time curve."

As noted previously, Reynolds' resulting theoretical definition of the ignition temperature, Eqn. (A2-30), is equivalent to that of the present investigation, Eqn. (II-57). The experimental definition is also equivalent. Thus agreement between theory and experiment, within the experimental error and the theoretical error in estimating the various parameters which appear in Eqn. (A 2-41) - (A2-43), is not unexpected. However, in the theory of Reynolds, the ignition temperature is predicted to be independent of sample size, and furthermore, no pressure dependence is predicted, because of the experimental indication that convective heat losses to the ambient gases are negligible.

d. Bulk Ignition According to the Theory of Talley

Talley (245) made a calculation of "the minimum temperature above which the combustion of boron is self-sustaining. . .by equating the rate of heat generation by chemical reaction with the rate of heat loss by radiation as functions of temperature." He referred to this temperature as an ignition temperature, but of course in the present model this temperature is defined as the critical temperature. Estimates of the reaction rate were acquired from data about 700^{o}C below the ignition temperature in

a temperature regime in which the evaporation of B_2O_3 from the metal surface is rate-determining.

As Talley recognized, because only a radiation heat loss mechanism is assumed, the theory is valid only for large samples. Under these assumptions, an ignition temperature of about 1925°C was predicted for large B samples in O_2. Because of the experiment employed to investigate the ignition process, critical and ignition temperatures could not be distinguished.

By introducing a 1 mm diameter B rod into an O_2-rich natural gas flame and using a corrected optical pyrometer to measure surface temperature, Talley made the following observations: "at temperatures about 1800°K the boron was observed to burn relatively slow. Between 1800 and 2100°K the rate increased evenly. A temperature of 2230°K (1957°C) was the highest temperature before there was a sudden increase in burning rate." The correspondence of the temperature of this sudden rate change and the calculated ignition temperature is excellent.

As is the case with most of the other theories discussed to this point, Talley's theory predicts that the calculated critical temperature is independent of sample size and oxidizer pressure.

e. Single Particle Ignition According to the Theory of Friedman and Macek

Friedman and Macek (15) developed an ignition theory in order to explain their experimental results on the ignition of Al particles. They later applied similar ideas to the ignition of Be (226); these experimental results have been discussed in Sections 4 and 5 of the present appendix.

The attempt to explain their results on the basis of a simple heat balance led to several discrepancies with their experimental results. The theory predicted a strong dependence of the ignition temperature on particle size and on ambient oxidizer concentration, whereas experimentally these parameters had little influence on ignition temperature. Furthermore, the predicted ignition temperatures were considerably higher than the measured temperatures.

In order to circumvent these difficulties, on the basis of the experimental association of the Al ignition temperature with the melting point of Al_2O_3 they assumed that a discontinuous increase in reaction rate occurs at the melting point of the oxide, T_{MP}^{MO} (T_s is the particle temperature):

$$\dot{q}_{chem} = Q_{chem}\, c_g K \qquad T_s < T_{MP}^{MO} \tag{A2-46}$$

$$\dot{q}_{chem} = Q_{chem}\, c_g K' \qquad T_s \geq T_{MP}^{MO} \tag{A2-47}$$

where Q_{chem} is the heat of reaction (cal/mole), c_g is the concentration of oxidizer at the particle surface (mole/cm^3), and k and k' are rate constants (cm/sec), with $k' >> k$.

Two heat fluxes in the ambient gas were considered:

$$\dot{q}_{cond,g} = 2K_g (T_s - T_g)/d \tag{A2-48}$$

$$\dot{q}_{diff} = 2Q_{chem} D (c_{g,\infty} - c_g)/d \tag{A2-49}$$

were $\dot{q}_{cond,g}$ is the heat lost by conduction, k_g is the

thermal conductivity of the gas (cal/cm sec ^{o}K), T_g is the gas temperature (^{o}K), d is the particle diameter (cm), $\dot{q}_{diff}$ is the heat flux due to oxidizer diffusion to the reaction zone, D is the oxidizer diffusivity (cm^2/sec), and $c_{g,\infty}$ is the oxidizer concentration at infinity ($mole/cm^3$).

Because the particle is assumed to be at uniform temperature T_s, conduction into the particle is neglected. Radiation losses are also neglected in the ignition process.

A temperature defined by an equilibrium:

$$\dot{q}_{cond,g} = \dot{q}_{diff} \qquad (A2-50)$$

$$\dot{q}_{chem} = \dot{q}_{cond,g} \qquad (A2-51)$$

exists below the oxide melting point; above this temperature the particle may self-heat (that is, this temperature is, in terms of the physical model, the critical temperature). The authors referred to this temperature as the minimum ambient temperature required for ignition.

Friedman and Macek proceeded in this manner in order to evaluate the oxidizer concentration at the particle surface from Eqn. (A2-50), (A2-48), and (A2-49):

$$c_g = c_{g,\infty} - K_g (T_s - T_g)/DQ_{chem} \qquad (\ -52)$$

Eqn. (A2-51) may be rewritten:

$$Q_{chem} c_g K = 2K_g (T_s - T_g)/d \qquad \text{(A2-53)}$$

Eqn. (A2-52) is then substituted into Eqn. (A2-53) and the expression for the minimum ambient temperature required for ignition is obtained:

$$T_g = T_s - c_{g,\infty} Q_{chem} / \left[K_g \left(\frac{1}{D} + \frac{2}{dK} \right) \right] \qquad \text{(A2-54)}$$

Since at ignition, $T_s = T_{MP}^{MO}$, Eqn. (A2-54) becomes:

$$T_g = T_{MP}^{MO} - c_{g,\infty} Q_{chem} / \left[K_g \left(\frac{1}{D} + \frac{2}{dK} \right) \right] \qquad \text{(A2-55)}$$

Friedman and Macek noted that the correction term, the second term on the right hand side of Eqn. (A2-55), is extremely small compared to T_{MP}^{MO}, which explains the observed small dependence of ignition temperature on d and D.

The theory is applicable only to small particles because conduction into the interior of the particle and radiation to the surroundings are neglected.

A major difficulty with the theory is that as the particle diameter is increased, the minimum ambient temperature required for ignition (or critical temperature) decreases. Also, k, the reaction rate, which appears in Eqn. (A2-55) is a function of temperature and pressure.

f. Dust Dispersion Ignition According to the Theory of Nagy and Surincik

Nagy and Surincik (246) have recently developed a theory for ignition of dust dispersions. Their theory was tested against experimental results on the ignition of cornstarch; nevertheless, inasmuch as DD experiments give ignition temperatures which have little correlation with transition temperatures, as has been shown in earlier sections of this appendix, the ignition temperatures of dust dispersions of cornstarch or metal powders are expected to be predicted equally well by a theory which does not include a transition temperature concept.

Again a simple heat balance is used to define ignition, so that in actuality a critical rather than ignition temperature is estimated:

$$\dot{q}_{chem} = \dot{q}_{loss} \qquad (A2-56)$$

Because of the nature of the sample configuration, somewhat more complicated expressions for the heat fluxes result. Also, heat fluxes per unit volume rather than per unit area are considered.

The following assumptions were made:

(1) The entire system (gas plus particles) is described by the equation of state $pV = RT$, where p is pressure, V is volume, R is the universal gas constant, and T is the temperature.

(2) The dispersion is uniform with respect to volume, and the volume of the particles is negligible with respect to that of the gas.

(3) Mass transfer is negligible during ignition.

(4) Heat capacities are temperature independent.

(5) Heat transfer occurs primarily by conduction and convection and is linearly proportional to the temperature difference.

(6) Any action of the addition of an inert dust to the dispersion is strictly thermal.

(7) A bimolecular oxidation process is assumed, and the rate variation of this process with respect to temperature is expressed by an Arrhenius-type function.

The heat release due to reaction per unit volume may then be expressed:

$$\dot{q}_{chem} = AQ_{chem}(F)^{\alpha}(OX)^{\beta}(p/RT)^{2}e^{-E/RT} \qquad \text{(A2-57)}$$

where all symbols have their previous meanings, and where α is the order of the reaction with respect to fuel (F) and β with respect to oxidizer (OX). (F) and (OX) are the relative molar concentrations per unit volume. Several simplifications of Eqn. (A2-59) are made as indicated below.

Since O_2 is the only reacting component of the gas phase, "the system may be considered unimolecular with respect to the gaseous phase. Thus the term p/RT is taken at the first power rather than at the second power, and the units of A become 1/sec. The system contains the inert gases nitrogen and admixed carbon dioxide, and the rate of reaction is lowered by the fraction θ, which represents the proportion of oxygen in the atmosphere." Since at ignition, by definition the concentra-

tion of products is negligible:

$$(F) + (OX) = 1 \tag{A2-58}$$

Because the number of moles of O_2 per unit volume is $p\theta/RT$, the weight of O_2 per unit volume, Z, is:

$$Z = p\theta \mathcal{M}_{O_2}/RT \tag{A2-59}$$

where $\mathcal{M}_{O_2}$ is the molecular weight of O_2.

The effective surface area of the dust is included in the chemical heat release rate by modification of the activation energy, that is, exp (-E/RT) is replaced by exp ($-\sigma$E/RT), where σ is the effective surface area of the dust, and E is a property only of the fuel. Finally,

$$(F) = (X/\mathcal{M}_d)/(X/\mathcal{M}_d + Z/\mathcal{M}_{O_2}) \tag{A2-60}$$

where X is the initial dust concentration in g/cm^3 and $\mathcal{M}_d$ is the molecular weight of the dust. Then:

$$(F)^\alpha[1-(F)]^\beta = [X/(X+bZ)]^\alpha[1-X/(X+bZ)]^\beta \tag{A2-61}$$

$$\equiv f(X) \tag{A2-62}$$

where

$$b \equiv \mathcal{M}_d/\mathcal{M}_{O_2} \tag{A2-63}$$

Thus combining Eqn. (A2-57) through (A2-62):

$$\dot{q}_{chem} = \{AQ_{chem} Z f(X)/\mathcal{M}_{O_2}\} e^{-\sigma E/RT} \tag{A2-64}$$

The rate of heat loss per unit volume is expressed in the following manner:

$$\dot{q}_{loss} = \left[\sum_i K_i N_i c_{p,i} + V'\right](T - T_f) \qquad \text{(A2-65)}$$

where subscript i includes all constituents of the dust and gas system, k_i is the coefficient of heat transfer of species i (including conduction, convection, and radiation), (1/sec), N_i is the concentration of species i at the furnace temperature T_f (g/cm^3), $c_{p,i}$ is the specific heat of species i at T_f (cal/g^oK), and V' is the rate of heat loss per degree per unit volume to the vessel walls (cal/sec^oKcm^3).

The experimental results indicated that the heat transfer coefficients, k_i, are all of the same order of magnitude. Thus

$$K_i = K \qquad \text{(A2-66)}$$

and

$$V = V'/K \qquad \text{(A2-67)}$$

Following Semenov, the approximation is made:

$$T - T_f \cong RT_f^2/\sigma E \qquad \text{(A2-68)}$$

and thus Eqn. (A2-65) becomes in its final form:

$$\dot{q}_{loss} = (KRT_f^2/\sigma E)\left[\sum_i N_i c_{p,i} + V\right] \qquad \text{(A2-69)}$$

The condition for ignition, Eqn. (A2-56), is then:

$$\{AQ_{chem}ZF(X)/M_{O_2}\}e^{-\sigma E/RT} = \{KRT_f^2/\sigma E\}\left[\sum_i N_i C_{P,i} + V\right] \qquad (A2\text{-}70)$$

Nagy and Surincik obtained the values of σ, k', V, α, β, and b, where

$$K' \equiv KRM_{O_2}/\sigma AQ_{chem}E \qquad (A2\text{-}71)$$

from their experimental results on the ignition of cornstarch. They then varied the furnace temperature and concentrations of fuel dust, inert dust, and oxygen over wide ranges, and found an excellent correlation between theory and experiment. Predictions of ignition limits were also verified experimentally.

The excellent agreement between this theory for the ignition of dust dispersions (in which in actuality a critical temperature is calculated) and the so-called measured "ignition temperatures" further substantiates the conclusion reached in earlier sections of this appendix that ignition temperatures measured in such experiments must be interpreted as critical temperatures.

g. Quiescent Pile Ignition According to the Theory of Anderson and Belz

Anderson and Belz (236) proposed a qualitative theory of the ignition of quiescent piles of metal powders. In particular, they considered the ignition of Zr in O_2.

It was assumed that a spherical mass of powder of radius r is in perfect contact with a heat reservoir at temperature T_0. This spherical mass of powder consists of spherical particles of diameter d. "If the rate of heat development at the center of the mass is greater than the rate at which the heat can be transported to the container, ignition eventually occurs. Then, the following condition is necessary to ignition: rate of exothermic heat development > rate of heat loss." Therefore, this theory is a discussion of the critical temperature for a quiescent pile experiment.

The appropriate reaction rate law for Zr in O_2 was taken as

$$w^2 = K_p t + \text{constant} \qquad \text{(A2-72)}$$

where w is the increase in weight of the metal sample per unit area. The reaction rate per unit area is then:

$$\frac{dw}{dt} = \frac{1}{2}\sqrt{\frac{K_p}{t}} = \frac{\sqrt{A'}\, e^{-E/2RT}}{2\sqrt{t}} \qquad \text{(A2-73)}$$

where all symbols have their previous meanings.

The total surface area per gram of a system of uniformly sized particles is $6/\rho d$, where ρ is the metal density.[8] Anderson and Belz then wrote the rate of heat generation by the center element as

$$\dot{q}_{chem} = (A' Q_{chem} / \sqrt{t}\, d)\, e^{-E/2RT} \qquad \text{(A2-74)}$$

---

[8] Anderson and Belz erroneously gave this expression as $6/\rho d^5$, but apparently used $6/\rho d$ in their subsequent calculations.

where A' includes all previous constants.

The heat loss term is assumed to be of the form:

$$\dot{q}_{loss} = K(T-T_o)/r \qquad \text{(A2-75)}$$

where k is the appropriate thermal conductivity of the particle plus void configuration. The criterion for ignition then becomes:

$$(A'Q_{chem}/\sqrt{E'}d)\,e^{-E/2RT} > K(T-T_o)/r \qquad \text{(A2-76)}$$

Anderson and Belz noted that this expression could not be solved for the ignition temperature T in terms of the ambient temperature T_0. However, simplifications are possible if the assumption that $(T - T_0)$ is equal to a small constant value is made. Then Eqn. (A2-76) may be written:

$$e^{-E/2RT_o} > A''\sqrt{E'}d/r \qquad \text{(A2-77)}$$

or

$$T_o > E/\{2R\ln(r/A''\sqrt{E'}d)\} \qquad \text{(A2-78)}$$

Anderson and Belz stated that "various interpretations of the time factor in this expression are possible. If it is interpreted as an inverse function of the external heating rate, then the expression predicts a decrease in ignition temperature with heating rate. This is the experimental case for small samples. In the

case of larger samples, the increase of ignition temperature with heating rate is attributed to increased lag of internal temperature with respect to external temperature. . . The expression is in qualitative agreement with the data, as regards particle size." The trend predicted is that the ignition temperature will decrease with decreasing particle diameter, d.

h. Quiescent Pile Ignition According to the Theory of Tetenbaum, Mishler, and Schnizlein

Tetenbaum et al. (233) correlated their experimental results on the ignition of quiescent piles of U powder in O_2 on the basis of the ignition theory of Frank-Kamenetskii. They also applied an ignition theory of Murray, Buddery, and Taylor, which was originally developed in light of the data of Anderson and Belz described in Section 7 of this appendix.

Using the stationary homogeneous ignition theory of Frank-Kamenetskii, which has been reviewed in detail in Section 1.a of Chapter II, Tetenbaum and coworkers found excellent agreement between their experimental results and ignition temperatures calculated on the basis of Eqn. (II-16) with $\delta = 0.88$, that is, for a one-dimensional container.

The agreement between a theory developed for homogeneous gas-phase systems with results obtained in a quiescent pile powder experiment no doubt results from the homogeneous nature of this latter experimental configuration, that is, the small metal particles separated by spaces filled with O_2. Again, since as shown in Chapter II, Eqn. (II-56) is the defining equation in this theory,

a critical temperature has been calculated.

Tetenbaum et al. then applied a theory due to Murray, Buddery, and Taylor; the physical basis of this theory is questionable. Here no heat losses are included, and all the heat generated by the chemical reaction is used to increase the temperature of the pile of powder. Effectively, then, the critical temperature for this theoretical model is zero, for as long as any exothermic reaction occurs, the temperature of the sample will increase until ignition occurs.

According to Murray et al. as quoted by Tetenbaum and co-workers, the rate of heating due to chemical reaction of a metal powder in the linear oxidation rate regime is:

$$\frac{dH}{dt} = \frac{6MQ_{chem}Ae^{-E/RT}}{\rho d} \qquad \text{(A2-79)}$$

where H is enthalpy, M is the mass of the powder, d is the diameter of a particle within the powder, and ρ is the density. If the container is heated at the rate $dT/dt = \phi$, then the total enthalpy generated upon heating from 298°K to T°K is:

$$H = \int_{298}^{T} \frac{6MQ_{chem}Ae^{-E/RT}}{\phi\rho d}\, dT \qquad \text{(A2-80)}$$

Also

$$H = Mc_p\Delta T \qquad \text{(A2-81)}$$

where c_p is the specific heat of the powder and ΔT is the

temperature rise resulting from reaction upon raising the container temperature from 298°K to T°K at a rate of ϕ °K/min.[9] Thus

$$\Delta T = \int_{298}^{T} \frac{6Q_{chem} A e^{-E/RT}}{\phi \rho c_p d} dT \qquad \text{(A2-82)}$$

After integration, Eqn. (A2-82) may be written:

$$\log\{R\rho d\phi c_p \Delta T / 6Q_{chem} AE\} = -E/4.56T_o + \log\left\{\left(\frac{RT_o}{E}\right)^2 - 2\left(\frac{RT_o}{E}\right)^3\right\} \qquad \text{(A2-83)}$$

where T_0 is the container temperature at which ignition occurs. ΔT is "the difference in temperature between the sample and container at ignition."

On the basis of the data of Anderson and Belz obtained with Zr powder (236), Murray and co-workers took $\Delta T = 50^{\circ}K$. Tetenbaum et al. used this value of ΔT and calculated ignition temperatures, T_0, for their experiments from Eqn. (A2-83). Again, excellent agreement between theory and experiment was obtained.

At first sight, there is an apparent contradiction between these two theories. Critical temperatures are calculated from the theory of Frank-Kamenetskii because of the starting equation, Eqn. (II-56). Because no heat losses are involved in the theory of Murray et al., the critical temperature is zero and the calculated temperature may be an ignition temperature. Yet temperatures

[9] There is a typographical error in the definition of H in Ref. (233), in which $H = Nc_p\Delta T$. Eqn. (A2-81) above is correct.

calculated from both theories agree extremely well with each other and with experiment. This could mean that the critical and ignition temperatures are equivalent in this particular experiment.

Firstly, however, it is not clear that the temperature calculated from the Murray theory if an ignition temperature, and particularly the ignition temperature as defined in the physical model of metal ignition. Secondly, in this theory, ignition is regarded to occur when the amount of sample self-heating over the container temperature, ΔT, is equal to $50^{\circ}K$. This value, however, was estimated on the basis of results of Anderson and Belz.

It was shown in the previous sections of this chapter that these latter investigators most likely measured critical temperatures rather than ignition temperatures. Thus the agreement of the Murray and Frank-Kamenetskii theories is not fortuitous, because the choice of $\Delta T = 50^{\circ}K$ was based on critical temperature data.

APPENDIX III-THE COMBUSTION OF MAGNESIUM AND ALUMINUM IN WATER VAPOR MIXTURES

The combustion of Mg ribbons and anodized Al wires in various H_2O mixtures, as observed in the wire-burning apparatus, is described in this section. Details of the apparatus are given in Chapter V, and the test points of interest and descriptions of the ignition characteristics are given in Chapter VI.

1. Magnesium

In H_2O-O_2 mixtures, as mentioned in Chapter VI, Mg ribbons generally ignited before they broke. The ignition and combustion flames appeared to be white. Burning rates were extremely rapid, as the approximately 9 cm length of ribbon exposed to the atmosphere was entirely consumed in less than one second. Flame spectra revealed no significant difference from the previously obtained Mg in O_2-Ar spectrum (7, 9).

After an experiment, a great deal of grey-white smoke was found on the electrode blocks and on the top of the chamber. The only recoverable products of combustion were a few white flakes of several mm^2 area.

In H_2O-Ar mixtures ignition also occurred before the ribbon's breaking. Beautifully colored vapor-phase flames were observed, usually either blue, green, or purple, or combinations of these. However, these flames were extremely dim.

Burning times were longer than in H_2O-O_2 mixtures; in particular, at, and only at 50%H_2O-50%Ar and a total pressure of 100 torr, the burning persisted for

10 to 15 sec. These flames were observed to consist of two colored zones, the inner of which was blue-green (perhaps discrete radiation from MgO (269)), and the outer purple (perhaps MgOH (269)). The long burning time occurred under these conditions each time that the sample was successfully ignited. No explanation can be offered for this abnormally long burning time at this particular test point.

Flame spectra obtained at this test point revealed only the Na D lines and complex bands in the 3700-3900 Å region which are due to either $(MgO)_n$ or MgOH (269). The dimness of the flames was such that only poor spectral plates could be obtained; thus definite identification was difficult.

The products of combustion in H_2O-Ar mixtures consisted of large white flakes which resembled the original ribbon shape. White smoke was also found.

On those few occasions in the H_2O-CO_2 mixtures when ignition occurred, the flames were of short duration and resembled the H_2O-Ar flames. Black areas were present on the large white flakes, but the products of combustion in all the gas mixtures studied consisted only of MgO, as determined by X-ray diffraction.[1]

In all the gas compositions, on these experiments at which ignition did not occur, the ribbon was twisted and blackened near its center where it had broken. A green spark, which may have been an electrical effect, was seen when the ribbon broke.

2. Aluminum

As was discussed in Chapter VI, unanodized Al

[1]The author wishes to acknowledge the assistance given in the X-ray diffraction analyses by Mr. Edward Lyden of Princeton University, Department of Geology.

wires could not be ignited in any of the wet gas mixtures which were studied; thus the description of the combustion mechanisms as given in the present section pertains only to the anodized wires.

In H_2O-O_2 mixtures, ignition occurred upon the breaking of the wire. Two types of combustion mechanisms were observed, depending on the total pressure. At 50 torr, large blue vapor-phase flames were observed at the ends of the wire. These flames generally regressed up the wire slowly and stabilized at a point at which the rate of heat generation by the flame equaled the rate of heat loss by conduction along the wire into the electrode blocks. Burning times were typically on the order of several sec. The flames and recoverable products of combustion resembled those found by Brzustowski at low pressures in O_2-Ar mixtures, denoted as Region 3 (7, 9), and by Mellor at low pressures in O_2-CO_2 mixtures, denoted as Regions 5 and 6 (19, 20).

Similar flames were also observed by Brzustowski and Glassman in H_2O-O_2 mixtures at a total pressure of 50 torr and are described in Ref. (270).

At total pressures of 100 or 200 torr in H_2O-O_2 mixtures a different type of combustion followed ignition upon the breaking of the wire. In this case, the wire was rapidly consumed by a white flame, which appeared at the exposed ends of the wire and regressed completely to the electrode blocks. Typical burning times were on the order of 1/2 sec. The products of combustion consisted of hard white spheres, most likely composed of α-Al_2O_3. A similar mechanism was observed by Brzustowski in O_2-Ar mixtures at higher pressures and was designated as Region 2 (7, 9).

In H_2O-Ar and H_2O-CO_2 mixtures, ignition

occurred in the form of a cylindrical vapor-phase flame before the wire broke, as discussed in Chapter VI.

After the breaking of the wire in either of these gas mixtures, dim vapor-phase flames persisted for times as long as 5 to 10 sec. The burning time after the breaking of the wire was observed to decrease with increasing pressure.

After the termination of an experiment, in the neighborhood of that part of the wire at which the flame had occurred, the wire surface was observed to be roughened and covered in places with a white deposit.

In general, in H_2O-Ar and H_2O-CO_2 mixtures, anodized Al wires exhibited combustion characteristics exactly similar to that observed in CO_2-Ar mixtures over a comparable pressure range, denoted previously as Region 1 in this latter case (19, 20).

Flame spectra were obtained only in H_2O-Ar mixtures and presented one major difference between these flames and those found in the other oxidizers studied earlier. Positive identification of AlH bandheads at 4241.0 and 4259.5 Å was made. This species was observed in emission. Its presence indicated that the presence of H_2O may affect the chemical mechanism of the flame, unlike the presence of CO_2 (19, 20).

3. Summary

Comparison of the combustion of Mg ribbons and anodized Al wires in H_2O-O_2 mixtures over the pressure range from 50 to 200 torr with that in O_2-Ar mixtures (7, 9) indicates that H_2O affects the chemical mechanisms proceding within the flame. In general, somewhat faster burning rates are observed in the former

oxidizer. Most likely the formation of H and OH radicals is responsible for this rate increase.

For Mg ribbons in H_2O-Ar mixtures, the observed colors indicate that new chemical processes are occurring in the flame, and these flames warrant further study.

Anodized Al wires were observed to burn in H_2O-Ar and H_2O-CO_2 mixtures in a manner which was generally similar to that in CO_2-Ar atmospheres (19, 20). However, one interesting difference was noted. In those mixtures containing CO_2, there appeared to be more oxide smoke formation in the flame, that is, the outer edge of the flame was more well-defined. This observation may be explained by the presence of C particles in the flame zone in mixtures containing CO_2; these particles would then provide nucleation sites for the condensation of the metal smoke.

To summarize, because the study of the ignition of Mg and Al in atmospheres containing H_2O was of paramount interest in the present investigation, only cursory observations on the combustion were made. However, the experimental results indicate that some differences are present between the combustion in H_2O containing oxidizers and in O_2-Ar and CO_2-Ar mixtures and deserve further study.

DISTRIBUTION LIST FOR NASA GRANT NSG-641

National Aeronautics and Space Administration
Western Support Office
150 Pico Boulevard
Santa Monica, California 90406
Attn: Eugene F. Wyszpolski

National Aeronautics and Space Administration
Langley Research Center
Langley Station
Hampton, Virginia 23365
Attn: Robert L. Swain (1)
Tech. Library (1)

National Aeronautics and Space Administration
George C. Marshall Space Flight Center
Redstone Arsenal
Huntsville, Alabama 35812
Attn: Alton L. Wheeler (1)
Tech. Library (1)
R. N. Eilerman R-PVE-PPS (1)

Chemical Propulsion Information Agency
Applied Physics Laboratory
8621 Georgia Avenue
Silver Spring, Maryland 20910

National Aeronautics and Space Administration
Manned Spacecraft Center
Houston, Texas 77058
Attn: Tech. Library (1)
J. G. Thibodaux (1)

National Aeronautics and Space Administration
Lewis Research Center
21000 Brookpark Road
Cleveland, Ohio 44135
Attn: Carl C. Ceipluch (1)
Mail Stop 500-313
Tech. Library (1)
Dr. Richard J. Priem (1)
Dr. L. A. Povinelli (1)

National Aeronautics and Space Administration
Goddard Space Flight Center
Greenbelt, Maryland 20771
Attn: Library

Jet Propulsion Laboratory
California Institute of Technology
4800 Oak Grove Drive
Pasadena, California 91103
Attn: Tech. Library (1)
Winston Gin (1)
Robert Sehgal (1)

National Aeronautics and Space Administration
Washington, D. C. 20546
Attn: SV/V. L. Johnson (1)
RV-1/C. Wood (1)
RV/M. B. Ames (1)
RC/J. L. Sloop (1)
RP/A. O. Tischler (1)
RTA/R. V. Hensley (1)
RTP/J. J. Phillips (1)
MGS/E. Hall (1)
MTA/M. C. Waugh (1)

Commander
Army Ballistic Missile Agency
Redstone Arsenal
Huntsville, Alabama 35812
Attn: Ordab-HSI

Ballistic Research Laboratory
Aberdeen Proving Ground,
Maryland 21005
Attn: Tech. Library (1)
Dr. Leland A. Watermeier (1)

Director
Advanced Research Projects Agency
The Pentagon, Room 3D154
Washington, D. C. 20301
Attn: Tech. Information Office

Department of the Air Force
Headquarters, USAF, DCS/D
Washington, D. C. 20545
Attn: AFDRT-AS

Air Force Systems Command
Space Systems Division
Air Force Unit Post Office
Los Angeles, California 90045
Attn: Col. H. Robbins

Commander
Air Force Systems Command
Hq. 6593 Test Group (Development)
Edwards Air F orce Base, California 93523
Attn: Mr. Don Hart (2)

Research and Technology Div. (AFSC)
Bolling Air Force Base
Washington, D. C.
Attn: Dr. Leon Green, Jr.

Commander Air Force Ballistic Missile Division
Hq. Air Research Development Command
P. O. Box 262
San Bernardino, California 92402
Attn: WDSOT

Department of the Army
Office, Chief of Ordnance
Washington, D. C. 20545
Attn: ORDTB

Commander
Army Rocket and Guided Missile Agency
U. S. Army Ordnance Missile Command
Redstone Arsenal
Huntsville, Alabama 35812
Attn: ORDXR-OTL (1)
Mr. Frank James (1)

Bureau of Naval Weapons
Department of the Navy
Washington, D. C. 20545
Attn: Code RMMP-2 (1)
Dr. O. H. Johnson (1)
Mr. Richard F. Gott (1)

Commander
U. S. Naval Ordnance Test Station
China Lake, California 93557
Attn: Dr. Alvin S. Gordon (1)
Tech. Library (1)

Professor Edward W. Price
Aerospace School
Georgia Institute of Technology
Atlanta, Georgia 30332

Naval Ordnance Laboratory
White Oak
Silver Spring, Maryland 20910
Attn: Dr. Carl Boyars (1)
Tech. Library (1)

Naval Propellant Plant
Indian Head, Maryland 20640
Attn: Tech. Library

Picatinny Arsenal
Dover, New Jersey 07801
Attn: Tech. Library

Institute for Defense Analyses
1666 Connecticut Avenue, N. W.
Washington, D. C. 20009
Attn: Tech. Library

Office of Naval Research
Navy Department
Washington, D. C. 20360
Attn: Mr. Roland D. Jackel, 429

Air Force Rocket Propulsion Laboratory
Edwards Air Force Base
California 93523
Attn: Mr. Richard Spann

Air Force Office of Scientific Research (SREP)
Propulsion Division
Washington, D. C. 20333
Attn: Dr. Bernard T. Wolfson

Air Force Systems Command
Research and Technology Division (RTGS)
Bolling Air Force Base
Washington, D. C. 20332
Attn: Dr. Leon Green, Jr.

United Technology Center
P. O. Box 358
Sunnyvale, California 94088
Attn: Librarian

Dr. Ralph Anderson, Vice President
Research and Development
CETEC Corporation
188 Whisman Road
Mountain View, California 94040

Allegany Ballistics Laboratory
Hercules Powder Company
Cumberland, Maryland 21502
Attn: Mr. T. A. Angelus

Rocketdyne
A Division of North American
Aviation, Inc.
Solid Propellant Operations
P. O. Box 548
McGregor, Texas 76657
Attn: Mr. S. C. Britton (1)
Librarian (1)

Chemical Propulsion Information Agency
The Johns Hopkins University
Applied Physics Laboratory
8621 Georgia Avenue
Silver Spring, Maryland 20910
Attn: Dr. Robert H. Cantrell (1)
Dr. Frank T. McClure (1)

Thayer School of Engineering
Dartmouth College
Hanover, New Hampshire 03755
Attn: Dr. Alvin O. Converse

Stanford Research Institute
333 Ravenswood Avenue
Menlo Park, California 94025
Attn: Mr. Lionel A. Dickinson

Aerojet-General Corporation
P. O. Box 296
Azusa, California 91703
Attn: Librarian

Amcel Propulsion Company
Subsidiary of Celanese Corporation
of America
1026-17th Street, N. W.
Washington, D. C. 20036

Hercules Powder Company
Allegany Ballistic Laboratory
P. O. Box 210
Cumberland, Maryland 21502
Attn: Librarian

Lockheed Propulsion Company
P. O. Box 111
Redlands, California 91409
Attn: Dr. Ralph L. Coates (1)
Helen Ashman, Librarian (1)

Space Technology Laboratories, Inc.
5730 Arbor Vitae Street
Los Angeles, California 90045
Attn: Librarian

Thiokol Chemical Corporation
Elkton Division
Elkton, Maryland 21921
Attn: Librarian

Aerojet-General Corporation
P. O. Box 1168
Sacramento, California 94086
Attn: R. G. Weitz, Head
Tech. Information Center

Aerospace Corporation
2400 East El Segundo Boulevard
El Segundo, California 90245
Attn: Librarian

Hercules Powder Company
Bacchus Works
Magna, Utah 84044
Attn: Librarian

Thiokol Chemical Corporation
Utah Division
Brigham City, Utah
Attn: Librarian

The Marquardt Corporation
16555 Saticoy Street
Van Nuys, California 91409
Attn: Technical Librarian

Rocket Power/Talco
A Division of Gabriel
Falcon Field
Mesa, Arizona 85201
Attn: Librarian

Atlantic Research Corporation
Shirley Highway at Edsall Road
Alexandria, Virginia 22314
Attn: Technical Librarian

Thiokol Chemical Corporation
Redstone Division
Huntsville, Alabama 35801
Attn: Technical Director

Rocket Research
233 Holden Street
Seattle, Washington
Attn: Librarian

Bolt, Beranek and Newman, Inc.
50 Moulton Street
Cambridge, Massachusetts
Attn: Dr. Ira Dyer

Brigham Young University
Provo, Utah 84601
Attn: Dr. Marvin D. Horton

Rocketdyne
A Division of North American Aviation, Inc.
6633 Canoga Park
Canoga Park, California 91304
Attn: Library, Dept. 596-306 (1)
Dr. Robert B. Lawhead (1)

California Institute of Technology
Pasadena, California 91109
Attn: Dr. Frank E. Marble (1)
Prof. B. H. Sage (1)

Purdue University
Jet Propulsion Center
Lafayette, Indiana
Attn: Dr. John R. Osborn

University of California
Dept. of Aerospace & Mechanical
Engineering Sciences
P. O. Box 107
La Jolla, California 92038
Attn: Prof. S. S. Penner

University of Utah
Department of Chemical Engineering
Salt Lake City, Utah 84112
Attn: Dr. Norman W. Ryan

Princeton University
Forrestal Research Center
Princeton, New Jersey 08540
Attn: Dr. Martin Summerfield

Rohm and Haas Company
Redstone Arsenal
Huntsville, Alabama 35808
Attn: William A. Wood (1)
Librarian (1)

Dr. Robert F. Sawyer
Mechanical Engineering,
Thermal Systems
University of California
Berkeley, California 94720